

https://dspace.org/

The amphibolite and the granulite facies rocks of southern Malawi.

Andreoli, Marco Achille Giacomo

1981
https://hdl.handle.net/10539/26581

Downloaded from a DSpace repository. https://dspace.org/

THE AMPHIBOLITE AND THE GRANULITE FACIES ROCKS OF SOUTHERN MALAWI

Marco Achille Giacomo Andreoli

A Thesis Submitted to the Faculty of Science

University of the Witwatersrand, Johannesburg

for the Degree of Doctor of Philosophy.

Johannesburg, 1981

DECLARATION

I declare that this thesis is my own, unaided work, unless otherwise acknowledged. It is being submitted for the degree of Doctor of Philosophy in the University of the Witwatersrand, Johannesburg. It has not been submitted before for any degree or examination in any other University.

.....

MARCO ANDREOLI

..... day of ..... 1981.

ABSTRACT

The Precambrian geology of southern Malawi forms a segment of the Mozambique Belt and includes important suites of amphibolite and granulite facies rocks. These grade into each other and comprise lithologies of supracrustal affinity, together with clearly intrusive varieties. In granulites and transitional rocks, hypersthene-augite-plagioclase-(edenitic pargasite) parageneses, or almandine-augite-plagioclase-(-quartz)(-tschermakitic pargasite) parageneses with affinities with eclogite, progressively replace amphibolite facies assemblages. The calculated metamorphic conditions were $\approx$900-950°C and $\approx$ 6-9 kbar for the medium-pressure two-pyroxene granulites, and 800-900°C at 9-12 kbar for the high-pressure garnet-clinopyroxene granulites. Terranes transitional between the amphibolite and the granulite facies were metamorphosed at 550-750°C and at 5-8 kbar; and these areas also include bodies, obviously allochtonous, of garnet lherzolite developed at pressures above 12 kbar. Thermodynamic calculations indicate that in certain granulites the activity of H_2O was low, suggesting that anatexis was on a minor scale and that the metamorphism was isochemical. However, the local influence of metasomatism is indicated by a swarm of biotitite bodies and by scapolitised granulites, particularly in Mozambique where CO_2-rich vapour also introduced widespread

Fe, Ti, U, REE, Mo and Cu mineralisation.

The granulites are chemically heterogeneous and comparable to lower crust rock suites from elsewhere in Africa. Apart from certain clearly metasedimentary types, the majority of the southern Malawi granulites define trends similar to those of the alkali olivine and high-alumina basalts and their differentiation products. In contrast, the amphibolite facies gneisses, include more frequent sedimentary compositions such as pelite and greywacke. Age determinations suggest that the climax of the metamorphism was c. 1 130 m.y. ago, when geothermal gradients of 30-40°C/km existed across the amphibolite to medium-pressure granulite terranes. Other granulites have given ages of c. 980m.y.; and a major uplift of high-pressure granulites, monitored by widespread retrogression to medium-pressure granulite facies or amphibolite facies parageneses, occurred probably between c.950 and 850 m.y. ago. The gneisses probably became closed isotopic systems c.830 m.y. ago and between c.750 and 600 m.y. ago. On a regional scale the climax of the Mozambiquian Orogenic Cycle in southern Malawi thus coincides with the Kibaran Orogeny of southern Africa, while its later waning stages are coeval with the Pan-African Orogeny.

It is tentatively suggested that the dome-like orthopyroxene isograds resulted from intense thermal anomalies

associated with large intrusions in the lower crust, and that the intrusions fractionated anorthosite and perhaps also the closely associated suites of charnockitic K-rich monzonite, syenite and granite, possibly by contamination with crustal material. In contrast, the garnet-clinopyroxene isograd reflects geothermal gradients of 20-25°C/km which prevailed further away from the intrusions.

This thesis is dedicated to the memory of Flavia, spouse and fleeting companion of Ph.D. studies, that of my father, Roberto, and of Lesley, the wife of my Supervisor.

... and Yet, from their
Living and Dying,
in Sorrow and Joy,
of Strength, Wisdom and Love
the Holier Meaning
I Felt.

TABLE OF CONTENTS

	Page
ACKNOWLEDGEMENTS	x
CHAPTER	
1. INTRODUCTION	1
1.1 Regional Setting	1
1.2 Outline of Malawi Pre-Karoo Geology ..	4
1.3 Previous Studies on Malawi	11
1.4 Aim of the Present Study, Methods Employed and Nomenclature	14
2. FIELD AND PETROGRAPHIC CHARACTERS OF MALAWI METAMORPHIC ROCKS AND PLUTONIC COMPLEXES ..	18
2.1 Introduction	18
2.2 Granulites	21
(a) Field characteristics	21
(b) Petrography	23
2.3 Amphibolite Facies Rocks	31
2.4 Amphibolite to Granulite Facies Transitional Rocks	34
(a) General characters and field relationships	34
(b) Petrography	38
2.5 Relationships between the Amphibolite and the Granulite Facies	39
2.6 Plutonic Rocks	51

CHAPTER		Page
3.	MINERAL CHEMISTRY	55
	3.1 Introduction	55
	3.2 Typical Minerals	57
	3.3 Interoxide Relationships	72
	(a) Pyroxene	72
	(b) Garnet	79
	(c) Hornblende	83
4.	PETROCHEMISTRY	87
	4.1 Introduction	87
	4.2 Granulite Facies Rocks	90
	(a) Major oxides	90
	(b) Trace elements	101
	4.3 Amphibolite and Amphibolite to Granulite Facies Transitional Rocks	108
	(a) Major oxides	108
	(b) Trace elements	114
	4.4 Plutonic Rocks	119
5.	DETERMINATION OF P-T METAMORPHIC CONDITIONS AND MINERAL PARAGENETIC SEQUENCES ..	125
	5.1 Introduction	125
	5.2 Granulite Facies Rocks	127
	5.3 Amphibolite to Granulite Facies Transitional Rocks and Amphibolite Facies Gneisses	143
	(a) Transitional rocks	143

CHAPTER Page

(b) Amphibolite facies gneisses .. 151

5.4 Retrogression of the Granulites .. 152

6. PETROGENESIS 155

6.1 Introduction 155

6.2 Granulites, Gneisses and Transitional Rocks 155

6.3 Plutonic Rocks 176

7. GEOCHRONOLOGY 184

7.1 Introduction 184

7.2 Results 186

7.3 Interpretation 190

8. CONCLUSIONS 198

APPENDIX

I LIST OF SAMPLES 219

II PETROGRAPHY 228

III ELECTRON-MICROPROBE MINERAL ANALYSES .. 254

IV X-RAY FLUORESCENCE ROCK ANALYSES 274

V DETERMINATION OF P-T METAMORPHIC CONDITIONS 298

VI GEOCHRONOLOGY 300

VII THE GRANULITES OF THE TETE AREA, MOZAMBIQUE 316

LIST OF REFERENCES 333

MAPS (In the pocket at the back of the thesis)

ACKNOWLEDGEMENTS

I would like to express my gratitude to all those people who have assisted in the completion of this work and in particular to my supervisor, Professor T.N. Clifford, for his patient guidance throughout my postgraduate studies and for providing important geochronological data. I wish also to thank the management of AGIP spa for granting me a period of unpaid leave to complete the work in time.

I am indebted to Dr. R.E. Robinson, Director General of the National Institute of Metallurgy; to Dr. G. Koen, Head of the Geology Laboratory at the Anglo-American Research Laboratory and to the Director of the South African Geological Survey for authorising the electron-microprobe mineral analyses. Miss S. Gasperrini, Messrs. G Hutchinson, E.A. Viljoen, L.W. Esterhuizen and Mr. G. Davies carried out the mineral analyses.

I wish also to thank Mr. J.H. Bean, Director of the Geological Survey of Malawi for his cooperation during my campaign of field work and providing samples from the Survey's collections. Mr. Chisale gave friendly and energetic assistance during the period of field work.

It is a pleasure to acknowledge the assistance received from Dr. T.S. McCarthy for the petrochemical and geochemical investigation and Mr. A. Bemath chemically analysed some of the samples.

Dr. Burger and Dr. D.C. Rex provided the age determinations of a suite of critical specimens.

The following people have also contributed to this study: Professor J. McIver, Drs. G. Cawthorn, J. Barton, M. De Wit, H. Haslam, J. Bertrand, J.D. Bennett, Messrs. R. Lipson, O. Barker, P. Horrocks, K. Smith, R.E.P. Fripp, B. Wyatt, M.J. Crow, M. Miles, and Mrs. E. Zingg, S. Eriksson, S. McCarthy and K. Lilly. Mr. V.P. Coelho of the Portuguese Geological Survey generously provided a suite of samples from Mozambique.

Mr. J. Chaplin and Mr. F. Magadla prepared the thin sections; Mr. M. Taylor, P. Stickler and Miss A. Saiet drew most of the text figures and Mr. H. Hudson carried out the photographic work. Miss E. Robinson did most of the editing.

I am also indebted to the University of the Witwatersrand, the CSIR and to the Stella and Paul Lowenstein Charitable and Education Trust for their financial support. I should also like to thank Mrs. Elaine Towsey for typing the thesis.

CHAPTER 1. INTRODUCTION

1.1 Regional Setting

The structural evolution of Africa has been described in terms of a number of tectonothermal events, frequently polyepisodic, spanning more than 3 000 million years of earth history. At least two major events prior to 2 500 m.y. ago were followed by orogenic episodes at 1 850 ± 250 m.y. ago (Eburnian and Huabian events), 1 100 ± 200 m.y. ago (Kibaran Orogeny), 600 ± 100 m.y. ago (Damaran-Katangan or Pan-African Orogeny), in mid-Paleozoic-early Mesozoic times and finally during the Tertiary (see Fig.1; Clifford, 1974). Of these events, the one most extensively preserved is the 600 ± 100 m.y. Pan-African event, of which an important segment extends along the eastern side of the continent and was originally designated as the Mozambique Belt by Holmes (1951).

In their type area (Mozambique), the rocks of the Mozambique Belt consist primarily of high-grade amphibolite facies gneisses, within which occurrences of hypersthene-bearing rocks akin to granodiorite, diorite, norite, anorthosite and pyroxenite are developed (Assunçao and Coelho, 1956; Araujo, 1967; Oberholzer, 1968). A similar association of amphibolite and granulite facies rocks including frequent anorthosite, is repeated elsewhere in the Mozambique Belt, notably in southern Malawi, eastern

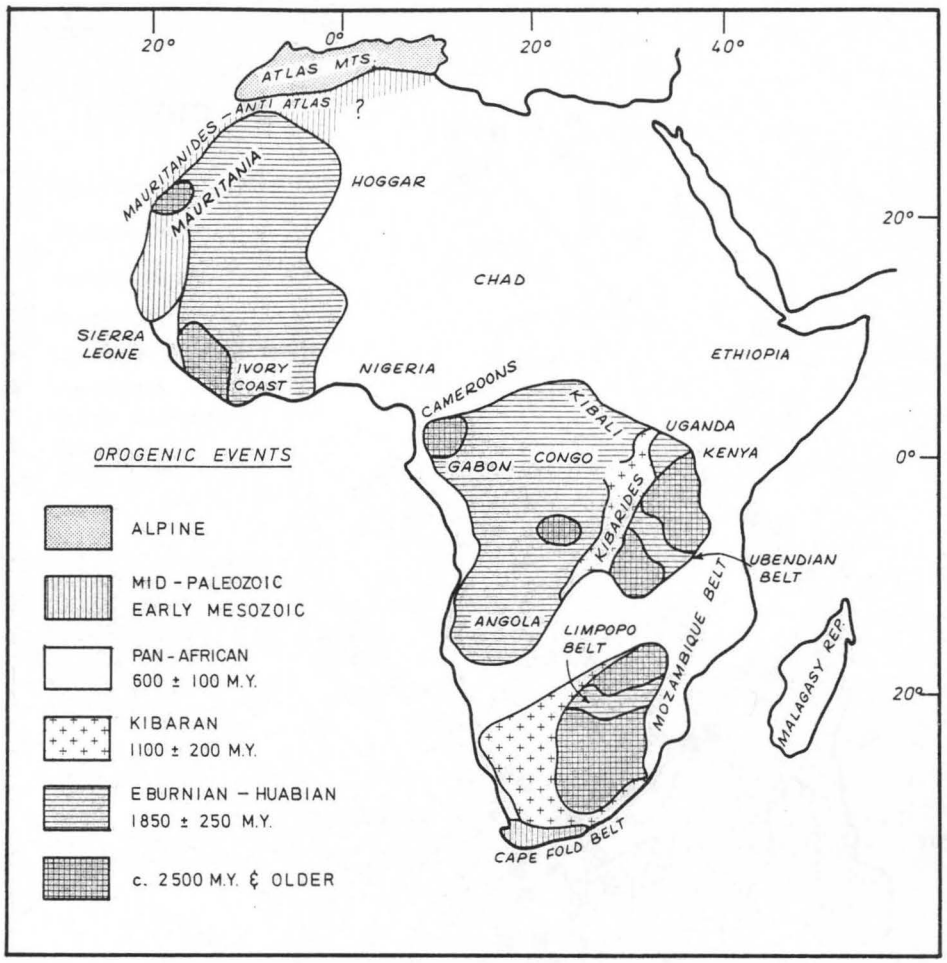


Fig.1. Generalized map of major structure units of Africa undisturbed by subsequent events (after Clifford, 1974).

Zambia, Tanzania and elsewhere (see Fig.2; Clifford, 1974; Ramsay and Ridgway, 1977). Perhaps the main problem concerning the geology of the Pan-African terranes in general and of the Mozambique Belt in particular is the relationship between the amphibolite and granulite facies suites. The latter are generally regarded as remnants of metamorphic and plutonic events older than the polyphase Mozambiquian (Pan-African) metamorphism (Clark, 1967; Clifford, 1974; Kröner, 1977).

Important shear zones affect the Mozambique Belt, particularly

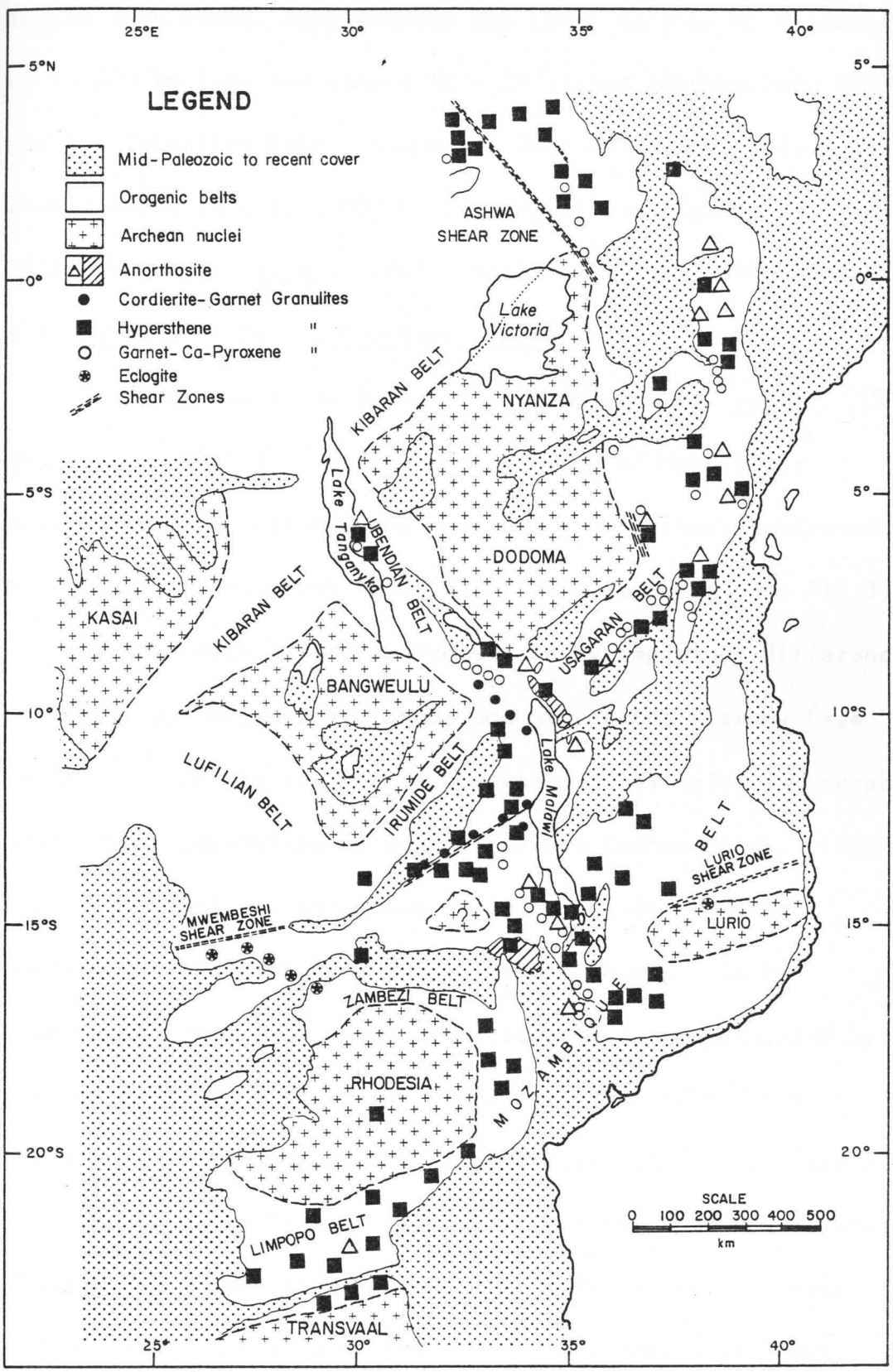


Fig.2. Main structural units in East Africa (modified after Vail, 1965; Saggerson, 1973; Saggerson and Turner, 1980).

in its type area: they include the Lurio Belt in NE Mozambique, up to 500 km long and with a NE - SW strike (Oberholzer, 1968), and the Chimaliro Belt - Mwembeshi Zone of Central Malawi and Zambia which is over 1 000 km in length (see Fig.2; Bloomfield, 1966; de Swardt et al., 1965; Snelling et al., 1972).

1.2 Outline of Malawi Pre-Karoo Geology

In review works by Bloomfield (1968), Cannon et al., (1969) and Thatcher (1973), the Basement geology of Malawi was subdivided into northern and southern subprovinces separated by a major transcurrent fault, the Chimaliro Belt (see Fig.3). The two subprovinces are characterised by important differences in lithology, metamorphic grade and geological history (see Table 1). In the northern subprovince three major metamorphic events were identified by Ray (1974) and Cannon et al., (1969). The first event was polyphase and accompanied by upper amphibolite and granulite facies metamorphism. In the granulites the most typical assemblages are characterised by the coexistence of garnet with sillimanite-cordierite ± biotite, while orthopyroxene-plagioclase-bearing rocks are rare.

According to Fitches (1968), this Basement and an overlying discordant sedimentary sequence, the 'Mafingi Group', were metamorphosed twice up to the amphibolite facies at about 1 200 and 550 ± 150 m.y. ago, when local downgrading to the greenschists facies occurred along the 600 km long Mugesse

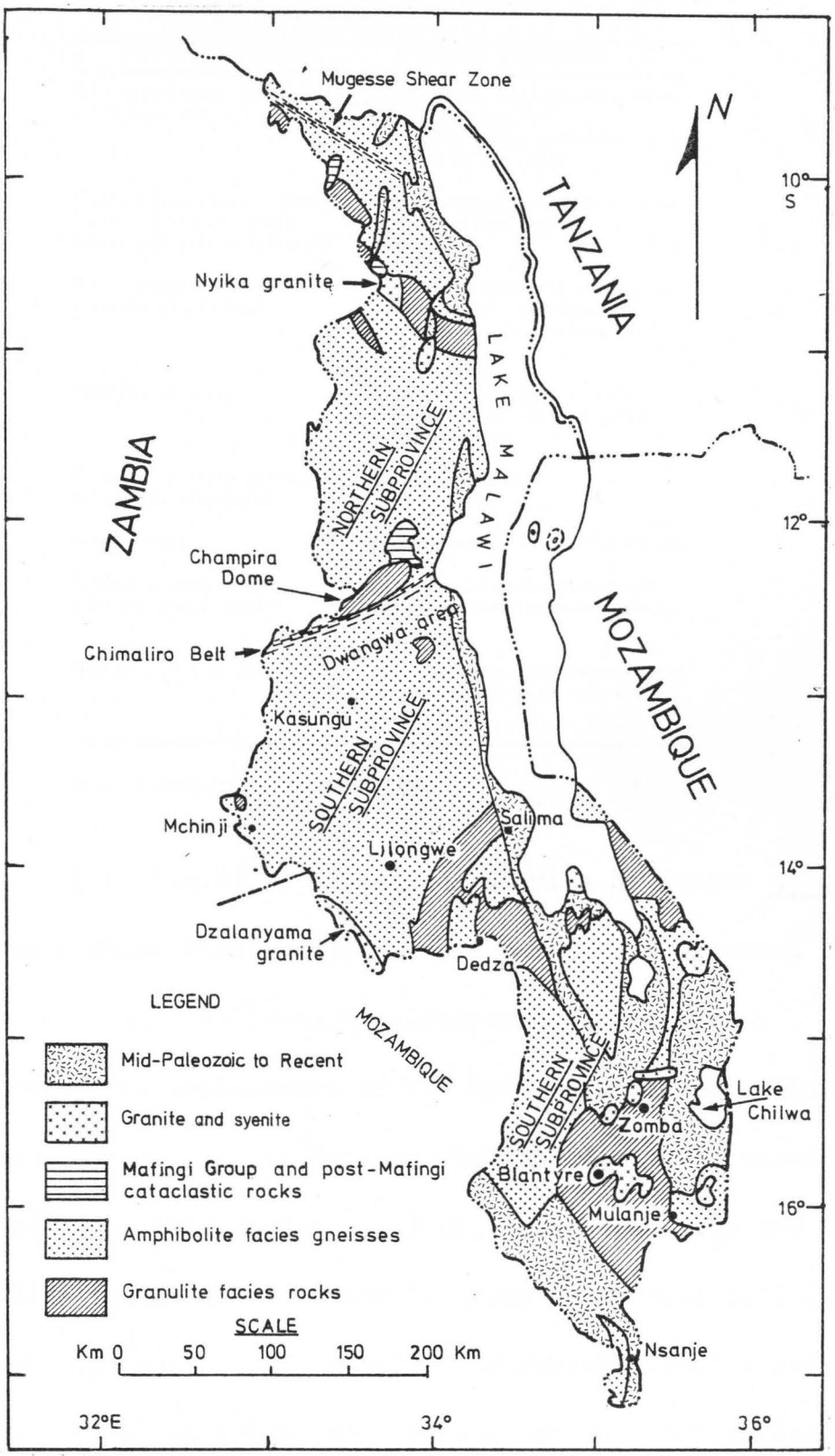


Fig.3. Major geological units of Malawi (modified after Carter and Bennett, 1973).

TABLE 1 - MAJOR DIFFERENCES BETWEEN THE GEOLOGY OF NORTHERN AND SOUTHERN MALAWI

Northern Subprovince	Southern Subprovince
Main metamorphic event about 2 000 m.y. old.	Amphibolite facies metamorphism 718 ± 25 m.y. old. Granulite facies metamorphism 1 126 ± 29 m.y. old.
Charnockites rare. Where present they are usually massive or weakly foliated.	Banded charnockitic gneisses and granulites common.
Marble absent. Calc-silicate gneiss rare.	Marble and calc-silicate gneiss common in both medium-grade gneisses and in charnockitic rocks.
Graphite absent.	Graphite widespread in both charnockitic rocks and medium-grade gneisses.
Banded cordierite granulite and gneiss widespread.	Cordierite rare.
Kyanite rare.	Kyanite common in pelitic gneiss.
Perthitic syenite and perthite gneiss absent.	Large Perthitic Complexes occur with associated perthite gneiss.
Meta-anorthosite absent.	Linthipe meta-anorthosite occurs in association with charnockitic rocks.

After Thatcher, 1973; Clifford, 1974.

Shear Zone (see Fig.3). Subsequent studies by Dodson et al., (1975) have shown that a major metamorphic event occurred at c. 2 000 m.y. ago, followed by widespread migmatisation accompanying the emplacement of the Nyika granite (see Fig.3). At present, therefore, it appears that the following tectonothermal events affected this region: (i) polyphase granulite and amphibolite facies metamorphism followed by igneous activity (c. 2 000 m.y. ago); (ii) erosion and deposition of a sedimentary sequence; (iii) polyphase amphibolite facies metamorphism (c. 1 200 m.y. ago); and (iv) shearing of Basement, with sporadic low-grade metamorphism (c. 550 m.y. ago).

The southern subprovince of Malawi includes two distinct

areas to the north-west and south-east of Lilongwe respectively (see Fig.3). The former region, generally referred to as central Malawi, is characterised by the predominance of amphibolite facies assemblages which cover an area of 14 500 km^2. Also present are rarer occurrences of 'charnockitic' orthopyroxene-bearing granulites (Thatcher and Walter, 1968; Peters, 1969; Walter, 1972a; Bellingham and Broomley, 1973) and sillimanite-cordierite-garnet granulites (Thatcher and Wilderspin, 1968; Kemp, 1974; see Fig.3). South-east of Lilongwe, in southern Malawi, pyroxene-, and garnet-bearing granulites and amphibolite facies gneisses and schists occur over extensive areas (see Fig.4). Typical regions of gneisses include the Kirk Range, the Middle Shire Valley, the country between Liwonde and Mangochi, and around Nsanje (see Fig.4); and their combined surface area is about 9 000 km^2. The most common rock types are monotonous hornblende-plagioclase gneisses with variable proportions of quartz, biotite and microcline. 'Pelitic' assemblages notably composed of kyanite-sillimanite-almandine-muscovite or sillimanite-almandine-orthoclase are common in the western Kirk Range and north-west of Lilongwe, whilst they are rare in the Middle Shire Valley. In addition, narrow and discontinuous belts of aegirine gneisses and granulites extend for about 100 km to the north of Lilongwe (Bloomfield, 1967), while in the south some occurrences of nepheline gneisses have been reported, particularly from Tambani, near the Mozambique Border (see Fig.4; Cooper

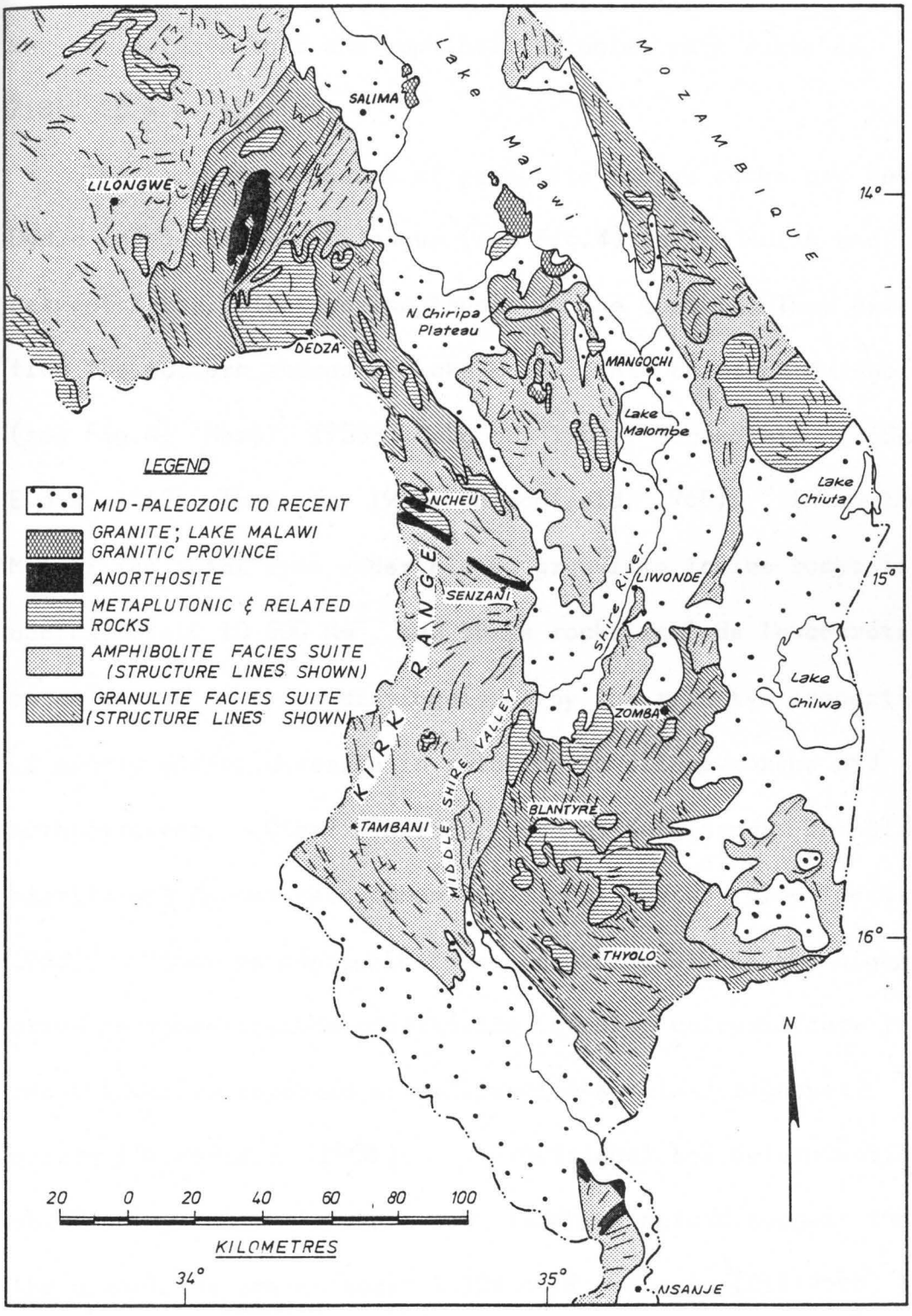


Fig.4. Geology of southern Malawi (after Bloomfield, 1968).

and Bloomfield, 1961). Provisional age determinations obtained by Clifford (1974) with Rb-Sr whole-rock isochron method indicate that the amphibolite facies rock suite is 718 ± 25 m.y. old.

The largest exposures of granulite facies rocks are between Dedza and Salima and Lilongwe (see Fig.4) in the north and between Zomba, Blantyre and Thyolo in the south. They extend from the eastern shores of Lake Malawi into adjacent Mozambique (see Fig.4; Morel, 1958; Habgood, 1959; Bloomfield, 1965a; Evans, 1965; Thatcher, 1968; Bloomfield, 1968). In southern Malawi the total area underlain by granulite facies rocks is approximately 10 500 Km^2, and these rocks include leucocratic to melanocratic types distinguished by the relative proportions of quartz and/or andesine in relation to clinopyroxene and orthopyroxene. Other minerals, such as K-feldspar, hornblende, biotite and garnet are common additional phases (Bloomfield, 1968). Other petrographic types occurring within the higher grade terranes include anorthosite, marble, calc-silicate rock, and khondalite composed of sillimanite-K-feldspar-garnet ± quartz (Bloomfield, 1968). Provisional age determinations obtained by the Rb-Sr whole-rock isochron method suggest that the granulites are at least 1 126 ± 29 m.y. old (Clifford, 1974).

The boundaries between the granulite and the widespread amphibolite facies rocks are generally transitional, and

orthopyroxene-clinopyroxene-plagioclase-hornblende-biotite assemblages are frequently present throughout southern Malawi. In particular these cover an area in excess of 7 000 Km^2 in the southern subprovince of Malawi with important developments in the Middle Shire Valley (Morel, 1958) and between Kasungu and the Dwangwa area (see Fig.3; Kemp, 1974).

Igneous rocks of various ages and emplaced within the metamorphic sequence are common in the southern subprovince of Malawi. In the predominantly gneissic terranes to the north and north-west of Lilongwe, pre-to late-kinematic igneous rocks are represented by frequent granitic orthogneiss, such as the sheared and epidotised Dzalanyama granite (see Fig.3; Thatcher and Walter, 1968). Unmetamorphosed igneous rocks include nepheline syenite at Kasungu and granitic stocks scattered along the shores of Lake Malawi (see Figs.3 and 4; Bloomfield, 1968). In contrast, the granulite facies terranes to the south-east of Lilongwe, particularly those of the Dedza and Zomba-Blantyre regions (see Fig.4), are intruded by the batholithic Perthitic Complexes constituted by syenitic to granitic rocks, often gneissic. In addition, in the south and to the west of Zomba five metamorphosed plutonic Ring Complexes, consisting mainly of syenitic rock, occasionally enclosing an ultramafic core and rimmed by granite, are aligned in an E - W direction (see Fig.5; Bloomfield, 1965b). Small synkinematic

to late-kinematic lenticular bodies of biotitite, serpentinised peridotite and pyroxenite are scattered throughout southern Malawi. Post-tectonic intrusive pegmatite and granite have been dated by the Rb-Sr whole-rock isochron method at 493 ± 16 m.y. ago (Clifford, 1974).

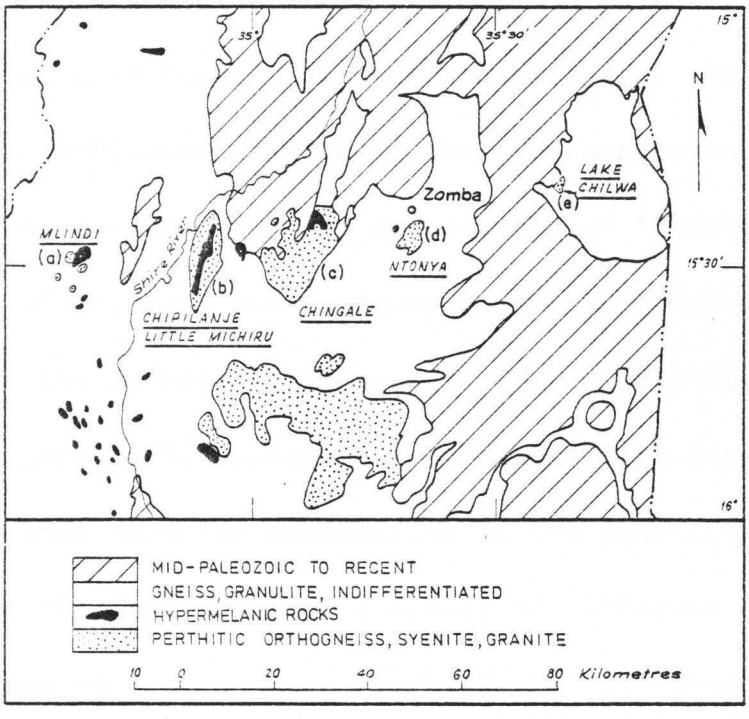


Fig.5. Geology of part of southern Malawi showing five plutonic Ring Complexes indicated by letters (a) to(e)and with their names underlined (after Bloomfield, 1965b).

1.3 Previous Studies on Malawi

The first account of the geology of Malawi was published in 1910 by Andrew and Bailey, who only incidentally mentioned occurrences of granulitic rocks. Systematic studies of the Precambrian Basement Complex began later and were conducted

by the geologists of the Malawi Geological Survey or by private mining groups. In particular, Bloomfield's (1968) memoir on the pre-Karoo geology of Malawi, occupies a place of outstanding importance. In this work Bloomfield summarised most of the information available at that stage and distinguished between supracrustal and infracrustal rocks. The former include not only probable metasediments such as marble and calc-silicate granulite but also banded types characterised by the diagnostic paragenesis orthopyroxene-plagioclase ± clinopyroxene. In contrast, anorthosite and rare occurrences of 'charnockitic' granulites of plutonic aspect found in parts of Malawi were included in the infracrustal group (ibid.). Granulites with coexisting garnet-clinopyroxene-plagioclase were interpreted as transitional from the amphibolite to the granulite facies.

During the past 20 years a number of different models have been proposed to explain the origin of the high-grade rocks occurring in the southern subprovince of Malawi. An essentially volcanosedimentary parentage (basalt, andesite and derivative greywacke) was advocated by Morel (1961b). However, most authors (Cooper and Bloomfield, 1961; Evans, 1965; Bloomfield, 1968; Peters, 1969; Carter and Bennett, 1973) preferred a metasedimentary origin from Na-enriched pelite, semipelite and calcareous marls for the rocks now occurring in the granulite facies. An overall sedimentary origin, with possible interbands

of basalt, was also suggested by Walshaw (1965), Thatcher and Walter (1968), and Dawson and Kirkpatrick (1968), while Holt (1961) envisaged the presence of former pyroclastic bands in the metasedimentary sequence occurring near the southern end of Lake Malawi.

With regard to the relationships between the granulite and the amphibolite facies rocks, Vail (1965a) suggested a basement-cover relationship obscured by recent faulting and the Mozambiquian metamorphism. However, most authors (Holt, 1961; Evans, 1965; Walshaw, 1965; Habgood, et al., 1973; Carter and Bennett, 1973; Thatcher, 1973) considered that the greater part of the amphibolite facies areas of southern Malawi are migmatised and retrograded pre-Mozambiquian granulite facies rocks. In contrast, Morel (1958, 1961a) and Bloomfield (1968) preferred a Mozambiquian age for the metamorphism that produced, in different crustal levels, the amphibolite and the granulite facies suites. The frequent interbanding of these rocks was attributed by the latter author to retrogressive metamorphism. In the Mchinji and Dwangwa areas (see Fig.3), Carter and Bennett (1973), Kemp (1974), and Ramsay and Ridgway (1977) advanced the hypothesis that an ancient basement, constituted by supracrustal rocks, was raised twice to the granulite facies. It first formed sillimanite-cordierite-garnet parageneses and

then, after an episodic retrogression to the amphibolite facies, produced orthopyroxene-bearing assemblages.

The anorthosite and certain bands of amphibolite were considered to be of igneous origin by Bloomfield (1968, p.60), Thatcher (1968) and Walter (1972b). A deep-seated magmatic crystallisation was proposed by Dawson and Kirkpatrick (1968) for certain dioritic-tonalitic charnockites from the northern Chiripa Plateau area (see Fig.4), while granulites occurring north of Mchinji (see Fig.3) were considered by Brewer et al. (1979) as unmetamorphosed hypersthene-bearing plutonic igneous rocks.

Considering the suite of perthitic rocks and the Ring-Complexes, Morel (1961b) suggested that these were consanguineous with the basalt and andesite that were later metamorphosed to the granulite facies. This view was not shared by later authors who considered the perthite-rich gneissic rocks as formed by a late-kinematic potassic metasomatism and ensuing migmatisation of pre-existing granulites and gneisses (Evans, 1965; Bloomfield, 1965b, 1968, 1970; Walshaw, 1965; Garson and Walshaw, 1969; Habgood et al., 1973; Carter and Bennett, 1973).

1.4 Aim of the Present Study, Methods Employed and Nomenclature

Granulite facies terranes occur in most orogenic belts of Africa and they represent therefore a major feature in the

continent evolution. A detailed study of these different suites could therefore provide a unique insight into the evolution of the African lower crust at different stages during its past 3 000 m.y. (Clifford, 1974). Since the continent represents almost 20 per cent of the earth's land surface it obviously constitutes the corner-stone of any reconstruction of the ancient Gondwanaland. Malawi was chosen because of the close areal association of granulite and amphibolite facies rocks. The high-grade suite occurring in the southern subprovince is also one of the largest and best exposed in the entire African continent. In fact, the total area underlain by pyroxene-bearing rocks is about 18 000 Km^2 and this exceeds the 13 000 Km^2 of the Lulua massif in the Kasai ancient nucleus of Zaire (Delhal, 1957, 1963), and the 15 000 Km^2 of the Bouca massif in the Central African Republic (Wacrenier and Wolf, 1965). It is, however, smaller than the Tanezrouft-Adrar zone in Hoggar, Algeria, where granulite facies rocks occupy some 34 000 Km^2 (Caby, 1970).

The material on which this investigation is based was largely collected by the author in 1974, supplemented by samples collected by Professor T.N.Clifford on previous visits to the area, and, by specimens kindly provided by the Malawi Geological Survey in Zomba. The locality maps for these specimens are found in a pocket at the back of this thesis (Maps 1 to 4).

In all, over 327 thin sections were obtained from 519 specimens and their complete list is presented in Appendices I-1, to 1-3.

Full silicate analyses were conducted on 74 samples, for 61 of which Rb, Sr, Y, Zr, and Nb were also determined and the data integrated with published information. Evans (1965) and especially Bloomfield (1965b, 1968) reported over 60 full silicate analyses plus a number of trace elements determinations for infracrustal and supracrustal rocks - mainly gneisses and granulites - of pre-Karoo age.

In addition, a total of 152 minerals, mainly coexisting orthopyroxene and clinopyroxene, garnet and hornblende, have been quantitatively analysed by electron-microprobe.

Finally, in order to clarify the time relationships between rocks of different metamorphic grade, a suite of samples from a carefully selected area was submitted for zircon U-Pb and whole-rock Rb-Sr isotopic age determinations.

The nomenclature of the orthopyroxene-bearing rocks is at present rather confused, and attempts to systematise the use of petrographic names were made by Pichamuthu (1969), Behr et al. (1971), Winkler and Sen (1973) and Streckeisen (1976). The more general term 'granulite' is used in this thesis for metamorphic rocks, of appropriate mineralogy, that crystallised in the granulite facies; while the terms like charnockite, norite etc. were only used for orthopyroxene-bearing intrusive rocks

crystallised primarily under granulite facies conditions (see Streckeisen, 1976). In the doubtful cases terms like charnockitic granulite have been adopted.

In accordance with studies by Green and Ringwood (1967) granulite facies conditions are indicated not only by the diagnostic coexistence of orthopyroxene with plagioclase but also of almandine-rich garnet with clinopyroxene, plagioclase and quartz in rocks of appropriate composition. Leucocratic, mesocratic and melanocratic gneisses and granulites define rocks with increasing proportions of ferro-magnesian minerals; and hypermelanic rocks are entirely constituted by pyroxene, hornblende and/or biotite. Following Winkler (1974) the term granoblastite applies to pyroxene-free rocks devoid of hydrous minerals, and the descriptive names for rocks of migmatitic aspect have been taken from Mehnert (1968).

Finally, a map of the metamorphic assemblages recorded in the literature, modified by the new petrographic data, is found in a pocket at the back of the thesis (Map 5).

CHAPTER 2. FIELD AND PETROGRAPHIC CHARACTERS OF MALAWI METAMORPHIC ROCKS AND PLUTONIC COMPLEXES

2.1 Introduction

In this chapter the field and petrographic characters, and interrelationships of granulites, amphibolite facies and amphibolite to granulite facies transitional rocks from southern Malawi have been considered. The principal areas of granulite facies and associated rocks extend south-east of Dedza and north-west of Namwera (see Fig.6) and between Blantyre and Zomba (see Fig.7). The following petrographic types have been identified: melanocratic, mesocratic and leucocratic orthopyroxene or garnet-bearing rocks, garnet granoblastite, calc-silicate and quartzo-feldspathic granoblastite and anorthosite. The amphibolite facies rocks are best represented north and west of Lilongwe, in the Balaka-Liwonde and the Kirk Range areas (see Figs.6 and 7): they lend themselves to a subdivision in amphibolite, mesocratic gneisses, calc-silicate rocks, pelites, quartzo-feldspathic and feldspathic rocks and aegirine gneiss.

Of particular interest are the rocks transitional between the amphibolite and the granulite facies, best represented in the area between Ncheu and Dedza (see Fig.6) and in the Middle Shire Valley (see Fig.7); and this thesis is mainly concerned

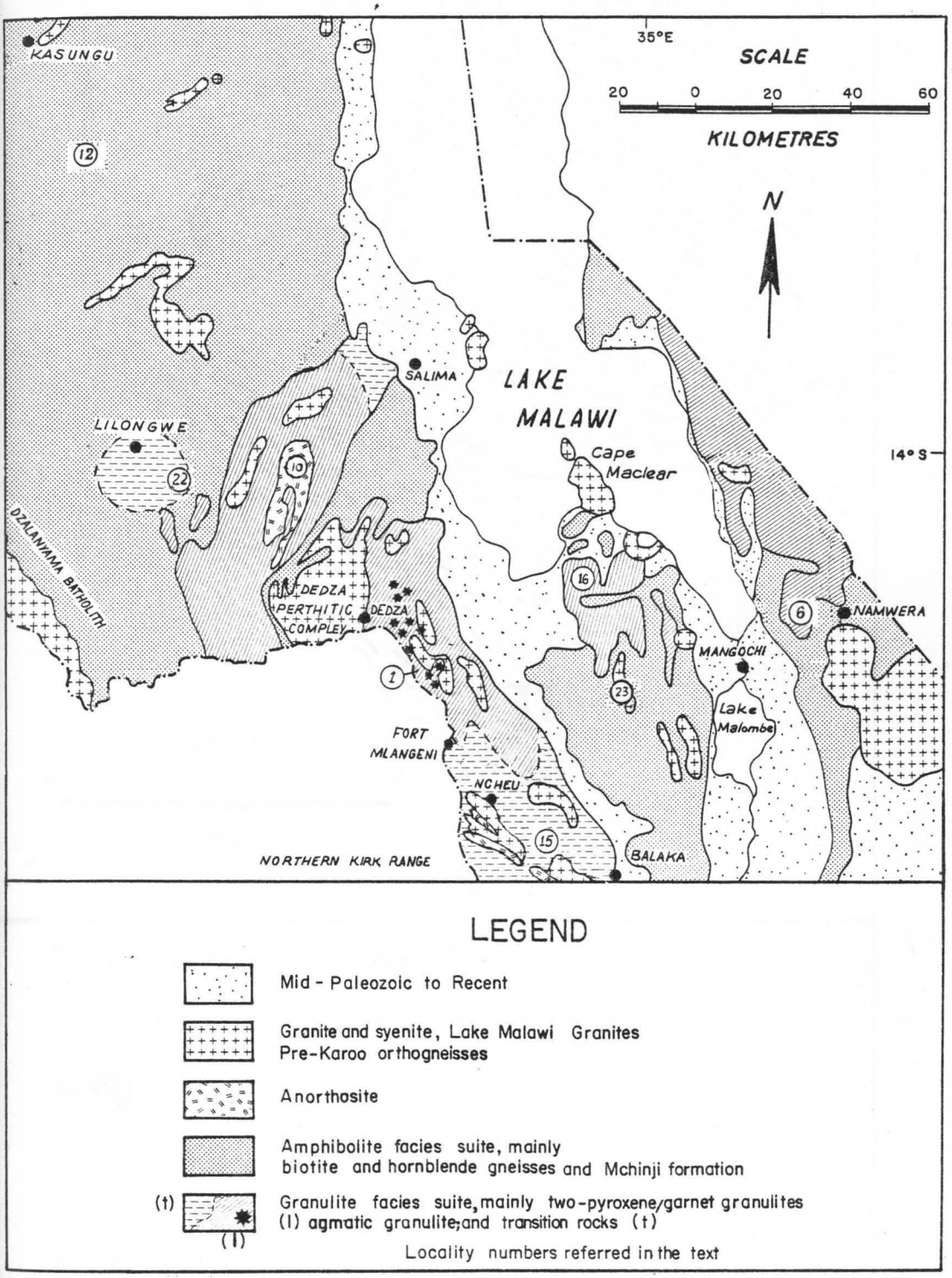


Fig.6. Locality map for southern and central Malawi (modified after Bloomfield, 1968).

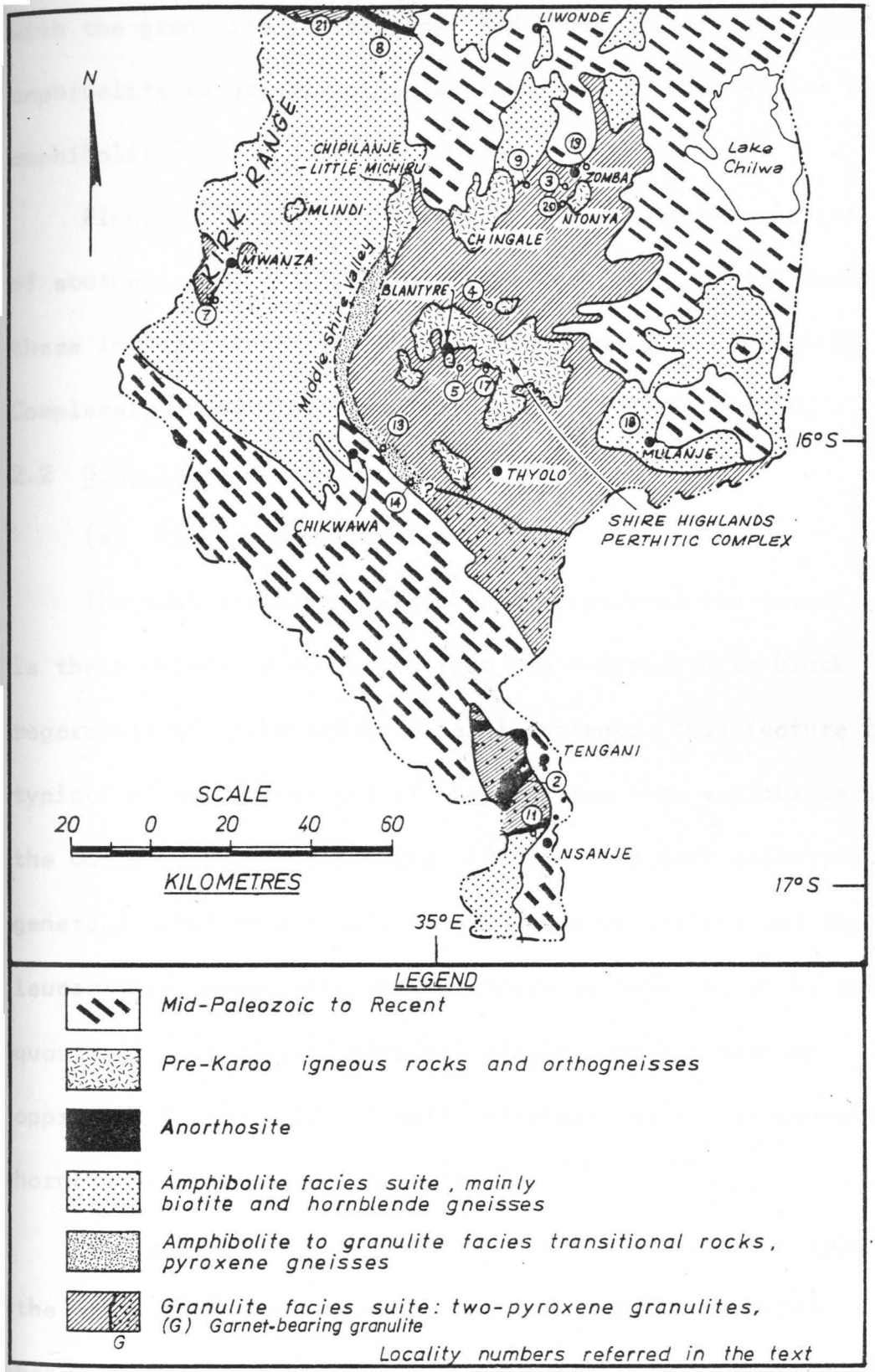


Fig.7. Locality map for southern Malawi (modified after Bloomfield, 1968; Morel, 1958).

with the granulite facies rocks and those transitional from the amphibolite to granulite facies, whilst the interest for the amphibolite facies suite is subordinate.

Finally, and for completeness, the main pre-Karoo intrusives of southern and central Malawi have been very briefly considered and these include ultramafic bodies, Ring Complexes, Perthitic Complexes, granite and granitoid rocks of various ages.

2.2 Granulites

(a) Field characteristics

The most striking field characteristic of the granulites is their colour which varies from light-greenish to black regardless of their felsic mineral content; this feature is typical of such rocks and of charnockites from various parts of the world (Oliver and Schultz, 1968). The dark colour is generally lost as a result of prolonged weathering and the terms leucocratic, mesocratic and melanocratic refer to rocks rich in quartz, intermediate (andesine) plagioclase but with an appreciable proportion of mafic minerals, or in pyroxenes ± hornblende and biotite respectively.

The granulites are subdivided into the following types on the basis of their mesoscopic and megascopic structures: banded, massive, agmatic, 'anatectic' and plutonic. Of these types, the banded granulites predominate especially in outcrops within the townships of Ncheu and Zomba (see Figs. 6 and 7)

and they are usually composed of very monotonous leucocratic and melanocratic layers ranging in thickness from a few millimetres to a few decimetres. In the Zomba area (see Fig. 7) individual bands may be continuous over a few hundred metres and minor, generally similar folds are present but are not frequent.

The massive granulites are very homogeneous and generally lack any kind of banding; and apart from a mineral lineation, no deformational features are generally visible. The agmatic or 'migmatitic' granulites are well developed to the south-east of Dedza (see Fig.6) where they occupy an area of at least ± 250 Km^2. On weathered surfaces the melanocratic elements within a mesocratic matrix appear like armoured inclusions being mantled by a reddish-coloured, fine-grained, 1 to 2 cm wide rim rich in pyroxenes. The shape of the inclusions is often angular and/or elongated, and in places they appear to maintain an original banding. In some cases the regional deformation has only partly obliterated former plagioclase augen. In other cases the banded granulites present nebulitic, stromatic-like structures which are characteristic of anatectic rocks (Mehnert, 1968).

Finally, the plutonic granulites (from melanocratic to leucocratic) exhibit intrusive and discordant contacts within the surrounding rocks like south-east of Dedza where intrusive

breccia-like structures in chevron-folded granulites are occasionally preserved (see locality 1, Fig.6). Discordant dykes of granulite also occur in the Tengani area (see Locality 2, Fig.7; Plate 1), near Zomba (see Locality 3, Fig.7) and at Njuli quarry (see Locality 4, Fig.7).

(b) Petrography

The textures of the Malawi granulites are all rather similar, mainly granoblastic, equigranular, often with straight, polygonal grain boundaries and triple-point junctions. Equigranular and seriate textures predominate in melanocratic types. In leucocratic rocks, quartz and sometimes plagioclase grains have interlobate to amoeboid boundaries, and xenoblastic, elongated quartz blebs tend to define a poor planar fabric. The quartz frequently resembles that of a late crystallisate, and in nearly all samples the pyroxenes have grain-boundary textures indicative of secondary growth with respect to quartz and feldspar.

In this chapter only the more typical or interesting assemblages have been recorded; however, the constituent and accessory minerals observed in the thin sections investigated are tabulated in Appendices II-1 and II-2. Petrographic descriptions of selected rocks are given in Appendix II-3.

The melanocratic granulites are best developed in the Zomba area (see Fig.7) and are characterised by the coexistence of orthopyroxene-clinopyroxene-andesine ± hornblende and biotite.

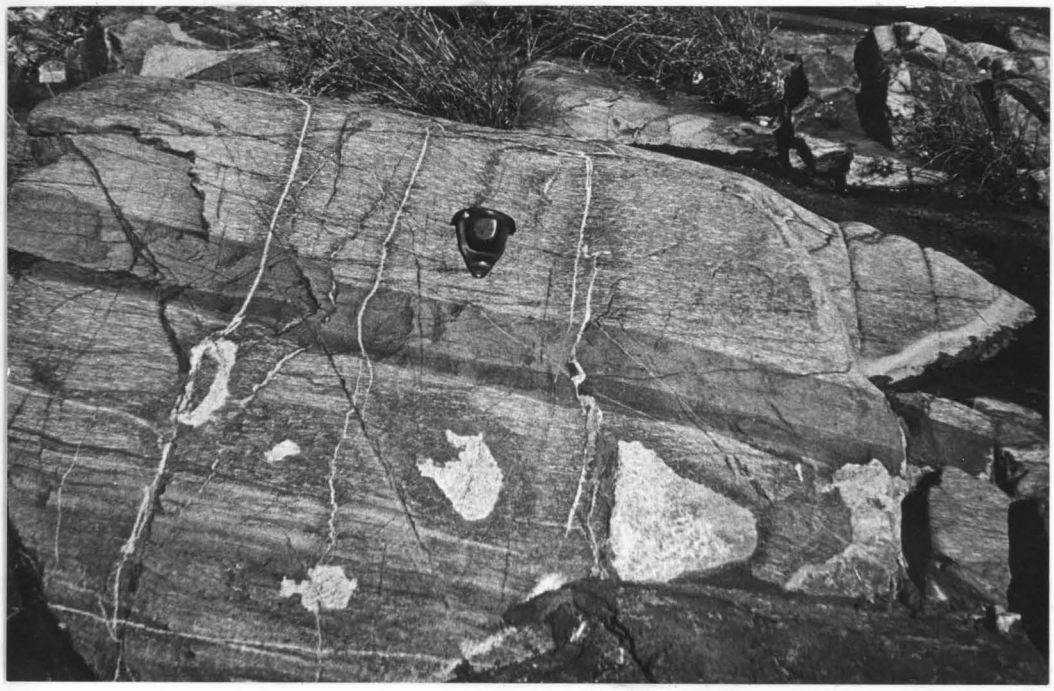


Plate 1. Discordant metadolerite in mesocratic garnet-clinopyroxene granulite with dark (hornblende-rich) haloes rimming leucocratic veins. Tengani, Nsanje (see locality 132, Map 1)

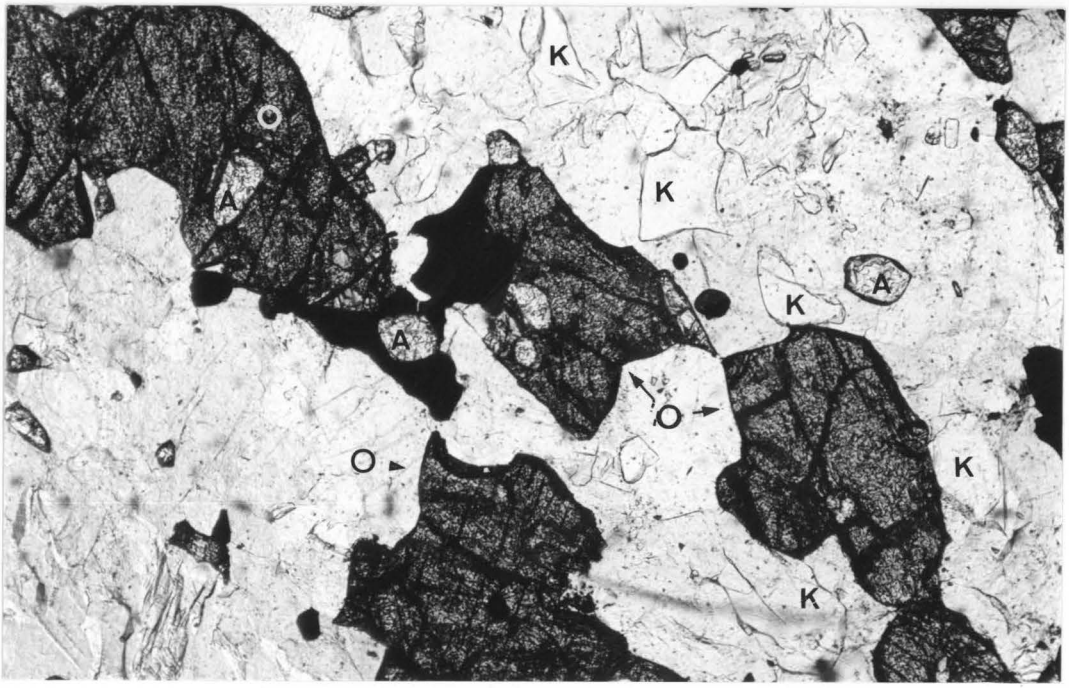


Plate 2. Mesocratic granulite, rich in orthopyroxene(o), perthite (K), and apatite (A). X50, Ncheu, (see locality 441, Map 3).

Except for some rare occurrences (see Locality 405, Map 2) in which orthopyroxene is the sole pyroxene, in most cases diopsidic pyroxene is much more common than the poorly pleochroic orthopyroxene. Feldspar has a rather constant composition, generally in the range An_{35} - An_{45}, and constitutes between 35 and 50 per cent of the mode; calcic oligoclase and labradorite are much rarer. The minor constituents include quartz, K-feldspar, and rare hercynite; while accessory components are ilmenite, magnetite, apatite, zircon and pyrite. In contrast the massive melanocratic granulites which are particularly well developed in the Njuli quarry near Blantyre (see Locality 4, Fig.7), are characterised by substantial amounts of perthitic K-feldspar and an unusual abundance of apatite and opaque minerals.

The mesocratic granulites are common both in the Zomba area and in the region west of Blantyre (see Fig.7). They are characterised by a banded, or less commonly massive structure and by the following mineral assemblage: antiperthitic andesine (forming up to 60 per cent of the mode) -orthopyroxene ±clinopyroxene, hornblende, biotite, quartz; apatite, ilmenite, magnetite ± zircon are the common accessories. Exceptions to this general mineralogy were found in the region south-east of Dedza (see Locality 429, Map 3) where the mesocratic granulites contain abundant graphite, pyrite, pyrrhotite, and little chalcopyrite. Moreover, certain massive mesocratic

granulites are characterised by the presence of perthite, for example: (a) the perthitic K-feldspar-oligoclase-orthopyroxene-clinopyroxene-quartz ± hornblende±biotite parageneses from the Soche quarry near Blantyre (see Locality 5, Fig.7) and from Ncheu township (see Fig.6 and Plate 2); (b) a perthite granulite with minor quartz, oligoclase and orthopyroxene from the area between Dedza and Ncheu (see Locality 432, Map 3) and (c) the perthite-oligoclase-augite-quartz ± orthopyroxene rocks from the Namwera area east of Mangoche (see Locality 6, Fig.6).

Leucocratic granulites with a banded structure are common in the Zomba area and between Blantyre and the Middle Shire Valley (see Fig.7). They are characterised by the assemblage: antiperthitic oligoclase/andesine-quartz-orthopyroxene ± perthitic K-feldspar ± clinopyroxene ± biotite ± garnet; accessory constituents in these rocks are rare but include ilmenite, magnetite, apatite and rounded zircons. For some of these rocks the microtextures are characterised by frequent myrmekitic intergrowths of quartz and sodic feldspar adjacent to K-feldspar, which appears to replace plagioclase. In contrast, most massive leucocratic granulites are characterised by the assemblage: perthite/mesoperthite-quartz-orthopyroxene ± oligoclase ± clinopyroxene ± hornblende ± biotite (see Plate 3), particularly those from the area north-west of Namwera (see Locality 6, Fig.6). In these rocks clinopyroxene lamellae are

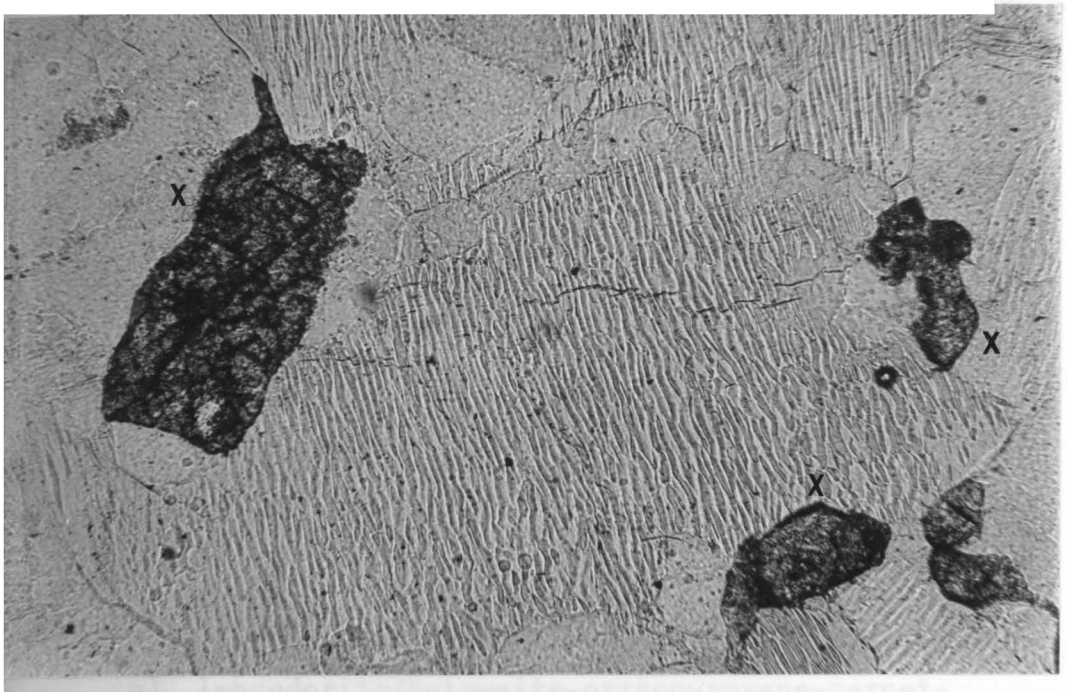


Plate 3. Leucocratic granulite rich in mesoperthite; note stable xenoblastic orthopyroxene (x). X120, Ncheu (see Locality 458, Map 3).

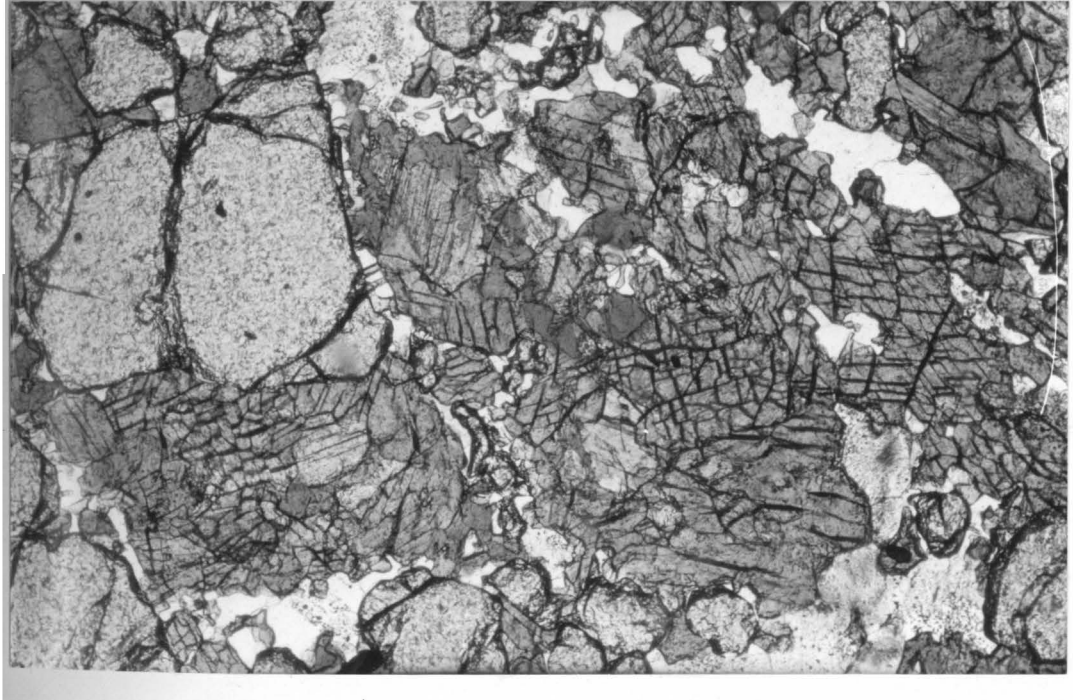


Plate 4. Melanocratic garnet-clinopyroxene-hornblende granulite. X50, Tengani area (see Locality 132, Map 1).

occasionally included in an igneous-like orthopyroxene and metamictic allanite is a common accessory. K-feldspar is found occasionally rimmed by myrmekitic sodic plagioclase in a charnockitic granulite dyke at Njuli quarry, near Blantyre (see Locality 4, Fig.7).

The garnet-granulites are an heterogeneous lithological group characterised by the following mineral assemblages:

(a) oligoclase/andesine-orthopyroxene-garnet-quartz ±biotite ± K-feldspar,

(b) labradorite/bytownite-orthopyroxene-garnet-scapolite-quartz,

(c) garnet-clinopyroxene ± hornblende ± quartz ± plagioclase ± biotite ± K-feldspar ± orthopyroxene ± scapolite,

(d) quartz-oligoclase/andesine-garnet-clinopyroxene ± hornblende ± perthitic microcline,

(e) quartz-oligoclase-kyanite-garnet ± sillimanite ± biotite.

Of these assemblages, (a) and (b) are generally interbanded with two-pyroxene granulites e.g. at Fort Mlangeni and Zomba (see Figs.6 and 7). Assemblages (c) and (d) on the contrary tend to have a regional development, mainly in the northern Kirk Range and Tengani areas (see Figs. 6 and 7; Plate 4). In the first region, rocks with assemblages (e) are locally interbanded with garnet granulites having assemblage (c).

Assemblages (c) and (d) are also scattered among the amphibolite facies terranes of the western Middle Shire Valley, at Mwanza (see Fig.7) and at Tambani (see Locality 7, Fig.7); and in central Malawi they occasionally occur near Lilongwe (Fig.6) and 30-50 km north-west of Kasungu (see Map 5). Assemblages (c) and (d) are also present in the poorly exposed terranes of the Thyolo region (see Fig.7), where both orthopyroxene-bearing granulite and amphibolite facies rocks have been described (Habgood et al., 1973). Assemblage (c) characterises melanocratic to mesocratic rocks with an (antiperthitic) plagioclase and frequent orthopyroxene. This mineral coexists with garnet only in the Fort Mlangeni-Ncheu area (see Fig.6), while elsewhere they appear to be in mutual disequilibrium. Leucocratic garnet granulites with assemblage (d) occurring in the Kirk Range are deficient in K-feldspar and have apatite and allanite as accessory constituents. In contrast, perthitic K-feldspar is a major constituent in massive granulites from Thyolo (see Fig.7; Locality 128, Map 1) and Mwanza (see Fig.7) where ilmenite forms symplectitic intergrowths with clinopyroxene (see Locality 358, Map 2). Finally, Bloomfield and Garson (1965, p.55) described the occurrence of a granulite characterised by about 70 per cent modal oligoclase with minor orthoclase, garnet and hornblende to the north-west of Senzani (see Locality 8, Fig.7).

Amongst the other rock types in the granulite facies

terranes, calc-silicate granoblastite is common west of Blantyre where it is characterised by the assemblage scapolite-clinopyroxene-labradorite-quartz ± sphene±hornblende±calcite±garnet±phlogopite. Wollastonite was mentioned in a marble from the important Changalume quarry (Bloomfield, 1968, p.129; see Locality 9, Fig.7). In addition, quartzo-feldspathic granoblastite is common north-east of Zomba and forms ridges up to a few kilometres long. It is characterised by a sugary texture and a mesoperthite-quartz-sodic oligoclase mineral assemblage; alkali feldspar always exceeds quartz and rare accessories are magnetite, hematite, zircon and allanite.

Finally, the granulite terranes of southern Malawi contain important bodies of <u>anorthosite.</u> Although the term anorthosite is generally employed for rocks with a plagioclase content of 95 per cent, it is used here for rocks with up to 15 per cent of mafic constituents: generally orthopyroxene, clinopyroxene hornblende, garnet and biotite. The largest body of anorthosite in Malawi is a refolded sill-like mass of 250 km^2 near the Linthipe river, east of Lilongwe (see Locality 10, Fig.6). Other occurrences in the south and south-east of Ncheu form long bands extended for a combined length of about 50 km (see Figs. 6 and 7), while west of Tengani (see Fig.7) strongly refolded anorthosite underlies an area of about 60 km^2. The plagioclase composition in this puzzling group of rocks ranges from

labradorite (An_{70}) at Linthipe to andesine/oligoclase at Tengani. In the latter locality and in the Ncheu area quartz and perthite are appreciable minor constituents (Bloomfield, 1968, p.136) while garnet is occasionally present; opaque minerals, apatite, graphite and zircon are among the accessory constituents. In addition, xenoliths of anorthosite occur in a dyke of charnockitic granulite at Njuli quarry, Blantyre (see Locality 4, Fig.7). The anorthosite is characterised by appreciable amounts of quartz and perthite interstitial between frequently hypidiomorphic and antiperthitic oligoclase (An_{28}); orthopyroxene and biotite are also present. The plagioclase is often dusted by very small inclusions of opaque lamellae, fluid and carbonate. The suite of accessories includes ilmenite, magnetite, idiomorphic apatite, carbonate (primary), allanite and zircon. Wide rims of quartz-plagioclase myrmekite are developed at the contact with the enclosing charnockitic perthite granulite.

2.3 Amphibolite Facies Rocks

The amphibolite facies suite is well developed both in southern and central Malawi (see Figs 6 and 7) and comprises a wide range of lithologies (Bloomfield, 1968); a brief general description will therefore suffice. Among the common lithological types, amphibolite is well developed in the Middle Shire, in the Kirk Range and elsewhere in central Malawi (ibid., p.67), and its mineral assemblage is generally hornblende-oligoclase-

andesine ± garnet±quartz±clinopyroxene±biotite. Relicts of igneous minerals in rocks previously referred to as metagabbro are sometimes preserved (ibid., p.66). Mesocratic gneisses, generally described as 'semipelitic' gneisses in the literature (ibid., p.29), are common in the Middle Shire Valley region, and in the south-east Kirk Range. These rocks have the assemblages: oligoclase/andesine-biotite ± quartz±hornblende or clinopyroxene-K-feldspar-epidote-garnet; magnetite, sphene, apatite and zircon are accessory minerals. Calc-silicate rocks are quite frequent in the Nsanje area, in the Middle Shire Valley region and also in central Malawi (ibid., pp.35-37; and pp.129-130) and are characterised by the assemblage labradorite-clinopyroxene ± calcite ± hornblende ± garnet ± epidote ± scapolite; gradation toward garnetite may also occur. Pelitic gneisses are more widely developed in the north-west Kirk Range (ibid., pp.32-33; and pp.126-127), where they are characterised by the assemblage: quartz-muscovite-albite-oligoclase ± kyanite ± sillimanite ± K-feldspar. Biotite ± garnet predominate in some bands, while staurolite is a rarer minor constituent. Pelitic schists particularly enriched in graphite, pyrite and pyrrhotite occur in the region south-west of Lilongwe in central Malawi (see Fig. 6; ibid., p.35), while an unusual 'khondalite' rock with the assemblage mesoperthitic feldspar-garnet-sillimanite-hercynite ±oligoclase, is interbanded with calc-silicate and biotite

(-graphite) gneisses near Nsanje (see Locality 11, Fig.7). Quartzo-feldspathic rock, generally referred to as psammite in the literature occurs in narrow lenses within the banded gneissic sequence (ibid., p.31) and its characteristic mineral assemblage is oligoclase/andesine-K-feldspar-quartz. Occasional minor constituents are biotite, diopside, hornblende, muscovite and kyanite whilst opaque minerals, apatite, rutile, sphene and allanite are the common accessory constituents. Feldspathic rocks of various types occur scattered within the gneisses of the northern Kirk Range (see Fig.7) and have the following mineral assemblages (Bloomfield and Garson, 1965, pp.44 and 55ff.):

(a) oligoclase (An_{14}) - hornblende-clinopyroxene-rutile,

(b) oligoclase/andesine-K-feldspar ± biotite±muscovite±garnet,

(c) oligoclase (An_{25}) ± quartz ± microcline,

(d) albite ± quartz,

(e) microcline-orthoclase-orthoclase/microperthite-oligoclase.

In assemblages (a), (b) and (c) plagioclase is the main constituent, ranging from 70 to 90 per cent of the mode which possibly suggests anorthositic affinities. Assemblage (d) is an albitite and in (e) microcline and orthoclase are the essential components. Aegirine gneiss, ranging from mesocratic to leucocratic, is common in parts of central Malawi (see Locality 12, Fig.6; Bloomfield, 1967) with the following mineral assemblage: quartz-albite-microcline-aegirine ±riebeckite.

Accessory constituents form up to 20 per cent of the mode, and include magnetite, zircon, leucoxene, allanite, monazite, sphalerite and sometimes pyrochlore.

2.4 Amphibolite to Granulite Facies Transitional Rocks

(a) General characters and field relationships

Granulite and amphibolite facies terranes are gradational in a number of areas throughout south and central Malawi with frequent interbanding of granulites and gneisses (Evans, 1965, p.26). In the present study emphasis has particularly been placed on the Middle Shire Valley transition zone where the boundary between amphibolite facies gneisses in the west and granulites in the east (the orthopyroxene 'isograde') transgresses recognisable metasedimentary horizons (Morel, 1958; 1961a; see Fig.8).

During the present study it was found that the transitional types of the Middle Shire were often barely distinguishable from typical granulites in colour and appearance. In other cases these transitional rocks have a strong superficial resemblance to the regional gneisses for their light colour and the widespread anatectic, migmatitic and nebulitic structures (see Plates 5 and 6). The presence of orthopyroxene in these lithotypes may only be established under the microscope. Significant observations were made in the present study at the Wakurumadzi River Bridge, about 12 km south-east of Mwanza

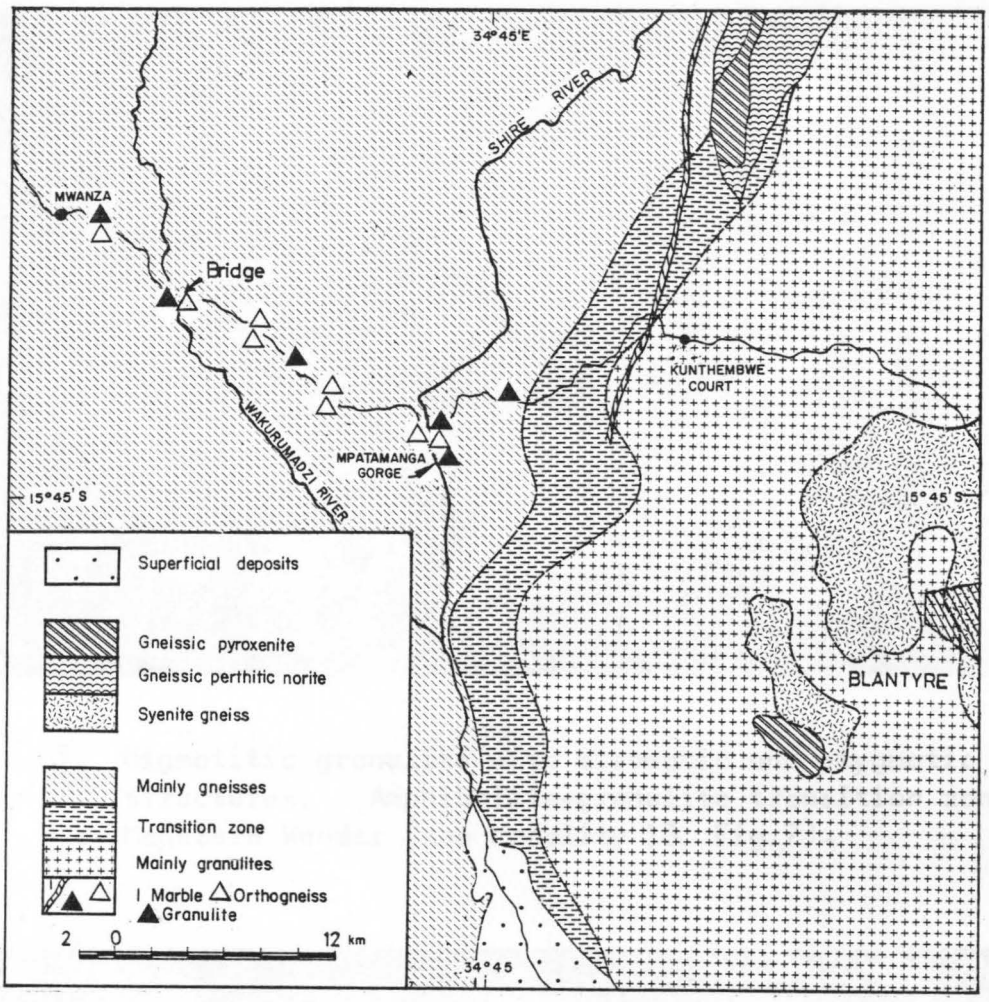


Fig.8. Geology of the Middle Shire area (after Morel, 1961a).

along the Blantyre-Mwanza Road (see Fig.8). In this locality a typical charnockitic granulite with melanocratic xenoliths, shown in Plates 7(a) and (b), crops out on the west bank of the river less than 50 metres from a very similar, but light coloured orthogneiss; these granitoid rocks, with or without orthopyroxene, are rather common in the area (see Fig.8). With the exception of the orthogneiss, rocks similar to those observed along the Blantyre-Mwanza Road (see Fig.8) were also found in the south-east extension of the Middle Shire

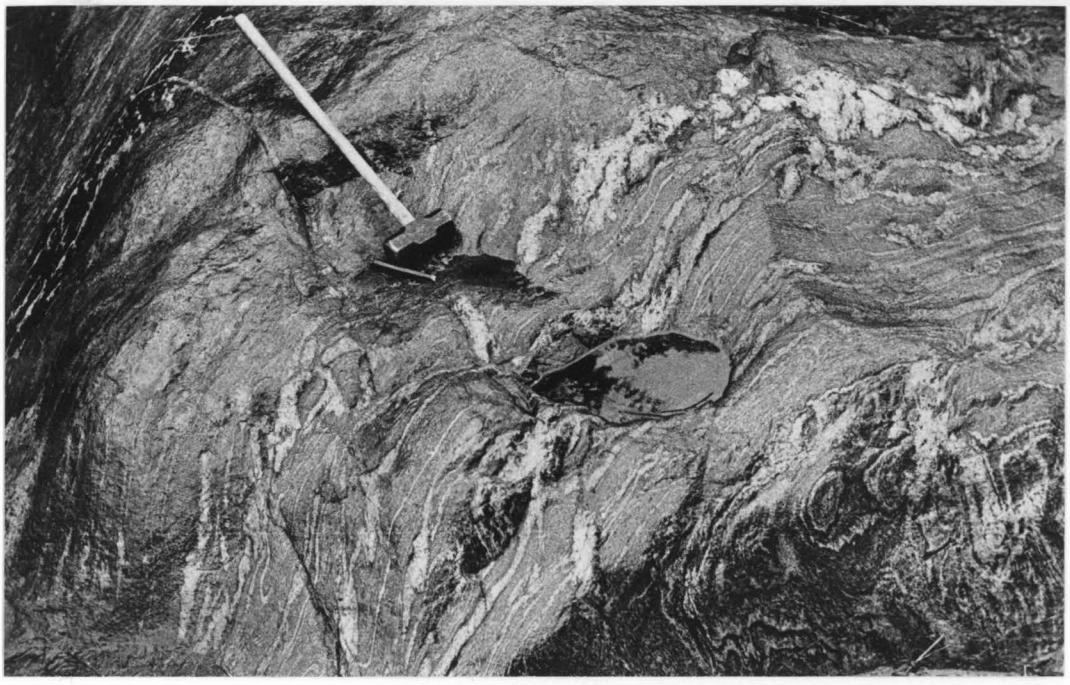
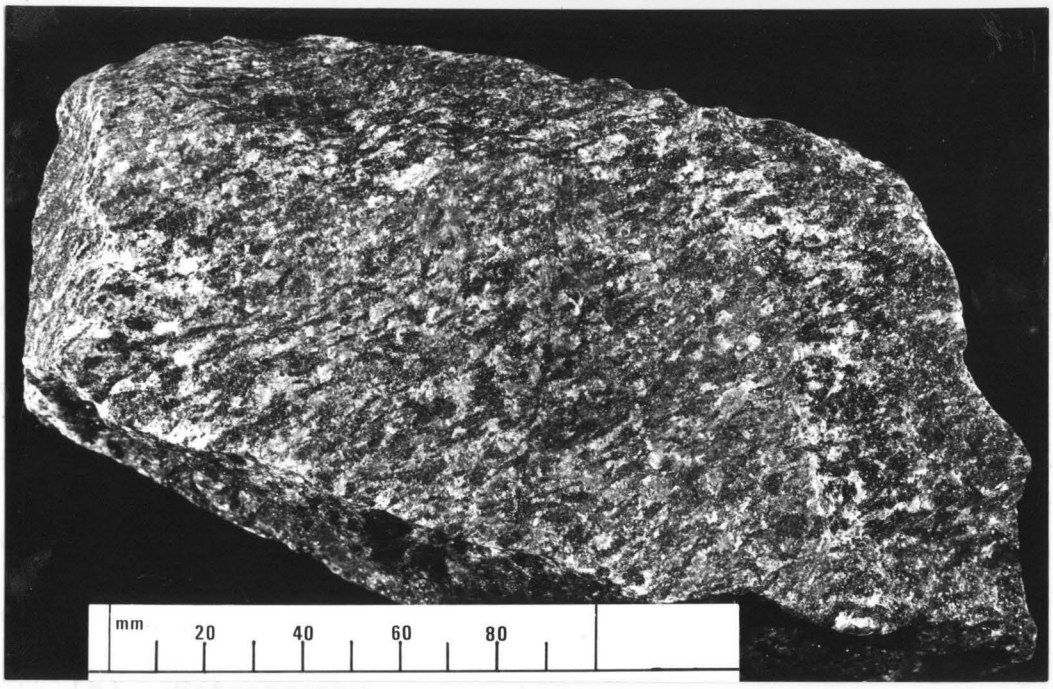


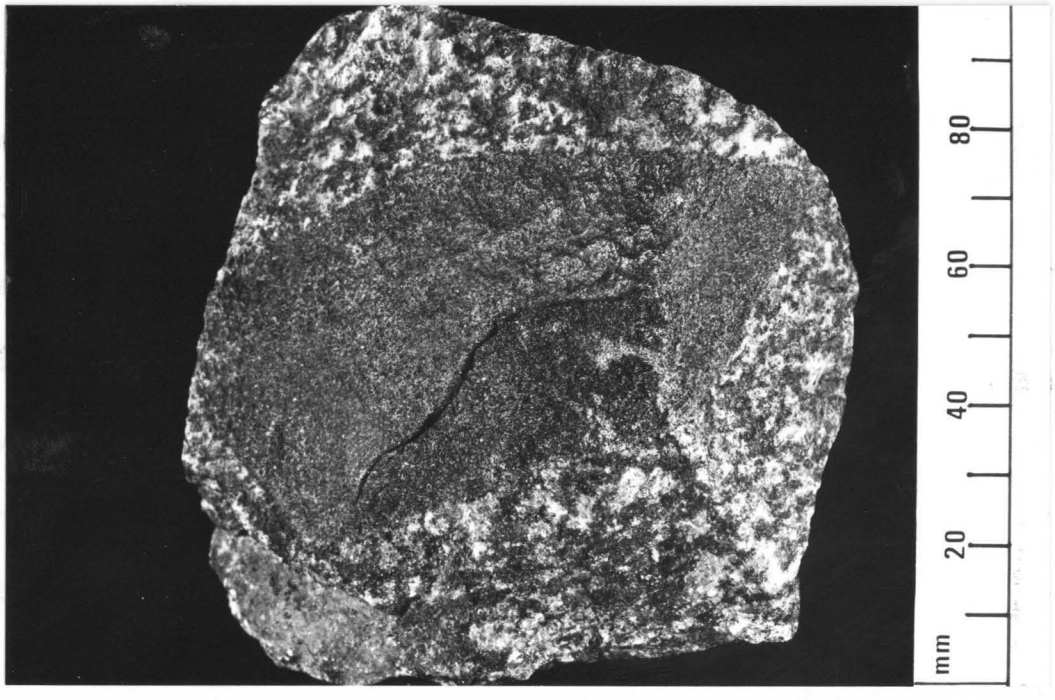
Plate 5. Migmatitic granulite with stromatic and ptygmatic structures. Amphibolite-granulite transition zone, Maperera Wander (see Locality 13, Fig.7).



Plate 6. Nebulitic granulite with melanocratic amphibolite bands. Amphibolite-granulite transition zone (see Mpatamanga Gorge, Fig.8: locality 331, Map 2).



(a)



(b)

Plate 7. (a). Charnockitic hornblende-biotite granulite. Amphibolite-granulite transition zone (see Wakurumadzi River Bridge, Fig.8, locality 351, Map 2).

(b). Charnockitic hornblende-biotite granulite with melanocratic xenolith. Same locality as Plate 14(a).

Valley transition zone, near Chikwawa (see Localities 13 and 14, Fig.7). In the north, near Nsipe (see Locality 15, Fig. 6), garnet-biotite granulites are interbanded with garnet-biotite gneisses which are sporadically cut by thin veins of greenish feldspar and orthopyroxene porphyroblasts (?) up to a few centimetres long. Finally, south of Cape Maclear (see Locality 16, Fig.6) anatectic quartzo-feldspathic garnet-biotite gneisses occur adjacent to biotite-rich granulites.

(b) Petrography

The basement suite in the Middle Shire Valley transition zone includes mainly melanocratic, mesocratic and leucocratic types with rare pelitic schist, quartzo-feldspathic rock and calc-silicate granulite. In these lithologic types the textures are generally granoblastic, equigranular to seriate, with interlobate, curved mineral boundaries and frequent myrmekites. Melanocratic rocks, grading to amphibolite, are characterised by an hornblende-oligoclase ± orthopyroxene ± clinopyroxene±spinel mineral assemblage. The mesocratic and leucocratic rocks share the typical colour and appearance of granulites and have the assemblage oligoclase-hornblende-quartz-biotite-K-feldspar ± orthopyroxene±clinopyroxene. This mineral assemblage is also characteristic of the charnockitic granulites and associated granitoid gneisses. Where leucocratic and melanocratic rocks are associated (see

Plate 6) orthopyroxene is absent or less frequent in the amphibolite interbands. A pelitic schist (see Locality 365, Map 2) interbanded with melanocratic rocks presents a unique microcline-quartz-muscovite-biotite-garnet assemblage.

Calc-silicate granulites are similar to those found in the granulite facies terranes except for presence of more abundant sphene.

2.5 Relationships between the Amphibolite and the Granulite Facies

There has been considerable debate during the past twenty years about the relationships between the amphibolite and the granulite facies assemblages as it was mentioned in the Introduction (see p.3). Yet, Holt (1961), Walshaw (1965) and Evans (1965) suggested that the gneisses generally represent granulites affected by retrograde Mozambiquian metamorphism. In contrast, Morel (1958, 1961a) asserted the view of a prograde metamorphism from the amphibolite to the granulite facies. Finally, Bloomfield (1968) proposed that the majority of higher- and lower-grade suites represent different structural levels in the same metamorphic event, the latter part of which was perhaps hydrous and retrogressive. In this work, a very careful field and petrographic investigation of critical outcrops, particularly those in transitional areas described in 2.4 (a) and (b), revealed the existence of simple geometric relationships between mineral assemblages of the amphibolite and granulite

facies. Such relationships are referred to here as Type I, II and III geometries. In prograde development geometry of Type I, a two-pyroxene-plagioclase mineral assemblage armours an amphibolite nucleus (see Plate 8). The alternative retrograde development geometry of Type I, at the interface between melanocratic pyroxene-bearing rocks and enclosing leucocratic assemblages characterised by a hornblende-biotite-rich paragenesis had not been previously observed in southern Malawi. The Type II geometry includes prograde and retrograde changes induced by cross-cutting veins of a different metamorphic grade from that of the wall-rocks. An example of prograde metamorphism is provided by Plate 9 in which an orthopyroxene-bearing vein cuts an amphibolite. In both Types I and II prograde geometries the rims and veins have generally sharp interfaces which may be characterised by changes in mineral size (see Plate 8) or by small pyroxenes growing at the expense of larger hornblendes (see Plate 10). In Type III geometry the replacement of minerals by others takes place without the strict control exerted in the Types I and II by physical or lithological discontinuities. Examples of such prograde and retrograde relationships are shown in Plates 11 and 12 respectively.

Morel's (1961a) amphibolite to granulite facies transition zone provides frequent well-developed examples of prograde Type I and Type II geometries, also visible on outcrop surfaces,

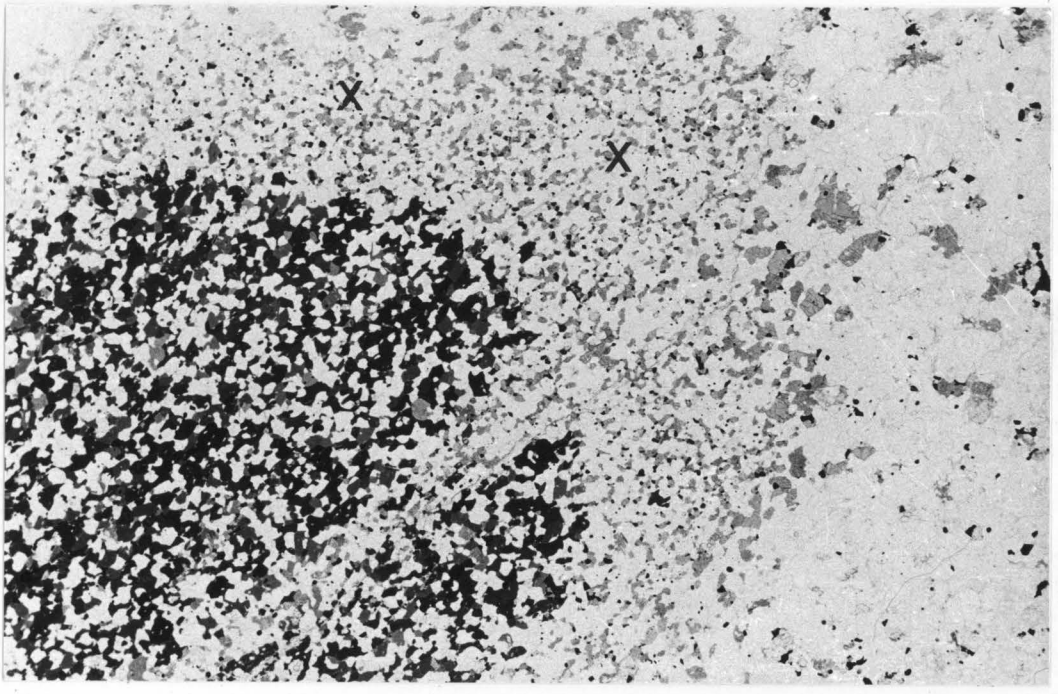


Plate 8. Type I prograde metamorphism geometry: 'anhydrous' granulite rim (X) shields an amphibolite nucleus. X4, Blantyre (see Locality 177, Map 2).

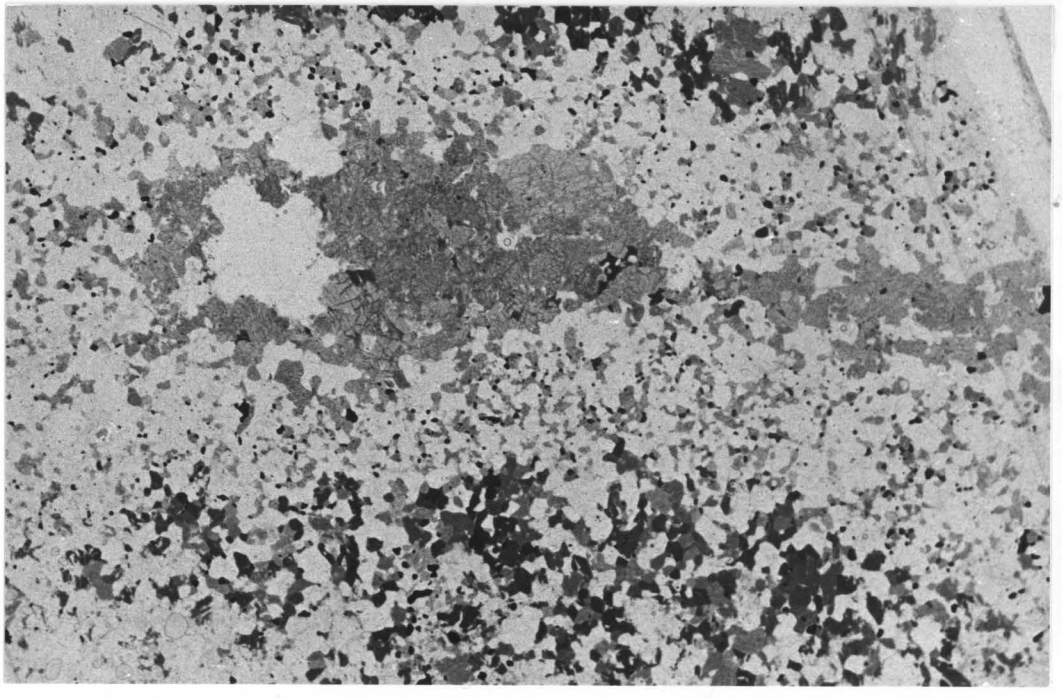


Plate 9. Type II prograde metamorphism geometry: pyroxene-rich vein cross-cuts amphibolite. X5, Blantyre (see Locality 179, Map 2).

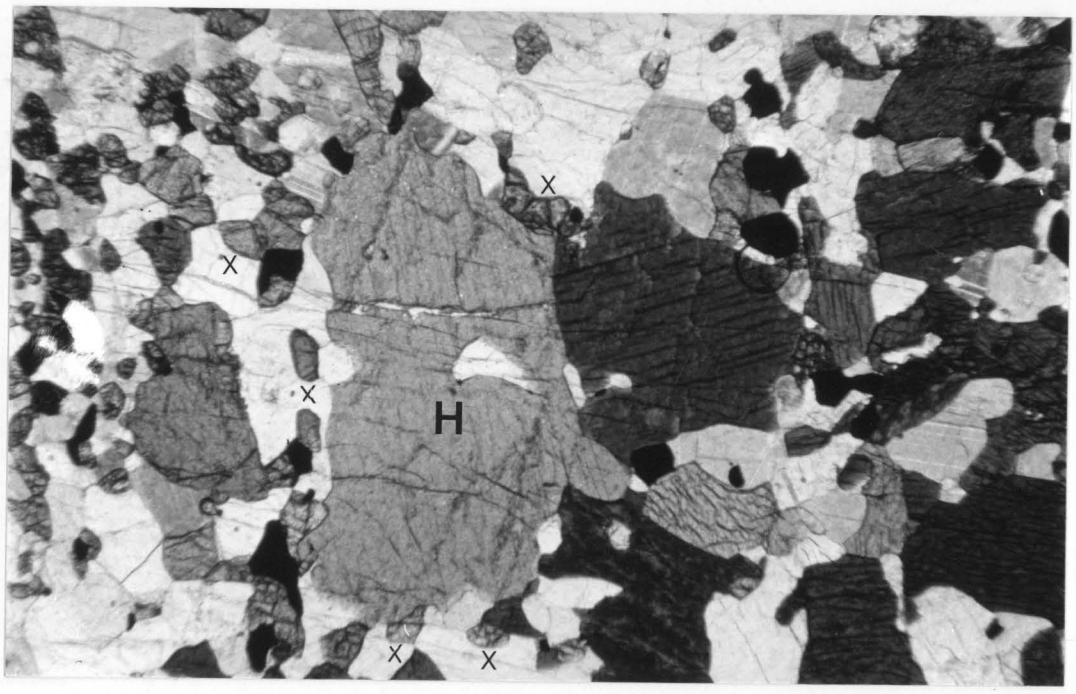


Plate 10. Type I prograde geometry: detail of interface between granulite (left) and amphibolite (right). Note the incipient growth of small orthopyroxene (X) from a large hornblende (H). X120, Middle Shire Valley transition zone (see Locality 322, Map 2).

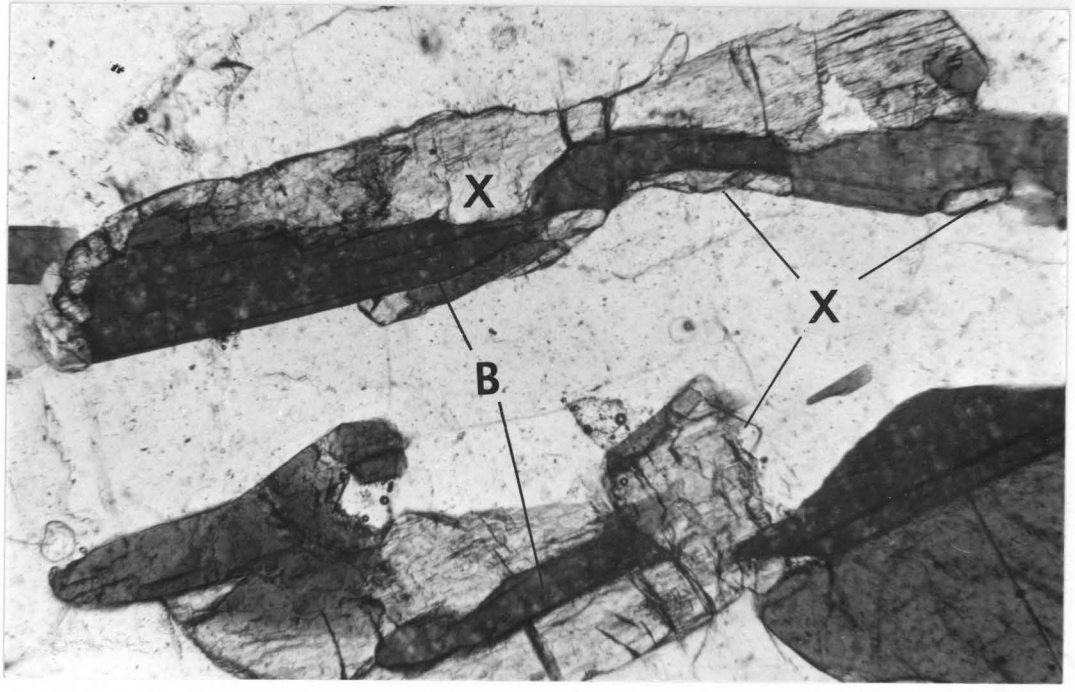


Plate 11. Type III prograde geometry: detail of orthopyroxene (X) replacing biotite (B) in a melanocratic biotite-hornblende-rich rock. X50, Chikwawa (see Locality 157, Map 1).

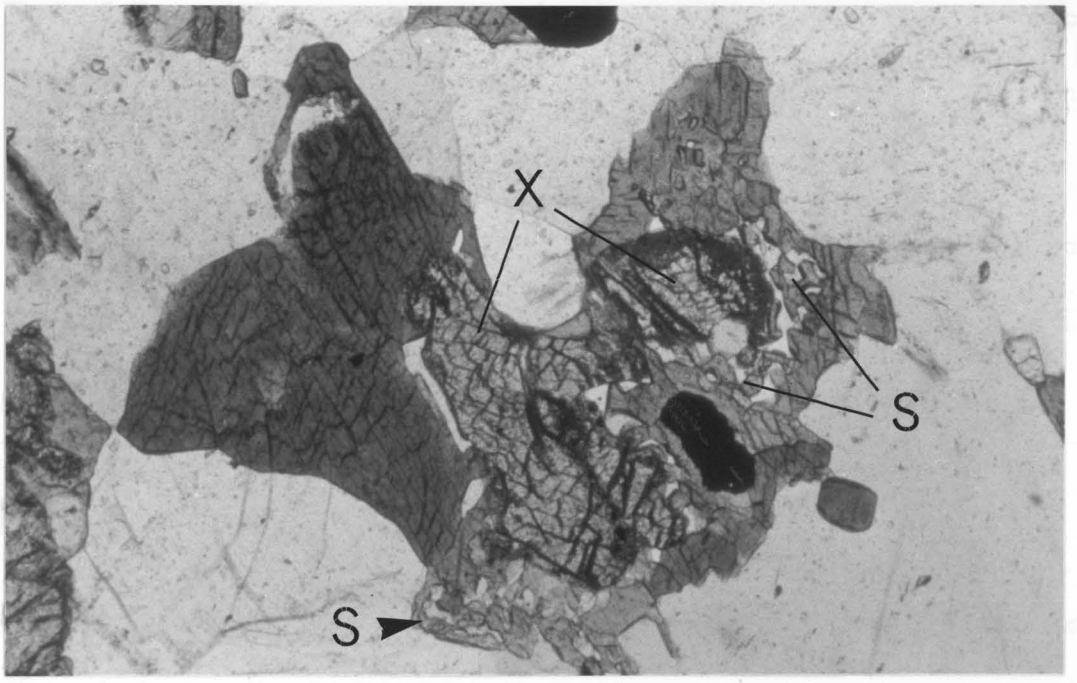


Plate 12. Type III retrograde geometry: detail of an orthopyroxene relict (x) rimmed by a hornblende-quartz symplectite (S). X50, Zomba area (see Locality 38, Map 2).

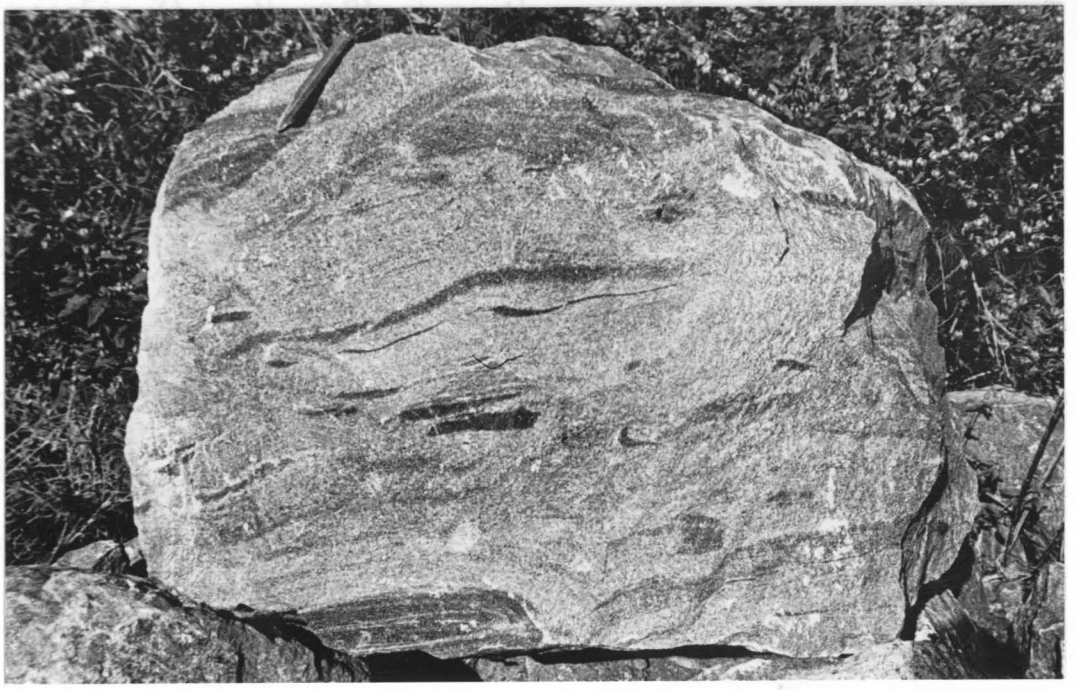


Plate 13. Migmatitic granulite, with stripes and boudins of amphibolite. Blantyre area (see Locality 242, Map 2).

and of Type III geometries, only detectable under the microscope. Rocks with various types of prograde geometries were found in many different localities beside the Middle Shire Valley transition zone, and in particular in the south near Chikwawa (see Locality 13, Fig.7 and Plate 11), and at the Wakurumadzi River Bridge (see Fig.8). More to the north, prograde geometries occur at Nsipe (see Locality 15, Fig.6 and p.38), at Fort Mlangeni (see Fig.6), 20 km south-east of Dedza (see Locality 1, Fig. 6) and near Salima on the western side of Lake Malawi (see Fig.6). On a broader scale, the prograde geometries of the Type I and Type II also occur in the area of highest metamorphic grade, namely the Shire Highlands - Zomba region (see Fig.7). Near Blantyre they were found in the Njuli and Malabwi quarries (see Localities 4 and 17, Fig.7 and Plates 8 and 9) and elsewhere. An interesting example of Type I geometries from the Blantyre area is offered by a leucocratic 'migmatitic' granulite in which biotite-hornblende-rich stripes present thin two-pyroxene-plagioclase reaction rims (see Plates 13 and 14). In addition, Type III prograde geometries were identified near Mulanje (see Locality 18, Fig.7) and also in various localities from the Zomba area, namely at Zomba quarry, at the north-western outskirts of the town and at the Chikala quarry (see localities 3, 19 and 20 respectively, Fig.7). At the latter locality, bands of quartz-free biotite-plagioclase

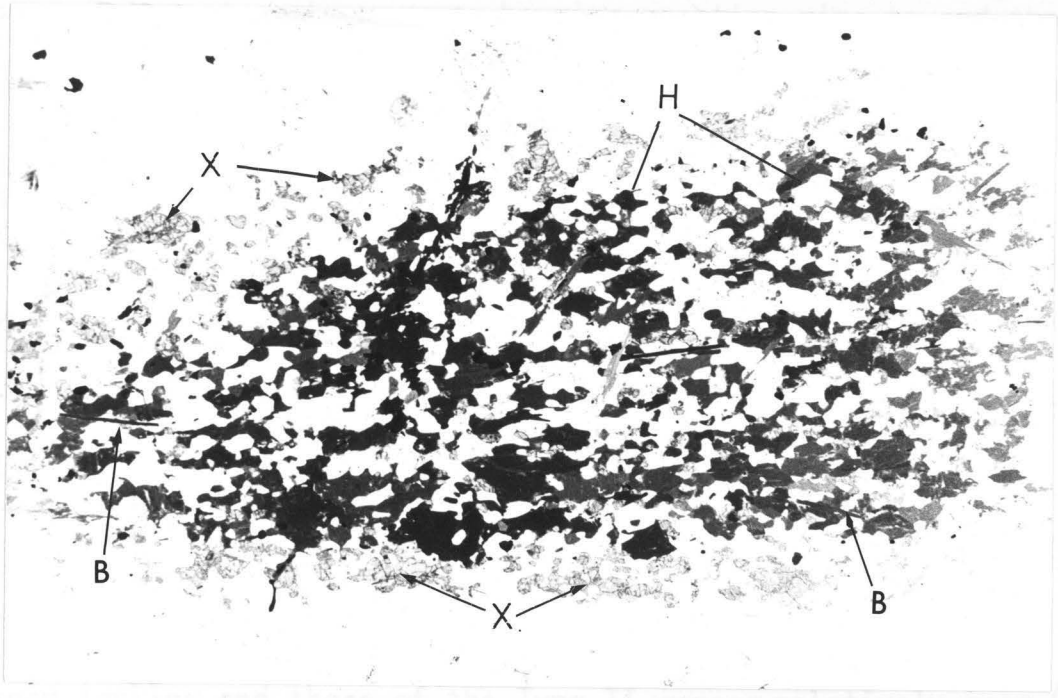


Plate 14. Photomicrograph of an amphibolite stripe from the sample of Plate 13, showing a Type I prograde geometry; note pyroxenes (X), hornblende (H) and biotite (B). X6, Blantyre area (see Locality 242, Map 2).

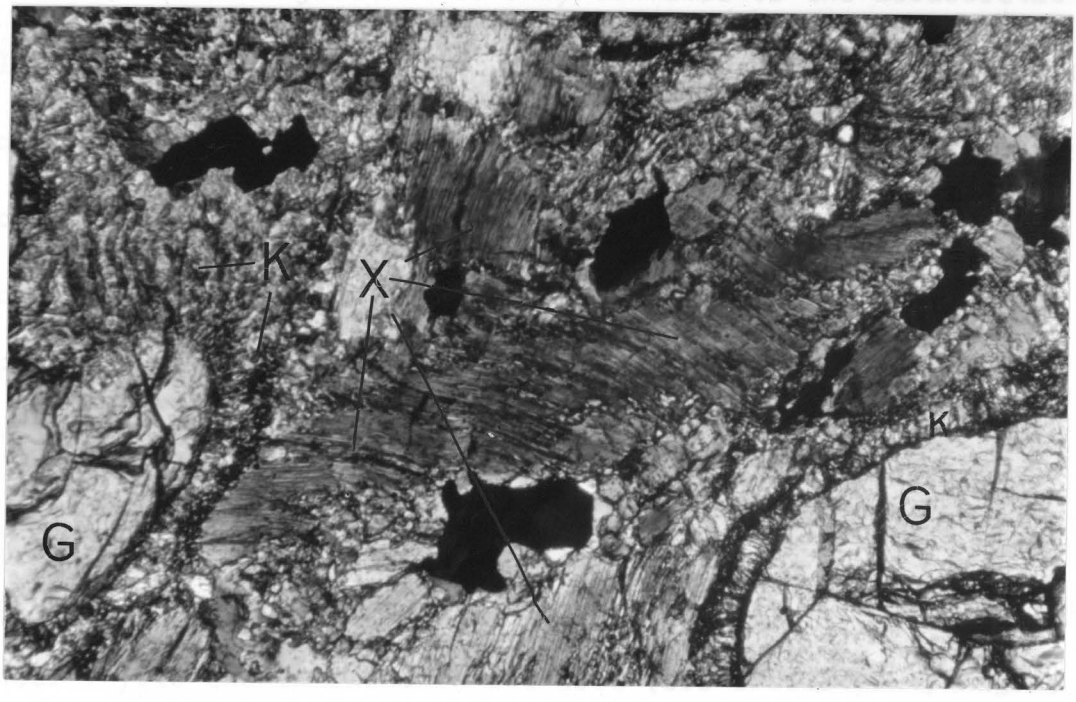


Plate 15. Sheared garnet-clinopyroxene granulite, note the partings in the clinopyroxene (X) and the kelyphitic rims (K) replacing the garnet (G). X50, Tengani area (see Locality 498, Map 1).

gneiss present orthopyroxene-bearing reaction rims toward the enclosing leucocratic granulites. Finally, type III prograde geometries occur in garnet-clinopyroxene granulites from the Kasungu area of northern Malawi (see Fig.6; and Localities 505 and 507, Map 4).

The retrograde metamorphism of the two-pyroxene granulites to the amphibolite facies, is generally represented by the widespread development of Type III retrograde geometries. In contrast, retrograde Type I geometries in melanocratic rocks seem lacking and those of the Type II appear relatively rare (see Plate 1 and Locality 55, Map 2). If the melanocratic and mesocratic transitional rocks are associated and interbanded, evidence of retrogression is only confined to the leucocratic lithotypes whereas the melanocratic ones retain good evidence of (Types I and II) prograde metamorphism. In various parts of southern and central Malawi garnet granulites frequently present Type III retrograde geometries to either amphibolite facies parageneses or to orthopyroxene granulites, indicating lower pressure conditions (Green and Ringwood, 1967).

Garnet breakdown to orthopyroxene-plagioclase kelyphitic rims was observed north-west of Tengani (see Locality 497, Map 1), near Thyolo and in the Chikwawa area (see Locality 14, Fig.7) and near Ncheu (see Fig.6 and Locality 456, Map 3). In central Malawi it was observed in rocks from an area north-west of

Kasungu (see Localities 505 and 506, Map 4). A more complex polymetamorphic pattern, such as: garnet-out/hornblende + biotite-in → garnet, biotite-out/orthopyroxene-in was observed in a group of granulites from a distinctive area west of Tengani. In these garnet granulites the minerals, mainly the clinopyroxene, are strongly zoned and sheared (see Plate 15). In addition, the clinopyroxene occasionally includes crystallographically oriented plagioclase lamellae (see Plate 16), while certain (sheared) orthopyroxene megacrysts from orthopyroxene-garnet veins in anorthosite include regularly spaced rods of garnet (see Plate 17) and more scattered plagioclase lamellae. The garnet is often rimmed by kelyphitic intergrowths of hornblende + scapolite and/or plagioclase (see Plate 18) which in some cases is poikiloblastic and includes minute pyrite grains (see Plate 19). The Tengani area is the only one of southern Malawi where rutile is a stable phase in melanocratic rocks.

To summarize, Table 2 presents the complex mineral paragenetic sequences observed in granulite facies terranes of contrasting assemblages. In particular, Table 2(a) indicates that in the regions where two-pyroxene granulites predominate, an older hornblende and biotite were replaced by ortho- and clinopyroxene during the main metamorphic event. Broken lines indicate the persistence of metastable (?) hornblende and less

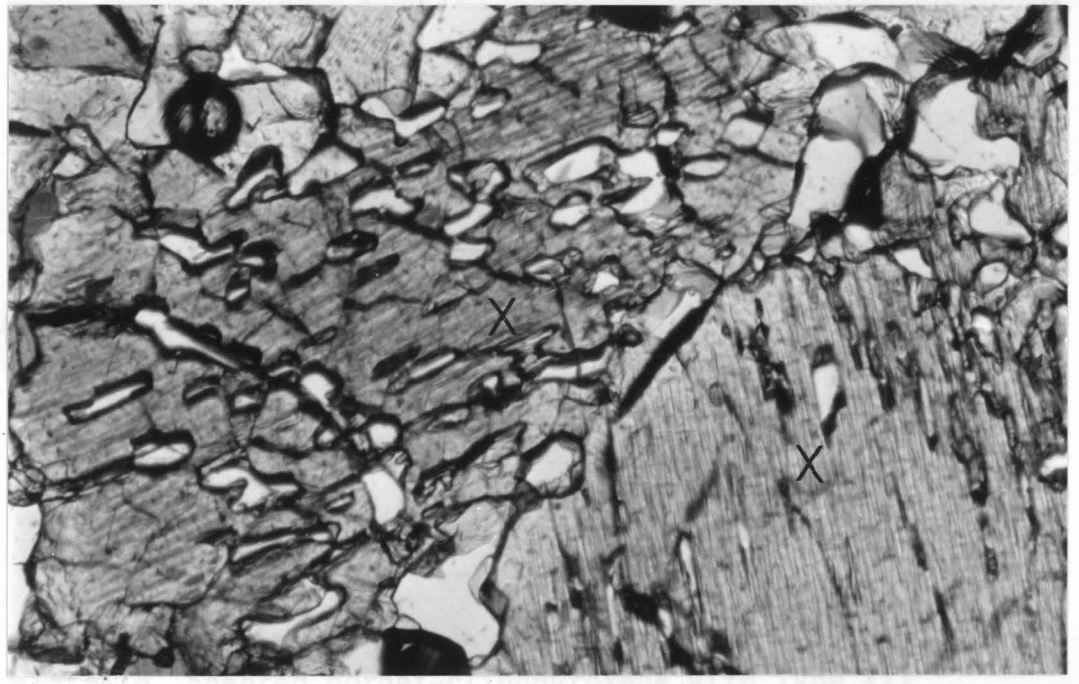


Plate 16. Garnet-clinopyroxene granulite: detail of poikiloblastic clinopyroxene (X) with crystallographically oriented plagioclase lamellae. X200, Tengani area (see Locality 132, Map 1).

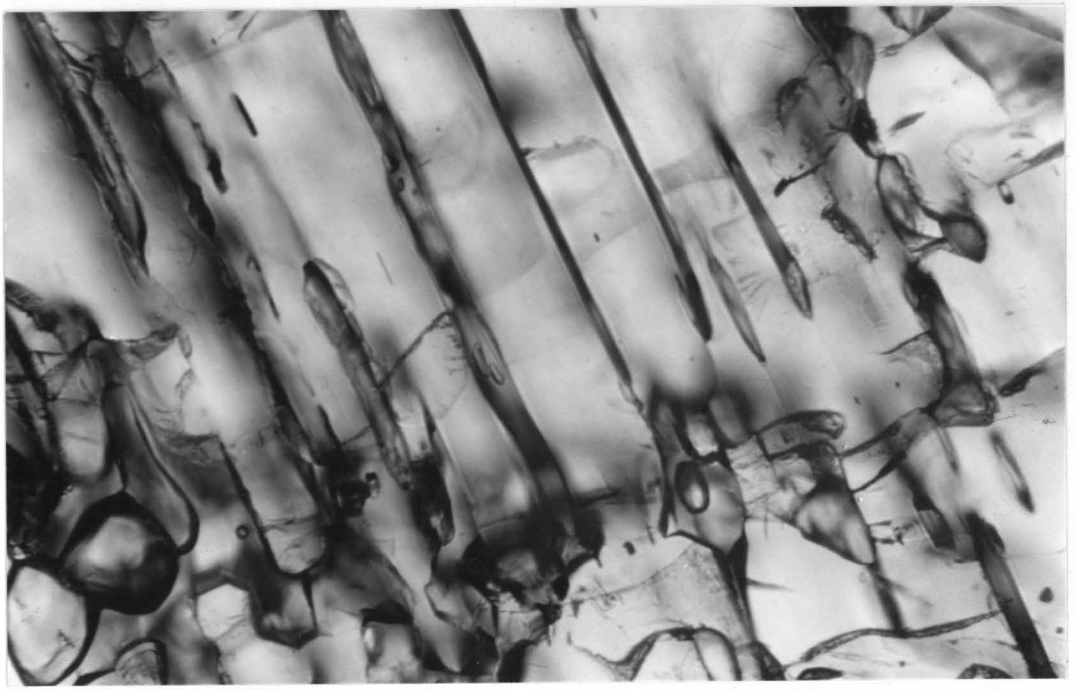


Plate 17. Detail of orthopyroxene megacryst with rods of garnet parallel to the C-axis of host. X200, crossed nicols, Tengani area (see Locality 132, Map 1).



Plate 18. Sheared garnet-clinopyroxene with Type III retrograde geometries; note the kelyphitic rim (K) of amphibole and scapolite replacing garnet (G); orthopyroxene (O), rutile (R), clinopyroxene (X), and hornblende (H). X120, Tengani area (see Locality 498, Map 1).

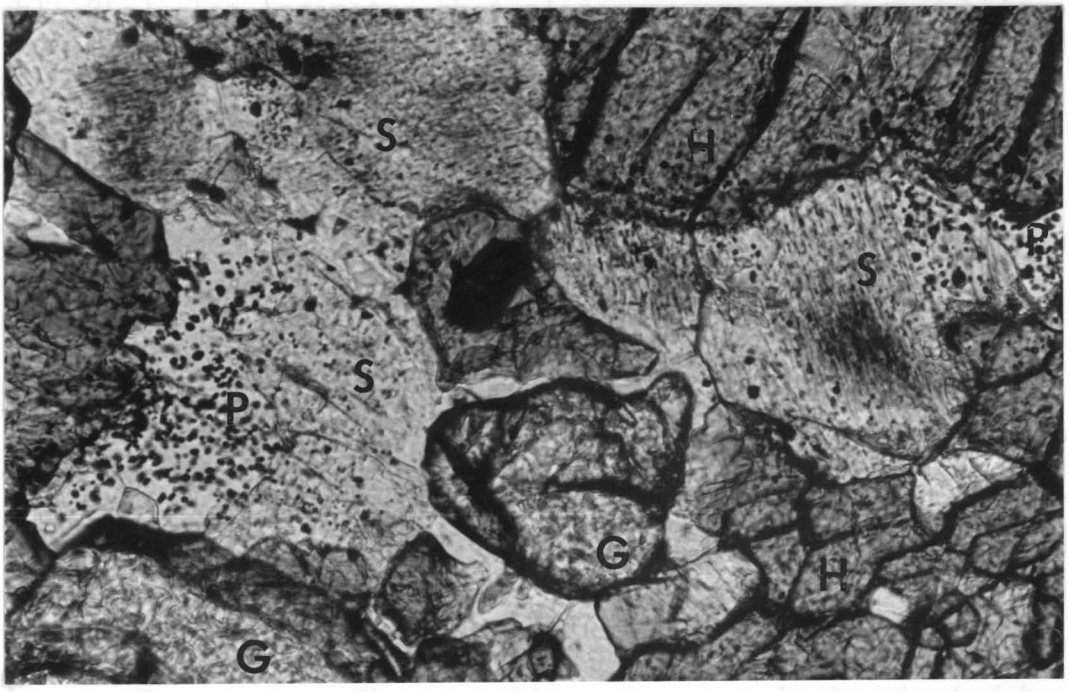
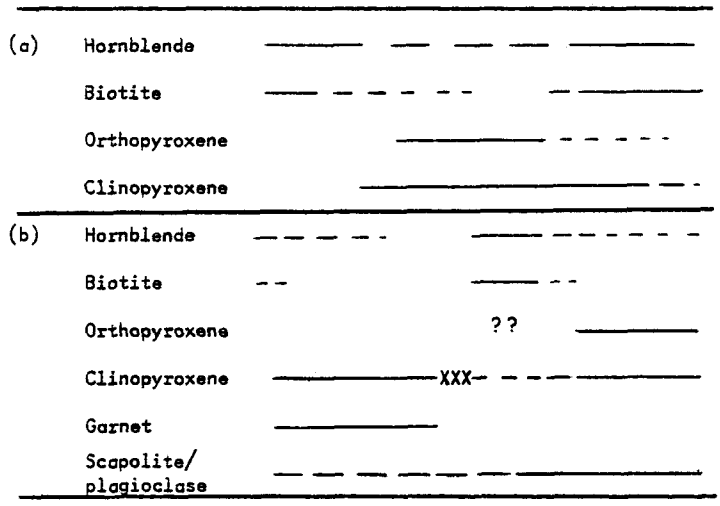


Plate 19. Garnet-clinopyroxene-hornblende granulite: note clouded scapolite (S), poikiloblastic plagioclase (P) with opaque inclusions of pyrite, garnet (G) and hornblende (H). X100, Tengani area (see Locality 132, Map 1).

TABLE 2 - MINERAL PARAGENETIC SEQUENCE IN GRANULITES



(a) two-pyroxene granulites.

(b) garnet-clinopyroxene granulites.

X shearing.

frequently biotite in particular lithologies or localities. Table 2(a) also indicates that clinopyroxene was formed before the orthopyroxene and it remained stable for a longer period even under later retrogressive amphibolite facies conditions. Plagioclase is not shown as it appears stable in all parageneses. In contrast Table 2(b) summarises the complex relationships of the regional garnet-clinopyroxene granulites found in the Tengani area. Garnet and clinopyroxene are the main and oldest minerals and occasionally include relict hornblende and biotite which testify to a possible even earlier prograde metamorphic event. The stability of garnet is terminated by a strong shearing episode, while clinopyroxene persisted in part during the development of hornblende, biotite, scapolite and

plagioclase. At an even later stage hornblende, biotite and garnet were finally replaced by orthopyroxene according to Type III prograde geometries.

2.6 Plutonic Rocks

Rocks of clear plutonic affinity are common in Malawi, and, although they do not form part of this research project, they cannot however be ignored because of their possible relationships to metamorphism. The rocks described here belong to hypermelanic bodies, the Ring Complexes, to the Perthitic Complexes and to granitic massifs and stocks.

With regard to the hypermelanic rocks, biotitite is typical of the Middle Shire Valley amphibolite facies terranes (see Map 5) and it is composed of phlogopite ± tremolite K-feldspar ± anthophyllite ± clinopyroxene ± apatite ± chromite (Morel, 1958). Meta-websterite is more common in granulite facies terranes and is characterised by clinopyroxene-orthopyroxene-spinel ± labradorite ± biotite ± olivine ± hornblende (see Bloomfield, 1968, pp.65-66), and p.138). At Ncheu, Walshaw (1965, pp.46-47) described intergrowths of poikiloblastic olivine and plagioclase, occasionally with spinel inclusions. A serpentinised peridotite mass from Chimwadzulu in the northern Kirk Range (see Locality 21, Fig.7) is associated to corundum amphibolite, garnet amphibolite, nephrite rock and with scapolitised garnet-clinopyroxene rock (Bloomfield and Garson, 1965, pp.84ff).

Finally, Thatcher and Walter (1968, p.34) mentioned garnet-olivine-hornblende metapyróxenite from the Lilongwe area (see Locality 22, Fig.6).

Many different petrographic types have been described by Bloomfield (1965b), in the Ring Complexes of Mlindi, Chipilanye - Little Michiru, Chingale and Ntonya from the Middle Shire and Zomba areas (see Fig.5). Typical rock of the Mlindi body is biotite-clinopyroxenite in which apatite may constitute up to 20 - 30 per cent of the mode (ibid., pp.29ff.). Melanocratic and hypermelanic rocks form the core of the largely syenite and syenite-gneiss bodies at Chipilanje-Little Michiru and at Chingale (see Fig.5). In contrast, the Ntonya structure is formed by a granite outer ring and a core of (quartz-)syenite, which presents charnockitic features including: a dark-green colour with a vitreous lustre, a granoblastic texture, late crystalloblastic orthopyroxene, and feldspar riddled with very fine needle-shaped opaque inclusions.

Lenticular or sill-like massifs of K-feldspar-rich, quartz-poor rocks of syenitic affinity occur within the high-grade granulite facies terranes of Malawi, south-east of Lilongwe (Bloomfield, 1968, pp.74ff. and 143-144). They are known as Perthitic Complexes of which the largest, near Dedza, underlies an area of over 600 km^2 (see Fig.6). The second largest mass is the Shire Highlands massif near Blantyre, covering

an area of 580 km^2 (see Fig.7). The Dedza massif is characterised by perthite-monzonite and granite (ibid.) while the Shire massif exhibits a complete gradation between perthitised granulites and gneisses, perthite gneiss, perthite syenite and minor granite (ibid.). In the Ncheu area smaller bodies concordant within the regional metamorphic sequence are generally made up of microperthite-hornblende-biotite-oligoclase-quartz ± orthopyroxene and clinopyroxene (ibid.). The accessory minerals in the Perthitic Complex rocks are titano-magnetite, pyrite, apatite, sphene, zircon and rare garnet, while the textures suggest replacement of plagioclase by microperthite and of the pyroxenes by hornblende and biotite indicating Type III retrograde texture (ibid., p.143).

Sheared, epidotised and porphyroblastic granite characterises the early-kinematic Dzalanyama Batholith (see Fig.6; ibid., p.155). Granitoid rocks, including 'permeation' augen gneiss and 'anatectic' granite are common throughout Malawi, particularly in the Middle Shire Valley area (see Fig. 8) and Chiripa Plateau (see Locality 23, Fig.6; Walshaw, 1965, pp.54-55). The granitoid orthogneiss of the Middle Shire area is foliated, lineated, and in certain cases presents incipient anatectic textures. The mineral assemblage of this rock is oligoclase/andesine-microperthite-biotite-quartz-hornblende. Accessory minerals are opaque grains, idiomorphic zircon and

apatite. In the Chiripa Plateau (see Locality 23, Fig.6) the same rocks range from predominantly potassic, microperthite-microcline rich, to almost sodic and are composed by quartz, K-feldspar and oligoclase in greatly variable proportions (Bloomfield, 1968, p.154). The final intrusive activity before the Karoo volcanic-sedimentary cycle is probably represented by a number of post-kinematic granite stocks scattered along the shores of Lake Malawi (see Fig.4).

CHAPTER 3. MINERAL CHEMISTRY

3.1 Introduction

Prior to the present investigation there were very few analyses of minerals from southern Malawi and other Mozambiquian metamorphic terranes. In particular, none are available from the Malawi granulites and, in this section, the results are presented for 29 orthopyroxenes, 8 garnets, 9 plagioclases, 3 ilmenites and 1 magnetite from orthopyroxene ± clinopyroxene ± garnet granulites. In addition, 5 clinopyroxenes, 11 garnets, and an ilmenite have been analysed from garnet-clinopyroxene ± orthopyroxene granulites. Finally, to understand the relationships between the granulite and the amphibolite facies assemblages, 29 hornblendes and 9 biotites were analysed in appropriate samples of contrasting metamorphic grade.

In Fig.9 the localities for the various specimens are shown and the majority of the samples studied are of comparable, melanocratic to mesocratic composition, in order to reduce problems caused by differences in the bulk chemistry (see Wilson, 1976a). All minerals were analysed with electron-microprobe techniques, details of which are provided in Appendix III. From the analytical data a computer programme written by Dr. G. Cawthorn has been used to recalculate the structural formulae and also the end-members of garnet and clinopyroxene.

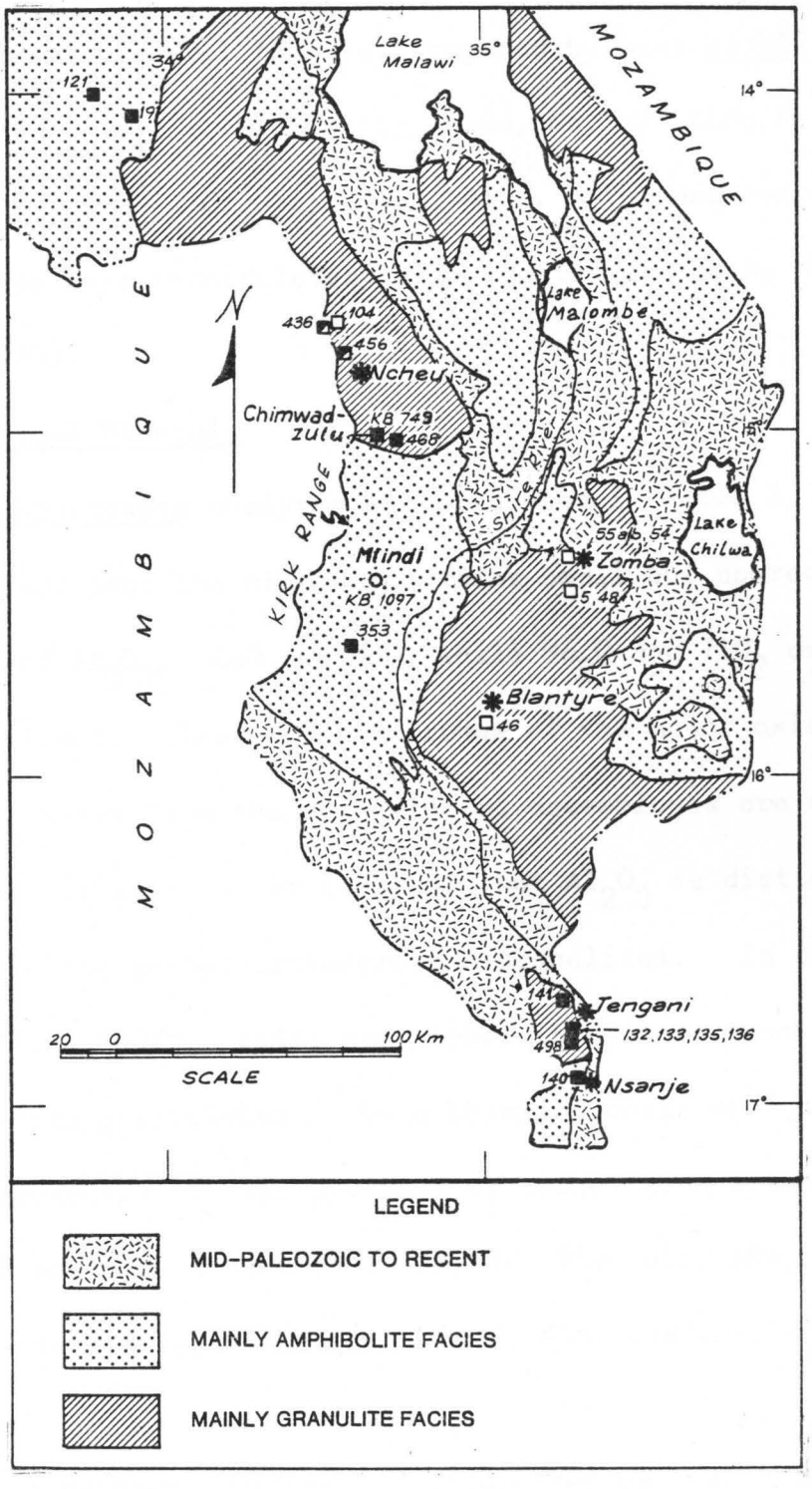


Fig.9. Locality map for samples of mineral analyses. Orthopyroxene granulite and associated amphibolite (□); garnet-two-pyroxene granulite (◩); garnet-clinopyroxene granulite and associated amphibolite (■); orthogneiss (○)(modified after Bloomfield, 1968).

The end-members of pyroxenes were recalculated on the basis of the following general formula, proposed by Deer et al. (1963): $W_{1-p}(X_1Y)_{1+p}Z_2O_6$ in which $p \leq 1$; W=Ca, Na, K; X=Mg, Fe^{2+}, Mn, Ni, Li; Y=Al^{VI}, Fe^{3+}, Cr, Ti; Z=Si, Al^{IV}. The end-members of hornblende were recalculated following the scheme by Misch and Rice (1975).

3.2 Typical Minerals

Orthopyroxene analyses are presented in Table 3, from which it is clear that the mineral contains small but appreciable amounts of Al_2O_3, CaO and MnO, while Na_2O and TiO_2 are insignificant. The variation range of the major oxides in the orthopyroxenes from the main mineral assemblages are compared in Table 4: SiO_2 is rather constant, but Al_2O_3 is distinctly higher in the garnet-orthopyroxene granulites. In contrast, CaO and the FeO/MgO ratio are higher in orthopyroxenes from garnet-free assemblages. On a chemical basis most of the orthopyroxenes from two-pyroxene or garnet granulites listed in Table 5 are hypersthene (nos. 43, 45, 55a, 55b, 104, 135b), a few are ferrohypersthene (nos. 5, 7, 436) and one is a bronzite (no.456).

Clinopyroxene analyses from garnet-free assemblages are presented in Table 6 while their recalculated end-members are given in Table 7. Chemical analyses of clinopyroxene coexisting with garnet and the relative end-members compositions are shown

TABLE 3 - ELECTRON-MICROPROBE ANALYSES OF ORTHOPYROXENE FROM GRANULITES

	A							B		C	
Sample	7		55a	55b	5	46	48	104	135b	436	456
No. of analyses	$6\bar{X}$	σ	$3\bar{M}$	$3\bar{M}$	$3\bar{M}$	$3\bar{M}$	$3\bar{M}$	$4\bar{M}$	1	$2\bar{M}$	1
SiO_2	49,56	0,61	51,06	50,35	51,82	51,74	51,09	50,04	52,76	50,27	51,95
TiO_2	0,07	0,02	0,08	0,13	0,14	0,10	0,17	0,11	0,03	0,22	0,12
Al_2O_3	0,82	0,10	1,02	1,96	1,56	1,23	1,06	2,56	1,67	1,48	3,30
*FeO	32,80	0,41	27,45	26,49	30,12	23,34	28,90	29,18	22,14	29,47	18,37
MnO	1,19	0,05	1,26	1,21	0,51	1,15	0,98	0,45	0,15	0,68	0,18
MgO	14,93	0,16	18,61	17,85	16,21	21,66	17,18	17,58	23,77	16,43	25,13
CaO	0,96	0,09	0,84	1,34	1,24	0,66	1,08	0,38	0,29	0,92	0,64
Na_2O	0,05	0,01	0,05	0,07	0,10	0,08	0,09	0,09	-	0,1	0,04
Total	100,38		100,37	99,40	101,74	99,96	100,56	100,39	100,77	99,47	99,73
CATIONS ON THE BASIS OF 6 OXYGENS											
Si	1,951		1,955	1,941	1,970	1,948	1,956	1,921	1,954	1,955	1,903
Al^{iv}	0,038		0,043	0,059	0,030	0,052	0,044	0,079	0,046	0,045	0,097
Al^{vi}	0,0		0,0	0,030	0,040	0,003	0,005	0,037	0,027	0,023	0,047
Ti	0,002		0,002	0,003	0,004	0,003	0,005	0,00	0,001	0,006	0,003
Fe	1,080		0,879	0,854	0,957	0,735	0,933	0,937	0,668	0,959	0,563
Mn	0,040		0,041	0,040	0,016	0,037	0,032	0,015	0,011	0,022	0,006
Mg	0,876		1,062	1,026	0,920	1,216	0,990	1,006	1,291	0,952	1,372
Ca	0,039		0,037	0,055	0,051	0,025	0,047	0,015	0,009	0,038	0,025
Na	0,004		0,004	0,006	0,008	0,006	0,007	0,007	-	0,007	0,003
Σz	1,989		1,998	2,000	2,000	2,000	2,000	2,000	2,000	2,000	2,000
Σxwy	2,041		2,025	2,014	1,996	2,025	2,019	2,021	2,009	2,007	2,022
Mg^{ox}	30,5		39,3	39,2	34,6	46,9	36,5	37,2	51,6	35,3	57,5

*All iron as FeO; 456 includes 0,11% Cr_2O_3.

$\bar{X}$: arithmetic mean; σ: standard deviation; $\bar{M}$: average

A: two-pyroxene granulite; B: garnet-orthopyroxene granulite.
C: garnet-two-pyroxene granulite. Sample localities are given in Fig.9.
Individual analyses are listed in Appendix III-12.

TABLE 4 - MAIN OXIDE VARIATIONS IN ORTHOPYROXENE
(SEE TABLE 3)

	A	B	C
SiO_2	49,56 - 51,82	50,04 - 52,76	50,27 - 51,95
Al_2O_3	0,82 - 1,96	1,67 - 2,56	1,48 - 3,30
*FeO	23,34 - 32,80	22,14 - 29,18	18,37 - 29,47
MgO	14,93 - 21,66	17,58 - 23,77	16,43 - 25,13
CaO	0,82 - 1,34	0,29 - 0,38	0,84 - 0,92

*All iron as FeO.
A = two-pyroxene granulite.
B = garnet-orthopyroxene granulite.
C = garnet-two-pyroxene granulite.

TABLE 5 - CLASSIFICATION OF ORTHOPYROXENES (SEE TABLE 3)

Bronzite	456	(R = 70,7)			
Hypersthene	46	(R = 61,2);	48	(R = 50,6);	55a (R = 53,6)
	55b	(R = 53,4);	104	(R = 51,3);	135b (R = 65,5)
Ferrohypersthene	5	(R = 48,6);	7	(R = 43,9);	436 (R = 49,2)

R = Mg x 100/(Mg + Fe + Mn).

TABLE 6 - ELECTRON-MICROPROBE ANALYSES OF CLINOPYROXENE FROM TWO-PYROXENE GRANULITE (SEE TABLE 3)

	A					
Sample	7	55a		55b	5	46	48
No. of analyses	$2\bar{M}$	$6\bar{X}$	σ	$3\bar{M}$	$4\bar{M}$	$2\bar{M}$	1
SiO_2	49,77	50,01	0,44	50,00	50,32	50,81	50,33
TiO_2	0,28	0,30	0,04	0,32	0,35	0,27	0,59
Al_2O_3	2,25	2,67	0,24	2,99	3,00	2,18	2,62
*FeO	15,32	12,67	0,22	11,46	13,22	10,16	11,60
MnO	0,51	0,57	-	0,62	0,39	0,50	0,46
MgO	10,57	11,56	0,28	11,83	11,11	13,17	12,13
CaO	19,79	20,00	0,63	21,80	21,32	21,15	21,83
Na_2O	0,53	0,48	-	0,51	0,57	0,75	0,42
Total	99,02	98,26		99,53	100,28	98,98	99,98
CATIONS ON THE BASIS OF 6 OXYGENS							
Si	1,931	1,931		1,907	1,913	1,932	1,910
Al^{iv}	0,069	0,069		0,093	0,087	0,068	0,090
Al^{vi}	0,034	0,052		0,042	0,048	0,030	0,028
Ti	0,008	0,009		0,009	0,010	0,008	0,017
Fe	0,497	0,409		0,366	0,420	0,323	0,368
Mn	0,017	0,019		0,020	0,013	0,016	0,015
Mg	0,611	0,665		0,672	0,630	0,746	0,686
Ca	0,823	0,828		0,890	0,867	0,862	0,887
Na	0,040	0,036		0,038	0,043	0,055	0,031
Σw	2,000	2,000		2,000	2,000	2,000	2,000
Σwxy	2,030	2,018		2,037	2,031	2,040	2,032
Mg^{ox}	40	46,6		49,5	44,9	55,3	50,1

* All iron as FeO.

$\bar{M}$: average; $\bar{X}$: arithmetic mean; σ: standard deviation.

Sample localities are given in Fig.9. Individual analyses are listed in Appendix III-13.

TABLE 7 - END MEMBERS OF CLINOPYROXENE FROM TWO-PYROXENE GRANULITE (SEE TABLE 6)

Sample	7	55a	55b	5	46	48
Jadeite	3,87	3,53	3,64	4,08	5,32	3
Ti-tschermak	0,79	0,86	0,89	0,97	0,74	1,63
Ca-tschermak	2,27	3,35	3,78	3,51	1,30	2,55
Wollastonite	38,43	38,56	40,65	39,89	40,43	40,96
Enstatite	29,68	32,69	32,44	30,54	35,90	33,28
Ferrosilite	24,96	21,02	18,60	21,00	16,31	18,57

in Tables 8 and 9. The data of Tables 7 and 9 indicate that the minerals are mainly augite , and in these analyses Al_2O_3 is variable but it can be rather high, up to 6,83 per cent; Na_2O, TiO_2 are generally very small but they are appreciable in a few samples (nos. 132, 133 and 136, Table 8) while MnO is insignificant. It is interesting to observe that the sum of cations in the clinopyroxenes ($\Sigma xwyz$) seldom approaches the theoretic 4,000 and that certain minerals (nos. 133a, b, and c, 353b and 468, Table 8) have a total in the 3,975 - 3,989 range. In other cases the clinopyroxenes have totals ranging from 4,018 to 4,071 (see Tables 6 and 8). This may not necessarily mean poor quality of the analyses since high totals may be induced by the presence of Fe^{3+} in the minerals and low totals are frequently reported in analyses of metamorphic clinopyroxenes of reputed good quality (Cawthorn and Collerson, 1974).

Table 10 summarises the chemical composition of clinopyroxenes from different areas and mineral assemblages. The SiO_2 content is relatively constant; Al_2O_3, TiO_2, Na_2O and MgO/FeO are generally higher in the Tengani augites (nos. 132, 133, 135,and 136, Table 8) which are also characterised by a variable CaO content. The strong variability in some samples is due to marked zoning of the minerals as in sample 133 from Tengani. An electron-microprobe scan across some zoned clinopyroxene grains indicated that the nucleus is enriched in

TABLE 8 - ELECTRON-MICROPROBE ANALYSES OF CLINOPYROXENE FROM GARNET-BEARING GRANULITE

	C		D												
Sample	436	456	468	353a	353b	121	19	140	136	132	498	498	133b	133a	133c
No. of analyses	$2\bar{M}$	1	1	1	1	1	1	1	1	1	nucleus 1	rim 1	$3\bar{M}$	1	1
SiO_2	48,55	50,03	53,93	50,34	52,48	50,29	50,85	50,59	49,46	49,49	50,96	50,71	51,03	49,76	50,93
TiO_2	0,42	0,64	0,24	0,48	0,18	0,19	0,29	0,30	1,09	0,74	0,65	0,53	0,93	0,89	0,43
Al_2O_3	2,27	5,15	2,88	3,15	1,53	5,93	5,76	2,35	6,83	4,80	3,98	3,85	4,35	6,60	5,96
Cr_2O_3	n.d.	0,17	n.d.	n.d.	n.d.	n.d.	n.d.	0,04	n.d.	0,09	0,03	0,03	n.d.	n.d.	n.d
*FeO	11,14	7,00	6,79	14,13	12,10	10,85	11,49	13,23	7,14	7,88	8,06	8,12	9,56	9,46	8,63
MnO	0,54	0,07	0,23	0,18	0,20	0,26	0,31	0,20	0,28	0,09	0,08	0,08	0,32	0,27	0,25
MgO	12,94	13,52	12,89	10,72	11,29	11,68	12,03	11,03	12,34	13,65	15,09	14,26	11,52	11,89	10,79
CaO	22,08	21,75	22,53	20,42	21,26	22,10	20,94	21,27	22,23	21,47	18,80	20,53	21,00	17,87	21,03
Na_2O	0,41	0,81	0,73	0,58	0,45	0,64	0,42	0,35	0,91	0,83	0,65	0,55	0,75	1,14	0,97
Total	98,35	99,14	100,22	100,00	99,49	101,06	102,08	99,36	100,28	99,05	98,30	98,65	99,46	98,08	98,11
CATIONS ON THE BASIS OF 6 OXYGENS															
Si	1,881	1,870	1,982	1,919	1,989	1,858	1,872	1,938	1,832	1,862	1,910	1,905	1,916	1,882	1,909
Al^{iv}	0,104	0,130	0,018	0,081	0,011	0,142	0,128	0,062	0,168	0,138	0,090	0,095	0,084	0,118	0,091
Al^{vi}	-	0,097	0,107	0,061	0,058	0,117	0,122	0,044	0,131	0,074	0,086	0,076	0,108	0,176	0,173
Ti	0,012	0,018	0,007	0,014	0,005	0,005	0,008	0,009	0,030	0,021	0,018	0,015	0,026	0,025	0,012
Cr	n.d.	0,005	n.d.	n.d.	n.d.	n.d.	n.d.	0,001	n.d.	0,003	0,001	n.d.	n.d.	n.d.	n.d.
Fe	0,361	0,219	0,209	0,451	0,384	0,335	0,354	0,424	0,221	0,248	0,253	0,255	0,300	0,299	0,271
Mn	0,018	0,002	0,007	0,006	0,006	0,008	0,010	0,006	0,009	0,003	0,003	0,003	0,010	0,009	0,008
Mg	0,747	0,753	0,706	0,609	0,638	0,643	0,660	0,630	0,681	0,765	0,843	0,799	0,645	0,670	0,603
Ca	0,917	0,871	0,887	0,834	0,864	0,875	0,826	0,873	0,883	0,865	0,755	0,827	0,845	0,724	0,845
Na	0,031	0,059	0,052	0,043	0,033	0,046	0,030	0,026	0,065	0,061	0,047	0,040	0,055	0,084	0,071
Σz	1,985	2,000	2,000	2,000	2,000	2,000	2,000	2,000	2,000	2,000	2,000	2,000	2,000	2,000	2,000
Σwxy	2,086	2,025	1,975	2,018	1,988	2,030	2,010	2,013	2,021	2,040	2,007	2,015	1,989	1,987	1,982
Mg^{ox}	52,6	65,6	64,7	42,8	47,9	51,2	50,5	45,1	62,4	63,1	64,9	63,0	53,8	55	54,9

*All iron as Feo; $\bar{M}$: average.

C: garnet-two-pyroxene granulite; D: garnet-clinopyroxene granulite.

Sample localities are given in Fig.9. Individual analyses are listed in Appendix III-13.

TABLE 9 - END MEMBERS OF CLINOPYROXENE FROM GARNET-BEARING GRANULITE (SEE TABLE 8)

	C		D											
Sample	436	456	468	353a	353b	121	19	140	136	132	498a	498b	133a	133b	133c
Jadeite	2,88	5,73	5,34	4,21	3,35	4,45	2,97	2,57	6,41	5,82	4,70	3,95	5,52	8,47	7,18
Ti-tschermak	1,14	1,76	0,68	1,35	0,52	0,51	0,79	0,85	2,98	2,01	1,82	1,48	2,66	2,56	1,24
Ca-tschermak	2,26	6,45	3,05	3,50	1,27	9,80	10,10	3,10	8,44	5,31	4,57	4,96	4,32	8,11	8,53
Wollastonite	41,12	38,28	43,64	38,57	42,83	37,33	35,46	41,09	37,53	37,88	34,30	37,51	39,22	31,34	38,11
Enstatite	34,91	36,75	36,21	29,93	32,29	31,23	32,68	31,08	33,38	36,79	41,89	39,36	32,59	33,94	30,70
Ferrosilite	17,69	10,79	11,07	22,43	19,75	16,67	18,00	21,24	11,27	12,06	12,68	12,70	15,69	15,59	14,84

C: clinopyroxenes from garnet-two-pyroxene granulite.

D: clinopyroxenes from garnet-clinopyroxene granulite.

TABLE 10 - MAIN OXIDE VARIATIONS IN CLINOPYROXENE (SEE TABLES 6 AND 8)

	A	D
SiO_2	49,77 - 50,81	49,46 - 53,93
TiO_2	0,27 - 0,59	0,18 - 1,09
Al_2O_3	2,18 - 3,00	1,53 - 6,83
*FeO	10,16 - 15,32	6,79 - 14,13
MgO	10,57 - 13,17	10,72 - 15,09
CaO	19,79 - 21,83	17,87 - 22,53
Na_2O	0,42 - 0,75	0,35 - 1,14
Wollastonite	38,4 - 41,0	31,3 - 43,6

* All iron as FeO.

A: clinopyroxenes from two-pyroxene granulite.

D: clinopyroxenes from garnet-clinopyroxene granulite.

Fe, Ti and Al relative to the more Si-rich rim, while Na does not change appreciably.

Analyses of garnet from Malawi granulites are listed in Table 11, from which it appears that these compositions are characterised by uniform SiO_2 and Al_2O_3 contents and only small amounts of TiO_2 and Na_2O. The concentration of the other oxides, mainly FeO with minor MgO and CaO, is however strongly dependent on both mineral parageneses and geographic location.

Chemical variations related to zoning were found in a garnet from Tengani (no.132, Table 11): the nucleus has a higher MgO and Cr_2O_3 concentration than the more FeO-, MnO-enriched rim. An electron-microprobe scan for Al on a hypersthene megacryst from the same area (see Plate 17) confirmed that the pink-coloured, rod-shaped inclusions are garnet.

The recalculated end-members are presented in Table 12 from which the minerals appear to be solid solutions of almandine, as the main component, with pyrope and grossular in substantial proportions. The spessartine end-member is quite small.

The ranges in the minimum and maximum oxide values in the garnet from various assemblages are shown in Table 13, indicating that the analyses of the garnet coexisting with orthopyroxene are characterised by the lowest CaO content. Moreover, garnets from Ncheu two-pyroxene-garnet granulites (nos. 436 and 456, Fig.9) are quite dissimilar, reflecting the fact that one

TABLE 11 - ELECTRON-MICROPROBE ANALYSES OF GARNET FROM GRANULITE

	B		C		D								
Sample	104	135b	436	456	353	468	506	121	19	140	498	132a	132b
No. of analyses	3M	1	3M	1	2M	2M	1	1	1	1	rim 1	nucleus 1	rim 1
SiO_2	38,66	38,72	37,37	39,81	38,17	38,01	37,92	37,84	38,29	38,11	38,66	39,24	38,68
TiO_2	0,02	0,06	0,24	0,09	0,02	0,18	0,03	0,05	0,04	0,07	0,11	0,1	0,11
Al_2O_3	21,95	22,38	20,98	23,01	20,52	20,30	20,30	19,79	20,16	22,00	22,59	22,79	22,47
Cr_2O_3	n.d.	0,19	n.d.	0,03	n.d.	n.d.	n.d.	n.d.	n.d.	0,05	0,04	0,33	0,22
*FeO	29,55	26,08	27,76	20,80	26,18	23,96	26,83	25,29	25,24	27.67	22,23	20,38	22,03
MnO	1,21	0,53	1,64	0,40	1,24	0,76	1,03	0,99	1,27	0,62	0,31	0,48	0,59
MgO	7,75	8,63	4,89	10,82	3,44	4,38	5,25	4,40	5,60	5,23	8.19	9,32	7,92
CaO	2,18	4,85	6,31	6,34	8,84	11,53	8,19	10,00	7,54	7,47	8,81	8,89	8,96
Na_2O	-	0,03	0,12	0,01	0,04	0,11	-	-	0,09	0,01	0,02	0,01	0,04
Total	101,32	101,46	99,31	101,32	98,45	99,23	99,28	98,36	98,53	101,23	100,96	101,54	101,02
CATIONS ON THE BASIS OF 24 OXYGENS													
Si	5,955	5,893	5,929	5,929	6,059	6,007	6,018	6,053	6,086	5,910	5,872	5,878	5,879
Al^{iv}	0,047	0,107	0,071	0,071	-	-	-	-	-	0,090	0,128	0,122	0,121
Al^{vi}	3,942	3,909	3,851	3,969	3,837	3,782	3,766	3,786	3,864	3,932	3,918	3,904	3,906
Ti	0,002	0,007	0,052	0,010	0,001	0,021	0,004	0,006	0,005	0,008	0,013	0,011	0,013
Cr	n.d.	0,023	n.d.	n.d.	n.d.	n.d.	n.d.	n.d.	n.d.	0,006	0,005	0,039	0,026
Fe	3,807	3,320	3,683	2,591	3,476	3,167	3,562	3,384	3,356	3,589	2,824	2,554	2,801
Mn	0,158	0,068	0,220	0,050	0,167	0,102	0,138	0,134	0,171	0,081	0,040	0,061	0,076
Mg	1,779	1,958	1,156	2,402	0,812	1,032	1,242	1,049	1,327	1,209	1,854	2,081	1,794
Ca	0,360	0,791	1,073	1,012	1,662	1,952	1,393	1,714	1,284	1,241	1,434	1,427	1,459
Na	-	0,009	0,037	0,003	0,012	0,034	-	-	0,028	0,003	0,006	0,003	0,012
Σ iv	6,000	6,000	6,000	6,000	6,059	6,007	6,018	6,053	6,086	6,000	6,000	6,000	6,000
Σ vi	10,049	10,085	10,074	10,040	9,995	10,009	10,104	10,074	10,034	10,070	10,093	10,080	10,087

* All iron as FeO; M: average; n.d.: not determined.
B: garnet-orthopyroxene granulite; C: garnet-two-pyroxene granulite;
D: garnet-clinopyroxene granulite.
Sample localities are given in Fig.9: for sample no.506, see Map in the pocket at the back of the thesis.
Individual analyses are listed in Appendix III-14.

TABLE 12 - GARNET END-MEMBERS (SEE TABLE 11)

	B		C		D								
	104	135b	436	456	353	468	506	121	19	140	nucl. 498	nucl. 132a	rim 132b
Pyrope	29,74	32,28	19,55	39,53	14,12	18,11	22,07	18,72	23,39	19,98	30,40	34,07	29,45
Uvarovite	-	0,56	n.d.	0,09	n.d.	n.d.	n.d.	n.d.	n.d.	0,15	0,20	0,96	0,65
Schorlomite	0,04	0,11	0,48	0,17	0,04	0,38	0,06	0,11	0,08	0,13	0,21	0,18	0,21
Grossularite	5,98	12,36	17,65	16,40	26,05	33,91	24,70	30,48	22,56	20,23	23,23	22,22	23,1
Spessartine	2,64	1,13	3,73	0,83	2,89	1,79	2,46	2,39	3,01	1,35	0,60	1	1,25
Almandine	61,60	53,55	58,59	42,99	56,89	45,81	50,71	48,31	50,95	58,16	45,34	41,57	45,35

n.d.: not determined; nucl.: nucleus.
B: garnet-orthopyroxene granulite.
C: garnet-two-pyroxene granulite
D: garnet-clinopyroxene granulite.

TABLE 13 - MAIN OXIDE VARIATIONS IN GARNET (SEE TABLE 11)

	(i)	(ii)
*FeO	20,80 - 29,55	20,38 - 27,67
MnO	0,40 - 1,64	0,31 - 1,27
MgO	4,89 - 10,82	3,44 - 9,32
CaO	2,18 - 6,34	7,47 - 11,53

* All iron as FeO.

(i) garnet-orthopyroxene ± clinopyroxene granulite (groups B and C, Table 11).

(ii) garnet-clinopyroxene granulite (group D, Table 11).

(no.456) is from an interband in anorthosite and has higher MgO but lower FeO and MnO of the other (no.436) which is associated with two-pyroxene (garnet-free) granulites. Finally the analysis of a garnet from an albite-prehnite-garnet-sericite rock (no.141, Fig.9), not shown in Table 11, is an almandine with appreciable grossular and pyrope components (total iron as FeO = 24,2 per cent; MgO = 6,4 per cent; CaO = 9,2 per cent). The complete analysis of this garnet is given in Appendix III-14.

Hornblende analyses are presented in Tables 14 (i) and (ii) while Table 15 shows the recalculated end-members, indicating that the amphiboles are mainly solid solutions of hastingsite with appreciable amounts of tschermakite, edenite and tremolite. The content of richterite and anthophyllite are quite insignificant. Considering the chemistry of the amphiboles in more detail, Table 16 shows the range of the main oxides in hornblendes from rocks of different assemblages. The hornblendes from garnet granulites have generally higher SiO_2, but lower TiO_2 than those from two-pyroxene granulites; in addition a higher MgO/FeO ratio distinguishes the amphiboles from Tengani (nos. 132a and 132b, Table 14(i)) from the majority of the others which were analysed. In particular, an early formed, reddish coloured amphibole (no. 132b, Table 14(i)) presents higher Al_2O_3, FeO and higher Na_2O/K_2O ratio than a latter developed green hornblende

TABLE 14(i) - ELECTRON-MICROPROBE ANALYSES OF HORNBLENDE

	A					D						E	
Sample	5	48		46	55b	468	436	353	132a	132b	498	KB749	54
No. of analyses	$3\bar{M}$	$5\bar{X}$	σ	$4\bar{M}$	$3\bar{M}$	$2\bar{M}$	$2\bar{M}$	1	$2\bar{M}$	$2\bar{M}$	1	1	$4\bar{M}$
SiO_2	41,63	41,68	0,19	41,95	40,69	44,30	40,32	41,31	40,63	40,15	45,42	45,07	41,65
TiO_2	2,63	3,26	0,06	2,19	2,23	1,31	3,00	2,07	2,12	2,03	1,87	0,44	1,97
Al_2O_3	11,12	11,68	0,17	10,77	12,15	11,67	12,96	11,69	13,88	16,98	10,85	13,10	11,98
Cr_2O_3	n.d.	n.d.		n.d.	n.d.	n.d.	n.d.	n.d.	n.d.	0,07	0,04	0,11	n.d.
*FeO	17,60	16,17	0,21	14,83	17,22	14,45	16,15	21,21	13,39	10,49	10,28	9,3	14,23
MnO	0,33	0,25	0,02	0,31	0,30	0,26	0,39	0,09	0,31	0,04	0,07	0,19	0,30
MgO	10,26	10,03	0,29	12,18	9,38	11,12	8,92	8,01	12,86	12,71	14,46	14,97	11,53
CaO	11,32	11,27	0,24	11,26	11,41	12,05	10,67	11,62	11,20	11,54	11,45	12,28	11,43
Na_2O	1,77	1,75	0,13	1,75	1,45	1,48	1,53	0,70	2,27	2,63	1,78	1,83	1,82
K_2O	1,44	1,83	0,06	1,63	2,29	0,51	2,49	1,73	1,41	0,69	0,50	0,29	1,86
Total	98,82	97,92		96,87	97,12	97,15	96,43	98,43	98,07	97,30	96,72	99,46	96,77

* All iron as FeO; $\bar{X}$: arithmetic mean; σ: standard deviation; $\bar{M}$: average; n.d.: not determined.
KB 749 (from Bloomfield and Garson, 1965, p.97), total includes 1,88% H_2O and 4,27% Fe_2O_3.

A: two-pyroxene granulite: D: garnet-clinopyroxene granulite: E: amphibolite.

Sample localities are given in Fig.9. Individual analyses are listed in Appendix III-15.

TABLE 14(ii) - CATION OF HORNBLENDES ON THE BASIS OF 23 OXYGENS* (SEE TABLE 14(i))

	A				D						E	
Sample	5	48	46	55b	468	436	353	132a	132b	498	KB749	54
Si	6,302	6,285	6,354	6,241	6,585	6,194	6,317	6,039	5,898	6,636	6,463	6,296
Al^{iv}	1,698	1,715	1,646	1,759	1,415	1,806	1,683	1,961	2,102	1,364	1,537	1,704
Al^{vi}	0,285	0,360	0,277	0,438	0,629	0,542	0,425	0,472	0,839	0,506	0,676	0,429
Ti	0,300	0,370	0,249	0,257	0,147	0,347	0,238	0,237	0,224	0,206	0,047	0,224
Cr	n.d.	n.d.	n.d.	n.d.	n.d.	n.d.	n.d.	n.d.	0,008	0,005	0,012	n.d.
Fe	2,559	2,039	1,873	2,208	1,797	2,075	2,713	1,665	1,289	1,256	1,115	1,826
Mn	0,042	0,032	0,040	0,038	0,032	0,051	0,012	0,039	0,005	0,009	0,023	0,039
Mg	2,316	2,254	2,743	2,145	2,463	2,043	1,826	2,849	2,783	3,145	3,198	2,598
Ca	1,836	1,820	1,828	1,874	1,918	1,757	1,904	1,748	1,817	1,793	1,886	1,851
Na	0,518	0,511	0,507	0,432	0,425	0,456	0,208	0,654	0,749	0,504	0,508	0,533
K	0,278	0,352	0,316	0,448	0,096	0,488	0,338	0,267	0,129	0,093	0,053	0,358
Σ iv	8,000	8,000	8,000	8,000	8,000	8,000	8,000	8,000	8,000	8,000	8,000	8,000
Σ vi	7,008	6,875	7,022	6,960	6,986	6,814	7,118	7,046	6,964	6,923	6,597	6,967
ΣA	0,798	0,863	0,823	0,880	0,521	0,944	0,545	0,922	0,878	0,598	0,561	0,891

*Structural formula of KB 749: recast to 24 (O,OH); H: 1,798; Fe includes 0,461 cations of Fe^{3+}.
n.d.: not determined; rock types are the same as in Table 14(i). Sample localities are given in Fig.9.

TABLE 15 - HORNBLENDE END-MEMBERS (SEE TABLES 14(i) AND (ii))

	A				D						E	
Sample	5	48	46	55b	498	132a	132b	468	436	353	54	KB 749
Richterite	-	12,5	-	4	3,8	1,8	5,6	1,4	18,6	-	3,3	4,3
Pargasite	58,5	61,3	54,8	69,5	44,3	84,2	69,7	49,3	56,9	53,6	65,3	47,5
Edenite	21,1	-	27,5	10,5	-	-	-	-	-	-	17,2	-
Tschermakite	-	5,8	-	-	13,7	10,9	20,4	21,4	16,0	5,8	-	36,0
Tremolite	12,2	17,6	9,1	11,7	29,8	-	-	24,4	5,0	34,2	8,4	8,6
Anthophyllite	8,0	2,7	8,6	4,3	6,9	2,7	4,3	3,5	2,5	6,4	5,8	3,6
Mg^{ox}	36,4	37,9	44,6	34,9	58,3	48,4	54,7	43,0	35,0	27,3	44,2	61,7

A: *two-pyroxene granulite*; D: *garnet-clinopyroxene granulite*; E: *amphibolite*.

TABLE 16 - MAIN OXIDE VARIATIONS IN HORNBLENDE (SEE TABLES 14(i) AND (ii))

	A	D	54	KB 749
SiO_2	40,69 - 41,68	40,15 - 45,42	41,65	45,07
TiO_2	2,19 - 3,26	1,31 - 3,00	1,97	0,44
Al_2O_3	10,59 - 12,15	10,85 - 16,98	11,98	13,10
*FeO	14,83 - 17,60	10,28 - 21,21	14,43	9,29
MgO	9,38 - 12,48	8,01 - 14,46	11,53	14,97
CaO	11,26 - 11,41	10,67 - 12,05	11,43	12,28
$Na_2O + K_2O$	3,21 - 3,74	1,99 - 4,02	3,68	2,12

* All iron as FeO.

A: two-pyroxene granulite; D: garnet-clinopyroxene granulite; 54 and KB 749: amphibolite.

(no. 132a, Table 14(i)). The data presented in Table 16 also suggest that hornblendes of amphibolites within high-grade terranes (no.54, Fig.9) may not be chemically distinguishable from those coexisting with pyroxenes in melanocratic granulites. In contrast, a published analysis from the northern Kirk Range (no. KB 749, Fig.9; Bloomfield and Garson, 1965, p.97) presents lower TiO_2 and FeO but higher SiO_2, Al_2O_3, MgO and CaO than the corresponding minerals from granulite facies terranes. As shown in Table 15, these chemical differences are reflected in a higher tschermakite / pargasite ratio for the Kirk Range sample.

Biotite compositions and structural formulae, listed in Table 17, indicate that the micas from two-pyroxene granulites and associated amphibolites are titanium-rich and transitional between biotite and phlogopite. Bulk chemical differences, suggested by the paragenesis garnet-hypersthene-biotite, may account for the appreciable content of Al^{VI} (siderophyllite component) in sample no.104 (see Fig.9). Like the amphibole from the northern Kirk Range (no. KB 749, Fig.9), the only mica analysis available from a low-grade area (no.KB 1097, Fig.9; Bloomfield, 1965b, p.30) is characterised by low TiO_2, FeO and high MgO. This is probably related to the bulk chemistry of the rock, which is a hypermelanic orthogneiss (see p.52). The mica is in fact a phlogopite since its Fe/Mg ratio is less

TABLE 17 - ELECTRON-MICROPROBE ANALYSES OF BIOTITE

	A	B	E	
Sample	48	104	54	KB1097**
No. of Analyses	$3\bar{M}$	$3\bar{M}$	$3\bar{M}$	1
SiO_2	36,38	36,18	36,98	37,74
TiO_2	5,60	5,33	4,54	2,68
Al_2O_3	13,53	14,90	13,72	13,57
*FeO	16,80	16,80	14,80	10,05
MnO	0,11	0,05	0,15	0,18
MgO	12,78	12,18	14,32	19,82
Na_2O	0,14	0,08	0,20	0,49
K_2O	10,59	10,45	10,64	8,75
BaO	-	-	-	1,80
H_2O	-	-	-	3,59
F	1,22	-	-	1,22
Total	95,93	95,97	95,35	99,89
CATIONS ON THE BASIS OF 22 OXYGENS				
Si	5,513	5,462	5,577	5,544
Al^{iv}	2,415	2,538	2,423	2,350
Al^{vi}	-	0,114	0,011	-
Ti	0,638	0,605	0,519	0,296
Fe	2,130	2,122	1,867	0,958
Mn	0,014	0,007	0,019	0,022
Mg	2,885	2,741	3,219	4,34
Na	0,040	0,023	0,058	0,140
K	2,047	2,011	2,047	1,753
Ba	-	-	-	0,069
H	-	-	-	3,521
F	-	-	-	0,567
ΣZ	7,928	8,000	8,000	7,894
ΣY	5,667	5,589	5,635	5,893
ΣW	2,087	2,034	2,105	1,961

*All iron as FeO; $\bar{M}$: average.
**FeO includes 2,50% Fe_2O_3; and structural formula is recast to 24 (O,OH,F) (after Bloomfield, 1965b, p.30).

A: two-pyroxene granulite; B: garnet-orthopyroxene granulite; E: amphibolite.

Sample localities are given in Fig.9. Individual analyses are listed in Appendix III-16.

than 0,5 (Deer et al., 1963). Plagioclase analyses are listed in Table 18 and they indicate an andesine (An_{39-45}) composition in accordance with petrographic observations.

Magnetite and ilmenite are typical accessory constituents in most rocks, and are particularly abundant in the melanocratic granulites, from which the analysed samples presented in Table 19 were selected. The composition of ilmenite, including one from an ilmenite-clinopyroxene symplectite (see Appendix III-13, no.353), is characterised by very low MgO, and MnO but traces of Al_2O_3. The electron-microprobe was also used to identify a silicate mineral from an albite-rich, garnet-bearing rock (no. 141, Fig.9) collected north of Tengani. Its chemical composition is simple (SiO_2 43,5 per cent; Al_2O_3 23,7 per cent; CaO 26,8 per cent) and matches that of prehnite if the balance to 100 per cent is due to water (see Deer et al., 1963).

3.3 Interoxide Relationships

(a) Pyroxene

In the literature much attention is paid to the partitioning of Fe and Mg between coexisting ortho- and clinopyroxene (Wood and Banno, 1973) because this parameter was found sensitive to the physical conditions of equilibration. In Fig.10, nearly all the tie-lines joining coexisting pyroxenes project to the enstatite-wollastonite side between Wo^{78} and Wo^{82}. Moreover they do not cross each other in the range Wo^{0-50}, a characteristic which is generally accepted as an indication of equilibrium

TABLE 18 - ELECTRON-MICROPROBLE ANALYSES OF PLAGIOCLASE FROM TWO-PYROXENE GRANULITE

Sample	55a	55b	5
No. of analyses	3M	3M	3M
SiO_2	56,68	55,69	57,81
Al_2O_3	26,50	26,51	25,56
CaO	9,01	9,51	8,16
Na_2O	5,91	5,72	6,79
K_2O	0,37	0,23	0,45
Total	98,47	97,66	98,77
CATIONS ON THE BASIS OF 32 OXYGENS			
Si	10,314	10,231	10,485
Al	5,682	5,739	5,462
Ca	1,757	1,871	1,584
Na	2,084	2,038	2,385
K	0,085	0,053	0,103
END MEMBERS			
or	2,18	1,36	2,54
ab	53,08	51,43	58,58
an	44,74	47,24	38,88

$\bar{M}$: average.

Sample localities are given in Fig.9. Individual analyses are listed in Appendix III-17.

TABLE 19 - ELECTRON-MICROPROBE ANALYSES OF ILMENITE AND MAGNETITE FROM GRANULITE

	ILMENITE				MAGNETITE
Sample	55	46	104	353	46
TiO_2	48,85	49,09	51,22	48,96	0,12
Al_2O_3	0,28	-	-	0,03	0,40
Cr_2O_3	0,02	-	-	0,08	0,23
*FeO	51,41	51,32	45,31	47,57	93,52
MnO	1,11	0,80	0,29	0,52	-
MgO	0,20	1,18	1,68	0,06	0,20
Total	101,87	102,39	98,61	97,22	94,27
CATIONS ON THE BASIS OF 6 OXYGENS					
Ti	1,864	1,858	1,964	1,936	
Al	0,017	-	-	0,002	
Cr	0,019	-	-	0,003	
Fe	2,182	2,161	1,932	2,092	
Mn	0,048	0,034	0,013	0,023	
Mg	0,015	0,089	0,128	0,005	
Σ iv	1,882	1,858	1,964	1,941	
Σ vi	2,245	2,283	2,073	2,120	

* All iron as FeO.

Structural formula of magnetite not calculated; poor totals relate to Fe_2O_3 or unsatisfactory microprobe working conditions.

Sample 46, 55, 104: two-pyroxene granulite.
Sample 353: garnet-clinopyroxene granulite.
Sample localities are given in Fig.9; individual analyses are listed in Appendix III-18.

crystallisation between mineral pairs. The main exception is represented by the pyroxenes of a garnet-bearing granulite (no. 436, Fig.3), which may indicate either a disequilibrium assemblage or an analytical imprecision, particularly on the iron determination, since metamorphic clinopyroxenes may

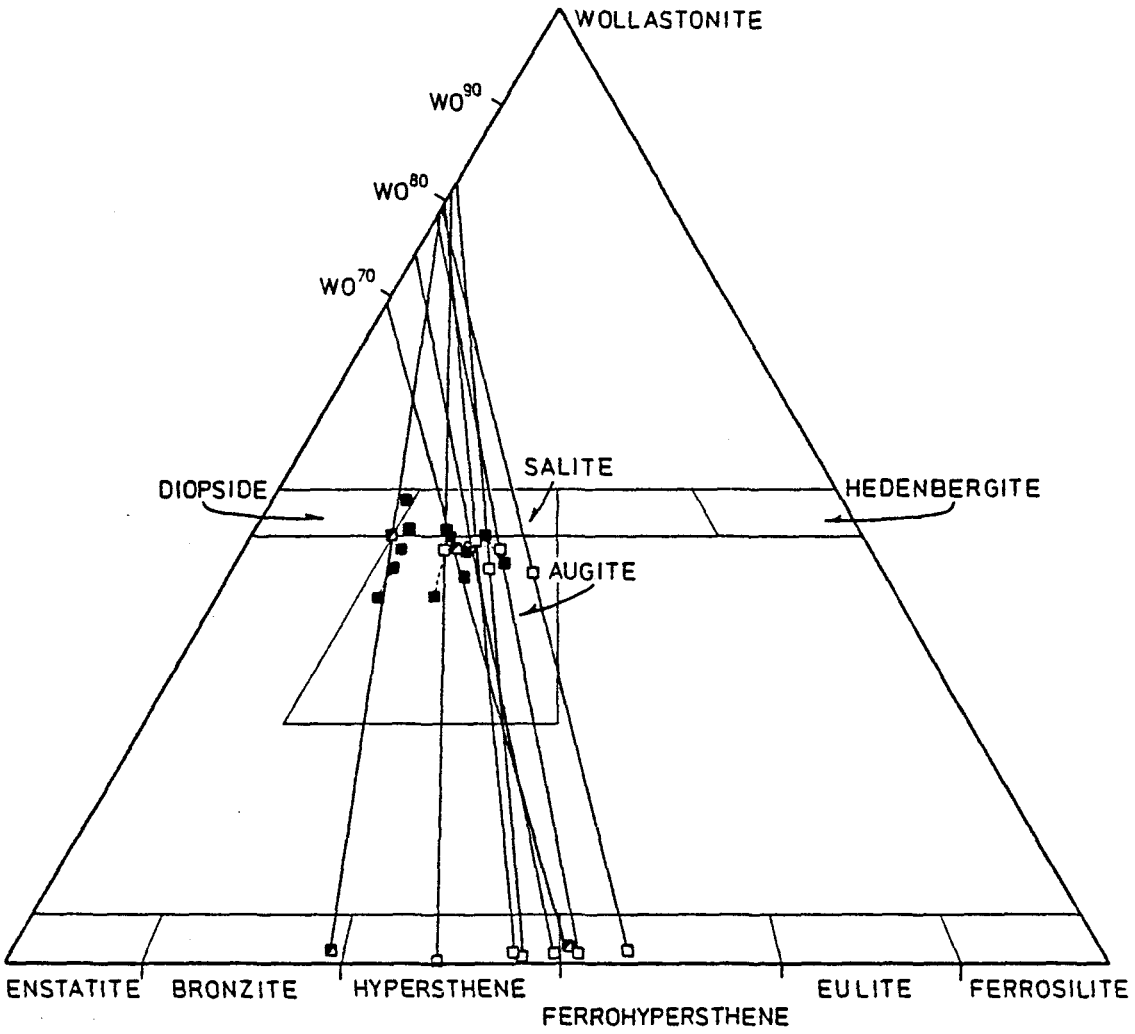


Fig.10. Distribution of wollastonite-enstatite-ferrosilite end-members in pyroxenes. Two-pyroxene granulites (□); garnet-clinopyroxene granulites (■); and garnet-two-pyroxene granulites (◩). Broken lines join analyses from zoned minerals and tie-lines join coexisting ortho- and clinopyroxenes.

contain a significant Fe_2O_3/FeO ratio (Deer et al., 1963). Attempts to recalculate the Fe^{3+} content from the structural formula with the scheme proposed by Cawthorn and Collerson (1974) do not however improve the plot significantly.

Equilibrium crystallisation for the majority of the pyroxenes is therefore suggested by the small variations in the composition of different grains from the same sample (see Tables 3 and 6), by the lack of visible zoning and by the rare overlapping of the tie-lines observed in Fig.10. The very same plot suggests a metamorphic origin for the hypersthene-augite granulites since the tie-lines intercept the wollastonite-enstatite join in the range of metamorphic pyroxene pairs (Bartholomé, 1962). A metamorphic origin for the clinopyroxenes of both pyroxene and garnet granulites is also suggested by Fig.11 in which all analyses except one plot in the appropriate field. The only pyroxene plotting in the igneous field (no. 436) occurs in a Type III prograde granulite which implies possible analytical errors. Fig.11 also indicates that augites in two-pyroxene granulites have in most cases not only a lower Al^{iv}, Al^{vi} content but also a lower Al^{vi}/Al^{iv} ratio than the clinopyroxenes coexisting with garnet. A few of the minerals have omphacitic affinities since they plot in the eclogitic field, but they are not true omphacites because their maximum Na_2O content (1,1 per cent) is well below the minimum accepted

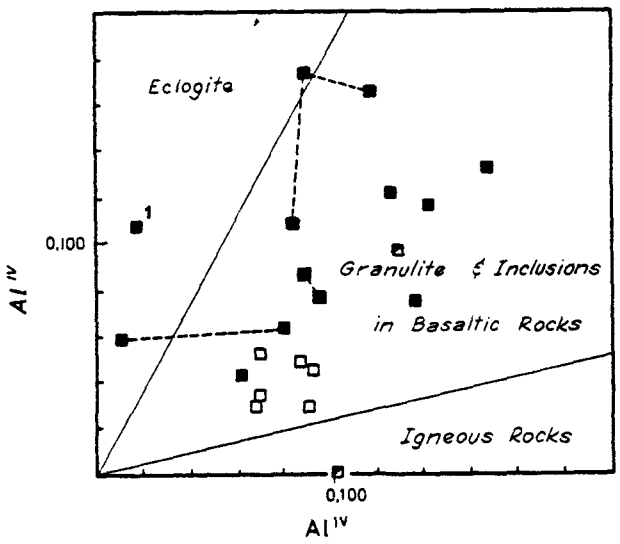
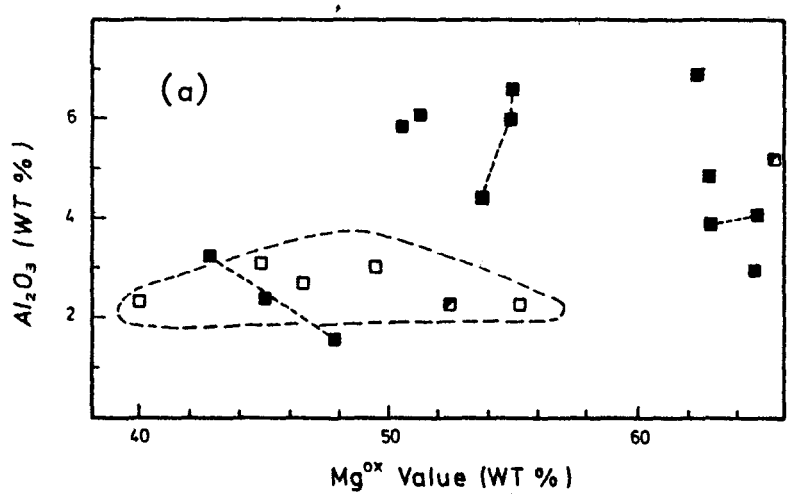


Fig.11. Distribution of Al^{iv} and Al^{vi} in clinopyroxenes. Two-pyroxene granulites (□); garnet-clinopyroxene granulites (■) and garnet-two-pyroxene granulites (◩). Labelled fields after Aoki and Kushiro (1968). See text for data on no.1.

value of 1,8 per cent (Deer et al., 1963). The same pyroxenes (nos. 133, 353b, 468) have $\Sigma_{xyz} < 4$ (see Table 8) and this may be related to observations by Cawthorn and Collerson (1974), that in omphacites the cation totals are statistically lower than the ideal 4,000. The data plotted in Fig.11 therefore may indicate that the garnet granulites did experience higher pressure than the two-pyroxene granulites.

Considering other interoxide relationships, various authors, particularly Wilson (1976a, b) have stressed the importance of the pyroxene gross composition as a control on the solubility of minor elements in their structure: in particular he suggested that alumina steadily increases with magnesia. To test Wilson's

studies, the variation of alumina relative to the magnesia content in clinopyroxenes is illustrated in Fig.12(a) where Al_2O_3 is plotted against Mg^{ox}, i.e. 100 MgO/(MgO + ΣFeO + MnO), in weight per cent. In this diagram the low-alumina clinopyroxenes from two-pyroxene granulites define a certain (outlined) trend; in contrast there is no trend at all amongst clinopyroxenes from garnet granulites. The flat-lying field suggests that the ratio Mg/Fe had a relatively minor effect on the concentration of Al in the augites. The higher concentrations shown by some minerals may therefore reflect other causes, such as the higher Al content of the rocks or differences in physical conditions during crystallisation. The distribution of the jadeite component in relation to ferrosilite is shown in Fig.12(b) where a number of clinopyroxenes, from the pyroxene granulites of Zomba, define a trend with a positive slope. This observation is consistent with the direct relationship existing between jadeite and ferrosilite in minerals recrystallised under the same P-T conditions and in rocks of comparable bulk chemistry (Wilson, 1976b). Fig.12(b) suggests that the higher jadeite content of some augites from garnet granulites cannot however be related solely to variations in ferrosilite component. On the contrary, since the minerals with higher jadeite are also more magnesian, the normalisation of the pyroxenes from garnet granulites with those from two-



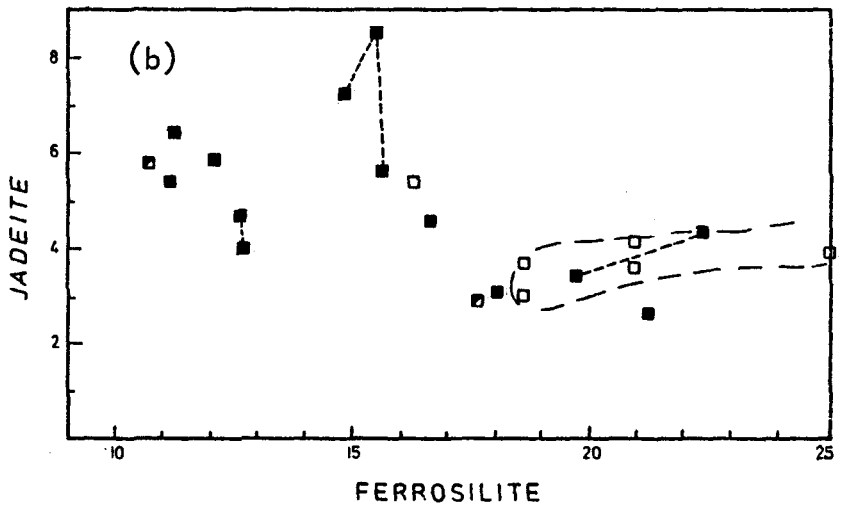


Fig.12(a). Distribution of Al_2O_3 and Mg^{ox} in clinopyroxenes. Two-pyroxene granulites (□); garnet-clinopyroxene granulites (■); and garnet-two-pyroxene granulites (◩). Broken lines join analyses of zoned pyroxenes; field of two-pyroxene granulites outlined.

Fig.12(b). Distribution of jadeite and ferrosilite in clinopyroxenes. Field of two-pyroxene granulites from Zomba outlined; for other symbols see explanation of Fig.12(a).

pyroxene rocks to the same ferrosilite value, as proposed by Wilson (1976b), would actually increase the differences between the two groups.

The relative proportions of the main components in the clinopyroxenes are shown in Fig.13 where the minerals from garnet and two-pyroxene granulites apparently occupy two fields. The garnet granulites are characterised by pyroxenes with a greater proportion of jadeite and Σtschermakite (Ca-Ti-tschermakite + Ca-Al-tschermakite) component perhaps related to a higher temperature and pressure of recrystallisation (Wilson, 1976b; Thompson, 1974).

(b) Garnet

In view of the interdependence of Mn and Fe in garnet, the affinity of spessartine and almandine components are shown in Fig.14 and illustrate a direct relationship, with a positive slope (see outlined field in Fig.14). In this diagram, a certain deficiency of spessartine of some of the garnets is probably related to their coexistence with orthopyroxene rather than clinopyroxene. Analytical data suggest that Mn enters preferentially into the hypersthene (range MnO in Table 3 = 0,45 - 1,26 per cent) than in augite-salite (range MnO in Tables 6 and 8 = 0,39 - 0,62 per cent), thus leaving less Mn available for solid solution in the coexisting garnet.

The composition of the garnets, expressed in terms of

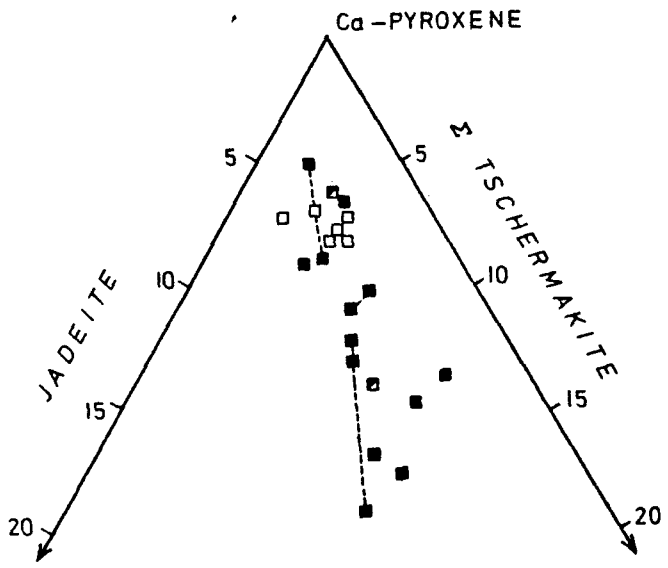


Fig.13. Distribution of jadeite - Σ tschermakite-Ca pyroxene end-members in clinopyroxenes. Broken lines join analyses of zoned pyroxenes. Symbols as in Figs.12(a) and (b).

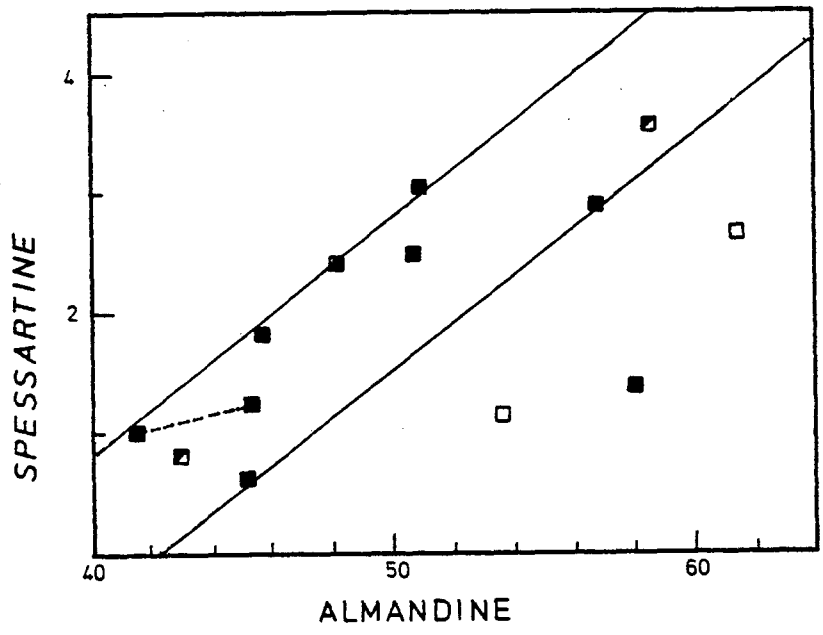


Fig.14. Distribution of almandine and spessartine end-members in garnets. Garnet-orthopyroxene granulites (□); garnet-clinopyroxene granulites (■); and garnet-two pyroxene granulites (◩). Broken line joins analyses of zoned garnet; for the field between lines, see text.

their end-members is shown in Fig.15, in relation to the fields typical of different metamorphic environments. Most of the analyses plot in the field where garnets from granulite and eclogite in medium- and high-grade terranes overlap (Winkler, 1974, p.262). Fig.15 also indicates that the grossular component is very low in the garnet associated to hypersthene but it becomes appreciable where Ca-rich augite is the only pyroxene present.

In a garnet-hornblende granulite from the northern Kirk Range (no.468, Fig.9) an eclogitic garnet (no.1, Fig.15) coexists with a clinopyroxene of omphacitic affinity (no.1, Fig.11); and it is likely that the host rock is transitional to eclogite.

It is now important to consider the distribution of Ca, Mg and Fe between coexisting garnet and clinopyroxene in view of recent studies on element partitioning (Raheim and Green, 1974; Ellis and Green, 1979). The cation proportions recalculated to 100 per cent from the structural formulae are plotted in Fig.16 where only one mineral pair exhibits tie-lines grossly discordant with the others and is probably related to the unknown Fe^{3+} content, zoning and differences in P-T conditions. The broad parallelism of most tie-lines in Fig.16 could be interpreted as indicating conditions of equilibrium between coexisting garnet and clinopyroxenes. In addition, a Mg-enrichment of certain clinopyroxenes relative to most others is remarkable, whilst zoning of both garnet

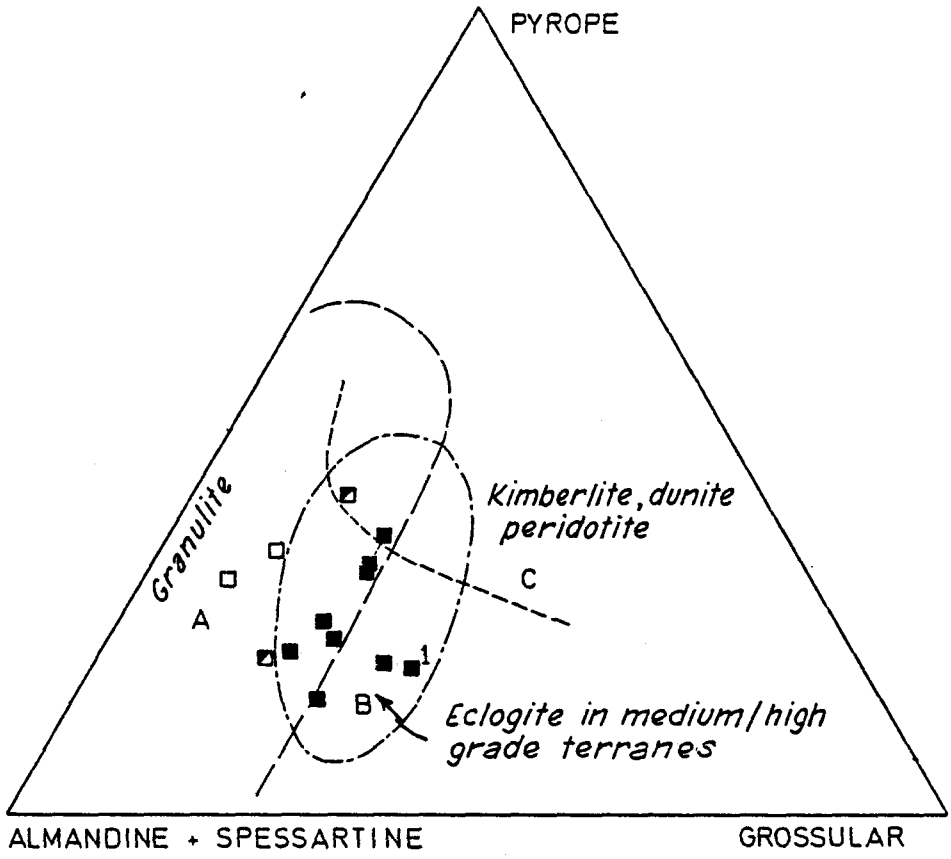


Fig.15. Distribution of end-members in garnet, showing the fields of garnet from granulite, eclogite, etc. from Winkler (1974, p.269). Garnet-orthopyroxene granulites (□); garnet-clinopyroxene granulites (■); and garnet-two-pyroxene granulites (◩). Broken line joins analyses of zoned garnet; for sample no.1 see text.

and clinopyroxenes in samples from Tengani (nos.132 and 498) is also significant (see Tables 8 and 11); and for this reason the tie-lines relate the compositions of adjacent garnet-clinopyroxene rims. In general, both petrographic and electron-microprobe data indicate that during the metamorphism in the Tengani area the Fe/Mg ratio increased in garnets (see Table 11) and decreased in clinopyroxenes (see Table 8). This may also be expressed by saying that the value of K_D = (Fe/Mg) ga: (Fe/Mg)cpx increased in these rocks during recrystallisation.

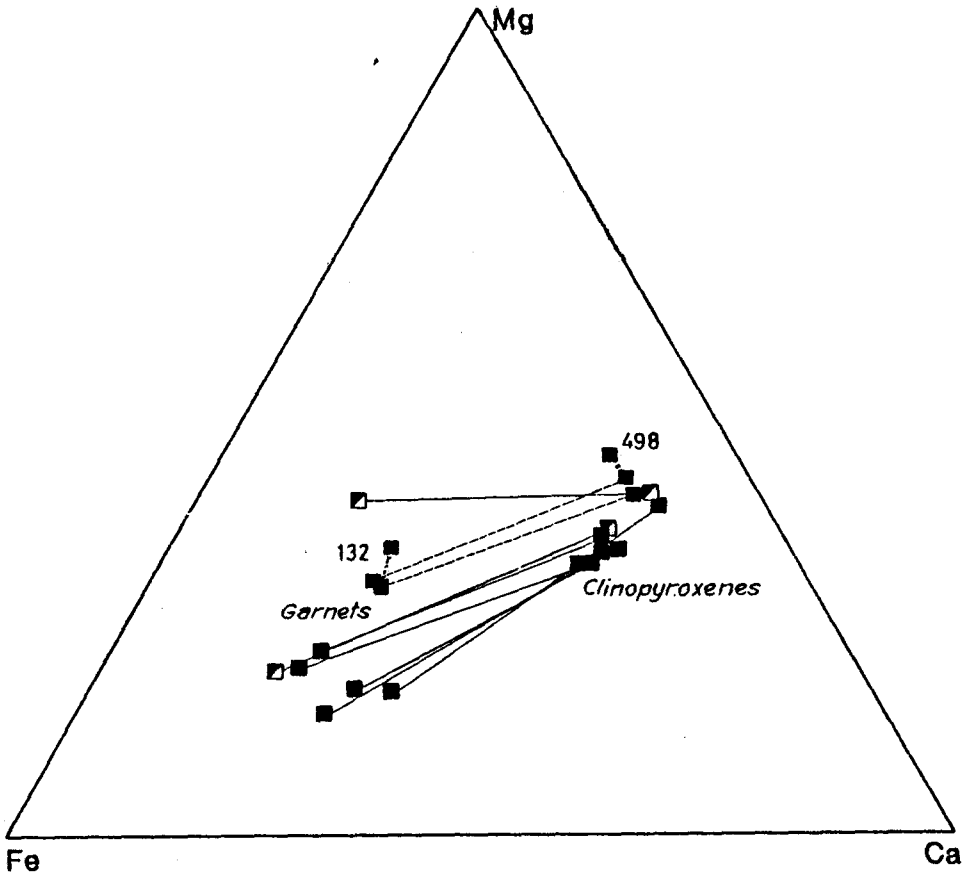


Fig.16. Distribution of Ca, Mg, Fe in coexisting garnet and clinopyroxenes from garnet-clinopyroxene granulites (■) and garnet-two-pyroxene granulites (◩); broken tie-lines link minerals nos. 132 and 498 from Tengani (see Fig.9); dotted lines join analyses of zoned minerals.

(c) Hornblende

Distribution of end-members amongst the hornblendes is investigated in Fig.17 where the main components (pargasite, edenite/tschermakite and tremolite + richterite) have been recalculated to 100 per cent. The last two components are added together since Deer et al., (1963) described these two amphiboles as formed under similar, low-grade environments. In the tschermakite triangle all amphiboles from garnet-

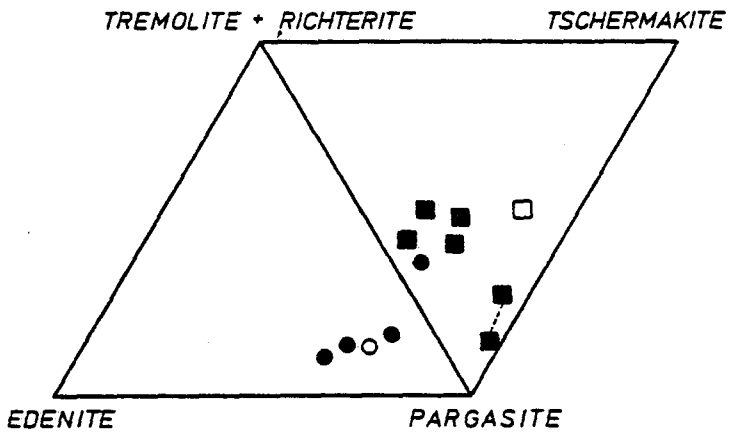


Fig.17. End members distribution in hornblendes. Two-pyroxene granulite (●), and an associated amphibolite (○); garnet-clinopyroxene granulite (■), and a related amphibolite (□). Dashed line joins analyses from the same sample.

clinopyroxene granulites and from associated amphibolite are plotted while in the edenite triangle most of the hornblendes from two-pyroxene granulites and associated amphibolite fall. The highest tschermakite content characterises a hornblende from Chimwadzulu (no. KB 749 Fig.9) for which the content of Fe^{3+} is known and therefore $Al^{'VI'}$ was taken as $(Al^{VI} + Fe^{3+} + Ti + Cr)$ following Misch and Rice (1975).

The interoxide variations in hornblendes are particularly complex because of the number of components present in the amphibole structure. The distribution of $Al^{'VI'}$ and Al^{IV} in hornblendes is shown in Fig.18(a) where most of the minerals from two-pyroxene granulites and a hornblende from a Zomba amphibolite (open dot) plot near the pargasite-edenite join. In contrast, the amphiboles from garnet-clinopyroxene

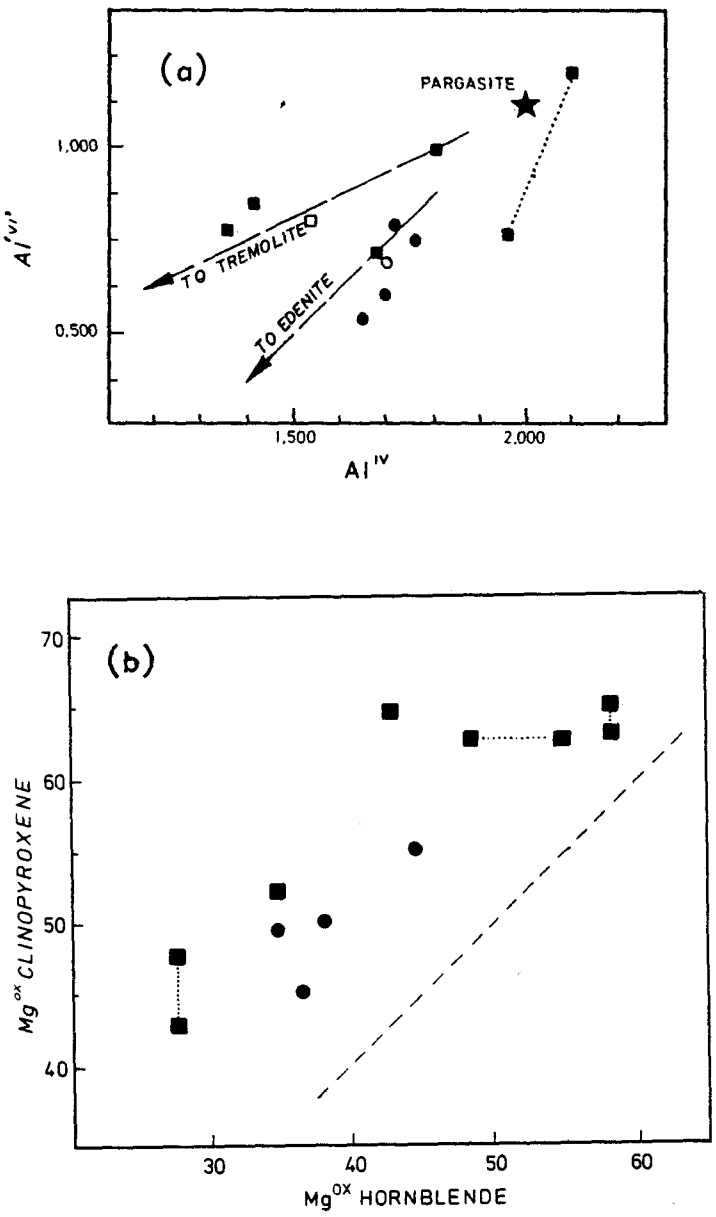


Fig.18(a). Distribution of Al^{IV} and $Al^{'VI'}$ (= Al^{VI} + Ti + Cr) in hornblendes. Two-pyroxene granulite (●) and an associated amphibolite (○); garnet-clinopyroxene granulite (■) and an associated amphibolite (□). Broken lines project towards amphibole end-members (Deer et al., 1963). Dotted line joins amphiboles from the same sample and (★) indicates where pargasite plots.

Fig.18(b). Distribution of Mg^{ox} (see p. 77) between hornblendes and associated clinopyroxenes. Dotted lines join analyses from the same sample and dashed line is trend of equal Mg^{ox} distribution.

assemblages and an amphibolite from Chimwadzulu (open square) are rather more scattered and in most cases they seem to plot along the tremolite-pargasite join.

The strict chemical relationships between hornblendes and associated clinopyroxenes are shown in Fig.18(b). In this plot the distribution of the Mg^{ox} values defines a crude trend with a positive slope which is parallel to and lying above the line of equal partitioning, indicating that magnesia is more abundant in the clinopyroxene.

The chemical characters of the hornblendes suggest that they equilibrated with their associated pyroxenes and/or garnet because substantial differences occur amongst amphiboles from different mineral assemblages. It is in fact significant that the clinopyroxenes and hornblendes coexisting with garnet have a higher $Al^{'VI'}/Al^{IV}$ ratio than those coexisting with orthopyroxene (see Figs. 11 and 18(a)). In addition, because tschermakitic amphibole is characteristic of hornblende eclogite (Deer et al., 1963), the more abundant jadeite component in clinopyroxene and tschermakite component in the associated amphibole are compatible with a common metamorphic environment of garnet granulite transitional to eclogite.

CHAPTER 4. PETROCHEMISTRY

4.1 Introduction

In this section the results of an extensive investigation on the chemical characteristics of the granulite facies rocks are presented and discussed. Most of these rocks were analysed for major and minor elements as well as Rb, Sr, Y, Zn and Nb. The granulites considered include melanocratic, mesocratic, leucocratic types and garnet granulites; but certain rock types such as khondalite, calc-silicate granulite and marble are omitted since their metasedimentary origin is generally undisputed. In addition to the granulites the chemical characteristics of about 18 gneisses and 11 amphibolite-granulite facies transitional rocks are also discussed, but the majority of the analyses of amphibolite facies gneisses used are taken from the literature. Finally whole-rock chemical analyses of 40 plutonic rocks are examined including amphibolite, metagabbro, metadolerite, Ring Complexes, Perthitic Complexes, granitoid orthogneisses and post-kinematic plutons.

The analytical data and analytical methods are given in Appendix IV, while the sample localities for the specimens analysed in this work are shown in Fig.19 and in Maps 1 to 4 in the pocket at the back of the thesis. A very generalised locality map for the published analyses is shown in Fig.20.

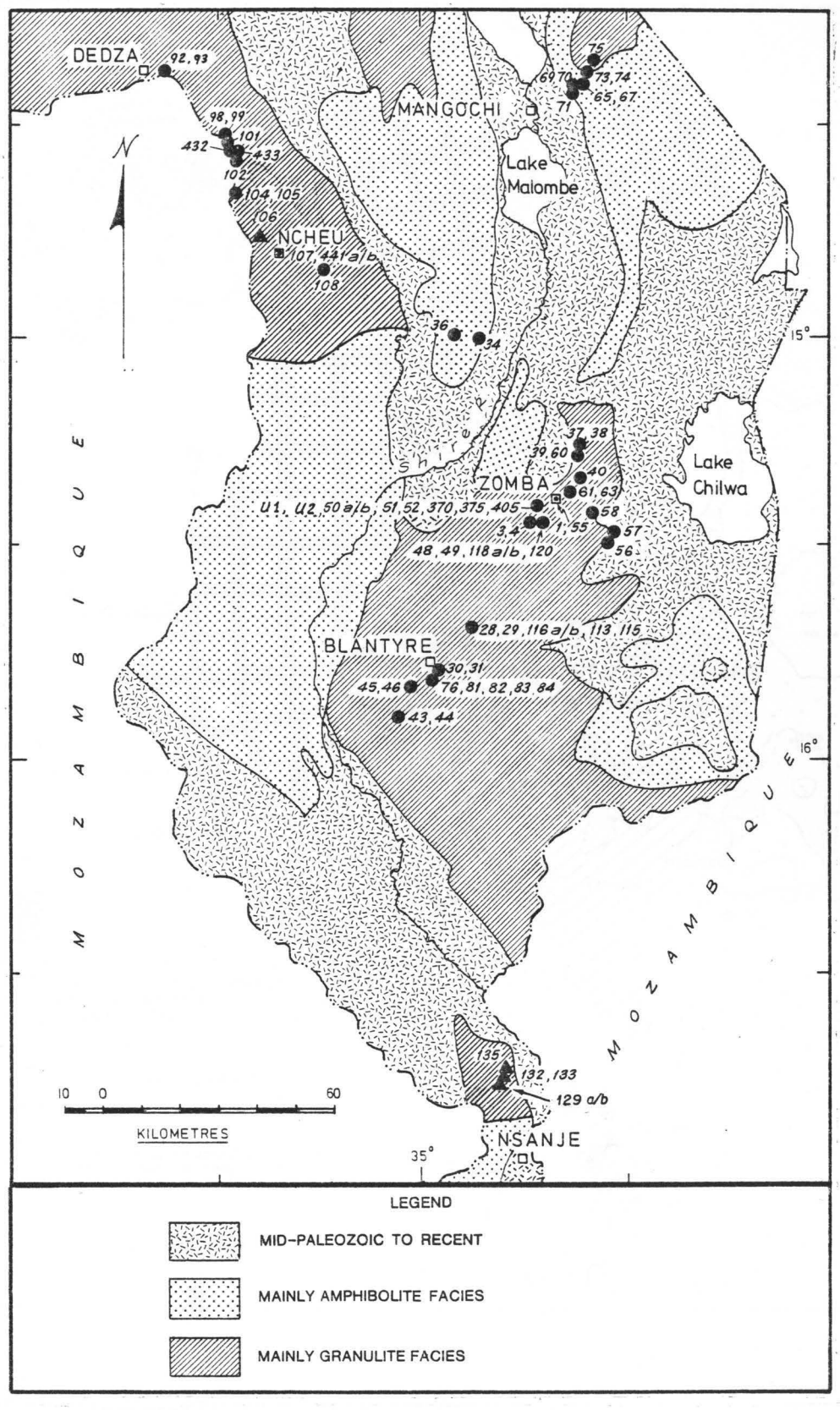


Fig.19. Locality map for analysed rock samples: orthopyroxene granulites (•); garnet-clinopyroxene granulites (▲); (modified after Bloomfield, 1968).

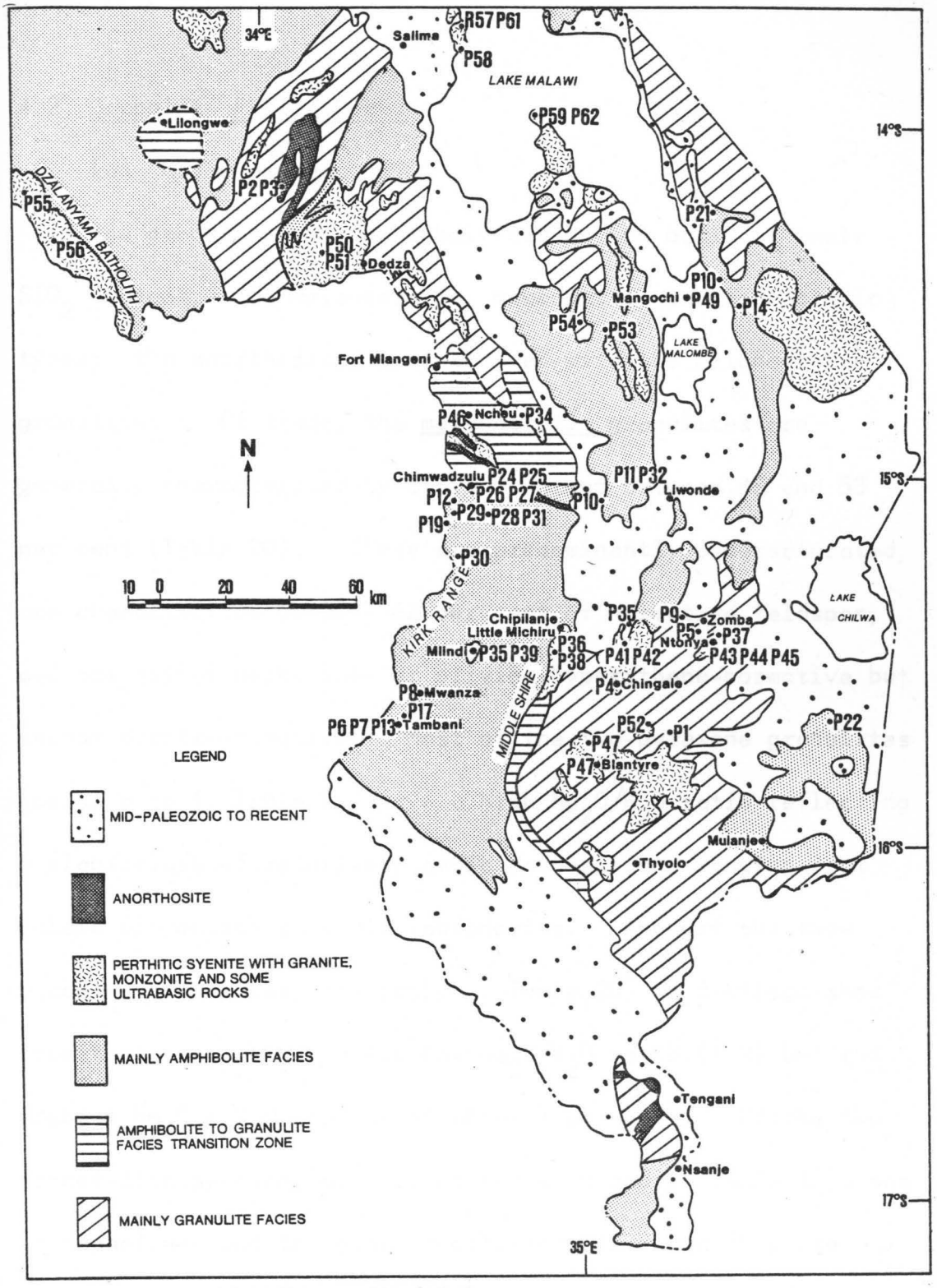


Fig.20. Generalised locality map for published rock analyses discussed in the text (modified after Bloomfield, 1968; Morel, 1961a).

4.2 Granulite Facies Rocks

(a) Major oxides

The granulites may be subdivided on the basis of their SiO_2 content, into melanocratic, mesocratic, and leucocratic types; the anorthosite is considered with the melanocratic granulites. Of these, the melanocratic granulites are generally characterised by a SiO_2 content between 43 and 53 per cent (Table 20). These are predominantly undersaturated, are characterised by 50 - 62 per cent of normative feldspar, and are either nepheline- or olivine-hypersthene-normative but seldom quartz-normative. Most of the two-pyroxene granulites (cols. a to f, Table 20) have a high Na_2O/K_2O ratio reflecting a plagioclase of relatively sodic composition, ranging from calcic oligoclase to sodic labradorite. Amongst the two-pyroxene granulites, one (col. d, Table 20) is distinguished from the other rocks by its low Na_2O/K_2O ratio (1.2) but the highest $Na_2O + K_2O$ content of about 7 per cent. Of the two garnet-clinopyroxene granulites (cols. h and i, Table 20), one is nepheline- and the other quartz-normative and they are markedly dissimilar from the other melanocratic rocks in their low Na_2O and K_2O contents and the high FeO, FeO/Fe_2O_3, MgO, and CaO contents. Table 20 also lists four analyses of anorthosite

TABLE 20 - COMPOSITIONS OF MELANOCRATIC GRANULITES AND ANORTHOSITE

	(a)	(b)	(c)	(d)	(e)	(f)	(g)	(h)	(i)	(j)	(k)	(l)	(m)
No. of analyses	1	1	1	1	4$\bar{M}$	1	1	1	1	1	1	1	1
SiO_2	43,01	43,56	48,20	49,60	50,32	51,70	51,92	46,17	46,69	49,74	51,40	52,17	57,87
TiO_2	4,30	2,48	1,69	1,39	1,81	1,73	1,57	1,41	3,41	0,16	0,44	0,15	0,11
Al_2O_3	14,62	15,89	15,02	17,09	15,00	13,91	15,48	14,23	14,10	27,16	28,95	28,43	26,87
Fe_2O_3	3,60	1,94	5,70	3,91	3,18	7,01	4,08	1,51	1,56	1,13	0,11	0,34	0,05
FeO	13,22	11,68	7,22	5,53	8,38	7,88	9,02	11,22	14,00	1,87	0,86	0,98	0,09
MnO	0,23	0,26	0,21	0,23	0,20	0,26	0,16	0,11	0,17	0,05	0,01	0,02	-
MgO	5,48	7,15	6,75	4,46	5,77	4,24	6,52	9,49	6,14	2,12	0,35	1,14	-
CaO	9,07	10,15	9,78	8,28	8,38	7,50	5,14	13,14	10,26	13,53	12,90	12,18	9,09
Na_2O	2,76	2,13	3,63	3,89	3,79	4,66	3,70	2,17	1,23	3,22	4,00	4,00	5,18
K_2O	0,60	1,21	0,99	3,03	1,25	0,61	1,01	0,42	0,48	0,21	0,31	0,56	1,03
P_2O_5	0,91	0,19	0,17	0,19	0,30	0,20	0,24	0,09	0,68	0,37	-	0,01	0,09
H_2O-	0,06	0,04	0,06	0,21	0,05	-	0,05	0,06	-	-	-	0,03	0,11
H_2O+	0,49	0,09	0,17	0,60	0,34	-	0,46	0,19	-	0,47	0,41	0,40	0,24
Total	98,35	98,07	100,41	99,41	98,77	99,35	99,37	100,21	98,79	100,13	99,74	100,41	100,73
CIPW NORMATIVE MINERALS (MOLECULAR PERCENTAGES)													
q	-	-	-	-	-	1,91	1,69	-	2,9	-	-	-	4,14
or	3,72	7,50	5,93	18,31	7,50	3,68	6,08	2,51	3,01	1,77	1,7	3,25	5,93
ab + an	53,01	47,70	53,05	46,43	55,45	58,24	56,92	40,43	44,81	86,39	94,2	91,60	88,58
ne	-	2,42	1,19	5,96	-	-	-	4,23	-	-	-	0,28	-
c	-	-	-	-	-	-	-	-	-	-	-	-	0,93
di + he	13,80	15,85	20,76	16,04	15,80	16,43	1,04	29,52	12,59	4,70	1,2	1,88	-
fo + fa	14,09	20,35	10,29	6,69	7,29	-	-	19,57	-	1,21	-	2,42	-
en + fs	3,12	-	-	-	7,39	8,93	27,18	-	28,49	2,62	0,8	-	-
ap	2,00	0,42	0,36	0,41	0,62	0,43	0,51	0,19	1,5	0,76	-	0,02	0,18
ma	3,95	2,13	6,03	4,18	3,39	7,48	4,34	1,58	1,72	1,16	0,2	0,35	-
il	6,29	3,62	2,38	1,98	2,56	2,46	2,23	1,97	5,00	1,34	0,7	0,2	0,15
An%	52	68	43	46	39	28	42	69	75	68	64	63	48

*: low totals are related to little carbonate, as observed in thin sections; $\bar{M}$: average. See p.92 for rock types.

TABLE 20 - COMPOSITION OF MELANOCRATIC GRANULITES AND ANORTHOSITE

(a) Two-pyroxene granulite: (29).

(b) Two-pyroxene-hornblende granulite: (48).

(c) Two-pyroxene granulite: (46).

(d) Charnockitic granulite: (P1).

(e) Average of melanocratic two-pyroxene ± hornblende granulites: (28), (40), (61) and (99).

(f) Two-pyroxene-hornblende granulite: (38).

(g) Orthopyroxene-plagioclase granulite: (107).

(h) Garnet-clinopyroxene-hornblende granulite: (132).

(i) Garnet-clinopyroxene-quartz granulite: (129).

(j) Gabbroic anorthosite: (P2).

(k) Anorthosite: (P3).

(l) Garnet-clinopyroxene-hornblende anorthosite: (106).

(m) Anorthosite: (135).

Numbers in brackets are samples from localities shown in Fig.19 and in Maps 1 to 3 in the pocket at the back of the thesis.

Analyst: M. Andreoli except for no.61, which was analysed by A.Bemath and for numbers preceded by P which are published analyses from localities shown in Fig.20.

Individual unpublished analyses are listed in Appendix IV-8; data sources for published analyses are listed in Appendices IV-9 and IV-10.

(cols. j to m), including nepheline-, diopside- and quartz-corundum-normative types. The recalculated feldspar ranges from Ca-labradorite (An_{68}) to andesine (An_{48}); K-feldspar is only a minor component.

The mesocratic granulites comprise banded and massive rocks in which SiO_2 ranges from 53 to less than 62 per cent (see Table 21); most of these rocks are quartz-, rather than olivine-normative; diopside is always present in the norm. However, the majority of the granulites seem to fall into two groups distinguished by their K_2O. In the main group (cols. b, c, and f, Table 21) K_2O is less than about 2 per cent and normative sodic andesine ($\simeq An_{35}$) constitutes between 50 and 74 per cent of the total. In the other groups (cols. d, e, g, h, and i, Table 21) K_2O is generally about 4 per cent or above that percentage and these rocks have a greater proportion (60 - 80 per cent) of normative albite + orthoclase. The garnet-clinopyroxene granulites (cols. k to h, Table 21) differ from the other groups being K_2O-poor and with a normative plagioclase which makes up between 47 and 65 per cent of the total.

The leucocratic granulites include a variety of types: perthite-rich orthopyroxene-bearing rocks, quartz-, and plagioclase-rich granulites, with or without biotite and garnet, and quartzo-feldspathic granoblastites (see Table 22). The silica content of these rocks is taken to be higher than 65 per cent SiO_2; however there are only two analyses of granulites with a SiO_2 content between 63 and 66 per cent

TABLE 21 - COMPOSITIONS OF MESOCRATIC GRANULITES

	(a)	(b)	(c)	(d)	(e)		(f)		(g)	(h)	(i)	(j)	(k)	(l)	(m)	(n)
No. of analyses	1	$2\bar{M}$	1	1	$6\bar{X}$	σ	$6\bar{X}$	σ	$2\bar{M}$	1	1	$2\bar{M}$	1	1	1	1
SiO_2	54,05	55,95	56,63	56,82	58,72	0,77	60,86	2,78	61,56	61,80	62,14	62,34	53,51	53,67	58,29	61,62
TiO_2	2,36	1,12	0,91	1,35	1,39	0,44	1,09	0,31	0,63	0,88	1	0,78	1,35	0,98	0,89	1,03
Al_2O_3	15,13	20,24	16,87	16,67	16,98	0,77	15,97	1,33	17,47	16,63	18,29	17,57	17,89	16,24	16,84	15,93
Fe_2O_3	12,74[△]	2,17	3,92	3,69	3,23	0,19	1,73	1,16	3,39	1,34	4,1[△]	0,75	2,41	1,13	1,73	1,82
FeO		3,30	4,67	3,90	*3,13	0,21	**4,7	1,05	3,28	4,34		3,86	6,03	7,73	5,86	4,77
MnO	0,16	0,11	0,18	-	0,09	0,04	0,12	0,04	0,19	0,09	-	0,08	0,05	0,16	0,14	0,11
MgO	2,49	2,35	3,81	3,18	2,17	0,45	2,74	0,76	0,13	2,19	1,11	2,64	3,88	6,20	3,04	2,39
CaO	6,80	6,80	6,98	4,86	4,27	0,15	5,35	1,01	3,5	4,03	2,73	5,00	8,54	9,26	6,38	4,58
Na_2O	3,35	5,34	4,60	4,44	4,54	0,19	4,40	0,34	4,14	3,72	3,64	4,34	4,53	3,36	4,05	3,42
K_2O	2,48	1,53	1,00	3,72	4,68	0,17	1,46	0,43	5,23	4,63	6,91	2,21	1,26	1,01	2,40	4,02
P_2O_5	1,26	0,33	0,15	0,93	0,72	0,03	0,26	0,09	0,16	0,35	0,32	0,25	0,32	0,26	0,38	0,29
H_2O	0,11	0,13	0,10	0,16	0,08	0,08	0,07	0,03	0,04	-	0,11	0,05	0,10	-	-	-
H_2O+	-	0,22	0,14	0,29	0,35	0,05	0,37	0,32	-	-	0,45	0,22	0,08	-	-	-
Total	100,93	99,59	100,49	100,01	100,35		99,12		99,79	100,0	100,8	100,09	99,95	100	100	100
CIPW NORMATIVE MINERALS (MOLECULAR PERCENTAGES)																
q	8,53	1,63	5,9	3,82	4,20		12,66		9,15	9,48	7,95	11,57	-	0,35	6,52	11,33
or	15,07	8,97	5,93	22,06	27,65		8,77		31,29	27,42	44,28	13,05	7,46	5,96	14,14	23,97
ab + an	50,33	74,30	63,90	54,61	52,82		59,96		51,20	46,59	47,76	59,66	65,35	56,31	54,75	47,32
di + he	n.c.	3,80	8,99	2,74	3,48		4,33		1,76	2,26	n.c.	1,01	12,41	14,34	7,01	3,70
fo + fa	-	-	-	-	-		-		-	-	-	-	1,84	-	-	-
en + fs	n.c.	6,75	9,57	9,05	5,05		10,35		1,64	10,17	n.c.	11,28	7,86	19,95	12,56	9,69
ap	n.c.	0,68	0,31	1,96	1,51		0,55		0,18	0,82	n.c.	0,53	0,67	0,54	0,88	0,61
ma	n.c.	2,25	4,11	3,87	3,37		1,84		0,89	1,58	n.c.	0,78	2,52	1,18	2,5	1,92
il	n.c.	1,55	1,27	1,88	1,93		1,54		0,44	1,68	n.c.	1,08	1,88	1,36	1,68	1,45
An%	40	37	37	28	24		34		29	32	27	37	39	48	38	36

$\bar{X}$: arithmetic mean; σ: standard deviation; $\bar{M}$: average; *: except 441b; **: except 69. n.c.: non calculated. See p.95 for rock types.

[△] All iron as Fe_2O_3.

TABLE 21 - COMPOSITION OF MESOCRATIC GRANULITES

(a) Porphyritic pyroxene-hornblende granulite: (405).

(b) Average of plagioclase-rich pyroxene granulites: (101) and (P4).

(c) Pyroxene granulite: (102).

(d) Perthite-rich granulite: (441a).

(e) Average and standard deviation of pyroxene-perthite ± hornblende granulites: (76), (81), (82), (83), (84) and (441b).

(f) Average of pyroxene ± hornblende-biotite granulites: (45), (49), (69), (98), (116a) and (118a).

(g) Average of perthite-rich pyroxene granulites: (74) and (75).

(h) Biotite-orthopyroxene granulite: (P5).

(i) Perthite-rich pyroxene granulite: (432).

(j) Average of pyroxene granulites: (118b) and (120).

(k) Garnet-clinopyroxene-quartz granulite (133).

(l), (m), (n) Clinopyroxene-hornblende-garnet-biotite granulites: (P6), (P7) and (P8) respectively.

Numbers in brackets are samples from localities shown in Fig.19 and in Maps 1 to 3 in the pocket at the back of the thesis.

Analyst: M. Andreoli except for numbers preceded by P which are published analyses of samples from localities shown in Fig.20. Individual unpublished analyses are listed in Appendix IV-8; data sources of individual published analyses are listed in Appendices IV-9 and IV-10.

(see nos. 45 and 116a, Appendix IV-8).

Considering the other oxides, the rocks are in some cases markedly sodic (cols. b, c, e, k, l, and m, Table 22), less

TABLE 22 - COMPOSITIONS OF LEUCOCRATIC GRANULITES

	(a)	(b)	(c)	(d)	(e)	(f)	(g)	(h)	(i)	(j)	(k)	(l)	(m)
No. of analyses	$2\bar{M}$	$2\bar{M}$	1	$2\bar{M}$	$4\bar{M}$	1	1	1	1	$4\bar{M}$	$3\bar{M}$	$2\bar{M}$	1
SiO_2	66,30	67,46	67,85	68,08	69,00	71,37	71,78	73,10	73,15	74,31	74,51	77,77	78,56
TiO_2	0,81	0,66	0,31	0,57	0,52	0,44	0,09	0,15	0,25	0,22	0,28	0,20	0,10
Al_2O_3	14,53	16,35	18,71	15,24	14,62	14,79	14,48	14,51	13,86	12,73	12,28	11,72	12,22
Fe_2O_3	0,96	1,29	2,85*	0,85	1,40	0,98	0,73	0,21	2,14	0,91	1,46	1,41	0,79
FeO	5,04	2,29		3,21	3,48	1,59	1,62	0,60	0,87	0,97	2,80	1,79	0,34
MnO	0,14	0,06	0,06	0,07	0,09	0,06	0,0	-	0,07	0,02	0,09	0,05	0,03
MgO	0,93	1,12	0,32	0,91	1,30	0,68	t	t	-	0,22	0,96	0,45	-
CaO	2,75	4,33	2,16	2,68	3,93	2,73	1,08	1,37	1,9	1,76	1,96	3,38	1,5
Na_2O	3,68	5,00	6,73	3,12	4,13	3,67	2,53	3,83	4,72	3,52	4,59	2,98	4,57
K_2O	4,36	1,03	1,53	4,39	0,67	3,48	7,86	5,85	2,89	4,36	0,97	0,36	2,22
P_2O_5	0,13	0,16	0,06	0,16	0,13	0,09	0,05	0,04	0,06	0,05	0,05	0,02	0,03
H_2O-	0,0	0,06	0,07	0,05	0,05	0,02	0,13	0,16	0,04	0,05	0,05	0,03	0,05
H_2O+	0,11	0,26	0,26	0,32	0,33	0,34	0,26	0,45	0,52	0,32	0,19	0,18	0,19
Total	99,74	100,07	100,91	99,65	99,81	100,24	100,61	100,27	100,47	99,44	100,19	100,32	100,6
CIPW NORMATIVE MINERALS (MOLECULAR PERCENTAGES)													
q	17,38	21,60	14,95	23,11	28,73	27,52	22,26	23,81	28,94	31,58	35,27	48,00	37,79
or	26,21	6,12	8,87	26,48	4,04	20,80	46,94	34,8	17,25	26,35	5,83	2,19	13,21
ab + an	43,99	64,23	69,37	41,06	56,81	46,40	27,87	39,68	50,88	38,48	51,05	44,67	47,59
c	-	-	2,35	0,96	0,03	0,26	-	-	-	-	0,43	0,37	-
di + he	2,08	1,08	-	-	-	-	0,07	1,08	-	1,32	-	-	-
en + fs	7,91	4,41	n.c.	6,33	7,42	3,18	1,84	-	1,81	0,26	5,81	2,92	-
ap	0,28	0,32	n.c.	0,34	0,28	0,19	0,11	0,08	0,35	0,11	-	0,04	0,06
ma	1,02	1,35	"	0,91	1,61	1,04	0,77	0,29	0,38	0,97	1,55	1,52	0,53
il	1,15	0,92	"	0,81	0,81	0,62	0,13	0,21	0,39	0,31	0,40	0,29	0,22
An%	25	31	15	32	35	29	18	14	17	17	20	40	14

$\bar{M}$: average; n.c.: non calculated; t: traces. See p. 97 for rock types.
* All iron as Fe_2O_3.

TABLE 22 - COMPOSITION OF LEUCOCRATIC GRANULITES

(a) Average of perthite-rich pyroxene granulites: (65) and (73).

(b) Average of leucocratic, plagioclase-rich granulites: (63) and (P9).

(c) Oligoclase-rich garnet granulite: (375).

(d) Average of garnet-pyroxene granulites: (55) and (P10).

(e) Average of quartz-plagioclase-rich ± biotite granulites: (37), (44) and (U1).

(f) Orthopyroxene-biotite granulite: (1).

(g) Perthite-rich charnockite: (115).

(h) Perthite-rich pyroxene granulite: (433).

(i) Plagioclase-biotite-pyroxene granulite: (39).

(j) Average of quartzo-feldspathic granoblastites: (57), (60), (113), and (116b).

(k) Average of plagioclase-biotite-pyroxene granulites: (51), (52) and (370).

(l) Average of plagioclase-rich, pyroxene-poor granulites: (3) and (U2).

(m) Quartzo-feldspathic granoblastite: (56).

Numbers in brackets are samples from localities shown in Fig.19 and in Maps 2 and 3 in the pocket at the back of the thesis.

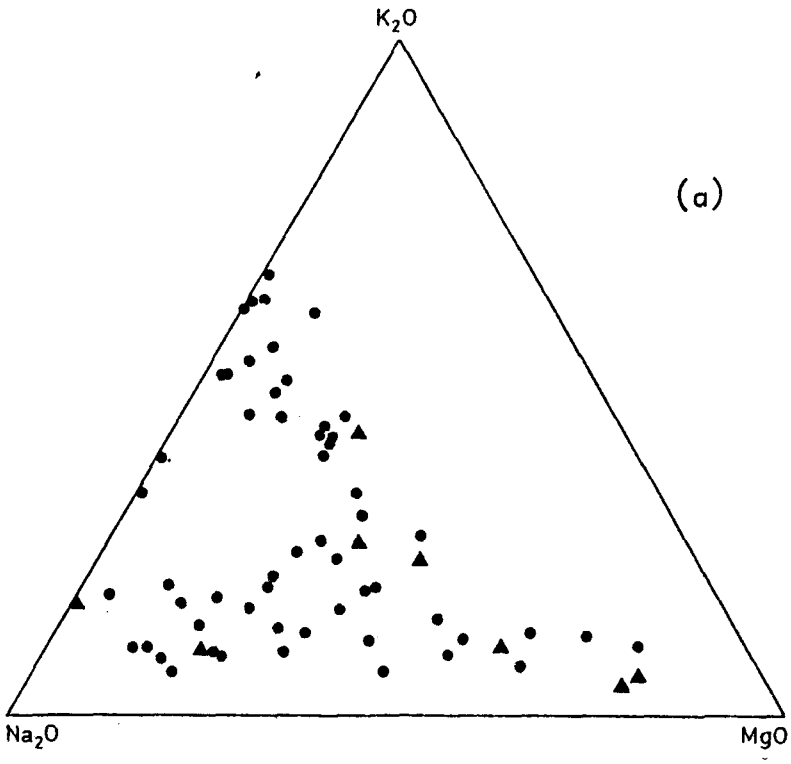
Analyst: M. Andreoli, except for samples nos. 44, 56 and 60 which were analysed by A. Bemath and nos. U1 and U2, which are unpublished analyses by E. Pinkney of Leeds University of samples from localities shown in Fig.19. Numbers preceded by P are published analyses of samples from localities shown in Fig.20.

Individual unpublished analyses are listed in Appendix IV-8; data sources of published analyses and individual compositions are listed in Appendices IV-9 and IV-10.

commonly potassic (cols. g, and h, Table 22), and in the remaining cases their alkali content is fairly well balanced ($Na_2O \approx K_2O$).

In the sodic group the normative albite constitutes between 30 and 40 per cent of the total and the normative plagioclase composition ranges from andesine (An_{35}) to oligoclase (An_{14}). In nearly all samples the albite/quartz ratio is greater than 1, while the albite/orthoclase ratio may be as high as 11; most of these analyses are either diopside- or only slightly corundum-normative. In two samples (col. 1, Table 22) Na_2O and K_2O are markedly lower than in all other leucocratic granulites. In the more potassic rocks (cols. g and h, Table 22) the MgO content is very low.

Despite the number of available chemical analyses, an average chemical composition for the southern Malawi granulites cannot be reliably calculated owing to the great variability of rock types encountered and to their largely unknown percentage of distribution. The broad chemical characters of this suite may however be investigated with the aid of the variation diagrams. When granulite facies rocks analyses are plotted in a K_2O-Na_2O-MgO diagram (Fig.21(a)) a 'Y'shaped field results, suggesting that low-magnesia granulites tend to be either potassic or sodic in character. In a plot of A (K_2O + Na_2O), F (total iron as FeO), and M (MgO) the granulites define a relatively narrow trend (Fig.21(b)), marked by variable proportions of alkalis.



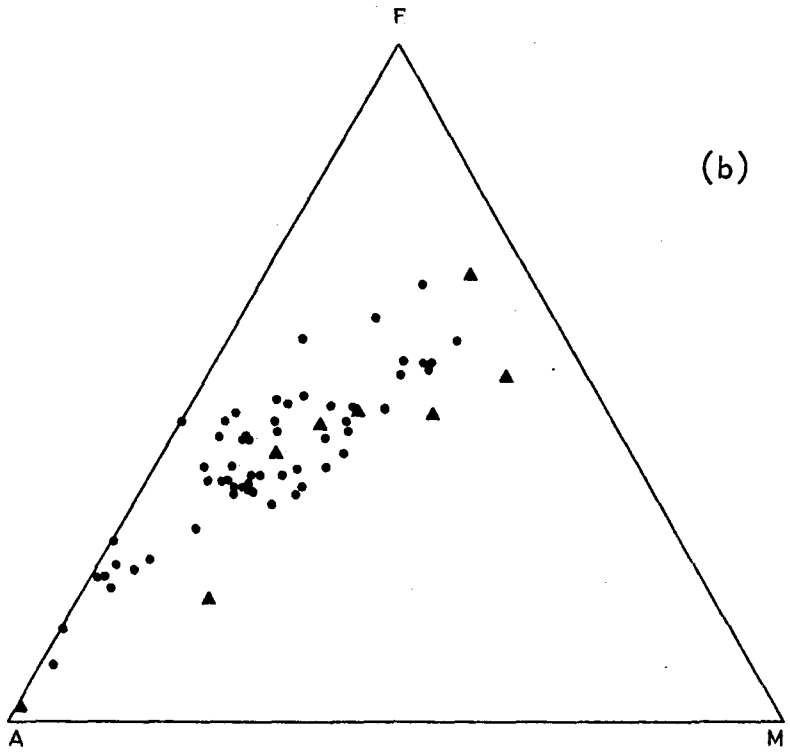


Fig.21(a). Na_2O-K_2O-MgO diagram (weight per cent) of all two-pyroxene granulites, (•); and garnet-clinopyroxene granulites, (▲) listed in Tables 20 to 22.

Fig.21(b). AFM diagram of all granulites listed in Tables 20 to 22. Symbols are the same as Fig.21(a).

The distribution of the alkalis in relation to silica amongst the granulites is shown in Fig.22 in which the majority of the two-pyroxene and garnet granulites define a broad trend.

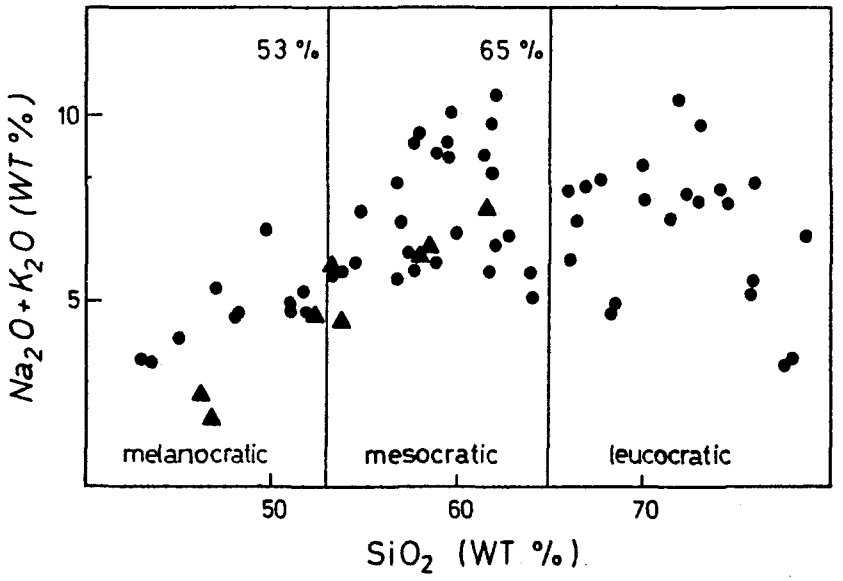


Fig.22. Distribution of (Na_2O+K_2O) and SiO_2 in all granulites listed in Tables 20 to 22. Two-pyroxene granulites, (●); and garnet-clinopyroxene granulites, (▲).

On the basis of their inter-oxide relationships the granulites appear as a suite of rocks characterised by a gradual increase both in silica and alkalis with a decrease in Fe and Mg (Figs. 21 to 22). The recalculated CIPW mineral compositions also indicate that the granulites are generally diopside-normative.

Few analytical data are available for garnet-clinopyroxene rocks; however sodic plagioclase generally predominates over K-feldspar in mesocratic to leucocratic types from the northern Kirk Range (no.500 in Appendix I-2 and no.501 in Map 2 in the pocket at the back of the thesis)and from many parts of central

Malawi (Bloomfield and Garson, 1965; Thatcher and Walter, 1968; Walter, 1972b; Bellingham and Broomley, 1973; Peters, 1969). It seems likely that these rocks are chemically akin to the main type of two-pyroxene granulites.

A few samples from the Tengani area (see Fig.19) were also analysed for Cl and S since the two light elements may be contained in scapolite. The results are presented in Table 23 which indicates that the chlorine content is directly related to the presence of (marialite-bearing) scapolite. Sulphur is probably present in larger opaque minerals and in minute opaque inclusions within scapolite and plagioclase (see Plate 19).

TABLE 23 - CHLORINE AND SULPHUR CONTENT IN SCAPOLITISED GRANULITES FROM TENGANI

Locality nos.	Cl ppm	S ppm	Rock type
132	2 460	780	Scapolite-rich melanocratic granulite.
129a	580	2 440	Scapolite-poor melanocratic granulite.
129b	360	5	Scapolite-poor anorthosite.
133	90	5	Scapolite-free mesocratic granulite.

For sample localities see Fig.19.

(b) Trace elements

The concentration of rubidium, strontium, yttrium, zirconium, niobium within the melanocratic, mesocratic and leucocratic granulites (listed in Tables 20 to 22) is summarised in Tables 24 to 26. The data presented in these Tables indicate that only Sr and Zr are present in appreciable

TABLE 24 - SELECTED TRACE ELEMENTS IN MELANOCRATIC GRANULITES

(1) Locality nos.	(29)	(48)	(46)	$\bar{M}1$	(38)	(107)	(106)
Rb	11	22	7	13	8	14	6
Sr	238	208	269	277	150	476	449
Y	68	29	29	35	37	26	3
Zr	273	109	85	136	52	65	33
Nb	31	5	5	7	-	4	-

(1) For sample localities see Fig.19. Individual trace elements concentrations are listed in Appendix IV-8.

$\bar{M}1$: average of samples nos. 28, 40, 61 and 99.

TABLE 25 - SELECTED TRACE ELEMENTS IN MESOCRATIC GRANULITES

*Locality nos.	(101)	(102)	$\bar{M}1$	$\bar{X}1$	σ	$\bar{M}2$	$\bar{M}3$
Rb	28	13	103	21	9	97	43
Sr	2 527	389	1 265	457	133	247	632
Y	20	29	32	19	12	51	12
Zr	159	78	432	129	39	1 154	140
Nb	10	4	24	6	3	41	6

*See Note 1, Table 24.

$\bar{M}1$: average of samples nos. 76, 82, 83 and 84.

$\bar{X}1$: arithmetic mean of samples nos. 45, 49, 98, 116a and 118a.

σ: standard deviation.

$\bar{M}2$: average of samples nos. 74 and 75.

$\bar{M}3$: average of samples nos. 118b and 120.

TABLE 26 - SELECTED TRACE ELEMENTS IN LEUCOCRATIC GRANULITES

*Locality nos.	$\bar{M}1$	63	55	$\bar{M}2$	1	39	$\bar{M}3$	$\bar{M}4$	3	56
Rb	120	11	79	10	73	32	90	21	3	26
Sr	152	382	251	234	240	215	310	149	142	54
Y	38	7	13	30	19	15	20	24	12	32
Zr	453	109	180	137	202	140	176	106	101	346
Nb	22	3	5	3	6	2	5	3	-	16

*See Note 1 in Table 24.

$\bar{M}1$: average of samples nos. 65 and 73.

$\bar{M}2$: average of samples nos. 4, 37 and 44.

$\bar{M}3$: average of samples nos. 57, 60, 113 and 116b.

$\bar{M}4$: average of samples nos. 51 and 52.

amounts, followed by less Rb and Y, whereas Nb is negligible. Despite the influence of sampling, distinctive overall characters distinguish the melanocratic, from the mesocratic and leucocratic group. The low-silica group has a very low concentration of Rb ($\bar{M} \approx 10$ ppm) but appreciable Sr ($\bar{M} \approx 300$ ppm) and 2,5 times less Zr ($\bar{M} \approx 120$ ppm). Mesocratic granulites are characterised by very high Sr ($\bar{M} \approx 800$ ppm) and appreciable Zr ($\bar{M} \approx 350$ ppm) while Rb has also substantially increased ($\bar{M} \approx 60$ ppm) despite the fact that in occasional samples it remains very low (10 - 15 ppm). Finally the leucocratic rocks possess the lowest content of Sr ($\bar{M} \approx 230$ ppm) while the Zr concentration is intermediate between the values in the melanocratic and mesocratic granulites ($\bar{M} \approx 220$ ppm). The concentration of Rb is about the same as in the latter group and ranges from 10 to 120 ppm ($\bar{M} \approx 50$ ppm). In contrast to the other elements Nb presents gradually decreasing values from melanocratic ($\bar{M} \approx 33$ ppm) to mesocratic ($\bar{M} \approx 26$ ppm) and leucocratic rocks ($\bar{M} \approx 23$ ppm). Finally little variation is shown by Nb through the melanocratic ($\bar{M} \approx 5$ ppm) to leucocratic ($\bar{M} \approx 4$ ppm) sequence, with the exception of a minor increase in the mesocratic range ($\bar{M} \approx 16$ ppm).

In considering now the individual trace elements, rubidium concentrations in the granulites range between approximately 5 to over 100 ppm. The lowest values characterise

certain low-K_2O melanocratic and leucocratic granulites while values over 50 ppm are present in K_2O-rich mesocratic to leucocratic rocks. Rubidium has close geochemical affinities with potassium and their relative distribution amongst the granulites is presented in Fig.23 which shows a broad trend of decreasing K/Rb ratio, from over 700 to less than 400, with increasing K content (1 to 4 per cent). The highest values are encountered in a few melanocratic to mesocratic granulites with ratios up to about 1 000, while the lowest values are presented by leucocratic, perthite-rich pyroxene granulites which are apparently separated from the other data points by a small hiatus.

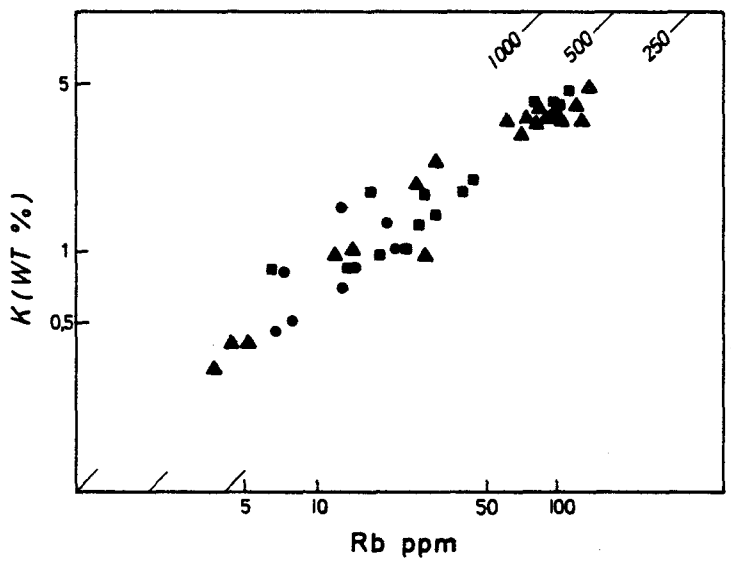


Fig.23. Distribution of K and Rb in melanocratic (•), mesocratic (■), and leucocratic (▲) orthopyroxene-bearing granulites listed in Tables 24 to 26.

Strontium concentration is generally below 800 ppm in the majority of the Malawi granulites, while a few intermediate,

K_2O-rich rocks from Blantyre localities (nos. 76, 82, 83 and 84, Fig.19) have contents between 1 200 and 1 500 ppm; however the highest value determined is about 2 500 ppm and characterises a mesocratic granulite with a high Na_2O/K_2O ratio (no.101, Fig.19). The relationship between Sr and TiO_2 shown in Fig.24 indicates the existence of a rather irregular trend of increasing Sr from melanocratic to mesocratic types, as monitored by decreasing TiO_2 content, up to a maximum of 600 - 650 ppm (at 1 per cent TiO_2). Thereafter, Sr rapidly decreases to low values (below 100 ppm)in the leucocratic granulites; while the group of high-Sr potassic granulites is enriched also in TiO_2 relative to the majority of the other mesocratic rocks.

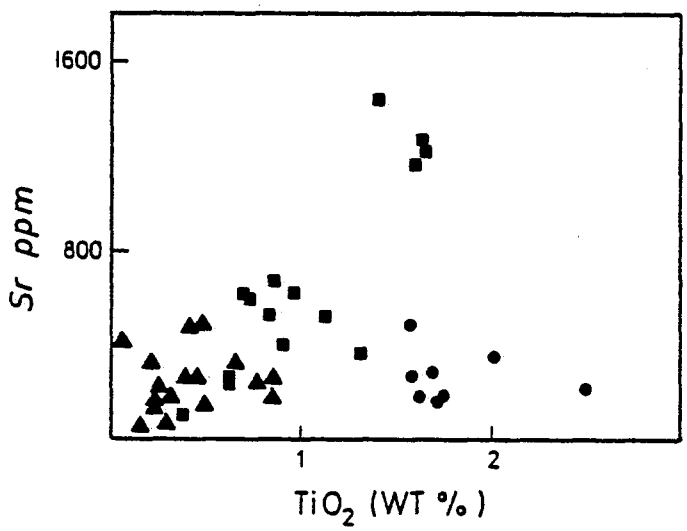


Fig.24. Distribution of Sr and TiO_2 in melanocratic (•), mesocratic (■), and leucocratic (▲) orthopyroxene granulites listed in Tables 24 to 26.

Yttrium concentration in Malawi granulites ranges from 10 to 70 ppm, although values above 40 ppm are relatively uncommon. In the melanocratic rocks, yttrium has a rather restricted range, between about 30 and 40 ppm, while a greater spread characterises the majority of the mesocratic and leucocratic types. Although yttrium has affinities with calcium (Lambert and Holland, 1974) no clear trend is observed amongst Malawi granulites in a CaO-Y diagram (see Fig.25).

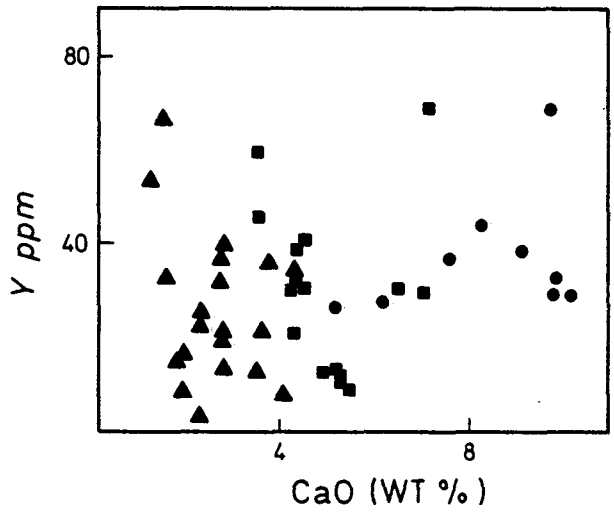


Fig.25. Distribution of Y and CaO in melanocratic (•), mesocratic (■), and leucocratic (▲) orthopyroxene granulites listed in Tables 24 to 26.

The concentration of zirconium amongst granulites shows a certain degree of bimodality since in most samples this element ranges between 50 and 200 ppm while in others it is between 350 and 500 ppm; moreover values of 1 000 and 1 300 characterise certain samples from the Mangochi area (nos. 74 and 75, Fig.19). Fig.26 shows the relatively uniform distribution of Zr relative to SiO_2 amongst granulites and no significant

variation of the trace element may be observed.

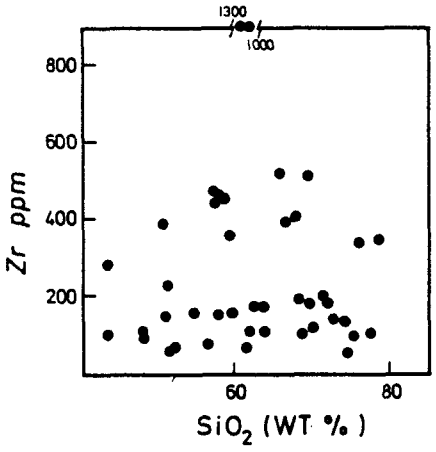


Fig.26. Plot of Zr and SiO_2 in orthopyroxene granulites listed in Tables 24 to 26.

Niobium contents of the granulites range from 1 to 50 ppm but the majority of the samples do not exceed 30 ppm. The distribution of niobium relative to yttrium is shown in Fig.27 where the majority of plagioclase-bearing melanocratic, mesocratic and leucocratic granulites cluster below ≈ 40 ppm Y and ≈10 ppm Nb.

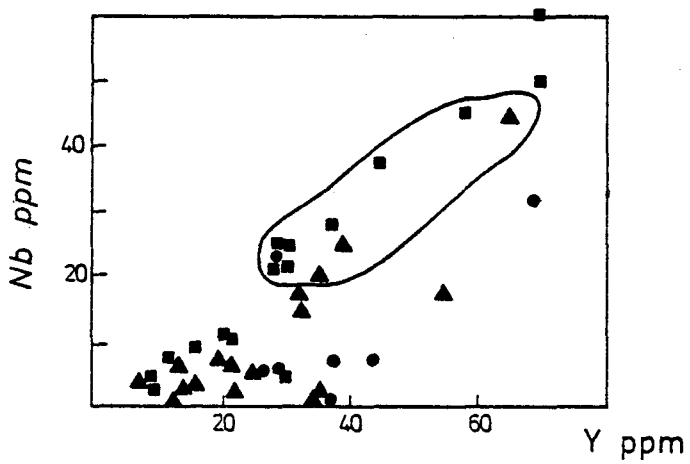


Fig.27. Distribution of Y and Nb in melanocratic (•), mesocratic (■), and leucocratic (▲) orthopyroxene granulites listed in Tables 24 to 26. The outlined field is discussed in the text.

In contrast, a number of mesocratic to leucocratic perthite-rich granulites from the Blantyre area (nos. 76, 82, 83 and 84, Fig.19) and Mangochi (nos. 65, 67, 73, 74 and 75, Fig.19) have an enrichment both in Y and Nb shown by the field outlined in Fig.27.

4.3 Amphibolite and Amphibolite to Granulite Facies Transitional Rocks

(a) Major oxides

The available chemical analyses of amphibolite facies gneisses are presented in Table 27 and illustrate a broad gradation in SiO_2 content from 54 to 77 per cent. This range is not accompanied by a significant variation in the Na_2O/K_2O ratio, which varies between 1,4 and 2. Nearly all gneisses are quartz-normative and in the norm corundum appears more frequently than Ca-pyroxene (diopside + hedenbergite); plagioclase is in the andesine range and constitutes between 43 and 62 per cent of the norm. Finally, the content of alkalis ($Na_2O + K_2O$) is sometimes relatively low, (e.g., cols. b and k, Table 27).

The analysis presented in col.c is unique as it is nepheline-normative and with a high proportion of normative feldspars (84 per cent) suggesting a relationship of this sample with the nepheline gneisses occurring in the same area (see p.7).

TABLE 27 - COMPOSITION OF AMPHIBOLITE FACIES GNEISSES

	(a)	(b)*	(c)*	(d)	(e)*	(f)	(g)*	(h)	(i)*	(j)	(k)*	(l)*	(m)	(n)*
No. of analyses	$2\bar{M}$	1	1	$2\bar{M}$	1	$2\bar{M}$	1	1	1	1	$2\bar{M}$	1	1	1
SiO_2	54,57	55,39	58,28	59,30	62,43	63,52	63,88	66,68	67,06	67,40	68,89	72,08	72,63	77,54
TiO_2	1,20	0,65	0,13	0,94	0,72	0,90	0,58	0,67	0,42	0,51	0,71	0,81	0,69	0,06
Al_2O_3	16,12	17,79	21,67	15,39	15,92	14,38	17,68	16,19	13,88	17,12	17,64	14,50	12,78	12,58
Fe_2O_3	3,28	3,40	1,12	1,63	3,04	2,04	1,49	1,06	2,70	1,93	4,46	1,85	1,20	1,45
FeO	4,95	8,41	5,58	5,23	5,58	5,44	3,06	2,80	4,46	1,94	3,63	0,49	3,35	0,94
MnO	0,15	0,22	0,26	0,13	0,10	0,14	0,08	0,06	0,08	-	0,07	0,02	0,07	-
MgO	4,65	5,15	0,01	3,63	3,05	3,12	2,13	1,41	2,02	1,19	0,86	0,26	1,78	0,48
CaO	8,00	4,18	1,44	5,62	0,44	6,22	5,00	2,60	1,45	2,08	0,11	1,48	2,24	0,73
Na_2O	4,77	4,40	7,06	2,83	2,29	2,38	4,58	3,60	2,33	4,49	0,55	4,02	2,73	4,37
K_2O	1,59	0,10	4,27	4,49	6,30	1,84	1,32	4,19	5,28	3,15	3,01	4,98	2,48	1,32
P_2O_5	0,41	0,31	0,09	0,28	0,13	0,20	0,20	0,27	0,32	0,13	0,07	0,10	0,14	0,03
Total	99,69	100,00	100,00	99,47	100,00	100,18	100,00	99,53	100,00	99,94	100,00	100,00	100,09	100,00
CIPW NORMATIVE MINERALS (MOLECULAR PERCENTAGES)														
q	-	7,62	**	7,47	15,78	22,1	17,19	19,91	24,23	21,2	49,75	24,52	36,96	40,10
or	9,37	0,59	25,31	26,86	37,81	11,11	7,79	25,03	31,91	18,6	18,65	29,60	13,81	10,90
ab + an	60,50	58,36	57,86	41,90	22,21	45,41	62,12	43,87	26,59	49,78	4,94	42,99	35,74	43,21
c	-	3,93	3,04	-	5,36	-	0,1	1,82	2,74	3,12	15,44	0,04	2,29	2,39
di + he	15,26	-	-	8,12	-	5,25	-	-	-	-	-	-	-	-
fo + fa	0,50	-	6,76	-	-	-	-	-	-	-	-	-	-	-
en + fs	8,44	24,37	-	12,00	14,31	12,26	9,08	6,72	10,37	4,24	5,78	0,72	8,62	1,71
ap	0,86	0,65	0,21	0,59	0,28	0,43	0,46	0,57	0,68	0,27	0,17	0,21	0,30	0,06
ma	3,42	3,56	1,88	1,72	3,22	2,18	2,15	1,12	2,88	2,02	2,63	0,54	1,28	1,53
il	1,67	0,98	0,25	1,32	1,03	1,28	1,1	0,94	0,6	0,71	1,03	0,40	0,98	0,08
An%	31	32	11	40	6	53	38	26	20	20	7	16	29	8

$\bar{M}$: average. *: Composition recalculated anhydrous to 100 per cent. **: Includes 4,69% normative nepheline. See p.110 for rock types.

TABLE 27 COMPOSITION OF AMPHIBOLITE FACIES GNEISSES

(a) Average of hornblende-biotite gneisses: (71) and (P11).

(b) Anthophyllite gneiss: (P12).

(c) Biotite-muscovite-plagioclase gneiss: (P13).

(d) Average of biotite-gneisses: (70) and (P63).

(e) Biotite-hornblende gneiss: (P14).

(f) Average of biotite ± hornblende-garnet gneisses: (P15) and (P16).

(g) Hornblende gneiss: (P17).

(h) Mesocratic biotite-garnet gneiss: (105).

(i) Mesocratic biotite-garnet gneiss: (P18).

(j) Quartzo-feldspathic gneiss: (P19).

(k) Average of biotite-garnet-sillimanite gneisses: (P20) and (P21).

(l) Quartzo-feldspathic rock: (P22).

(m) Quartzo-biotite-garnet gneiss: (108).

(n) Quartzo-feldspathic schist: (P23).

Numbers in brackets are samples from localities shown in Fig.19 and in Maps 2 and 3 in the pocket at the back of the thesis.

Analyst: M. Andreoli, except for numbers preceded by P which are published analyses of samples from localities shown in Fig.20.

Individual unpublished analyses are listed in Appendix IV-8; data sources of published analyses and individual compositions are listed in Appendices IV-9 and IV-10.

Chemical analyses of a number of rocks transitional from the amphibolite to the granulite facies are shown in Table 28 and they comprise melanocratic, mesocratic and leucocratic types, showing a wide range in SiO_2 contents (47 to 75 per cent). Only two analyses of melanocratic rocks of this type are available, of which one (col.a, Table 28) is olivine-hypersthene normative, with $Na_2O/K_2O \approx 1$ and $MgO > CaO$ while the other, (col.b, Table 28) is silica undersaturated and nepheline normative with $CaO > MgO$ and $Na_2O/K_2O > 2$.

The mesocratic rocks(cols. c to g, Table 28) have a SiO_2content ranging from 59 to 62 per cent, and in general possess a high Na_2O/K_2O ratio and normative plagioclase in the oligoclase-andesine range. In contrast two hornblende-perthite-bearing rocks (col.e, Table 28) have $K_2O > Na_2O$ and about 77 per cent of normative orthoclase + oligoclase (An_{25}). These rocks also have relatively high P_2O_5 and a ratio $Fe_2O_3/FeO \simeq 1$.

The leucocratic transitional rocks have a SiO_2 content above 67 per cent and their compositions are rather heterogeneous, most oxides showing large variations, particularly those of potassium, magnesium and iron; Na_2O is however relatively constant. Normative andesine and quartz largely predominate in certain K_2O-poor rocks (cols. f and j, Table 28) but leucocratic granulites enriched in K_2O are also present (col.i, Table 28).

TABLE 28 - COMPOSITIONS OF AMPHIBOLITE-GRANULITE FACIES TRANSITIONAL ROCKS

	(a)	(b)	(c)	(d)	(e)	(f)	(g)	(h)	(i)	(j)
No. of analyses	1	1	1	1	2$\bar{M}$	1	1	1	1	1
SiO_2	47,37	47,94	59,17	59,45	59,63	60,91	61,96	67,57	69,92	74,35
TiO_2	1,92	1,72	1,54	1,16	1,56	1,19	0,97	0,92	0,37	0,43
Al_2O_3	15,20	13,54	15,53	12,79	16,20	16,90	15,59	14,81	13,80	11,88
Fe_2O_3	2,46	3,42	1,89	1,40	3,07	2,59	1,31	0,98	1,73	0,93
FeO	10,50	9,31	8,80	6,41	3,17	4,86	5,95	4,38	1,71	2,61
MnO	0,23	0,23	0,19	0,15	0,10	0,13	0,11	0,09	0,07	0,07
MgO	9,33	6,97	3,94	6,77	2,15	2,15	3,75	1,39	0,06	1,74
CaO	7,56	11,41	3,28	5,60	4,30	4,18	3,82	2,72	1,47	3,46
Na_2O	2,28	2,85	3,76	2,21	4,14	4,51	3,79	3,01	3,04	3,43
K_2O	2,05	1,14	1,02	1,78	4,58	1,11	1,91	4,20	5,66	0,54
P_2O_5	0,28	0,13	0,02	1,01	0,73	0,12	0,18	0,25	0,08	0,10
H_2O	0,1	0,02	0,06	0,07	0,05	0,13	0,10	0,02	0,08	0,07
H_2O^+	0,09	0,30	0,05	0,67	0,45	1,00	0,09	0,30	0,31	0,67
Total	99,37	98,98	99,25	99,47	100,13	98,87	99,53	100,64	98,30	100,29
CIPW NORMATIVE MINERALS (MOLECULAR PERCENTAGES)										
q	-	-	14,11	15,90	7,62	15,41	14,51	22,61	25,91	39,18
or	12,25	6,90	6,17	10,78	27,26	6,70	11,43	25,16	34,72	3,27
ab + an	46,14	44,62	51,03	40,51	49,60	61,69	52,40	39,38	35,33	47,37
ne	-	1,72	-	-	-	-	-	-	-	-
c	-	-	2,6	-	-	1,08	0,85	1,07	0,21	-
di + he	8,48	28,65	-	1,19	3,58	-	-	-	-	0,88
fo + fa	20,78	11,72	-	-	-	-	-	-	-	-
en + fs	6,45	-	21,83	26,29	4,94	10,42	17,68	8,92	1,25	7,46
ap	0,59	0,28	0,04	2,16	1,55	0,26	0,38	0,53	0,17	0,21
ma	2,6	3,66	2,02	1,50	3,23	2,76	1,38	1,04	1,88	1,00
il	2,7	2,45	2,19	1,65	2,19	1,69	1,37	1,30	0,53	0,61
An%	57	49	34	33	25	34	36	32	21	35

$\bar{M}$: average; see p.113 for rock types.

TABLE 28 - COMPOSITIONS OF AMPHIBOLITE-GRANULITE FACIES TRANSITIONAL ROCKS

(a) Melanocratic biotite-two-pyroxene granulite: (92).

(b) Melanocratic hornblende-clinopyroxene granulite: (34).

(c) Mesocratic garnet-biotite granulite: (104).

(d) Mesocratic biotite granulite: (50a).

(e) Average of mesocratic hornblende-perthite granulites: (3), and (31).

(f) Mesocratic biotite granulite: (43).

(g) Mesocratic biotite-pyroxene granulite: (93).

(h) Leucocratic garnet-pyroxene granulite: (36).

(i) Leucocratic hornblende granulite: (67).

(j) Leucocratic biotite-andesine granulite: (50b).

Numbers in brackets are samples from localities shown in Fig.19 and in Maps 2 and 3 at the back of the thesis.

Analyst: M.Andreoli, except for samples nos. 31, and 50b which were analysed by A. Bemath. Individual analyses are listed in Appendix IV-8.

Considering the interoxides relationships, Fig.28 shows the distribution of Na_2O-K_2O-MgO in amphibolite and amphibolite to granulite facies transitional rocks in relationship to the trend defined by the granulites. The amphibolite facies gneisses are scattered and many fall outside the field of the granulites, while the majority of compositions of amphibolite to granulite facies transitional rocks fall within the field of the granulites. The distribution of Na_2O and K_2O amongst

granulites is shown in Fig.29(a) and amongst gneisses and transitional rocks in Fig.29(b). It seems that the latter type plots within or near the granulites field, in contrast with a somehow greater scatter of the gneisses.

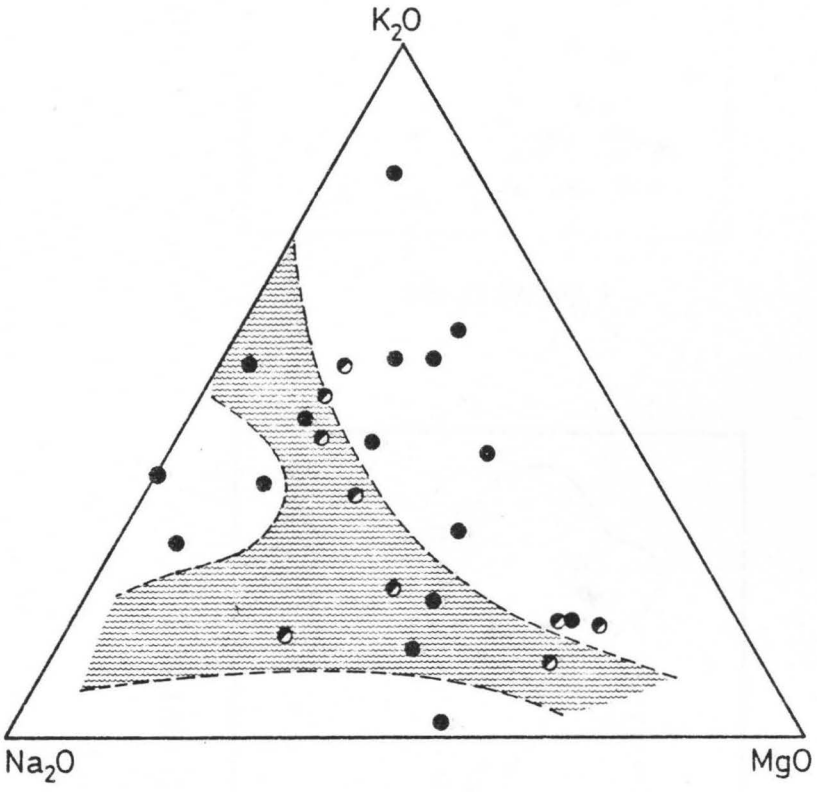


Fig.28. Na_2O-K_2O-MgO diagram (weight per cent) of all amphibolite facies gneisses (●) and amphibolite to granulite facies transitional rocks (◒) listed in Tables 27 and 28, in relationship to the field (shaded) of granulites in Fig.21(a).

(b) Trace elements

Only scanty data shown in Table 29 are available for amphibolite facies gneiss and amphibolite-granulite facies transitional rocks. The abundance of rubidium in them varies from about 10 ppm to over 100 ppm, with a hiatus from 15

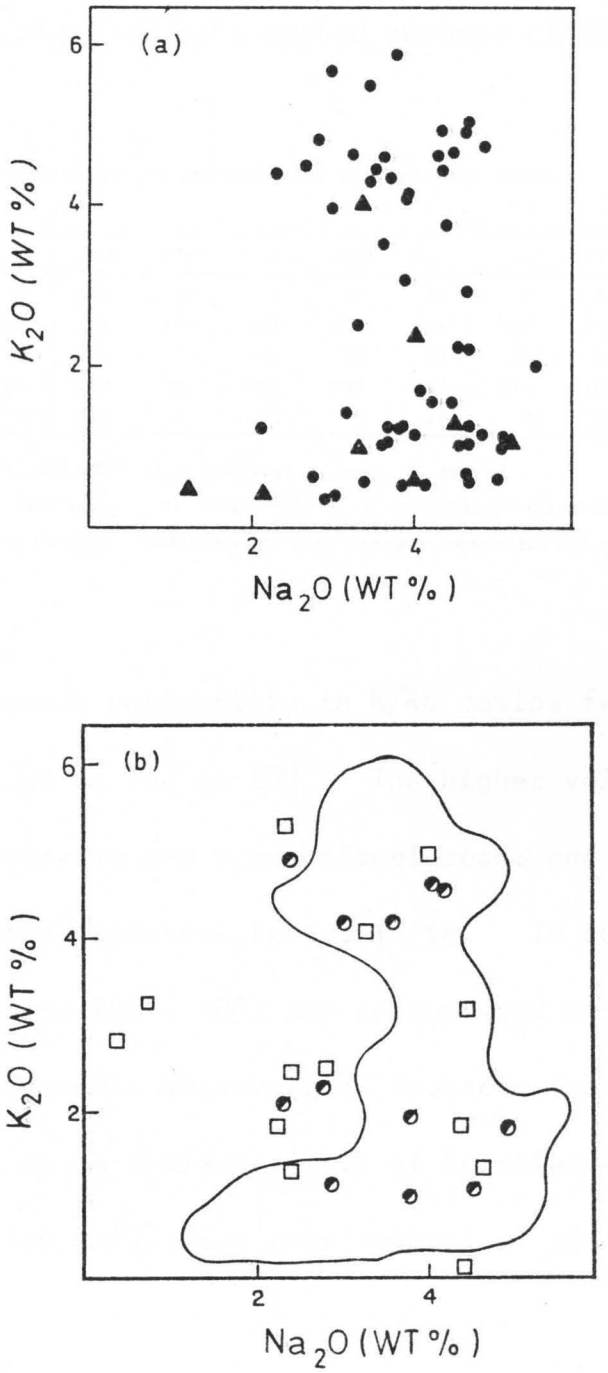


Fig.29(a). Distribution of K_2O and Na_2O in all two-pyroxene granulites (●) and garnet-clinopyroxene granulites (▲) listed in Tables 20 to 22.

Fig.29(b). Distribution of K_2O and Na_2O in all amphibolite facies gneisses (□) and transitional rocks (◐) listed in Tables 27 and 28. The outlined area is the field of distribution of granulites in Fig.29(a).

to 50 ppm and the distribution of rubidium relative to potassium (Fig.30) is characterised by a marked scatter of the data points.

TABLE 29 - SELECTED TRACE ELEMENTS IN GNEISSES AND TRANSITIONAL ROCKS

	A			B								
Locality nos.	(71)	(70)	$\bar{M}_1$	(92)	(34)	(104)	(50a)	$\bar{M}_2$	(43)	(93)	(36)	(67)	(50b)
Rb	51	171	73	118	11	9	65	55	6	64	107	140	9
Sr	855	118	308	125	144	697	897	946	326	335	205	96	513
Y	19	30	29	32	30	58	46	33	23	26	32	64	15
Zr	171	189	267	118	90	580	293	394	116	189	407	514	214
Nb	10	15	6	15		12	16	24	4	9	14	44	3

$\bar{M}_1$: average of nos. 105 and 108; $\bar{M}_2$: average of nos. 30 and 31.

A: amphibolite facies gneisses; B: amphibolite to granulite facies transitional rocks.

For sample localities see Fig.19. Individual trace element compositions are listed in Appendix VI-8.

There is a great variability in K/Rb ratios from 1 300 to 300, with one value as low as 150. The higher values apparently characterise the transitional rocks and these fall in the field of the granulite facies suite. In contrast, low K/Rb ratios (down to 200 - 400) are encountered amongst the gneisses. Petrographic observations indicate that the high K/Rb ratios tend to be characteristic of hornblende-bearing rocks while the low ratios are more typical of biotite-rich types.

The strontium content in amphibolite facies gneisses is quite variable and in one sample it exceeds 800 ppm while in the others it is ≤ 300. Equally, the majority of the transitional rocks are characterised by Sr values not exceeding 350 ppm although some samples (nos. 104, 50a, 30 and 31, Table

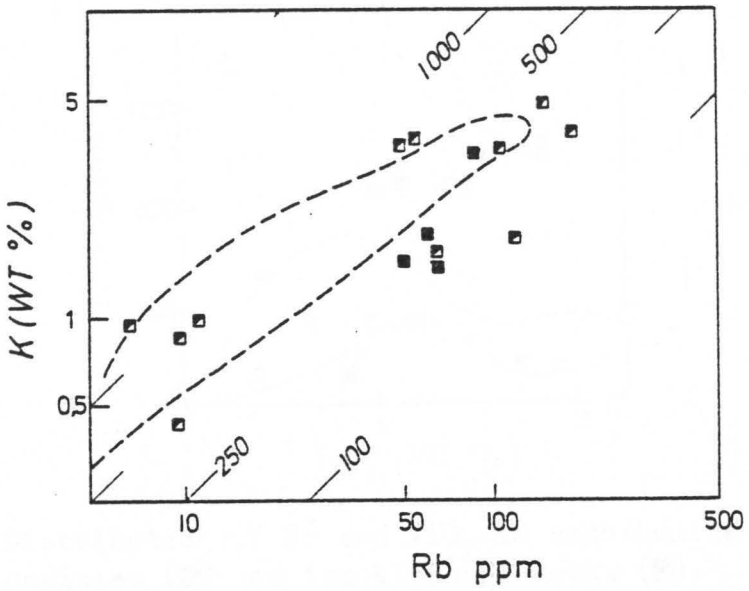


Fig.30. Distribution of K and Rb in all amphibolite facies gneisses (■) and transitional rocks (◩) listed in Table 29. The outlined area is the field of the granulites in Fig.23.

29) have Sr contents between 700 and 1 000 ppm. The distribution of Sr and TiO_2 is shown in Fig.31; this plot suggests that the amphibolite and granulite facies rocks have a wider compositional range than the granulite facies rocks. In addition, an enrichment in Sr and Ti characterises perthite-rich mesocratic rocks (nos. 30 and 31, Fig.19) similar to those described from a neighbouring locality (nos. 76 to 84, Fig.19).

The niobium content of the amphibolite and amphibolite to granulite facies transitional rocks ranges between a few ppm to about 40 ppm, and above-average values between 20 and 27 ppm characterise certain perthitic transitional rocks (see col. M̄2, Table 29 and Appendix IV-8).

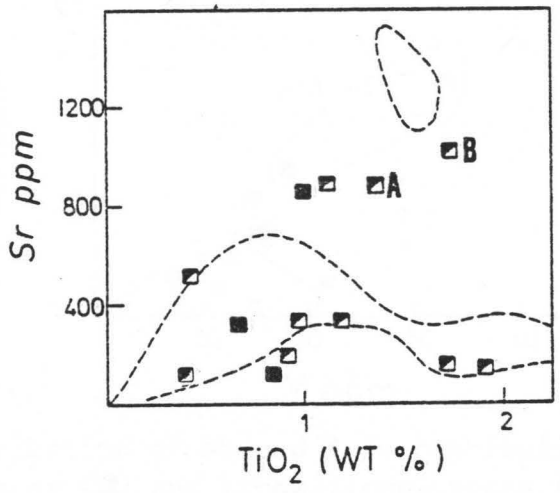


Fig.31. Distribution of Sr and TiO_2 in amphibolite facies gneisses (■) and transitional rocks (◩). A and B are samples from localities nos. 30 and 31 (see Fig. 19). The outlined areas are the fields of granulites in Fig.24.

Yttrium concentrations do not differ significantly between amphibolite and amphibolite to granulite facies transitional rocks and the values range between 13 and 45 ppm. The distribution of Y relatively to Nb in these suites is shown in Fig.32 where, as in Fig.31, the amphibolite and amphibolite granulite facies transitional rocks are more scattered than the granulites.

Zirconium distribution in gneisses and transitional rocks (see Fig.33) is characterised by values generally in the range 100 ppm to 400 ppm: no differences between the two suites are evident.

In conclusion, there is no clear and simple relationship between the restricted (major and trace element) chemistry of the granulites and the chemistry of the amphibolite and amphibolite to granulite facies transitional rocks.

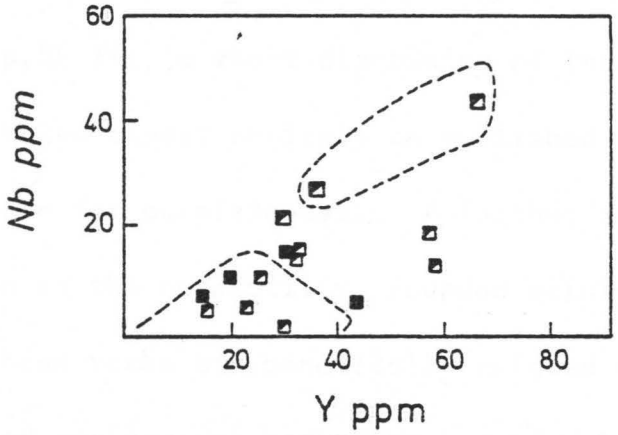


Fig.32. Distribution of Nb and Y in amphibolite facies gneisses (■) and transitional rocks (◩). The outlined areas are fields of granulites in Fig.27.

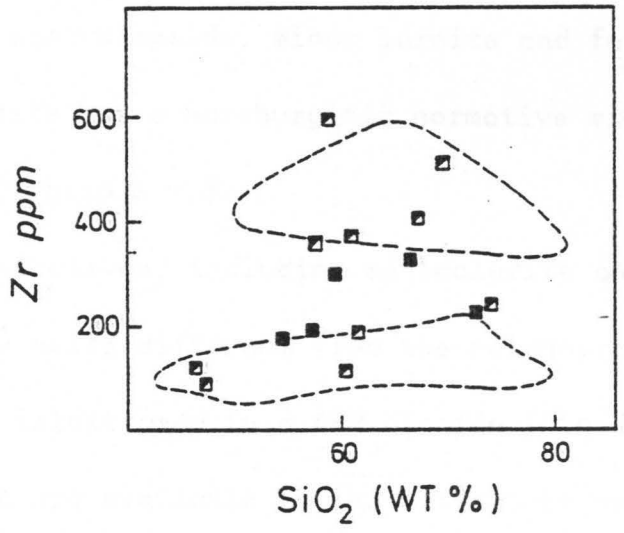


Fig.33. Distribution of Zr and SiO_2 in amphibolite facies (■) and transitional rocks (◩). The outlined areas are fields of granulites in Fig.26.

4.4 Plutonic Rocks

There is a large number of rock types in Malawi that were considered of clear intrusive origin, despite their frequent metamorphic overprint and their geographic distribution is

shown in Fig.20. Whilst the petrography of these rocks is outlined on p.51 ff., a short discussion of their chemical characters (based almost entirely on published analyses), is introduced here for completeness. A further reason for their investigation is the possibility, founded mainly on petrographic data, that these rocks are genetically related to granulites.

Published analyses of corundum, and garnet amphibolite, serpentinite, metadolerite, and metagabbro are presented in Appendix IV-11. An important feature of the amphibolite rocks from Chimwadzulu (see Fig.20) is their high normative anorthite content with some diopside, minor larnite and feldspathoid. The serpentinite has a harzburgitic normative mineral composition and a MgO/FeO ratio = 9,5.

These intrusives, including metadolerite and metagabbro, are chemically quite different from the melanocratic pyroxene granulites as illustrated in a AFM diagram (Fig.34).

Few data are available in the literature on the geochemistry of amphibolite, metadolerite, metagabbro; however the corundum amphibolite from Chimwadzulu contains about 500 ppm Sr, and traces of Li (Bloomfield and Garson, 1965, p.101), while appreciable U or Th may be suspected from common pleochroic haloes to epidote grains (see no.16, Map 2).

The Ring Complexes (see Figs.5 and 20) include a large number of different petrographic types and their composition is

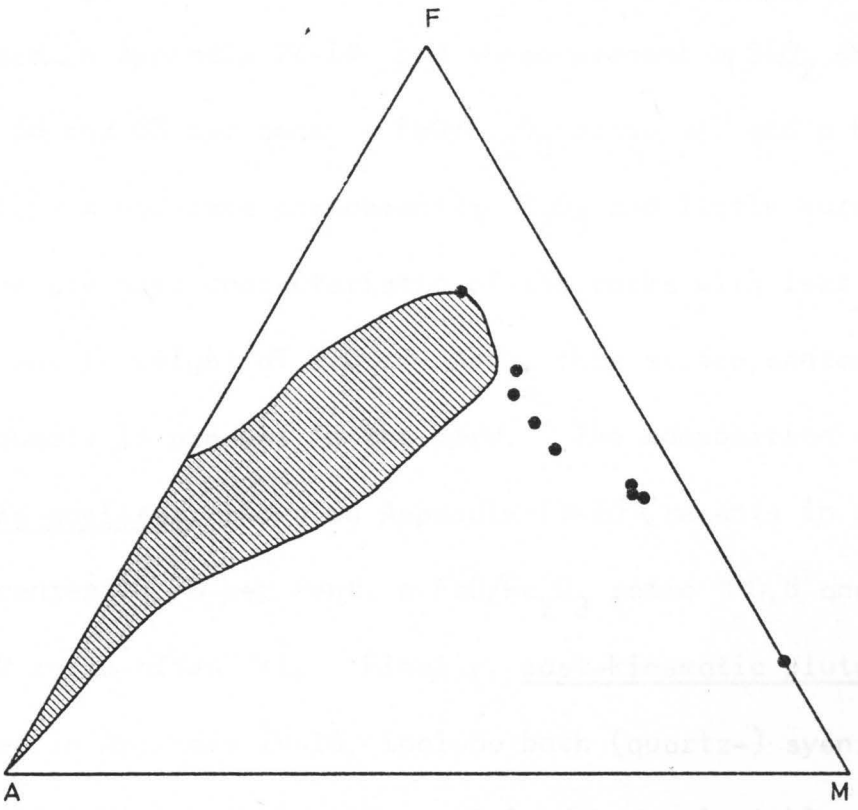


Fig.34. AFM diagram of all amphibolite, metadolerite, metagabbro and related rocks (•), listed in Appendix IV-11. Shaded area is the field of pyroxene granulites in Fig.21(b).

presented in Appendices IV-12 and IV-13. The pyroxenites are enriched in Al_2O_3, Fe_2O_3, CaO, and SrO, and those rich in biotite (see P35, Appendix IV-12) have a high K_2O content (70 per cent), a ratio $FeO/Fe_2O_3 \approx 1,3$ and olivine, leucite, clinopyroxene and larnite as normative minerals. In addition, the syenites and syenitic gneisses are nepheline normative and are characterised by enrichment in K_2O (between 6 and 7 per cent) and of P_2O_5 and Fe_2O_3 with low MgO and CaO. Granitic rocks are corundum-normative with neglectable MgO, FeO/Fe_2O_3 ratio $\approx 2,4$ and a K_2O/Na_2O ratio > 2.

Analyses of syenitic rocks from the Perthitic Complexes are listed in Appendix IV-14, and these present a SiO_2 content between 56 and 63 per cent, a FeO/Fe_2O_3 ratio ≈ 1 and a $K_2O/Na_2O > 1$. A moderate enrichment in P_2O_5 and little normative nepheline are also characteristic of the rocks with less than 60 per cent in weight of SiO_2. Above this silica content little quartz is present in the norm. The composition of the granitoid gneisses, shown in Appendix IV-15 presents in general a SiO_2 content < 70 per cent, a FeO/Fe_2O_3 ratio $\approx 0,8$ and K_2O/Na_2O ratio often > 1. Finally, post-kinematic plutons presented in Appendix IV-16, include both (quartz-) syenite and granite types and they are characterised by neglectable MgO, and K_2O/Na_2O ratio $\approx 1,7$ and $K_2O + Na_2O \approx 10 - 11$ per cent.

The analyses of two perthitic granulites are compared in Table 30 with the average composition of certain rocks from the Perthitic Complexes and the Ring Complexes, suggesting distinct chemical similarities between the various suites. Sample no. 432 in Table 30 has a higher SiO_2, Al_2O_3 and K_2O but lower FeO, MgO, CaO and Na_2O than the syenites from the Ring Complexes; its composition is however generally within the standard deviation range of a few syenite rocks from the Perthitic Complexes. Sample no.115 is not exactly comparable, yet two granites from the Ring Complexes share with it certain common features, mainly a high K_2O/Na_2O ratio > 2. Despite

the scarcity of data, there is also evidence that the plutonic rocks described above have certain similarities with the perthitic granulites even in regard to the trace elements concentrations.

TABLE 30 - CHEMISTRY OF PERTHITIC GRANULITES IN RELATION TO PRE-KAROO PERTHITIC ORTHOGNEISSES

Locality nos.	(432)	$\bar{M}1$	$\bar{X}1$	σ	(115)	$\bar{M}2$
SiO_2	62,1	58,2	59,6	2,6	71,8	68,2
TiO_2	1	1	0,75	0,2	0,1	0,5
Al_2O_3	18,3	17,5	17,4	1,2	14,5	13,5
Fe_2O_3	4,1*	2,4	2,9	0,7	0,7	1,5
FeO		3,1	2,1	0,8	1,6	3,6
MgO	1,1	1,6	1,6	0,9	t	0,2
CaO	2,7	3,8	3,1	1,9	1,1	1,9
Na_2O	3,6	4,6	4,5	0,9	2,5	3,1
K_2O	6,9	6,3	6,8	1,0	7,9	6,7

*All iron as Fe_2O_3. σ : standard deviation.
(432): pyroxene-perthite granulite (col.i, Table 21).
$\bar{M}1$: average of 3 syenite rocks from Ring Complexes (cols. c, d, and e, Appendix IV-13).
$\bar{X}1$: arithmetic mean of 7 syenite rocks from Perthitic Complexes (cols. a to g, Appendix IV-14).
(115): leucocratic charnockite dyke (col.g, Table 22).
$\bar{M}2$: average of granites from Ring Complexes (cols. f and g, Appendix IV-13).
For sample localities: see Appendices IV-13, IV-14 and Figs. 19 and 20.

Trace elements data listed in Appendix IV-17 indicate that the syenites from the Ring Complexes and the Perthitic Complexes are enriched in Sr which varies between 700 and 1 300 ppm up to a maximum of 2 000 ppm and thus cover the $\approx$ 1 200 ppm range of the perthitic mesocratic granulites (see col.$\bar{M}1$, Table 25 and Fig.24). Moreover, the range of Y and Nb in Ring Complexes and in Perthitic Complexes encompasses the values of the perthitic granulites (see Figs.25 and 27). Similarly, Zr ranges in the plutonic rocks between 80 to over 1 000 ppm while

the perthitic granulites have an average concentration of about 430 ppm (see col. $\bar{M}1$, Table 25). These similarities are particularly important since the perthitic granulites are generally closely associated to the Perthitic Complexes. In the Blantyre area, a charnockitic dyke (see no.115, Table 30 and Fig.19) intrudes melanocratic, perthitic granulites 1 km west of the Chimwadzulu Mountain perthitic massif (see Map 2 in the pocket at the back of the thesis). Moreover, south-east of Dedza mesocratic, massive, perthitic granulites occur adjacent to small masses of perthitic rocks (see no.432, Table 30 and Map 3). Perthite-rich, hornblende-, and biotite-free mesocratic granulites (see Plate 2 and cols.d and e, Table 21) occur in Ncheu at a few hundred metres from a massif of perthitic syenite shown in Fig.20. Finally perthite-rich, hornblende-, and biotite-free mesocratic two-pyroxene granulites (see col. g, Table 21) occur north-east of Mangochi near a lenticular body of perthitic syenite (see Map 3).

CHAPTER 5. DETERMINATION OF P-T METAMORPHIC CONDITIONS AND MINERAL PARAGENETIC SEQUENCES

5.1 Introduction

The available petrographic, petrochemical and mineral-chemical data may now be considered in relation to published theoretical and experimental studies in order to examine the P-T conditions of the different mineral assemblages identified in southern Malawi. For this purpose a number of areas (shown in Fig.35) for which most information is available, have been selected. In particular the Zomba-Blantyre and the Tengani areas were chosen as typical examples of regions with pyroxene and garnet granulites respectively. The former area is characterised by rocks with the mineral assemblage hypersthene-augite-plagioclase ± quartz, hornblende and biotite, which range from melanocratic to mesocratic and leucocratic. The Tengani area contains rocks with the assemblage garnet-clinopyroxene-plagioclase ± quartz, hornblende and biotite. The chapter will then deal with the metamorphic conditions in a number of other areas where amphibolite and granulite facies rocks are either associated or grade into each other and special attention was given to the terranes extending around Fort Mlangeni, Ncheu and the northern Kirk Range respectively (see Fig.35). Between the two former localities (see Fig.35),

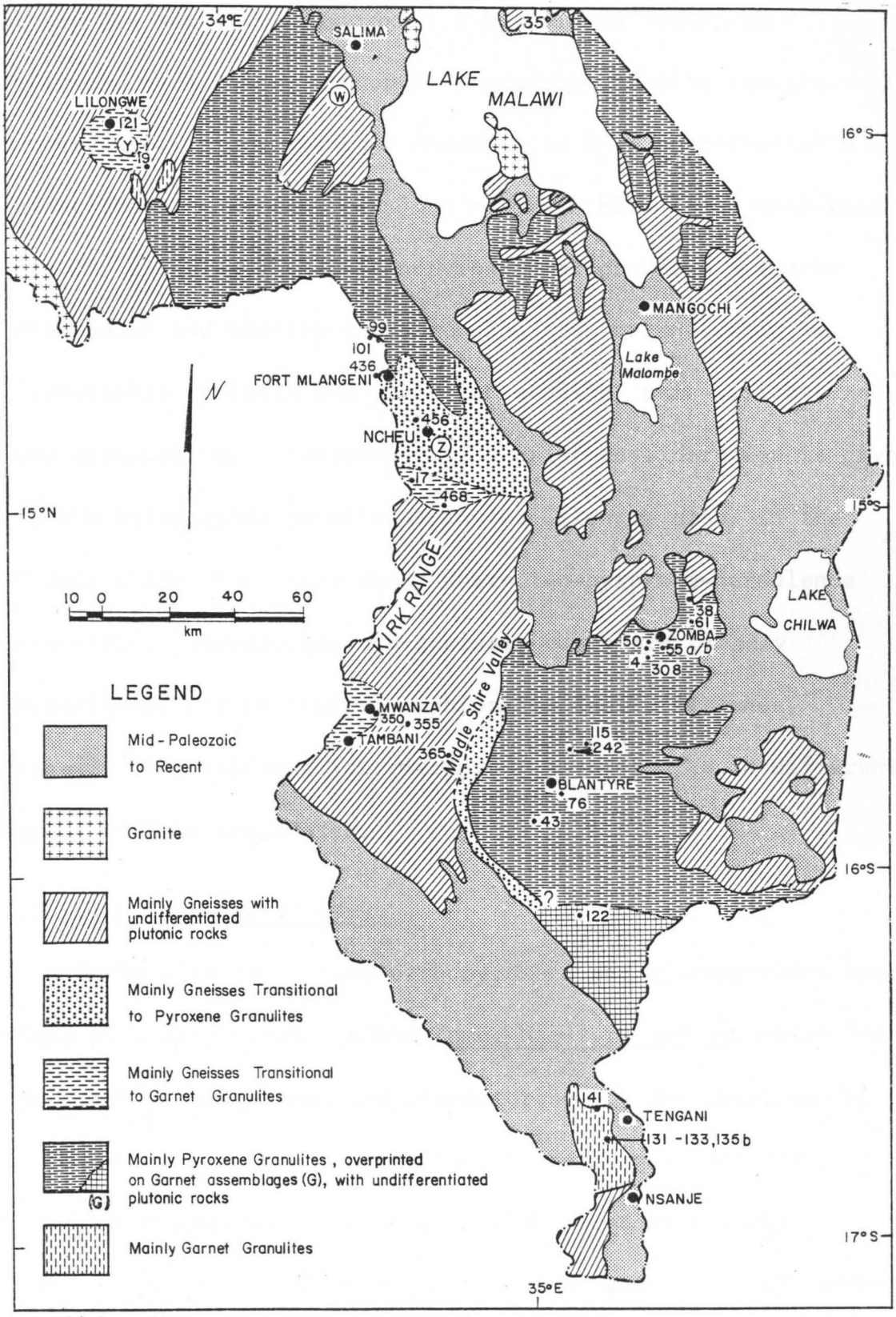


Fig.35. Generalized map of localities referred to in Chapter 5 (see also Maps 1 to 4 in the pocket at the back of the thesis; modified after Bloomfield, 1968; Morel, 1961a).

there are garnet- two-pyroxene ± hornblende rocks, two-pyroxene granulites, orthopyroxene-garnet-biotite transitional rocks, biotite gneisses and anorthosite in a characteristic association. In contrast, the northern Kirk Range area (see Fig.35) contains garnet-clinopyroxene-plagioclase ± quartz, hornblende and biotite rocks ranging from melanocratic to leucocratic, pelitic and graphitic schists, calc-silicate rocks and amphibolite. Subsequently, a brief consideration is given to the metamorphic conditions in the Lilongwe area, in the Middle Shire transition zone, where two-pyroxene-hornblende granulites, amphibolite and gneissic rocks are closely associated, and in typical amphibolite facies terranes. Finally, the evidence for retrograde metamorphism in different areas will be considered.

5.2 Granulite Facies Rocks

Rocks with coexisting orthopyroxene and clinopyroxene have their best development in the Zomba-Blantyre region, where the typomorphic parageneses are characterised by the coexistence of orthopyroxene with plagioclase. The main assemblages, found in melanocratic, mesocratic and leucocratic rocks, respectively are: (a) hypersthene-augite-andesine; (b) andesine-hypersthene-augite-quartz ± perthite; and (c) quartz-oligoclase-perthite-hypersthene.

In these assemblages, hornblende and biotite are sometimes present and the rocks range from two-pyroxene granulites to

hornblende ± biotite granulites, amphibolite or gneisses. Of these, the most melanocratic granulites, with or without hornblende, are silica undersaturated, olivine- and even nepheline-normative. The discrepancy between norm and mode may be explained by the aluminous nature of the pyroxenes in relation to ideal mineral reactions of the type: nepheline + albite = 2 jadeite; and anorthite + olivine = enstatite + Ca-tschermak pyroxene. The jadeite and the Ca-tschermak molecules formed from these reactions enter in solid solutions within the pyroxenes.

In regard to the P-T metamorphic conditions in the Zomba-Blantyre area (see Fig.35) there is now a considerable volume of published experimental data on the stability of orthopyroxene or garnet with plagioclase under different pressures and temperatures. In particular Green and Ringwood (1967) and Irving (1974) investigated the stability of olivine in the presence of plagioclase and clinopyroxene, with or without hypersthene, in basaltic rocks of differing Mg/(Mg + Fe) ratios. This parameter was found to have a great influence on the breakdown of olivine and more magnesian compositions raise its stability field toward high pressures. Rocks of olivine-tholeiitic composition (with Mg/(Mg + Fe) $\approx$ 0,5) and characterised by stable hypersthene and absence of olivine, were designated intermediate pressure granulites by Green and Ringwood (1967).

With recent advances in experimental techniques, analytical probe chemistry and thermodynamic investigations there is at present a number of reasonably precise geothermometers. These are semi-empirical formulae relating partitioning of dominant cations, mainly Mg and Fe, between coexisting phases in function of changes of T and subordinately P.

As the geothermometers are derived from experimental data it was found that the T values obtained are generally within 50°C of the experimental conditions. This suggests that for the practical purpose of this study, the values obtained will be ± 50°C (or at worst 100°C) from true geological conditions. Apart from possible inaccuracies of the electron-microprobe discussed in Appendix III, a further source of error in the calculated conditions is the unknown amount of Fe^{3+} in garnet and pyroxenes. However, a study conducted on this subject by Horrocks(1980) on a suite of Archean granulites from the Limpopo Belt, S.Africa, suggests that the stoichiometric estimate of Fe^{3+} does not lower the T estimates by more than 50°C in most cases, while it is generally much less (ibid.).

Of particular importance for the determination of T in the Zomba-Blantyre granulite facies terranes is the thermodynamic behaviour of the following exchange reaction:

$$MgSiO_3 + CaFeSi_2O_6 = FeSiO_3 + CaMgSi_2O_6 \quad (1)$$

enstatite hedenbergite ferrosilite diopside

Wood and Banno (1973) have determined the following semi-quantitative equation:

$$T^{\circ}K = \frac{-10202}{\ln\left[\frac{a^{cpx}_{MgSiO_3}}{a^{opx}_{MgSiO_3}}\right] \times \left(-7,65 \times X^{opx}_{Fe} + 3,88 \times X^{opx\,2}_{Fe} - 4,6\right)} \qquad (2)$$

For equation (2) the authors considered that activities of enstatite in coexisting pyroxenes could be estimated by an ideal two-site solution model, accordingly:

$$X^{opx}_{Fe} = \text{Fe/(Fe+Mg) in orthopyroxene} \qquad (3)$$

More recently, Wells (1977) has proposed a new equation (4), based on the thermodynamics of reaction (1) which he claims to be accurate within $\pm 70^{\circ}C$ from experimental results and to be less sensitive to aluminium content in MgO-rich pyroxenes:

$$T = \frac{7\,341}{3,355 + 2,44\, X^{cpx}_{Fe} - \ln K} \qquad (4)$$

$$\ln\left\{\frac{a^{cpx}_{Mg_2Si_2O_6}}{a^{opx}_{Mg_2Si_2O_6}}\right\} - 7.65 \times X^{opx}_{Fe} + 3.88\,(X^{opx}_{Fe})^2 - 4.6 \qquad (5)$$

and X^{opx}_{Fe} is expressed as in (3).

However, Powell (1978) criticised Woods and Banno's (1973) equation and from the following mineral reaction

$$CaMgSi_2O_6 + Mg_2Si_2O_6 = CaMgSi_2O_6 + Mg_2Si_2O_6 \quad (6)$$

clinopyroxene orthopyroxene orthopyroxene clinopyroxene

he derived a formula (7) that takes better account of the non-ideal solid solution behaviour of pyroxenes:

$$T = \left\{ -1\,600 + 80P + (x_{Ca,M2} - x_{Mg,M2})_{cpx} \right.$$
$$\left. (6\,670 - 88P) - 1\,900x_{Fe,M2,opx} \right\} : \ln K_D. \quad (7)$$

$$\text{where } K_D = \left(\frac{x_{Ca,M2}}{x_{Mg,M2}}\right)_{opx} \left(\frac{x_{Mg,M2}}{x_{Ca,M2}}\right)_{cpx} \quad (8)$$

and P is in Kbar.

The site occupancies of Ca, Mg, Fe in coexisting pyroxenes are calculated after Wood and Banno (1973) assuming that the Mg/Fe ratios in the M1 and M2 sites are equal to the Mg/Fe ratio of the mineral.

Such an assumption was however questioned by Ellis and Green (1979) who argued that the partitioning of Mg and Fe^{2+} between M1 and M2 is sensitive to T and $CaSiO_3$ content of clinopyroxene. Metamorphic temperatures derived from equations (2), (4) and (7) applied to mineral chemical data from the Zomba-Blantyre area are listed in Table 31.

In the light of the approximations introduced (unknown Fe^{3+} content or the Fe/Mg partitioning between M1 and M2 sites) and of the sensitivity limits of the methods ($\pm 50^{\circ}C$), there is a substantial agreement between temperatures obtained with equations (2) and (4) on hornblende-bearing and hornblende-free

TABLE 31 - GEOTHERMOMETRY OF TWO-PYROXENE GRANULITES FROM ZOMBA-BLANTYRE

Locality no.		T^1	T^2	T^3	
				5Kbar	10Kbar
A	(7)	825	886	907	921
	(55a)	803	849	882	895
B	(5)	794	828	942	950
	(46)	820	826	843	853
	(48)	795	824	937	942
	(55b)	771	781	924	928

(A) two-pyroxene granulites; (B) two-pyroxene-hornblende granulites. T^1, T^2, T^3 are temperatures in ^oC calculated according to equations (2), (4) and (7) respectively. Sample localities are shown in Fig.9 and in Map 2 in the pocket at the back of the thesis; mole fractions and partition coefficients are listed in Appendix V-1.

granulites from different localities. However, the more refined Powell's (1978) geothermometer provides temperatures up to 130 - 150^o higher than values obtained from Wood and Banno (1973) and Wells (1977). The determination of pressure (P) is a more complex exercise since there are no available thermodynamic formulae applicable to the mineralogy investigated. Some broad indications may be obtained from published experimental data if the composition of the rocks used in such studies can match that of at least some of the granulites investigated. The CIPW norms presented in Table 32 indicate

that there is a crude resemblance between certain melanocratic granulites of the Zomba-Blantyre area and the experimentally determined rocks. In particular, the granulites listed in cols. 1 and 4 compare respectively to the basalts of cols. 5 and 7 which were investigated by Green and Ringwood (1967); and the rock of col. 3 matches the granulite of col. 8 which was studied by Irving (1974). It is then reasonable to conclude that since orthopyroxene + clinopyroxene and not garnet + clinopyroxene or olivine + plagioclase are the stable phases in the granulites, P ranged between 7 and 9 Kbar at 800 - 950°C (see Fig.36) in the Zomba-Blantyre granulite terranes.

TABLE 32 - CIPW NORMS OF SELECTED GRANULITES AND EXPERIMENTALLY INVESTIGATED MATERIALS

	(i)				(ii)			
	1	2	3	4	5	6	7	8
ab + an	47	53	55	45	44	42	45	57
ne	2	1	-	-	2	-	-	-
di + he	16	21	16	13	16	17	20	18
fo + fa	20	10	7	-	26	22	-	10
en + fs	-	-	7	28	-	12	24	10
Mg/(Mg + Fe)	0,3	0,4	0,3	0,3	0,4	0,5	0,5	0,4
An%	68	43	39	75	59	66	65	58

(i): Nos.1 to 4, melanocratic granulites: see cols.(b), (c), (e) and (i) in in Table 20.

(ii): Nos.5 to 7, basalts(Green and Ringwood, 1967); no.8, two-pyroxene granulite (Irving, 1974).

It is now important to consider the significance of the prograde geometries of Types I, II and III in amphibolite to granulite facies transitional rocks. These may be related to the interaction of two main causes. The first cause is

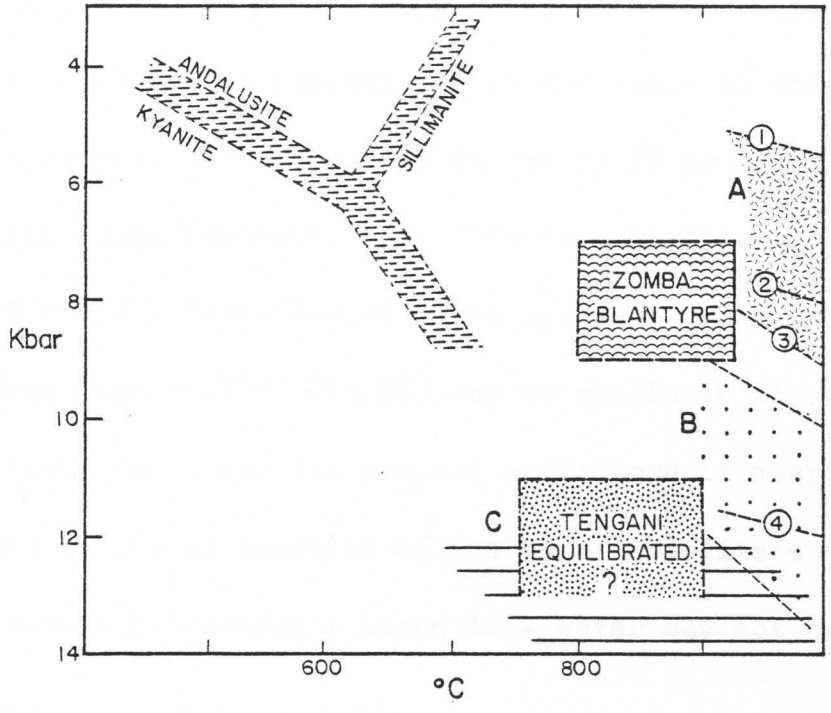


Fig.36. Some experimental data relevant to the determination of the P-T conditions in parts of southern Malawi. Fields of Al-silicates are from Richardson et al. (1968; 1969), and Althaus (1967; 1969a,b). Numbered curves are: 1, high-pressure stability limit of olivine in olivine-tholeiites (Irving, 1974); 2, first appearance of garnet in iron-rich alkali-olivine basalt (Green and Ringwood, 1967); 3, high-pressure stability limit of olivine + plagioclase in basalts with $Mg/(Mg+Fe)^{2+} \approx 0,6$ (ibid.); and 4, high-pressure stability limit of orthopyroxene in olivine-tholeiites (Irving, 1974). The shaded areas are: A, P-T field over which olivine may coexist with plagioclase (Green and Ringwood, 1967); B, range in P-T conditions for first appearance of garnet in quartz-tholeiites with $Mg:(Mg + Fe^{2+}) \approx 0,4 - 0,7$ (ibid.); and C, range in P-T conditions associated to disappearance of plagioclase in quartz-tholeiite compositions (ibid.).

chemical: most melanocratic granulites and transitional rocks are undersaturated and the activity of tremolite in hornblende, as determined from electron-microprobe analyses listed in Tables 14(i) and 15 is low. In such rocks upgrading occurs preferentially if silica is added to the pargasite-rich amphibole at the contact with leucocratic granulites (geometry I) or along cross-cutting quartz veins (geometry II). Certain biotite-rich transitional rocks interbanded with the pyroxene granulites in the Zomba area (see no.308, Fig.35) may be similarly interpreted: within the biotitic bands, the mineral assemblage is quartz-deficient and a mineral reaction of the type: biotite + quartz = orthopyroxene + K-feldspar + ilmenite + water may not have taken place.

Biotite is however completely replaced by pyroxene at the interface with the leucocratic granulite and the resulting reaction rim does not exceed a width of a few millimetres.

A further reason for the prograde texture is the activity of H_2O and there is the clear petrographic evidence that, in Zomba and Blantyre, Type III prograde geometries resulted from a delicate equilibrium in the reaction of hornblende with quartz to produce pyroxenes, plagioclase, ilmenite and vapour. Petrographic evidence therefore contrasts with the suggestions of Sen and Ray (1971) that the stability of the amphibole in hornblende granulites is not influenced by the relative P_{H_2O}.

The amphiboles and pyroxenes of southern Malawi are solid solutions of a number of end-members; however, a crude approximation of P_{H_2O} can be obtained by considering the reaction:

$$Ca_2Mg_5Si_8O_{22}(OH)_2 = 2CaMgSi_2O_6 + 3MgSiO_3 + SiO_2 + H_2O \quad (9)$$

tremolite diopside enstatite quartz vapour

Three samples were initially taken into consideration for calculation of P_{H_2O}: nos. 43, 55b and 436 (see Fig.35); however, specimen no. 43 is a hornblende-rich, quartz-free granulite lacking prograde textures. In addition, no. 436 is devoid of quartz and shows the replacement of biotite by hypersthene and garnet; reaction (9) may not therefore be applied to these rocks. In contrast sample 55b (see Fig.35) is characterised by a hypersthene-augite-andesine-hornblende-quartz mineral assemblage. This rock also shows Type III prograde and Type II retrograde geometries, and perhaps in relation to this, two different amphibole compositions have been obtained. Three analyses show a high content of alkalis and are comparable to the amphiboles from other granulites. The fourth analysis (see Appendix III-15) has in contrast a relatively low Na_2O + K_2O content which could be related to an analytical error ($M_1 + M_3 = 3,716$) or to the difficulty of recognizing prograde from retrograde amphibole in probe petrography. For these reasons the latter analysis was not discussed in Chapter 3.

The $a_{H_2O}^{vapour}$ in a granulite of the Zomba area may be calculated using the following equation by Smith (1973) together with approximations by Fisher and Zen (1971):

$$\Delta\mu = \Delta\mu^{\circ}_{(1,298)\ solids} - \Delta S^{\circ}_{solids\ (1,298)}\ (T-298) + G^{*}\ H_2O + \\ + \Delta V^{\circ}_{solids}\ (P-1) + RT\ \ln K. \qquad (10)$$

Under equilibrium conditions $\Delta\mu = 0$ and

$$(1)\ K = \frac{(a_{diop}^{cpx})^2\ (a_{enst}^{cpx})^3\ (a_{SiO_2}^{qz})\ (a_{H_2O}^{vapour})}{(a_{trem}^{amph})} \qquad (11)$$

To solve equation (11) relative to $(a_{H_2O}^{vapour})$ the value of K has been derived from (10) using available values of ΔV°_{solid}, ΔS°_{solid} and $\Delta\mu^{\circ}_{solid}$ (Dr. S. Richardson, personal communication) and the function of $G^{*}H_2O$ from Fisher and Zen (1971). The above values are listed in Table 33 and yield values of

K = 0,7765 (800°C, 7 000 bar)

K = 2,4187 (950°C, 9 000 bar)

Diopside activity in clinopyroxene is calculated from analytical data using the general formula:

$$a_{diop}^{cpx} = (X_{Ca}^{M2})(X_{Mg}^{M1})(X_{Si}^{Tet})^2 = 0,4872 \qquad (12)$$

while $a_{enst}^{opx} = 0,2591$ (see Appendix V-1). The determination

---

(1) diop = diopside; cpx = clinopyroxene; qz = quartz; enst = enstatite; amph = amphibole; trem = tremolite.

of the tremolite activity in amphibole is more complex, due to the problems of site occupancy in hornblende (see Deer et al., 1963; Misch and Rice, 1975)

$$a_{trem}^{amph} = \left(X_{Si}^{tet}\right)^8 \left(X_{Mg}^{M2}\right)^2 \left(X_{Ca}^{M4}\right)^2 \left(X_{M_g}^{M1M3}\right)^3 \left(X_{\square}^{A}\right) = \quad (13)$$

$$= \text{(a) } 0{,}000353 \text{ and } \text{(b) } 0{,}000554$$

where (a) and (b) refer to the prograde and retrograde amphiboles respectively. Tremolite activity is in both cases very low but the recalculation of up to 14% FeO as Fe_2O_3 (Powell, 1975) does not change the above activity values significantly (P. Horrocks, personal communication).

TABLE 33 - THERMODYNAMIC VALUES USED FOR CALCULATIONS

$\Delta\bar{H}^o$ (cal)	$\Delta\bar{S}^o$ (cal deg^{-1})	$\Delta\mu^o$ (cal)	$\bar{V}$ (cal bar^{-1})	Mineral
-2946575	-582,92	-2772865	6,5229	tremolite (i)
- 766590	-139,55	- 725004	1,5795	diopside
- 370030	- 69,58	- 349295	0,7522	enstatite
- 217650	- 43,62	- 204652	0,5423	quartz

ΔS^o solids (cal deg^{-1})	$\Delta\mu^o$ solids (cal)	$\Delta\bar{V}$ solids (cal bar^{-1})
51,46	70318,4	-0,5650

(ii) G* H_2O (800°C, 7000b) = -25943 cal/mole
(950°C, 9000b) = -19780 cal/mole

R = 1,9872 cal/deg mole

(i) Data source: S. Richardson, personal communication.
(ii) Data source: Fisher and Zen (1971).

Using the above data the following values have been obtained:

	amph.(a)	amph.(b)	
$a^{vap}_{H_2O}$ =	0,07	0,10	(800°, 7 000 bar)
	0,21	0,32	(950°, 9 000 bar)

These values indicate that, at the peak of the granulite facies metamorphism in the Zomba area, a $^{vapour}_{H_2O}$ was probably low and did not exceed 30 - 35 mole per cent of the total vapour phase. It is therefore very probable that the latter was mainly CO_2 as suggested by the presence of scapolite in a Type II prograde geometry from Blantyre (Locality no.179, Map 2).

Granulitic rocks characterised by coexisting almandine-rich garnet, clinopyroxene, plagioclase and quartz occur in a number of areas in southern and central Malawi, but only the Tengani region has been studied in detail (see Fig.35). The typical rock types are mesocratic granulites with an augite-garnet-plagioclase-quartz ± hornblende±biotite mineral assemblage. Anorthosite with melanocratic and hypermelanic interbands is also frequent.

The presence of garnet, plagioclase and the absence of orthopyroxene in quartz-tholeiitic compositions is a clear indication of the influence of pressure (Green and Ringwood, 1967), and garnet-clinopyroxene rocks of appropriate composition would be classified as high-pressure granulites according to these authors. It is of particular importance therefore that a melanocratic rock (no.4, Table 32) from Tengani is quartz-

normative but unfortunately only broadly comparable, in its chemistry, to one of the quartz-tholeiites used by Green and Ringwood for their experimental investigation (no.7, Table 32). Indications on the temperatures, for fixed P, at which the Tengani granulites equilibrated may be obtained from the thermodynamic behaviour of the following reaction:

$$CaMgSi_2O_6 + \frac{1}{3} Fe_3Al_2Si_3O_{12} = CaFeSi_2O_6 + \frac{1}{3} Mg_3Al_2Si_3O_{12} \qquad (14)$$

diopside almandine hedenbergite pyrope

Raheim and Green (1974) first proposed the following semi-empirical equation based on (14):

$$T(^oK) = \frac{3\,686 + 28{,}35P}{\ln K_D + 2{,}33} \qquad (15)$$

where P is in Kbar and

$$K_D = \frac{(FeO/MgO)ga}{(FeO/MgO)cpx} \qquad (16)$$

On the basis of experimental data, Wells (1979) developed the following equation approximate to $\pm 40^oK$:

$$T = \frac{24\,440 + 0{,}06524\,(P-1)}{13{,}41 - 3R\ln\left(\frac{X_{Mg}^{ga}\, X_{Fe}^{cpx}}{X_{Fe}^{ga}\, X_{Mg}^{cpx}}\right)} \qquad (17)$$

where P is in bars and R is the gas constant (see Table 33).

In addition X_{Mg}^{ga} = Mg/(Mg + Fe + Mn + Ca) in garnet (18)

and X_{Fe}^{ga} = Fe/(Fe + Mg + Mn + Ca) in garnet (19)

A further improvement was claimed by Ellis and Green (1979) with the following formula, based on experimental crystallisation of natural and synthetic compositions:

$$T(^{o}K) = \frac{3\ 104\ X_{Ca}^{ga} + 3\ 030 + 10,86\ P(Kbar)}{\ln K_D + 1,9034} \quad (20)$$

in which

$$X_{Ca}^{ga} = Ca/(Ca + Mg + Fe) \text{ in garnet} \quad (21)$$

and, since the minerals are assumed to be ideal solid solutions, K_D is calculated according to (16).

An interesting aspect of equation (20) is that it takes into account the grossular component of garnet, which is present in appreciable amounts in the Tengani minerals (see Fig.15)

Since a garnetiferous orthopyroxene megacryst (135b, Fig.35) has been identified in the hills of the Tengani area, the following reaction may be considered:

$$2MgSiO_3 - MgAl_2SiO_6 = Mg_3Al_2Si_3O_{12} \quad (22)$$

enstatite solid solution pyrope

The pressure-temperature dependence of (22) was investigated by Wood (1974) who developed the equation:

$$P = \frac{\overset{*}{RT}}{\Delta V_r} \ln \frac{X_{Al}^{M1}\left(1 - X_{Al}^{M1}\right)}{(1-Y)_{ga}^{3}} + \frac{\left(7\,012 - 3,89T\right)}{\Delta Vr} \times 41,860$$

$$- C(X_{Fe}^{opx})(1 - 2\ X_{Al}^{M1}) \quad (23)$$

This equation has been modified to reduce all constants to the same reference system".

where *R = 83.143 cm^3 bars/mole K; C = 10 450 and T = °K

In addition $X_{Al}^{Ml} = \frac{(Al^{vi} + Al^{iv})}{2}$ in orthopyroxene (24)

and $(1-Y)_{ga} = X_{Fe}^{ga} + X_{Mg}^{ga}$ (25)

Finally, $\Delta Vr = f(X_{Al}^{Ml})$ is shown in Appendices V-2 and V-3; and X_{Fe}^{opx}, X_{Mg}^{ga}, X_{Fe}^{ga} are as in equations (3), (18) and (19)respectively. The pressure value obtainable from equation (23) must be taken with particular care in view of the problems of Al solubility in pyroxenes (O'Hara and Yarwood, 1978).

Available mineral chemical data for three samples of garnet-clinopyroxene granulite and for a garnet-bearing hypersthene megacryst were applied to equations (15), (17), (20) and (23); the calculated P-T values are listed in Table 34. Pressure estimates may also be inferred from available experimental data on the transition: garnet-in/orthopyroxene-out in quartz-normative basaltic compositions (Irving, 1974; Green and Ringwood, 1967; see Fig.36). Data presented in Table 34, in conjunction with curve 4 and fields C and B in Fig.36, suggest that near Tengani the conditions attained were T $\approx 750^{\circ}$ - 900°; P $\approx$ 11 - 13 kbar . It must also be added that such P-T data were obtained from the analyses of coexisting outer rims.

TABLE 34 - GEOTHERMOMETRY AND GEOBAROMETRY OF GARNET-CLINOPYROXENE GRANULITES FROM TENGANI

Sample	(132)		(498)		(140)		(135b)	
Equation no.	T(5Kbar)	T(10Kbar)	T(5Kbar)	T(10Kbar)	T(5Kbar)	T(10Kbar)	P(T=750)	P(T=900)
(15)	708	744	710	747	731	768	-	-
(17)	814	828	799	813	840	854	-	-
(20)	827	843	806	822	823	839	-	-
(23)	-	-	-	-	-	-	9,3	19,4

Sample localities are shown in Fig.35 and in Map 1 in the pocket at the back of the thesis.
T = °C; and P = Kbar ; mole fractions and partitioning values are listed in Appendix V-2.

Moreover, analytical results on samples from Tengani suggest that during an earlier phase K_D in equation (16) was smaller than the value presently calculated (see p. 82 , and Appendix V-2). This implies that the following conditions were probably attained before equilibration: $T \geq 900°$; $P \geq 12$ kbar .

5.3 Amphibolite to Granulite Facies Transitional Rocks and Amphibolite Facies Gneisses

(a) Transitional rocks

Rocks with variable proportions of hornblende, biotite, pyroxenes and garnet are common in various parts of southern Malawi, but only those occurring in the Fort Mlangeni-Ncheu area, in the northern Kirk Range, at Lilongwe and finally in the Middle Shire Valley transition zone (see Fig.35) will be successively considered.

In the Fort Mlangeni area (see Fig.35) melanocratic garnet-two-pyroxene granulites and leucocratic garnet-orthopyroxene

transitional gneisses are associated with one another. The following mineral assemblages are common:(a) clinopyroxene-orthopyroxene-garnet-hornblende-biotite-andesine; and (b) garnet-biotite-andesine-orthopyroxene-perthite-quartz. Replacement textures of hornblende and biotite by garnet and pyroxenes are frequent in the above assemblages and they have probably been derived from the reaction of quartz with biotite and hornblende to yield garnet, clinopyroxene, orthopyroxene, alkali-feldspar and water. Broad indications on the temperatures during metamorphism are obtained by the application of equations (2), (4), (7), (15), (17) and (20) to samples of which mineral chemical data are available. The calculated values are listed in Table 35, together with information derived from the following reaction:

$$Fe_3Al_2Si_3O_{12} + KMg_3AlSi_3O_{10}(OH)_2 = KFe_3AlSi_3O_{10}(OH)_2 + Mg_3Al_2Si_3O_{12} \quad (26)$$

almandine phlogopite annite pyrope

The partitioning of Fe-Mg between garnet and biotite as a function of P and T was experimentally investigated by Ferry and Spear (1978) and yielded the equation:

$$T(^{o}K) = \frac{0,057P + 12\ 454}{4,662 - 3R\ln K} \quad (27)$$

$$\text{where } K = \frac{(Mg/Fe)^{ga}}{(Mg/Fe)^{bi}} \quad (28)$$

either as oxides or on an atomic metal basis; and P is in bars.

TABLE 35 - GEOTHERMOMETRY OF AMPHIBOLITE-GRANULITE FACIES TRANSITIONAL ROCKS FROM FORT MLANGENI, THE NORTHERN KIRK RANGE AND AN ANORTHOSITE MASS NEAR NCHEU

	FORT MLANGENI				KIRK RANGE		NCHEU	
Sample no.	436		104		468		456	
Equation no.	T^{5Kbar}	T^{10Kbar}	T^{5Kbar}	T^{10Kbar}	T^{5Kbar}	T^{10Kbar}	T^{5Kbar}	T^{10Kbar}
(2)	742		-		-	-	860	
(4)	751		-		-	-	841	
(7)	805	807	-		-	-	800	807
(15)	636	669	-		547	577	779	817
(17)	732	745	-		632	644	894	909
(20)	684	698	-		682	695	849	866
(27)	-	-	920	931	-	-	-	-

Sample localities are shown in Fig.35, and in Map 3 in the pocket at the back of the thesis.

T = °C and P = Kbar. Mole fractions and partitioning values are listed in Appendix V-3.

The values obtained from equation (27) on samples of the Fort Mlangeni area are listed in Table 35 and appear about 50° - 150°C higher than temperatures calculated from other equations, such as (2), (4), (7), (15), (17) and (20). Moreover, pressure data obtained from equation (23) are presented in Table 36.

TABLE 36 - GEOBAROMETRY OF AMPHIBOLITE-GRANULITE FACIES TRANSITIONAL ROCKS FROM THE FORT MLANGENI AND NCHEU AREAS

	FORT MLANGENI		NCHEU
Sample no.	436	104	456
$P^{600°}$	0,8	0,5	-
$P^{700°}$	-	-	1,9
$P^{800°}$	10,5	10,0	-
$P^{900°}$	-	-	10,2

Sample localities are shown in Fig.35 and in Map 3 in the pocket at the back of the thesis.

P = Kbar is calculated according to equation (23); mole fractions and partitioning values are listed in Appendix V-3.

Additional information about pressure in the terranes near Fort Mlangeni is provided by the absence of garnet in quartz and clinopyroxene-bearing rocks and by the presence of a little sillimanite in sample no. 104 (Fig.35). There is also evidence that garnet and clinopyroxene coexist in melanocratic rocks of nepheline-normative composition. This is consistent with experimental results by Green and Ringwood (1967) that garnet appears at lower P in alkali-olivine basalt relative to a quartz-tholeiite. The metamorphic conditions as shown in Fig.37 indicate that near Fort Mlangeni (see Fig.35) T ranged between 650° and 850° while P was between 6 and 8 kbar .

In contrast, the metamorphic conditions characterising a sheared anorthosite from Ncheu (no.456, Fig.35), based on data presented in Tables 35 and 36, are as follows: T ≃ 800° - 900°C and P ≃ 8 - 11 kbars.

Of additional interest are the transitional rocks occurring at the northern end of the Kirk Range between 20 and 30 km south-south-east of Ncheu (see Fig.35). The main typomorphic mineral assemblages are: (a) hornblende-garnet-augite/salite-andesine ± biotite±quartz; (b) andesine-hornblende-biotite-clinopyroxene-garnet ± perthite; and (c) oligoclase-quartz-perthite-hornblende-biotite-garnet-clinopyroxene.

The mineral relationships observed in these granulites indicate the replacement of hornblende and/or biotite by garnet and clinopyroxene.

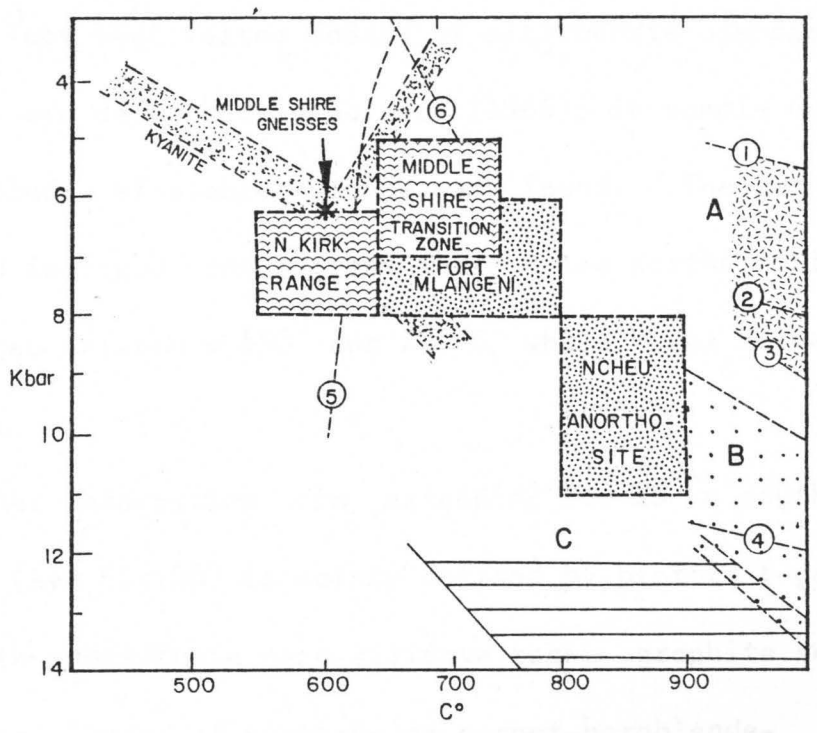


Fig.37. Some experimental data relevant to the determination of the P-T conditions in parts of southern Malawi. The fields of Al-silicates, the shaded areas A, B and C and the numbered curves 1 to 4 are the same as in Fig.36; curve 5 is beginning of melting in granitic rocks (Merril et al., 1970; Tuttle and Bowen, 1958); and 6 is the high-temperature stability limit of muscovite + quartz (Althaus et al., 1970).

Data on the P-T conditions in the northern Kirk Range are obtainable by introducing mineral chemical data for sample 468 (see Fig.35) in equations (15), (17) and (20) and the results are presented in Table 35. Additional information is provided by experimental curves relating bulk rock (basaltic) chemistry to the garnet-in/orthopyroxene + plagioclase-out transition (see Green and Ringwood, 1967; Irving, 1974). In addition, hornblende-diopside gneisses, with or without garnet are associated

to a kyanite-ore deposit 18 km south of Ncheu (no.17, Fig.35). Despite the fact that felted masses of sillimanite associated with kyanite are described by Walshaw (1965), in sample no.17 only large blades of stable kyanite were found. The above data are combined in Fig.37 and suggest that in the northern Kirk Range T ranged between ≃ 550° and 700°C, while P was between 6 and 8 kbar .

Another interesting area, extending for 25 km south-east of Lilongwe (see Fig.35) is mainly defined by biotite (-garnet) gneisses with subordinate calc-silicate rocks, graphite schists and occasional lenses of pyroxene or garnet-hornblende-clinopyroxene granulite in sheared gneisses (Thatcher and Walter, 1968). Granulite with the assemblage hornblende-clinopyroxene-biotite-plagioclase-quartz-garnet-K-feldspar, forms occasional narrow interbands within the gneisses. Although the overall relationships between amphibolite and granulite facies mineral assemblages are unclear, in certain samples (nos. 121 and 19, Fig.35) garnet and clinopyroxene have formed from biotite ± hornblende gneisses presumably according to reactions between biotite, plagioclase and quartz to yield K-feldspar, clinopyroxene, garnet and water. Temperature data, calculated with equations nos. (15), (17) and (20) from mineral analyses, are listed in Table 37 and indicate that sample no. 19 was metamorphosed between 700° and 850°C while sample no.121

TABLE 37 - GEOTHERMOMETRY OF TRANSITIONAL GARNET GRANULITES FROM THE LILONGWE AREA

Sample no.	(19)			(121)		
Equation no.	ln K_D	T^{5Kbar}	T^{10Kbar}	ln K_D	T^{5Kbar}	T^{10Kbar}
(15)	1,5516	713	750	1,8222	649	683
(17)	-1,5508	820	835	-1,8232	747	760
(20)	1,5508	808	824	1,8232	782	796

Value of X_{Ca}^{ga} (21) for no.19 = 0,2092, and for no.121 = 0,2729.

Sample localities are shown in Fig.35 and in Map 4 in the pocket at the back of the thesis; T = C^{o}.

records a temperature 50 - 100°C lower, yet within the experimental error of the method.

Information on pressure is scanty. Isolated masses of olivine-bearing metapyroxenite were reported by Thatcher and Walter (1968) from a few sites between localities (121) and (19), (see Y, Fig.35) and the rock is characterised by the assemblage hornblende-orthopyroxene-olivine-garnet.(2) Spinel and ilmenomagnetite are additional mineral constituents and apatite is a common accessory.

Following earlier investigations by MacGregor (1964) on a Ca-free system, experimental data by O'Hara et al. (1971) on the reaction:

(2) Other occurrences of rocks with the assemblage garnet + hornblende + olivine ± spinel ± plagioclase have been described from the Salima area (see W, Fig.35) by Walter (1972b p.13). Further, the assemblage olivine-clinopyroxene-hypersthene-hornblende-biotite-garnet is recorded in the Ncheu-Balaka area (see Z, Fig.35) by Walshaw (1965, p.28).

$Mg_2SiO_4 + Mg_2CaAl_2Si_3O_{12} = 2\ MgSiO_3 + CaMgSi_2O_6 + MgAl_2O_4$ (29)

forsterite Ca-pyrope enstatite diopside spinel

demonstrated that forsterite can coexist with garnet only if $P > 12$ kbar over a wide temperature range below 1 200°C. It was also found by O'Hara et al. (1971) that the rightward reaction rate for (29) is particularly rapid at temperatures of about 850°C and pressures less than 12 kbar . It has also been known for a long time that garnet-olivine ultramafic rock (lherzolite) is, among other lithotypes, typical of the eclogite facies (Eskola, 1921). Yet, no eclogite nor comparable rocks have so far been reported from the mainly amphibolite facies terranes in the region south-east of Lilongwe. Therefore, the logical conclusion to the above experimental results, and to field and petrographic observations, is that the olivine-metapyroxenite bodies were tectonically emplaced in the present position and cannot be used to derive pressure data for the area.

Finally, the critical assemblages in the Middle Shire Valley transition zone are: (a) hornblende-orthopyroxene-clinopyroxene-oligoclase/andesine; (b) andesine-hornblende-orthopyroxene-clinopyroxene-quartz ± biotite; and (c) oligoclase/andesine-quartz-biotite-orthopyroxene-clinopyroxene-hornblende.

In these assemblages, particularly in the mesocratic ones, biotite and hornblende have reacted with quartz according to

reactions yielding orthopyroxene, clinopyroxene, plagioclase, alkaline feldspar, ilmenite and water. The lack of electron-microprobe data precludes the application of the various two-pyroxene geothermometers. However, temperatures between 650° and 750° are suggested by (a) the coexistence of K-feldspar-quartz-muscovite in a pelitic gneiss (no.365, Fig.35) occurring at 800 m from the nearest granulite outcrop (see Storre and Karotke, 1972); and (b) the frequent occurrence in the region of anatectic rocks (see Plates 5 and 6).

There are also scarce data on pressure during metamorphism, but it was possibly in the 5 to 7 kbar range (see Fig.37) because: (a) In the Middle Shire area Morel (1958, p.23) mentioned the development of sillimanite from kyanite in metapelites; and (b) in melanocratic rocks, such as hornblende-rich two-pyroxene granulites and amphibolite, garnet is absent.

(b) Amphibolite facies gneisses

Amphibolite facies rocks have their maximum development in central Malawi and are limited in the south. In this investigation, a number of assemblages have been studied from the (western) Middle Shire region and the south-east Kirk Range (Fig.35) and typical rocks have the following mineralogy:
(a) hornblende-oligoclase/andesine-biotite ± epidote±garnet;
(b) oligoclase/andesine-hornblende-biotite-quartz ± epidote; and
(c) quartz-oligoclase/perthite/microcline ± biotite ± garnet.

In the (western) Middle Shire area the following pelitic assemblage is characteristic (Morel, 1958): (d) quartz-K-feldspar-sodic plagioclase-muscovite-sillimanite. In the Kirk Range there are also muscovite and kyanite-bearing schists with the following assemblages (Bloomfield, 1968, p.56): (e) quartz-kyanite-staurolite-muscovite-biotite-oligoclase; and (f) quartz-almandine-muscovite-biotite-oligoclase.

Since this study is mainly concerned with rocks of granulite facies or those characterised by the presence of pyroxenes and/ or garnet, no detailed study on the P-T conditions within the amphibolite facies terranes has been conducted. Experimental data by Hoschek (1969) on staurolite appearance in rocks of appropriate composition and the presence of kyanite and sillimanite (but no andalusite) suggest that temperatures of $\backsimeq 600^{\circ}C$ and pressures of $\backsimeq 6$ kbar were attained (see Fig.37).

5.4 Retrogression of the Granulites

Retrogression of granulites is a rather common observation and generally involves the growth of biotite or hornblende from the pyroxenes and/or garnet.

As previously mentioned (see p. 46) Type I retrograde geometries in two-pyroxene granulites have not been observed but those of Type II are occasionally present (no.38, Fig.35) and of Type III are quite common even in high grade terranes. Examples of this are provided among many others by samples

from localities nos.4, 38, 55a, 61, 76, 99 and 101 (see Fig.35).

In most cases retrogression is characterised by sporadic rimming of pyroxenes by bluish-green amphibole or brown mica indenting garnet and hypersthene. In certain samples (see Plate 12 and no.38, Fig.35) symplectites of quartz with hornblende or biotite derive from a reaction between orthopyroxene, clinopyroxene, plagioclase, ilmenite and water to produce hornblende, quartz and some biotite if K-feldspar was present.

Available analytical information is at present insufficient to define P-T conditions that controlled this reaction, mainly because variations of $a_{H_2O}^{Vap}$ are involved. In garnet-clinopyroxene rocks, the frequent kelyphitic replacement of garnet by orthopyroxene + plagioclase may be interpreted in terms of the following reaction under conditions of decreasing P and increasing T (Green and Ringwood, 1967):

2 garnet + 1 clinopyroxene + 2 quartz = 3 orthopyroxene + 2 anorthite (30)

In this mineral reaction the availability of quartz is vital and its absence will cause the garnet to occur in a metastable state at lower pressure. However, if water and alkalis are present, they would react with garnet and clinopyroxene to yield hornblende and quartz. These retrogressive reactions have frequently been observed, not only at Tengani (nos. 131 and 133, Fig.35) but also in the Middle Shire (nos. 350 and 355, Fig.35), in the Thyolo area (No.122, Fig.35) and near Ncheu

(no.456, Fig.35). Other interesting textures observed in the rocks from the Tengani area are the inclusions of plagioclase lamellae in clinopyroxene and rods of garnet ± plagioclase lamellae in orthopyroxene. The former texture could probably be derived from the exsolution of excess tschermak component under decreasing pressure. In fact, the plagioclase lamellae in clinopyroxene are generally concentrated in the Al-rich nuclei and are rarer in the colourless rims. Likewise, the origin of the garnet rods in orthopyroxene is probably related to the exsolution of excess alumina from the host; but for the garnet it is unclear whether this texture indicates decreasing or increasing P-T metamorphic conditions. The occasionally associated plagioclase lamellae were most probably derived from Al and Ca exsolved under decreasing P-T conditions (Emslie, 1975). The sporadic presence of plagioclase filled by minute pyrite inclusions in scapolitised rocks from the same area (no. 132, Fig.35 and Plate 19) remains unexplained.

The presence of the unusual mineral assemblage prehnite-albite-sericite in a rock of anorthositic origin (no.141, Fig. 35) from the Tengani area implies that the anorthosite underwent probable shearing, hydration and recrystallisation at a temperature between 200° and 400°C (Liou, 1971; Winkler, 1976, pp.158 and 189). No indication on pressure is available.

CHAPTER 6. PETROGENESIS

6.1 Introduction

One of the major problems confronting the study of high-grade metamorphic suites is the identification of the parent rock types of granulites, gneisses, etc. In the simpler case of an isochemical metamorphism, the detailed study (involving binary, and ternary diagrams) of a large number of rock analyses, including major and trace elements, may provide reliable clues to the nature of the original rocks. This approach is much less reliable if the influence of metasomatism and partial melting are suspected. The relative effects of these processes and their importance will be discussed later as they have often been described by previous authors of southern Malawi geology. This chapter is therefore first concerned with a discussion of the affinities and similarities between granulites, gneisses and unmetamorphosed sedimentary and igneous rocks. After consideration of the various physico-chemical processes that may have affected the high-grade southern Malawi suite, a discussion on the origin of certain associated intrusions is given. The localities mentioned are shown in Fig.38.

6.2 Granulites, Gneisses and Transitional Rocks

Average analyses of greywacke, gabbro, andesite, rhyodacite,

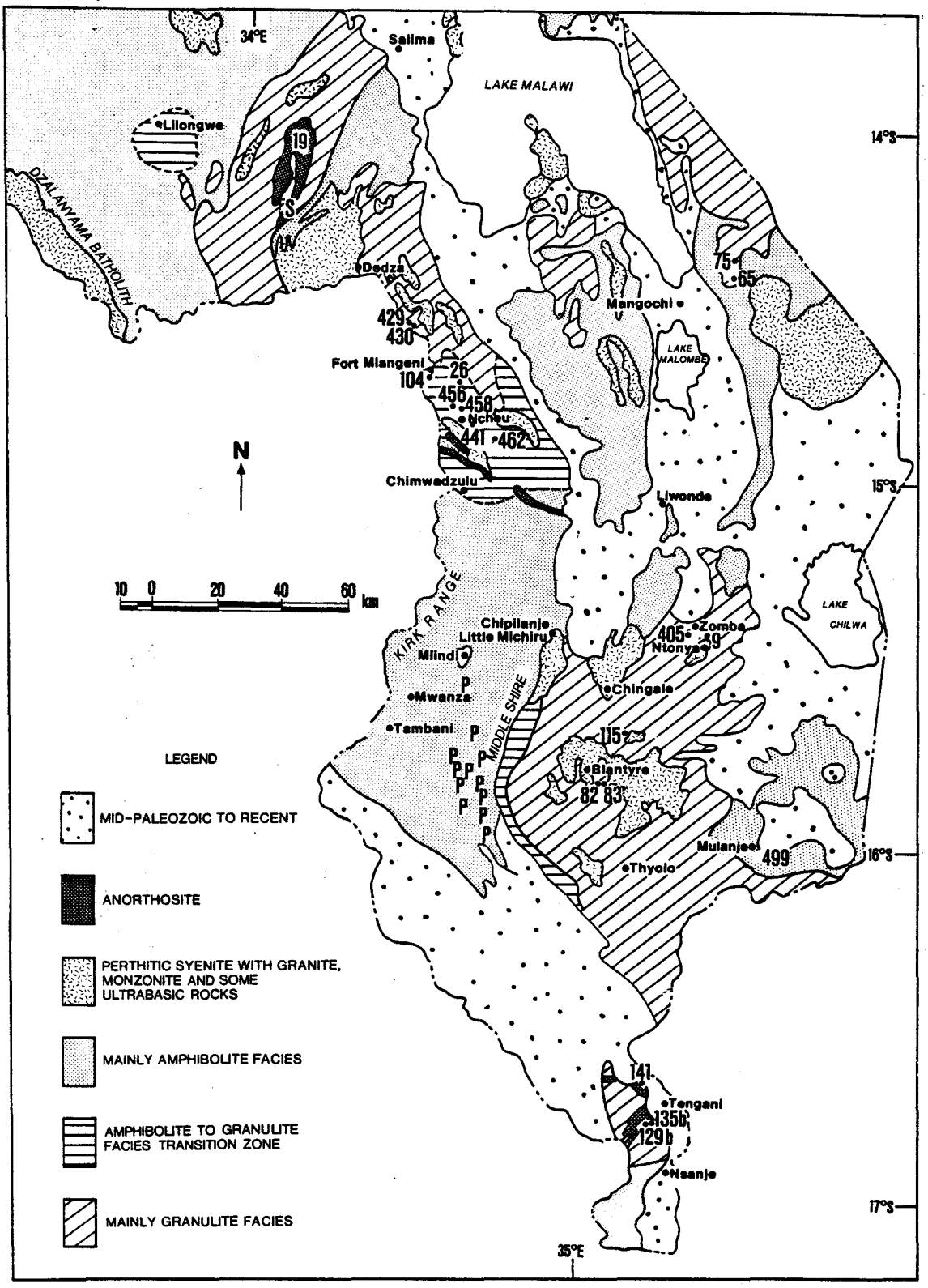
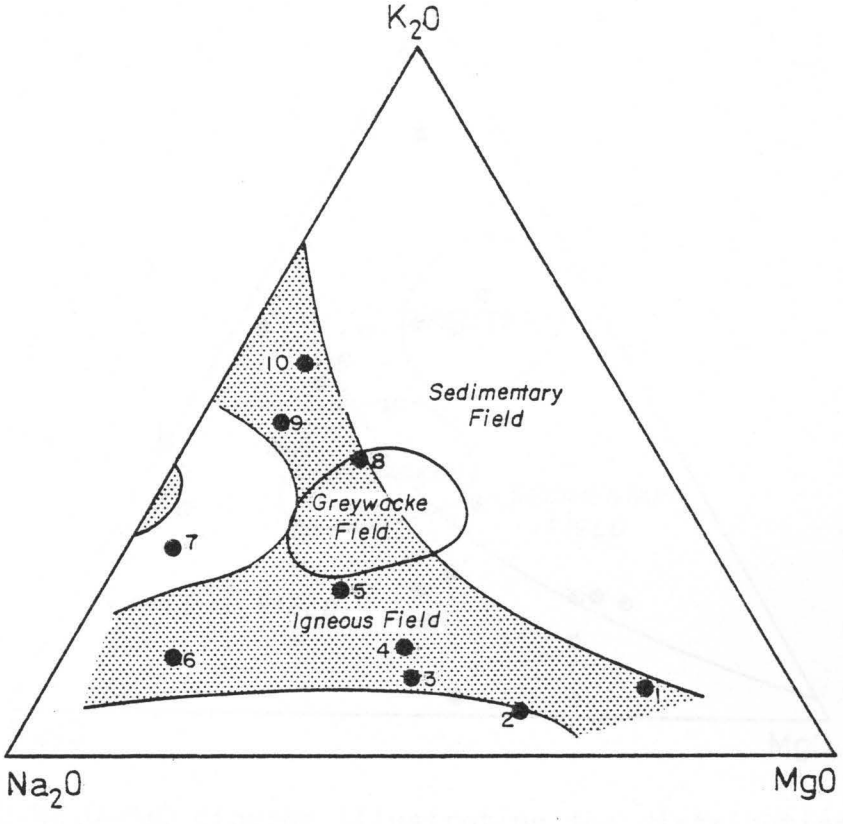


Fig.38. Generalized map of localities referred to in Chapter 6; P: biotitite rocks(modified after Bloomfield, 1968; Morel, 1961a).

syenite and granite have been plotted in the Na_2O-K_2O-MgO ternary diagram shown in Fig.39 (nos. 1-10). This demonstrates the wide range of granulites compositions and their apparent affinity with the chemistry of igneous rocks.

The amphibolitic gneisses and transitional rocks are shown in Fig.40 and are equally distributed between the igneous and the sedimentary fields. Rather similar relationships are presented by an ACF diagram (see Fig.41) in which the granulites define a rather well-marked trend stretching from the basalt-andesite field toward the median point on the C-A join (anorthite). Only a few analyses fall in or near the greywacke/pelite region. In contrast, the majority of the amphibolite facies gneisses and transitional rocks fall in the domain of greywacke, pelite, Al-rich clay and shale (Fig.42). Some of these differences are most likely due to sampling bias. In Fig.43 the granulites are plotted in an AFM diagram which also shows the trends of Hawaii tholeiite and alkali basalt differentiation products. The distribution of the granulites closely compares with that of calc-alkaline igneous rocks (Robinson and Leake, 1975). The same diagram indicates that alkali-poor granulites tend to be enriched in total iron, whilst amphibolite has a distinctly higher MgO proportion.

In Fig.44 the distribution of alkalis and silica amongst the granulites is compared with some igneous and sedimentary



Figs.39. K_2O-Na_2O-MgO diagram illustrating the distribution of the southern Malawi granulites (shaded area; see Fig. 2)(a) in relation to sedimentary and igneous fields (given by de La Roche, 1966). Dots (●) 1 to 10 are average plots of: (1), alkali gabbro; (2), Ural spilite; (3), spilite; (4), and (5), andesite; (6), Fiji (low-K) rhyodacite; (7), New Zealand quartz-keratophyre; (8), monzonite; (9), alkali syenite; (10), calc-alkali granite. Sources of data are: (1), (4), (5), (8), (9), and (10), Nockolds (1954); (2), Sharfman (1968); (3) Sundius (1930, p.9); (6), Gill and Gordon (1973); and (7), Bartrum (1936, p.417, n.1).

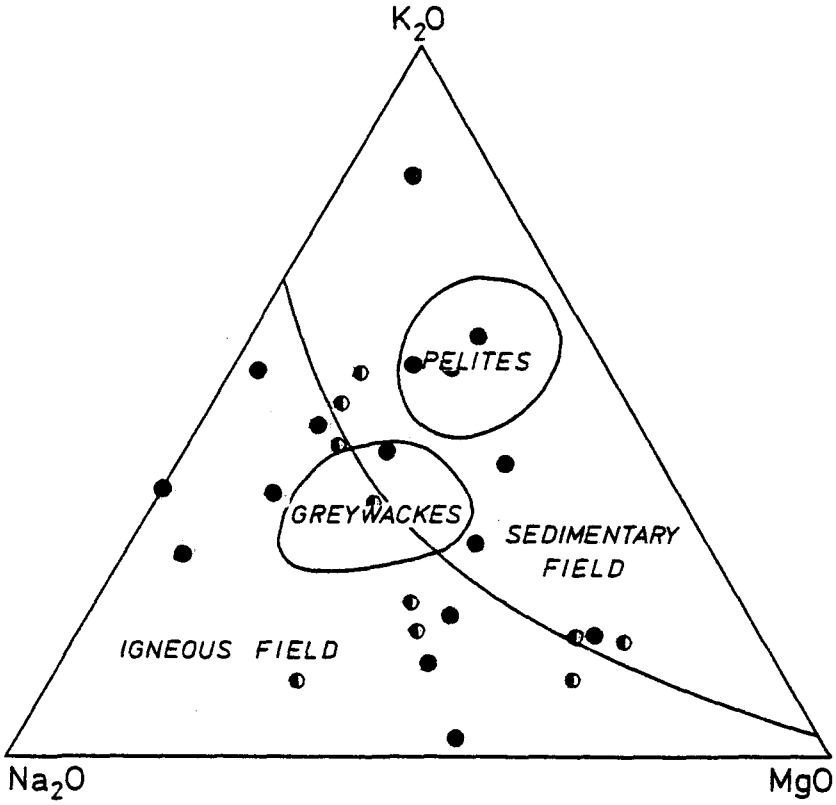


Fig.40. K_2O-Na_2O-MgO diagram illustrating the distribution of the southern Malawi amphibolite facies gneisses (●), and amphibolite to granulite facies transitional rocks (◐) (see Fig.28), in relation to sedimentary and igneous fields (given by de La Roche, 1966).

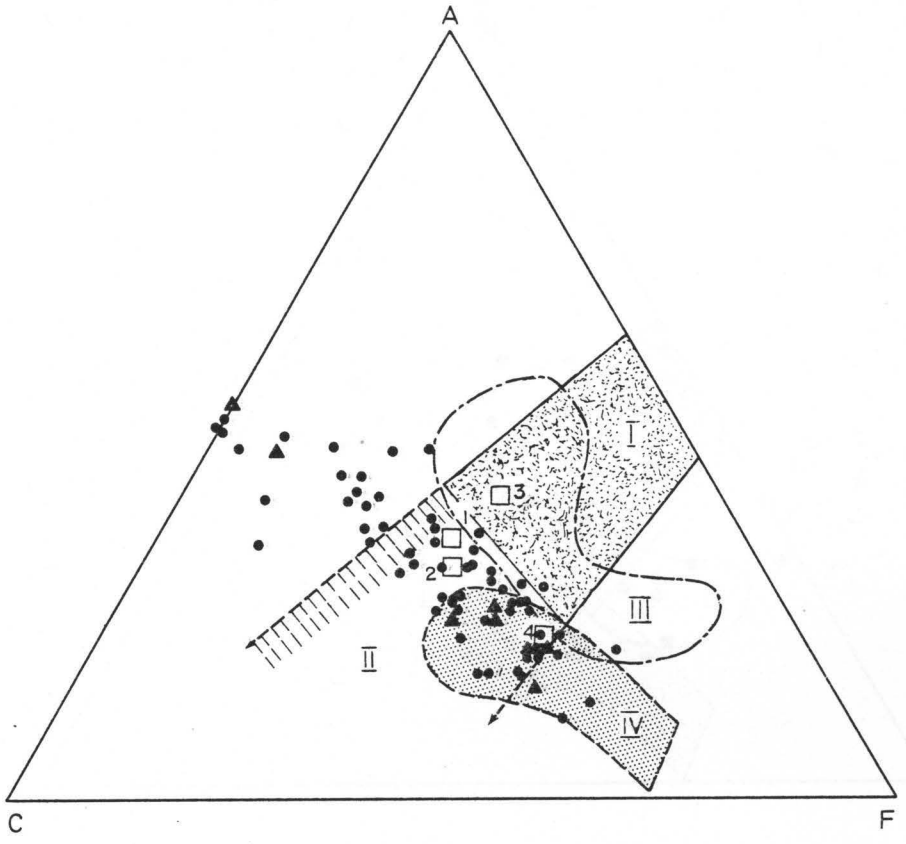


Fig.41. ACF diagram illustrating the distribution of all southern Malawi two-pyroxene granulites (●) and garnet-clinopyroxene granulites (▲) listed in Tables 20 to 22, in relation to sedimentary and igneous fields of: (I), clays and shales with up to 35 per cent carbonate; (II), marls; (III), greywacke; (IV), basaltic and andesitic rocks (given by Winkler, 1967, p.56). Squares (□) 1 to 4 are average plot of: (1), granodiorite; (2), tonalite; (3), calc-alkali granite; (4), basalt (Nockolds, 1954).

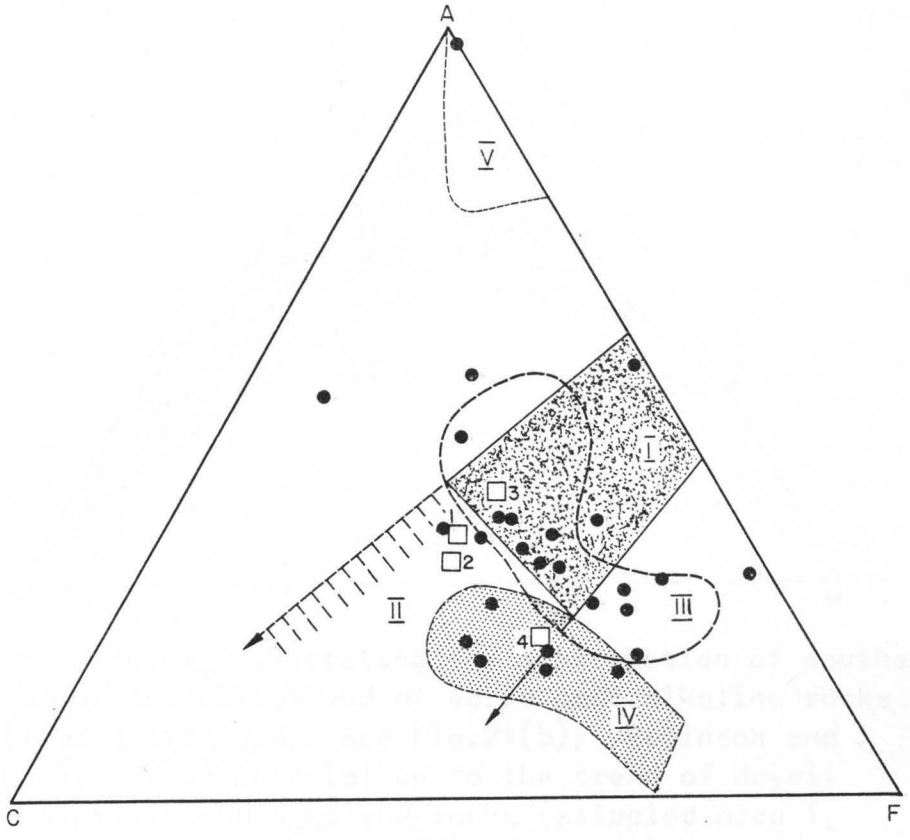


Fig.42. ACF diagram illustrating the distribution of southern Malawi amphibolite facies gneisses and amphibolite to granulite facies transitional rocks (•) listed in Tables 27 and 28, in relation to the sedimentary and igneous fields and average composition of igneous rocks referred to in Fig.41. Field (V): Al-rich clay and shale (given by Winkler, 1967, p.56).

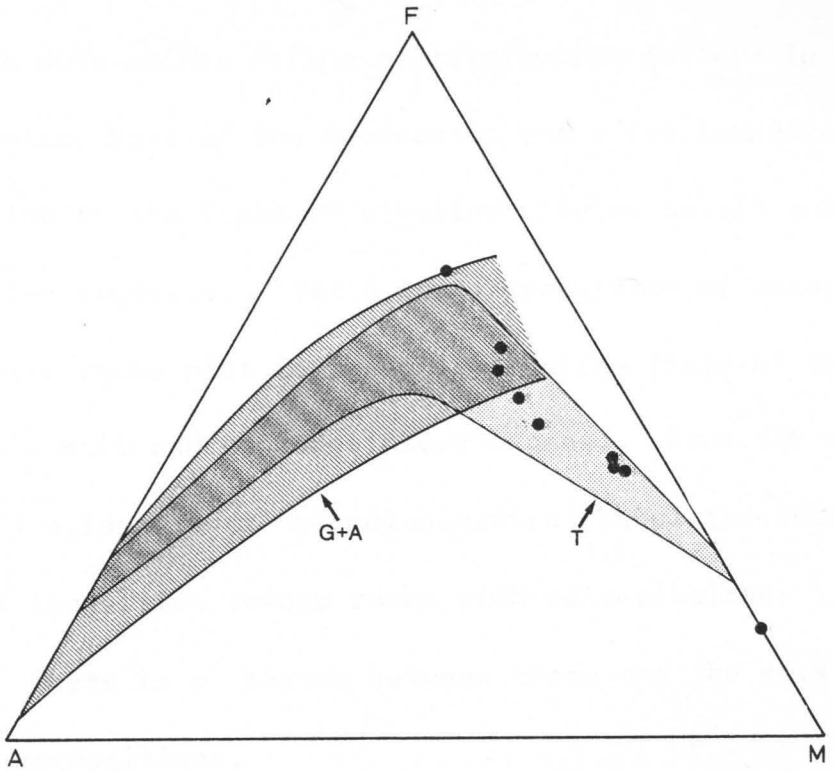


Fig.43. AFM diagram illustrating the distribution of southern Malawi granulites and of world calc-alkaline rocks (shaded area G+A; see Fig.21(b); Robinson and Leake, 1975) in relation to the trend of Hawaii tholeiitic and alkaline rocks (stippled area T, given by MacDonald, 1968). Dots (•) are plots of northern Kirk Range amphibolite, metagabbro and peridotite (see Fig.34 and Appendix IV-11).

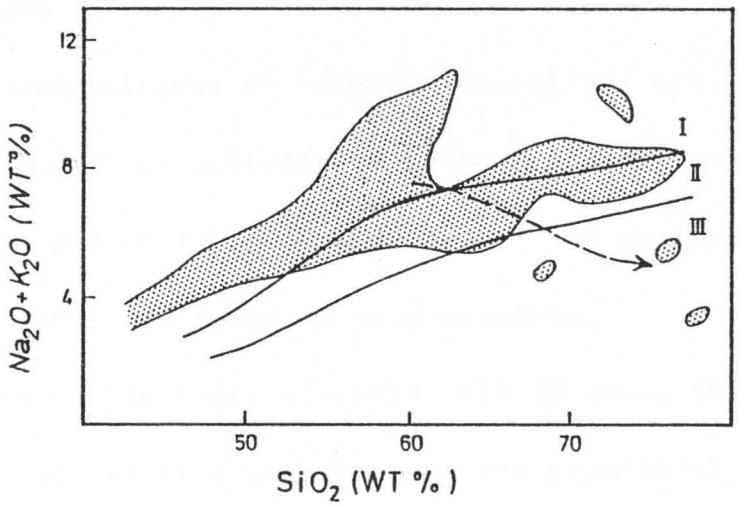


Fig.44. Alkali-silica diagram illustrating the distribution of the southern Malawi granulites (shaded area; see Fig.22) in relation to fields of (I), alkali-olivine basalt; (ii) high-alumina basalt; and (III), tholeiite (given by Kuno, 1968). The arrow defines the trend of pelitic rocks from Japanese Paleozoic geosynclinal deposits (ibid.).

trends. The data points define a distribution pattern in which the melanocratic, part of the mesocratic, and a few leucocratic granulites plot in the field of alkaline olivine basalt and its differentiation products. Yet a large proportion of mesocratic and leucocratic rocks plot in the calc-alkaline field of the high-alumina basalt and consanguineous magmas. From the same diagram it is evident that the melanocratic granulites show a very gradual transition toward rocks with calc-alkaline character. There is a hiatus between these and the more alkali-rich compositions.

Figs. 39 and 41 illustrate that the granulites exhibit strong igneous affinities, while Figs.40 and 42 suggest that a greater number of the amphibolite facies gneisses and amphibolite-granulite facies transitional rocks have a possible metasedimentary parentage from greywacke, pelite and shale. Some average compositions of selected granulites are compared in Tables 38 and 39 to analyses of igneous rocks from elsewhere in the world; and in Table 40 a number of the gneisses and transitional rocks are compared to greywackes.

In regard to the trace elements, Fig.45 shows the distribution pattern of K and Rb among the granulites in relation to the average trend of island-arc volcanics (Jakés and White, 1970). For K values up to about 1 per cent the

TABLE 38 - AVERAGE COMPOSITION OF SOME MELANOCRATIC, MESOCRATIC AND LEUCOCRATIC GRANULITES AND COMPARABLE IGNEOUS ROCKS

	I	A	II	B	III	C	IV	D	V	E	VI	F
SiO_2	50,3	49,0	51,7	53,1	60,90	63,60	68,50	67,4	74,3	73,6	74,5	74,5
TiO_2	1,8	3,1	1,7	1,5	1,1	0,6	0,6	0,7	0,2	0,3	0,3	0,3
Al_2O_3	15,0	15,2	13,9	14,4	16.	16,7	15,2	15,3	12,7	14,0	12,3	12,9
Fe_2O_3	3,2	3,7	7,0	1,3	1,7	2,2	1,4	1,1	0,9	0,4	1,5	
FeO	8,4	8,3	7,9	9,3	4,7	3	3,1	3,9	1,	1,4	2,8	3,3
MgO	5,8	5,00	4,2	4,7	2,7	2,1	1,2	1,2	0,2	0,4	1	0,5
CaO	8,4	8,8	7,5	7,0	5,3	5,5	4,1	4,5	1,8	1,4	2	2,1
Na_2O	3,8	3,7	4,7	4,6	4,4	4	4,4	4,7	3,5	4,0	4,6	4,6
K_2O	1,2	1,2	0,6	1	1,5	1,4	0,8	0,9	4,4	4,3	1	0,9

I, Average composition of four melanocratic granulites (col.e, Table 20).
A, Average trachybasalt from Ascension Island (Borley, 1974, p.322).
II, Melanocratic hornblende granulite (col.f, Table 20).
B, Spilite from Oregon (Gilluly, 1935, p.235).
III, Average composition of six mesocratic granulites (col.f, Table 21).
C, Average dacite (Nockolds, 1954, p.1015).
IV, Average composition of six leucocratic granulites (cols.b and e, Table 22).
D, Augite-hypersthene andesite, Japan (Kuno, 1950, p.1004).
V, Average composition of four quartzo-feldspathic granulites (col.j, Table 22).
E, Rhyolitic obsidian,Medicine Lake Highlands (Anderson, 1941, p.399).
VI, Average composition of three leucocratic granulites (col.k, Table 22).
F, Metakeratophyre,Hoggar (Caby, 1970, p.106).

TABLE 39 - AVERAGE COMPOSITION OF SOME MESOCRATIC AND LEUCOCRATIC GRANULITES AND COMPARABLE IGNEOUS ROCKS

	I	A	II	B	III	C	IV	D	V	E
SiO_2	58,7	58,5	61,6	63,0	66,3	65,9	71,5	72,1	71,8	72,1
TiO_2	1,4	1,4	0,6	0,8	0,8	0,8	0,	0,4	0,1	0,1
Al_2O_3	17,0	15,7	17,5	16,0	14,5	15,1	14,1	13,9	14,5	14,6
Fe_2O_3	3,2	3,3	3,4	2,3	1,0	1,7	1,0	0,9	0,7	0,3
FeO	3,1	4,0	3,3	3,1	5,0	2,7	1,2	1,7	1,6	0,3
MgO	2,2	2,5	0,1	1,0	0,9	1,4	t	0,5	t	0,3
CaO	4,3	5,5	3,5	3,3	2,8	3,4	1,4	1,3	1,1	0,4
Na_2O	4,5	3,5	4,1	4,5	3,7	3,5	3,4	3,1	2,5	3,1
K_2O	4,7	4,6	5,2	5,0	4,4	4,6	5,7	5,5	7,9	8,2

I, Average composition of six mesocratic granulites (col.e, Table 21).
A, Average hornblende-biotite monzonite (Nockolds,1954; p.1017).
II, Average composition of two mesocratic granulites (col.g, Table 21).
B, Quartz-syenite, Dyana Complex, Adirondacks (Buddington, 1939; p.103).
III, Average composition of two leucocratic granulites (col.a, Table 22)
C, Average hornblende-biotite adamellite (Nockolds,1954, p.1012).
IV, Average composition of two leucocratic granulites (col.h, Table 22, and col. i, Table 28).
D, Average calc-alkali granite (Nockolds, 1954, p.1012).
V, Charnockitic granulite (col.g, Table 22).
E, Potassic granite, Finland (Harme, 1965, p.19).

TABLE 40 - COMPOSITION OF SOME AMPHIBOLITE FACIES GNEISSES AND TRANSITIONAL ROCKS AND COMPARABLE SEDIMENTARY ROCKS

No.	I	A	II	B	III	C
SiO_2	59,2	61,4	63,0	60,5	72,6	69,7
TiO_2	1,5	0,6	0,8	0,9	0,7	0,7
Al_2O_3	15,5	17,0	16,4	15,4	12,8	14,8
Fe_2O_3	1,9	0,4	2,0	0,8	1,2	0,7
FeO	8,9	5,3	4,8	7,6	3,3	3,2
MgO	3,9	3,8	3,4	3,4	1,8	1,8
CaO	3,3	3,2	4,5	2,1	2,2	1,8
Na_2O	3,8	2,9	2,4	2,5	2,7	2,6
K_2O	1,0	1,3	2,4	1,7	2,5	2,3

I, Mesocratic garnet-biotite granulite (col.c, Table 28)
A, Greywacke from Minnesota (Pettijohn et al., 1972, p.200).
II, Garnet-biotite gneiss (pl6, Appendix IV-10).
B, Greywacke (Pettijohn, 1957, p.306).
III, Biotite-garnet gneiss (col.m, Table 27).
C, Greywacke (Caby, 1970; p.68).

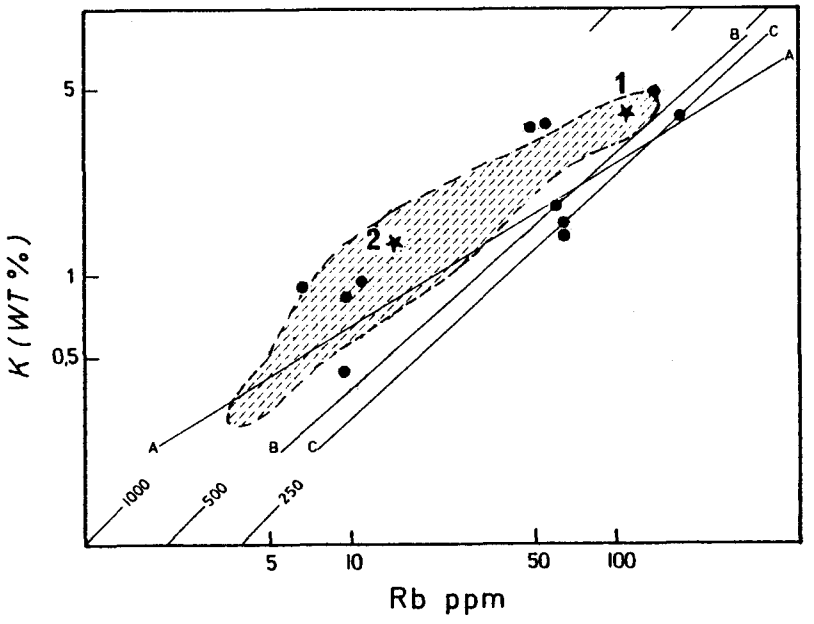


Fig.45. Distribution of K and Rb in southern Malawi granulites (shaded area; see Fig.23) and in gneisses and transitional rocks (dots (•); see Fig.30), in relation to igneous trends of: (A), island-arc igneous suites (given by Jakés and White, 1970); (b), lower crust granulite and charnockite suites (given by Lewis and Spooner, 1973); and (c), high-level igneous rocks (given by Shaw, 1968). Stars (★) are: (1), average of five rhyolites (Groome and Hall, 1974); and (2), Saipan dacite (Taylor et al., 1969).

Malawi rocks overlap the island-arc trend while, above this value, the Malawi rocks appear Rb-depleted relative to the island-arc, but not relative to certain silicic igneous rocks such as dacite. The granulites of Malawi are also strongly deficient in Rb relative to K if compared either to the high-level igneous trend (Shaw, 1968) or to the world granulite trend. The distribution of Sr against Rb, shown in Fig.46, illustrates that the granulites plot in the general basalt-andesite-rhyolite trachyte trend defined by Hedge (1966). From these data it may be concluded that the granulites have, in a very general way, an igneous-like composition even in regard to trace elements like Rb and Sr.

Data plotted in Fig.45 also indicate that some gneisses and transitional rocks have a K and Rb distribution which is characteristic of world high-level and island-arc igneous suites. However, a few other rocks have an enrichment in Rb relative to K which is not consistent with a direct igneous origin.

Before considering a genetic model for the granulites and gneisses it is necessary to consider whether or not the high-grade metamorphism has been allochemical or isochemical. The main processes responsible for such chemical changes include anatexis and depletion in the granitophile components, metasomatism and metamorphic segregation. Of these, <u>partial melting</u> and separation of the liquid fraction is considered to be a major petrogenetic process in lower crustal regions

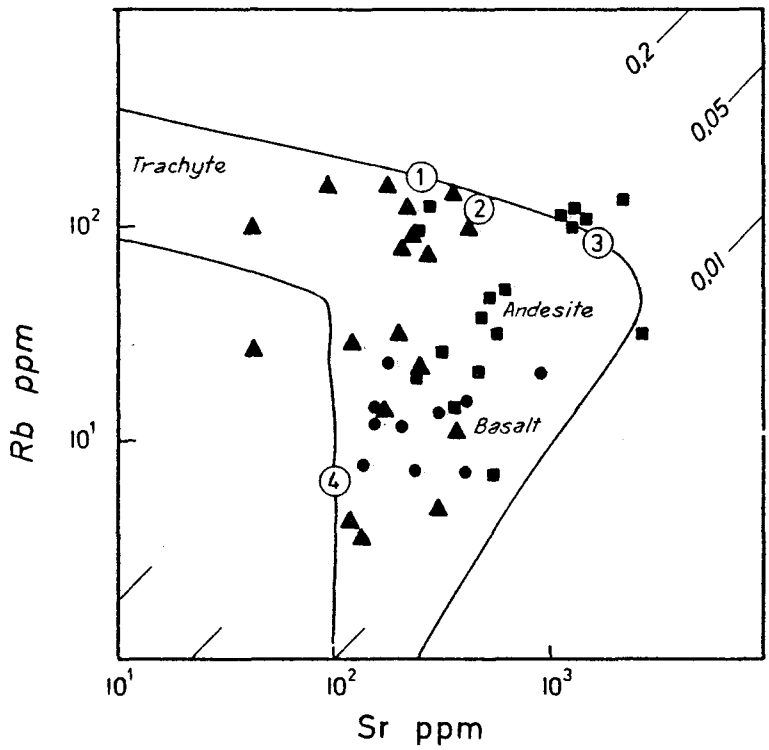


Fig.46. Distribution of Rb and Sr in southern Malawi melanocratic (•), mesocratic (■) and leucocratic (▲) granulites in relation to the basalt-rhyolite/trachyte trend (given by Hedge, 1966). Numbers indicate: (1), granite (ibid.); (2), rhyolite and rhyodacite (Groome and Hall, 1974); (3), latite (Nockolds and Allen, 1954); and (4), Fiji keratophyre (Gill, 1970).

and its importance has been stressed by a number of authors, including Lambert and Heier (1968), Sighinolfi (1969), Lewis and Spooner (1973), Field and Clough (1976), and McCarthy (1976). The experimental anatexis of rocks with mineralogy and composition comparable to that of the southern Malawi biotite-plagioclase-quartz ± hornblende gneisses was investigated by Steuhl (1962), Knabe (1970), Büsch et al.(1974). From their data it appears that at temperatures approaching those of the granulites and transitional rocks (750 - 850°C) nearly complete melting would take place in water-saturated compositions. There is indeed field and petrographic evidence of melting not only of the granulites and transitional rocks (see Plates 5, 6 and 13) but also of the amphibolite facies gneisses as emphasised by Bloomfield (1968, p.69). Many of the granulites and transitional rocks have migmatitic structures (see Plates 5 and 13) and, in the Zomba area, leucocratic transgressive veins with very coarse idiomorphic orthopyroxene crystals are present. In addition, the leucocratic granulites exhibit amoeboid, poikiloblastic quartz similar to that of late crystallisate in granitoid rocks. It is therefore crucial to evaluate the degree of partial melting and segregation of the residue if one wants to define the primitive composition of the granulites; and this should not be grossly affected by the depletion of only limited amounts of liquids. Definite evidence of element

depletion (mainly K, Al, Si, Rb and OH) from granulite facies rocks is offered by petrographic and geochemical studies. Yet, among the numerous thin sections of amphibolite to granulite facies transitional rocks investigated,only very few (e.g. nos. 104, 430, and 499, Fig.38) provide definite evidence of a prograde replacement of biotite by orthopyroxene in the absence of K-feldspar. The stoichiometry of the reaction requires in fact the development of a K-bearing phase; and if this is missing, it is deduced that K-feldspar, quartz, plagioclase and H_2O formed a granitic liquid later removed from the sample investigated. Geochemical evidence for elements depletion is derived from the high K/Rb ratios of the K-rich granulites as previously described (see p.167 and Fig.45) while K-poor granulites appear less affected. This may be explained in terms of decreasing melt fractions which can be generated in increasingly melanocratic granulites. Having established that partial melting and element depletion did affect at least a few granulites, the problem is to assess at least in broad terms what percentage of the granulite facies suite was molten at the time of metamorphism. In this regard, the field data suggest that only a relatively minor amount of melt was present because the granulites often preserve their lithological individuality of well-banded rocks. The scarcity of melts may be explained by the water deficiency in the granulites as

made evident by the thermodynamic calculations presented in Chapter 5, which show that melanocratic transitional rocks had $a_{H_2O}^{vapour} \approx 7$ - 35 mole per cent.

This result should be considered in relation to experimental data by Yoder and Tilley (1962) which indicate that for temperatures of about 800°C the plagioclase in rocks of alkali basalt composition starts to melt if P_{H_2O} = 5 - 6 kb. Since at least some of the melanocratic granulites do have an alkali basalt composition, it is likely that, because of the low activity of H_2O, partial melting affected these rocks only in a small way. Considering the leucocratic granulites, Tuttle and Bowen (1958), Brown and Fyfe (1970) and Winkler (1976, p.306) stressed the control exercised by the concentration of H_2O on the percentage of melt in rocks experiencing conditions of high pressure and temperature. Only small amounts of melts may be formed at 800°C in leucocratic granulites if little water was available, and which was provided by the breakdown of hornblende and biotite in the reaction rims, discordant veins and in Type III prograde geometries.

The conclusion that only limited quantities of melt were sporadically formed in leucocratic granulites indicates two things. The first is that it was difficult for the partial melts to be removed on a large scale from their residues and secondly that the depletion of anatectic liquids did not alter

considerably the chemical characters of the granulite suite. These conclusions are strengthened from the observation that certain common rock types maintain their distinctive lithological characters throughout the P-T range encompassed by amphibolite facies gneisses and two-pyroxene granulites.

In the northern Kirk Range (see Fig.38) the granulites recrystallised at temperatures about 150 - 200°C lower than in the Zomba-Blantyre area (see Figs. 36 and 37) and yet in both regions comparable, leucocratic, sodic plagioclase-quartz granulites occur.(3) In the Kirk Range area, K-feldspar-poor hornblende-biotite-gneisses are extensively developed (Bloomfield and Garson, 1965). Rocks similar to these are also frequent in the Middle Shire area (see p. 32) and their careful petrographic investigation across the amphibolite-granulite facies transition zone has failed to indicate gross changes in the plagioclase/K-feldspar ratio, in the anorthite content of the feldspar, and in the percentage of quartz or of the mafic constituents.

Metasomatism is a petrogenetic process believed by certain authors such as Sheraton et al. (1973) and Robinson and Leake (1975) to be operative on a large scale in deep crustal regions

---

(3) Experimental data also indicate that at temperatures in the 600°-650° range only melting of water-saturated granite is possible (Tuttle and Bowen, 1958; Merril, et al., 1970; see Fig.37).

during metamorphism. In southern Malawi this hypothesis appears to be unsupported by the widespread occurrence of banded granulites which maintain well-defined chemical differences between adjacent, often massive, layers. In addition, the Types I and II prograde textures which in general do not exceed 1 - 2 cm in width, point toward a very limited mobility of water, the transporting agent, in unsheared rocks. A more specific metasomatism was advocated by Bloomfield (1968, pp. 89ff,) for the development of perthitic gneisses (in cases remobilised to syenite/granite) from pyroxene granulites by progressive introduction of H, O_2, K, Al, Na, and Ba. It was considered that these elements were derived from lower crustal levels affected by progressive dehydration during high-grade metamorphism. However, this hypothesis does not appear compatible with the occurrence of certain perthitic granulites with a H_2O-deficient mineralogy and an enrichment in elements like P, Ti, and Sr. The absence of hornblende and biotite in certain orthopyroxene-perthite granulites (see Plates 2 and 3) is in fact difficult to reconcile with the high activity of H_2O that should characterise metasomatic rocks. Moreover, the refractory behaviour of elements such as P, Ti and Sr in crustal anatectic processes has been described by McCarthy (1976), Lambert and Heier (1968) and Lewis and Spooner (1973), who observed that these elements tend to be concentrated on the

granulites depleted of granitophile components (U, Th, Rb, K, etc.).

The only area of Malawi where metasomatism has probably been operative is near Tengani (see Fig.38). In this area the granulites and anorthosite have been intensely sheared, scapolitised and retrograded to hornblende-biotite assemblages by a fluid phase composed of H_2O, Cl and CO_2 as suggested by petrographic evidence and geochemical data. Finally, a prehnitised anorthosite from a nearby locality (no.141, Fig.38) probably suffered H_2O and Ca metasomatism to convert anorthite (Ca = 1 atom/mole) into prehnite (Ca = 2 atoms/mole) if no other Ca-mineral had been present.

The last process possibly relevant to the petrogenesis of granulites and gneisses is metamorphic segregation, investigated extensively by Bowes and Park (1966), and Evans and Leake(1960). According to these authors, the rocks redistribute their cations under the effect of tectonic stress, and concomitant mineral blastesis produces leucocratic and melanocratic bands often several metres long and ± 1mm to ± 2cm wide. The contacts between striped and unstriped amphibolites are generally gradational in the examples referred by Evans and Leake (1960). While it is possible that metamorphic segregation could have produced the banding in melanocratic transitional rocks (see Plates 5, 6 and 13), the thick melanocratic layers within

banded granulites and gneisses in Malawi are massive, homogeneous and with contacts generally sharp. Further, since in southern Malawi rocks of undoubted sedimentary origin such as marble and calc-silicate granulite are interbanded with typical granulites, a primary origin for the typical regional layering is generally acceptable.

In this regard, the banded granulites are most likely of supracrustal origin, and probably represent either volcanic rocks (see Figs. 39 and 41, and Tables 38 and 39) or chemically similar greywackes, perhaps together with metamorphosed plutonic igneous rocks.

The petrochemistry of the amphibolite facies gneisses and of the amphibolite to granulite facies transitional rocks indicates either equivalence to diopside-normative granulites of basaltic, andesitic, rhyolitic, keratophiric composition, or to greywacke, shale and pelite (see Figs. 40 and 42, and Table 40). The affinity of the gneisses of the Tambani area (see Fig.38) to basalt, andesite, quartz-monzonite was mentioned by C.E. Tilley (quoted in Cooper and Bloomfield, 1961, p.15). In addition, bands of basaltic rocks with relict andesine/labradorite, augite and olivine (see cols. a, and b, Table 20) occur in the same area and these were considered of supracrustal volcanic origin and contemporaneous to the enclosing gneisses by Cooper and Bloomfield (1961, p.185).

The presence near Ncheu of a quartz-Mn-pyroxene-spessartine rock (no.462, Fig.38) fits the above interpretation as it may be derived from a manganese chert, a sediment typical of volcanosedimentary environments (Stanton, 1972, p.492). In the same way a nepheline gneiss from Ncheu (no.26, Fig.38) may be derived from analcime-bearing argillites or ashes (Bloomfield, 1968, p.55). Similar tuffs were reported from a New Zealand geosyncline sequence (Blatt et al., 1972, p.566). In addition, the aegirine gneisses and granulites of central Malawi were also considered of igneous origin by Carter and Bennett (1973).

6.3 Plutonic Rocks

In addition to the granulite and amphibolite facies rocks, there are a number of clearly plutonic types emplaced within the Basement Complex of southern Malawi. Of these, the anorthosite and the Perthitic Complexes are generally restricted to granulite facies terranes while pyroxenite, amphibolite, the Ring Complexes and finally the granitoid orthogneisses occur both in the granulite and in the amphibolite facies terranes.

Anorthosite occurs in southern and central Malawi as large sill-like uniform bodies, with a Na_2O content ranging from 3 to 5 per cent and a scarce content of mafic minerals. In the Tengani area (no.129b, Fig.38) anorthosite includes lenses and layers of Fe-Ti (magnetite-ilmenite-rutile ± garnet) ore with veins of orthopyroxene ± garnet rock (Bloomfield, 1958, p.19).

Well developed bands of melanocratic to hypermelanic garnet-two-pyroxene ± hornblende rocks were also observed in anorthosite from the Ncheu area (no.456, Fig.38) while in the north, at Linthipe (no.19, Fig.38) the massive plagioclase rock is bordered by a more melanocratic variety. Finally, near Blantyre, inclusions of anorthosite in a charnockitic granulite dyke present cumulus textures of plagioclase laths with intercumulus quartz and K-feldspar (no.115, Fig.38). A meta-sedimentary origin of anorthosite from marl and greywacke, with or without an intervening partial melting + liquid depletion event, was proposed by Hietanen(1969) and de Vore (1975). This interpretation may not be a priori excluded at least for some of the minor occurrences. However the main bodies of southern Malawi are in general too large in size, uniformly massive and leucocratic to be explained in the above way, and for example the anorthosite of Linthipe is ± 200 km^2 in area.

The possibility that anorthosite represents the product of partial melting of amphibolite under high P_{H_2O} and P-T compatible with those of the granulite facies was investigated by Yoder and Tilley (1962). However, southern Malawi amphibolites and related rocks were probably characterised by a very low P_{H_2O} to allow partial melting, complementary bodies of (pyroxene-) hornblendite with an adequately large size are not present in the terranes where anorthosite occurs.

The above discussion, based on petrological and field evidence suggests an igneous parentage for the massifs of anorthosite characterised by oligoclase/andesine to labradorite-type plagioclase. However, the origin of this rock is problematic, mainly since the majority of anorthosite bodies are 1 300 ± 200 million years old and they generally occur in two main belts when plotted on a predrift continental reconstruction (Herz, 1969).

A general model involving plagioclase fractionation from a basaltic-andesitic liquid rather than simple crystallisation of an anorthositic magma was stressed by many authors (Isachsen, 1969; ; Sighinolfi and Gorgoni, 1975; Bridgwater and Windley, 1973; Wynne-Edwards, 1976; Higgins and Doig, 1977).

A mantle origin of the parent magma was inferred by Emslie (1975) from the occurrence in Quebec anorthosites of sheared aluminous orthopyroxene megacrysts formed at P = 15 ± 5 kbar. This model by Emslie (1975) seems perhaps applicable to the anorthosite bodies of Tengani. These include probable cumulate bands of ilmenite-magnetite ± rutile ore (Bloomfield, 1958, p.64ff.). Associated veins of aluminous orthopyroxene(in occasional megacrysts) ± garnet ± rutile, were recrystallised at P ≥ 12 kbars (see no.135b, Fig.38 and Plate 17; Bloomfield, 1958, pp.17 and 64ff.).

Syenite is the main lithotype constituting the Perthitic Complexes, which occur in massifs of variable dimensions within

the granulite facies terranes (see Fig.38). Beside the perthitic gneisses and associated granulites, these rocks may grade into either (quartz-) monzonite or quartz-syenite and granite. In addition, this suite of perthitic rocks appears spatially associated with anorthosite, for example:(i) masses of syenite and syenitic gneiss surround the Linthipe anorthosite, intruded by dykes of perthite rock on the Linthipe river (see S, Fig.38); (ii) sill-like masses of syenitic, granitic gneiss and granulite alternate with anorthosite west-south-west of Ncheu (see Fig.38 and Map 4 in the pocket at the back of the thesis); and (iii) xenoliths of anorthosite are included within a dyke of perthite-rich charnockitic granulite near Blantyre (no.115, Fig.38).

On the basis of the reasons previously expressed, the Perthitic Complexes did not probably form by metasomatism (Bloomfield, 1968, 1970) but represent metamorphosed plutonic igneous rocks. In this second case the Perthitic Complexes might be comparable for origin, geological setting, lithological association, and petrochemistry to certain plutonic igneous rocks (see Table 39) often accompanying anorthosite in Precambrian granulite facies terranes (de Waard, 1969; Anderson and Morin, 1969; Krank, 1969; Bridgwater and Windley, 1973). The association of anorthosite with (pyroxene-bearing) igneous rocks of monzonite (quartz-) syenitic and K-rich granitic

composition was defined as the 'anorthosite suite' by Emslie (1973). This association is possibly related to the rapakivi granites, an acidic suite characterised by $K_2O/Na_2O > 2$ (Krank, 1969; Carmichel et al., 1974).

With regard to plutonic rocks within amphibolite and granulite facies terranes, insufficient analytical data is available for the isolated masses of ultramafic rocks, mainly meta-websterite and rare garnet-olivine-metapyroxenite described by Bloomfield (1968, p.138). An igneous origin and a primary crystallisation under spinel-peridotite facies conditions (O'Hara, 1968) was asserted by Haslam et al. (1976) for the amphibolite and serpentinised peridotite rock from Chimwadzulu in the northern Kirk Range (see Fig.38). Moreover, the chemical resemblance of the Chimwadzulu serpentinised peridotite to alpine-type peridotitic rocks was described by Bloomfield (1968, p.138). In contrast, a metasomatic origin is probable for the bodies of biotitite, scattered within the metamorphic terranes of the western Middle Shire Valley and possibly related to the Mlindi Complex (see Fig.38, Bloomfield, 1968, p.68). Rocks similar to biotitite were described by Gittins et al. (1975) as formed by localised fenitisation in an ultramafic carbonatite complex in Ontario, Canada. However, there is no evidence as yet of any alteration of the enclosing gneisses nor of the presence of marbles akin to metamorphosed carbonatite in

Malawi (Morel, 1958). As a consequence, the bodies of phlogopitite are probably exotic masses formed by metasomatism of pyroxenite or peridotite at greater depth. This is in accordance with a model put forward by Lloyd and Bailey (1973) and Aoki (1975) for certain mantle-derived xenoliths in alkaline volcanics from Uganda, the Eifel region of Germany and South Africa.

Within the amphibolite and granulite facies terranes, more or less concordant bodies of metagabbro with relic igneous textures, and homogeneous bands of amphibolite are common. General field relationships suggest that these rocks may be comparable to certain melanocratic granulites and that their chemistry was not altered during metamorphism. Like many among the granulites, these rocks plot in the field of Hawaiian tholeiitic and alkalic rocks (see Fig.43). In addition, the chemical analyses of a melanocratic granulite and of an amphibolite are broadly comparable (cf. col. a, Table 20, and col.e, Appendix IV-11).

The infracrustal Ring Complexes of the Middle Shire Valley and Zomba areas (see Figs. 5 and 38) occur in a variety of metamorphic environments, but only the Mlindi Complex lays within amphibolite facies terranes while the others are in granulite or amphibolite to granulite facies transitional areas. According to Morel (1961b) this suite was igneous and pre-kinematic; however this assertion was criticized by Bloomfield (1965b, 1968 and 1970) who maintained a late-kinematic and

metasomatic genesis. An updated petrogenetic model for the Ring Complexes must satisfy the following evidence: (a) the Chipilanje - Little Michiru body (see Fig.38) was emplaced within the amphibolite to granulite facies transitional area in the Middle Shire Valley; (b) the same complex has a strongly deformed canoe-shaped zoned structure, yet no widespread shearing and cataclastic textures have been described in the literature (see Morel, 1958; Bloomfield, 1968); (c) perthitic norite from the Chipilanje - Little Michiru Complex was described with a granulitic texture and intrusive contacts into melanocratic granulites (Morel, 1958, p.44); and (d) quartz-syenite from the Ntonya Complex (no.9, Fig.38) is characterised by a charnockite-like dark-green colour, a waxy lustre and a clearly metamorphic orthopyroxene. The most logical interpretation of the above data is that the Ring Complexes are probably of igneous origin and emplaced before or during an important tectonometamorphic event which affected the region. This induced occasional recrystallisation under conditions prograde from the amphibolite facies to the granulite facies and variations of a $^{Vapour}_{H_2O}$, $X^{rock}_{Si,}$ and T mainly influenced the attainment of a granulite facies mineralogy.

Considering the granitoid orthogneisses, those of the Middle Shire Valley (see Fig.38), previously not recognised, are similar to granodiorite, relatively deficient in perthitic

K-feldspar and richer in oligoclase-andesine, hornblende and biotite. The metamorphic grade of these rocks is variable and a garnet-clinopyroxene paragenesis is possibly preserved at Mwanza while further east, amphibolite and orthopyroxene-bearing transitional assemblages are characteristic (see Fig.8 and Plates 7(a) and (b)). The frequent occurrences of cognate melanocratic xenoliths and the absence of metasedimentary, anatectic resistors suggest that this large granitic-granodioritic mass is of igneous origin. It is however unclear whether this is an early- to synkinematic intrusion or perhaps the relict of a cratonic infrastructure of greater antiquity. Comparable granodioritic gneisses with melanocratic amphibolite layers and schlieren are in fact typical of many Precambrian, mainly Archean terranes (Tarney, 1976).

Among the felsic plutonic rocks of central Malawi, the Dzalanyama Batholith (see Fig.20) occupies a prominent place as it extends into adjacent Mozambique. Its pre-kinematic and anatectic origin was argued by Thatcher and Walter (1968, p.38). An anatectic origin for the quartz-syenitic to granitic 'permeation gneisses' of central Malawi was also suggested by Bloomfield (1968, p.154); and finally the granite and quartz syenite emplaced along the shore of Lake Malawi were regarded as high-level, post-kinematic intrusions by Bloomfield (1968, p.95).

CHAPTER 7. GEOCHRONOLOGY

7.1 Introduction

To date there is very little detailed information on the age of the metamorphic terranes in southern Malawi, and, in most cases, it was obtained by dating micas from amphibolite facies rocks of the Middle Shire Valley and the Kirk Range areas. The present chapter therefore presents and discusses data for granulite facies and amphibolite facies rocks of southern Malawi kindly supplied by Professor T. N. Clifford and other geochronologists of South Africa and the United Kingdom whose help is acknowledged. Most of the dated samples were collected by Professor T. N. Clifford, but a group of 12 specimens was taken by the candidate.

A review of previous age determinations, ranging between 550 and 380 m.y. ago, was made by Bloomfield (1968), and they are listed in Appendix VI-1.

More recent preliminary Rb/Sr (whole-rock) dating on three suites of granulites, amphibolite facies rocks and discordant dykes yielded 1 126 ± 29; 718 ± 25 and 493 ± 16 m.y. old ages respectively (Clifford, 1974).

In accordance with the multidisciplinary approach followed in this thesis, it was considered crucial to date amphibolite and granulite facies rocks from the Middle Shire Valley

transition zone where they coexist and grade into each other by primary gradients.

The samples dated (gneisses, granulites and transitional types) include supracrustal and metaplutonic rocks, whose localities are shown in Fig.47 and in Appendix VI-A and VI-B.

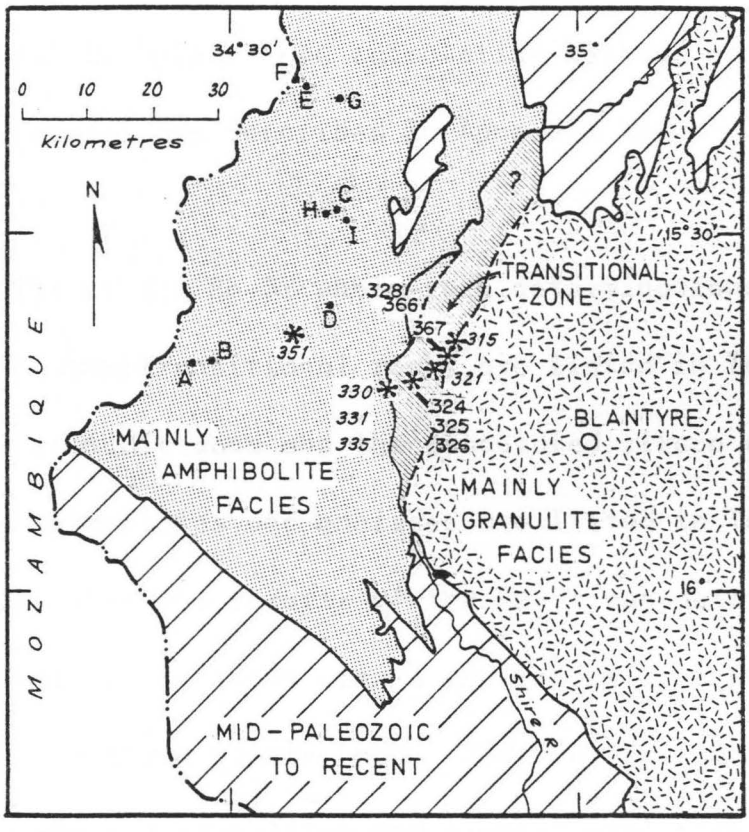


Fig.47. Locality map of samples from the Middle Shire area used for age determinations (nos. 315 to 367). (A) to (I) are the localities of published radiometric mineral ages listed in Appendix VI-1. (Geology modified after Bloomfield, 1968; Morel, 1958)

In addition, the results of Rb-Sr whole rock age determinations previously carried out by Professor T. N. Clifford on suites of

regional granulites, gneisses and intrusive dykes will be considered.

The rocks of southern Malawi were dated with the zircon U-Pb method by Dr. A.J. Burger of the CSIR, Pretoria and by the Rb-Sr whole-rock technique by Messrs. D.C. Rex and A. Gledhill and Miss J. Gronow of Leeds University. Details of the analytical techniques and calculating methods adopted on dating the samples are described in Appendix VI(iii)

7.2 Results

The results of the Rb-Sr whole-rock determinations on the Middle Shire area transitional rocks are listed in Table 41, while the U-Pb isotopic data and the calculated zircon ages for a number of granulites and gneisses are listed in Table 42.

Fig.48 presents the results of the Rb-Sr age determinations, and the main isochron is shown with a continuous line which was recalculated using three points, nos. 330, 331 and 335, representing anatectic granulites and transitional rocks from nearby outcrops in the same locality (see Appendix VI-A). This isochron gives an age of 1 128 $\pm$ 14 m.y. with a R_o = 0,7027 and a MSUM value = 0,757. Two lines parallel to this isochron and the data points for the remaining samples from other Middle Shire localities are also shown in Fig.48. Considering the zircon isotopic data, two different graphic interpretations are considered here. In Fig.49(a) the points representing

TABLE 41 - Rb-Sr ISOTOPIC DATA AND PETROGRAPHIC DESIGNATION FOR GRANULITES AND ASSOCIATED ROCKS FROM THE MIDDLE SHIRE

Sample[1] no.	Slide no.	Name	Rb_{ppm}	Sr_{ppm}	Rb^{87}/Sr^{86}	Sr^{87}/Sr^{86}
315	X21356	Quartzo-feldspathic granulite	34	604	0,164	0,70620
321	X21753	Granulite with leucocratic bands	42	642	0,190	0,70594
330	X21245	Granitic gneiss	90	352	0,736	0,71448
331	X21246	Quartzo-feldspathic granulite	29	897	0,094	0,70418
335	X21247	Mesocratic gneiss	82	407	0,584	0,71218
351	X21224	Charnockitic granulite	69	464	0,428	0,71035
324	MA 203	Mesocratic granulite	70	411	0,491	0,71268
325	MA 204	Mesocratic granulite	35	422	0,239	0,70944
326	MA 205	Mesocratic granulite	54	450	0,349	0,70925
328	X21752	Charnockitic gneiss	57	555	0,299	0,70922
366	X21750	Melanocratic granulite	4	437	0,025	0,70357
367	X21751	Mesocratic hornblende granulite	4	744	0,017	0,70328

Analyst: A.Gledhill.

(1) See Fig.47 and Appendices VI-A, VI-B and VI-2 for localities, and Appendix II-3 for petrographic descriptions.

TABLE 42 - U-Pb ISOTOPIC DATA FOR ZIRCONS OF GRANULITES AND ASSOCIATED ROCKS FROM THE MIDDLE SHIRE AREA

		ppm		isotopic ratios			calculated ages (m.y.)			atomic ratios	
Sample[1]	Fraction	U	Pb	206 Pb / 204 Pb	207 Pb / 204 Pb	208 Pb / 204 Pb	207 Pb / 235 U	206 Pb / 238 U	207 Pb / 206 Pb	207 Pb / 235 U	206 Pb / 238 U
315	composite	292	24	3 331	230	2 781	766	378	318	0,45	0,05
321	composite	106	10	1 851	128	167	655	588	570	0,78	0,09
330	composite	247	31,8	12 084	857	13	922	807	769	1,22	0,12
330	100-150µ	302	32	9 070	630	923	922	687	632	0,97	0,10
330	75-100µ	334	22	8 681	609	921	881	490	410	0,62	0,07
331	composite	236	26	3 117	220	428	802	655	639	0,94	0,10
331	75-100µ	219	24,5	9 132	629	1 031	846	710	670	1,01	0,11
331	75-100µ	247	27,8	7 252	495	1 007	818	691	664	0,97	0,11
331	<50µ	285	27,3	4 927	344	703	834	619	563	0,84	0,09
335	composite	223	26	6 803	477	739	870	746	705	1,08	0,12
335	>150µ	190	25	4 702	330	764	840	777	751	1,14	0,12
351	composite	218	26	6 723	487	885	936	750	691	1,09	0,11
351	100-150µ	134	21	4 572	329	634	902	892	884	1,41	0,15

Analyst: A.J. Burger.

(1) See Fig.47 and Appendices VI-A, VI-B and VI-2 for localities and Appendix II-3 for petrographic descriptions.

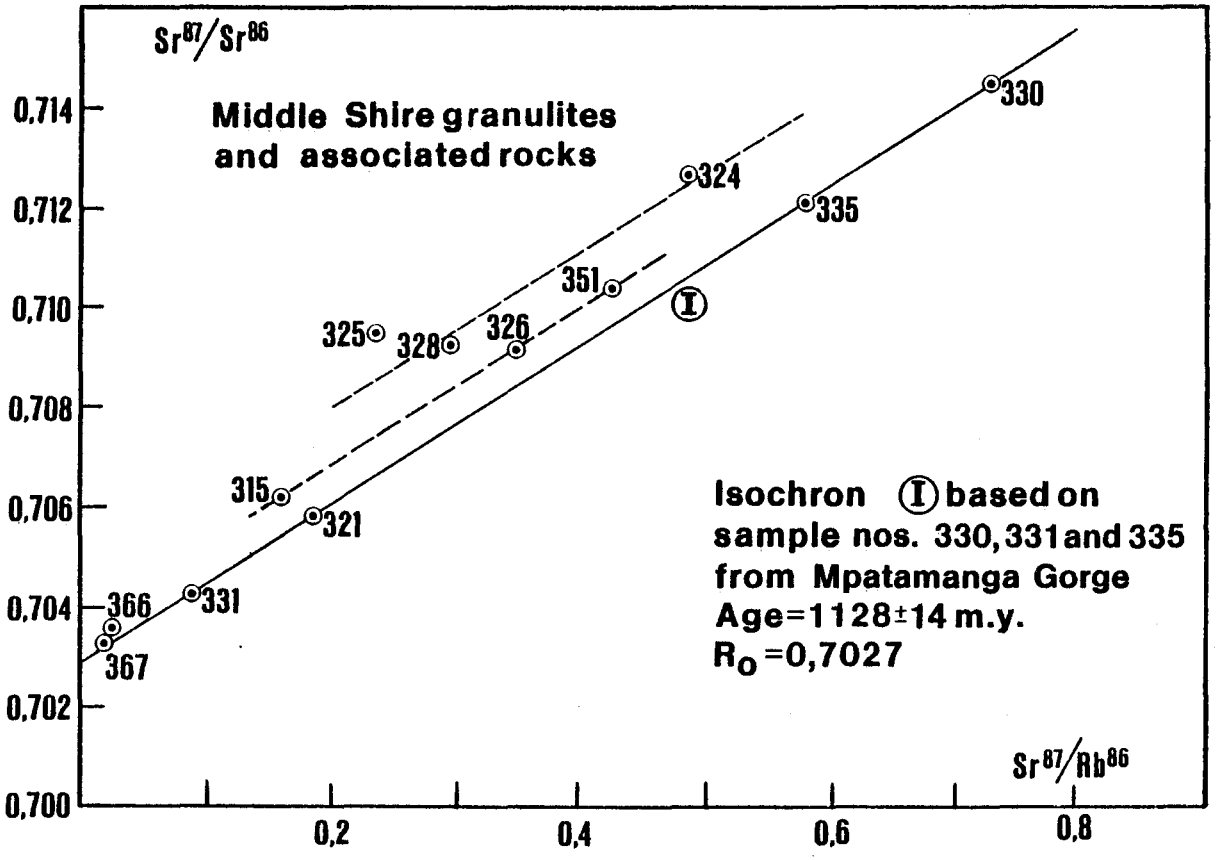


Fig.48. Rb-Sr whole-rock isochron diagram (after York, 1969) for the Middle Shire granulites, and associated rocks (see Fig.47 and Appendices VI-A, VI-B and VI-2 for localities and Appendix II-3 for petrographic data).

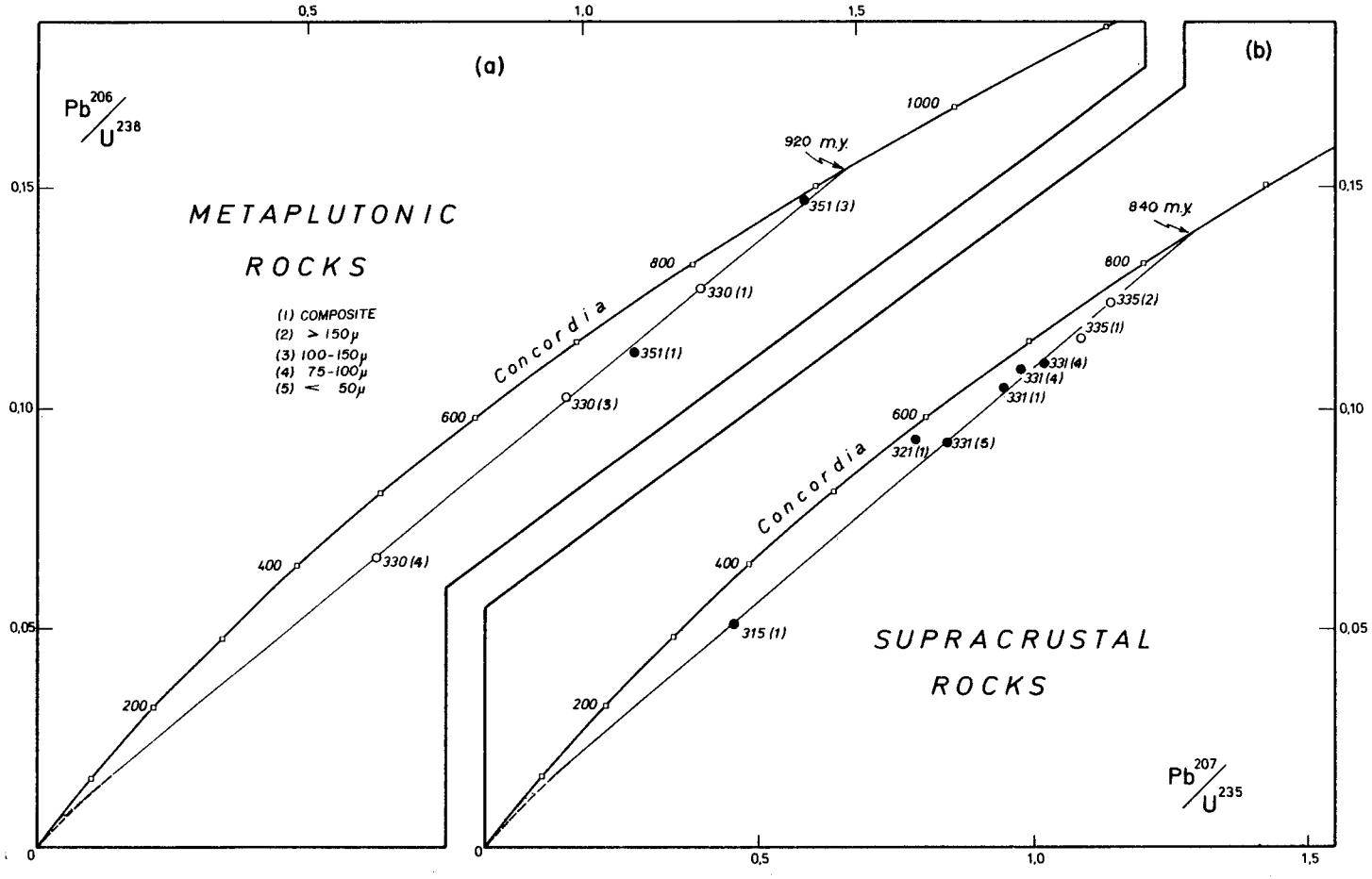


Fig.49(a). Concordia plot for zircon fractions from metaplutonic rocks of the Middle Shire area; (●) hypersthene-bearing rocks, and (o) gneisses and orthogneisses (see note 1 to Table 42).

Fig.49(b). Concordia plot for zircon fractions from supracrustal rocks of the Middle Shire area (the symbols are the same as in Fig.49(a); see note 1 to Table 42).

whole zircon concentrates and size fractions from metaplutonic rocks, charnockitic granulite (no. 351) and granitoid orthogneiss (no.330), define a chord with an upper intercept age of 920 m.y.; the lower intercept of 40 m.y. is probably spurious and the spread of data points is more readily understood in terms of continuous Pb-diffusion.

supracrustal granulite (nos. 315 and 321), amphibolite facies (no. 335) and transitional rocks (no.331) present a relative scatter and more than one chord may be calculated. However, a 7-point regression line, calculated excluding the composite fraction of granulite no.321 , provides a concordia upper intercept age of 840 m.y. The MSUM values calculated for the chords of the metaplutonic and supracrustal rocks are 0,44 and 0,55 respectively, indicating that the scatter of the data points is less than what is predicted by experimental uncertainties.

7.3 Interpretation

The lateral extent and degree of Rb-Sr isotopic homogeneity in igneous and metamorphic suites during mineral (re) - crystallisation is a process not yet fully understood and which for igneous complexes has only recently begun to be investigated (McCarthy and Cawthorn, 1980). It is therefore appropriate to consider Rb/Sr ratios and isotopic distributions in a suite of prograde transitional rocks from an area of the Middle Shire Valley which is sufficiently narrow to keep the geological disturbances to a minimum.

The small scatter of data points for nos. 330, 331 and 335 from the ideal straight line is possibly consistent, among other possibilities, with a model of near-complete homogenisation at the scale of the outcrop, up to a distance of about 200m (see Appendix VI-A). This is particularly true since considerable difficulty was experienced in the field in establishing whether or not the orthogneiss no.330 could represent a total melt product of the mesocratic gneisses associated (no.335). With increasing distance between each other, the remaining samples present in Fig.48 show a clear tendency to scatter. No isochron can in fact be calculated for samples nos. 324, 325 and 326 collected in an area about 1 km wide. Even greater reciprocal distances separate the remaining samples nos. 315, 321, 328, 351, 361 and 367 and their corresponding data points also present a substantial scatter in Fig.48. Yet, it is perhaps significant that 8 out of 9 samples from the separate localities plot either on (or very near to) the main Mpatamanga Gorge isochron (Ⓘ in Fig.48) or otherwise on (or near to) a set of lines parallel to it. This observation suggests that the granulites and gneisses of the Middle Shire transition zone had perhaps different Ro (Sr^{87}/Sr^{86}) initial ratios ranging from about 0.7027 to at least 0,7045. The age obtained is particularly significant since it is nearly coincident with the 1 085 ± 71 m.y. old isochron (with Ro = 0,7066) calculated by Clifford et al. (in prep.) from a

suite of regional granulite facies rocks of the Zomba, Blantyre, Mangochi and other areas (see Appendices VI-B and VI-C).

In addition, the results of the Rb-Sr isotope age determinations confirm petrographic observations that, in the Middle Shire, amphibolite facies gneisses grade into granulite facies rocks by primary P-T gradients. For consistency with the method adopted in the Middle Shire area, an attempt was made to calculate separate isochrons for the Zomba, Blantyre, Dedza and Mangochi areas using the data of Appendix VI-3. However most of the data points presented an excessive scatter with the exception of the three samples, nos. 65, 67 and 75, from an area north-east of Mangochi which yielded an errorchron of 981 ± 34 m.y. with a Ro = 0,7103 and a MSUM = 3,4 (see Appendix VI-D). Of additional interest is the slope of the line joining two samples of interbanded melanocratic (no. 92) and leucocratic (no.93) retrograded granulites from the Dedza area, and which is less steep than a 750 m.y. reference isochron (see Appendix VI-C). The age of 1 128 ± 14 m.y. obtained dating the gneisses from the Mpatamanga Gorge of the Middle Shire is strikingly different from an unpublished age of 835 ± 65 m.y. with a Ro = 0,7051 obtained on regional amphibolite facies gneisses (Clifford et al., in prep.; see Appendices VI-4 and VI-E). The latter age is strictly comparable to the age of 826 ± 32 m.y., with a Ro = 0,7048 and MSUM = 2,4 provided by

an isochron based on samples from a single quarry near Liwonde (see Appendices VI-B and VI-F). The near coincidence of the Ro of the regional gneisses with that of the Liwonde gneisses might perhaps imply that the amphibolite facies terranes of southern and central Malawi either evolved from a pre-existing material with a Sr^{87}/Sr^{86} initial ratio, which was very uniform over large areas, or that they experienced an episode of exceptional isotopic homogenisation.

Finally the Middle Shire granulites appear far older than the granite and syenite dykes from various localities in southern Malawi and whose scatter precludes the calculation of a single reliable isochron (Clifford et al., in prep.; see Appendices VI-5 and VI-G).

Considering now in detail the U-Pb age determinations, the metaplutonic rocks seem to indicate an event at about 920 m.y. ago; and the closeness of one of the fractions of sample no. 351 to the concordia curve suggests the possibility that the crystallisation of the zircons occurred shortly before the 920 m.y. old metamorphic event (Dr. J. Barton, personal communication). A narrow time interval is suggested by the lack of significant scatter of the analytical points relative to the 920 m.y. chord as otherwise expected for a multistage model. In contrast, the rocks of supposed metasedimentary origin associated with the former indicate a metamorphic event

which is about 80 m.y. younger. This apparently took place about 840 m.y. ago.

In addition, Fig.49(a) indicates that the granitoid orthogneisses were affected by the same event recorded in the charnockitic granulites; and similarly Fig.49(b) shows that also supracrustal gneisses and granulites yield a common age.

The study of the zircon morphologies supports field observations on the intrusive nature of sample no.351. The crystals have predominantly idiomorphic, double terminated, stout shapes indicative of primary magmatic generation (see Plate 20). However, the majority of the gneisses and granulites often carry rounded and oval, probably corroded zircons (see Plates 21 to 23), which are a common feature in high-grade metamorphic rocks (Professor T.N. Clifford, personal communication). Refacetted zircons and slender, uncorroded crystals are also present in leucocratic granulites (see Plate 22). These various morphologies, particularly the ghost zircon nuclei rich in older lead (see Plate 20), could possibly account for age differences the metaplutonic and supracrustal rocks yield. Therefore, the 920 m.y. event would either represent a 'mixed' age, or it represents the time at which T dropped below a 'threshold' value for the re-equilibration in the coarser idiomorphic zircons of the metaplutonic rocks (Dr. V. Köppel, personal communication).

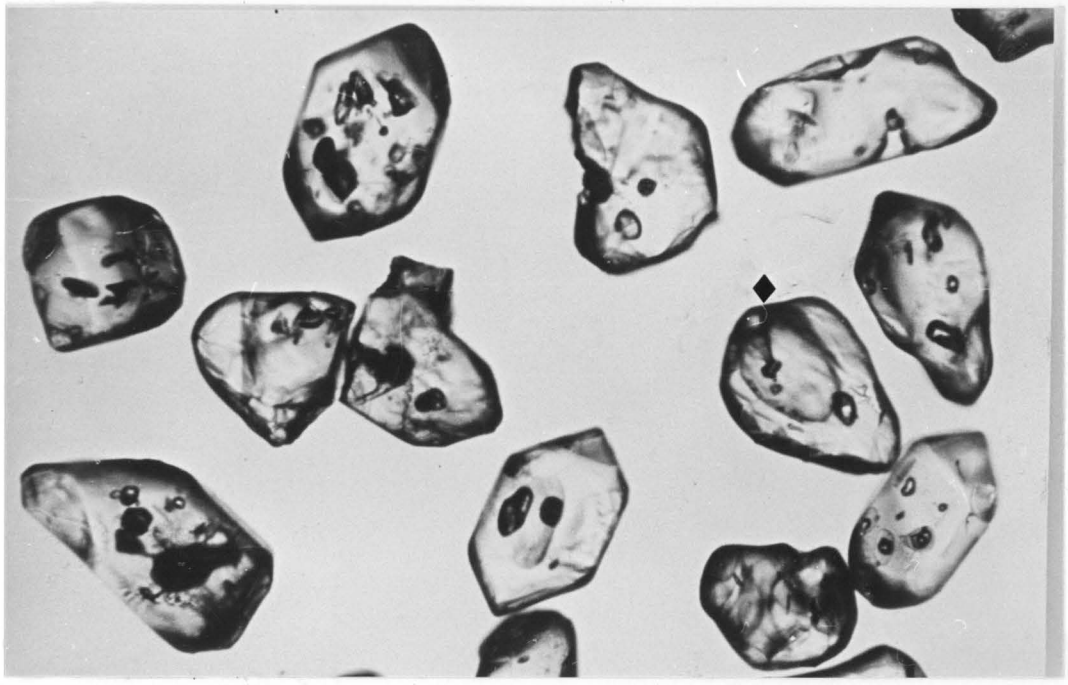


Plate 20. Zircon population of a charnockitic granulite; (♦), crystal carrying ghost inclusion of older zircon. X100 (no.351, see Fig.47).



Plate 21. Zircon population in orthogneiss. X90 (no.330, see Fig.44).



Plate 22. Zircon population of a leucocratic migmatitic granulite; (◆), new facet developed. X90 (no. 331, see Fig.47).

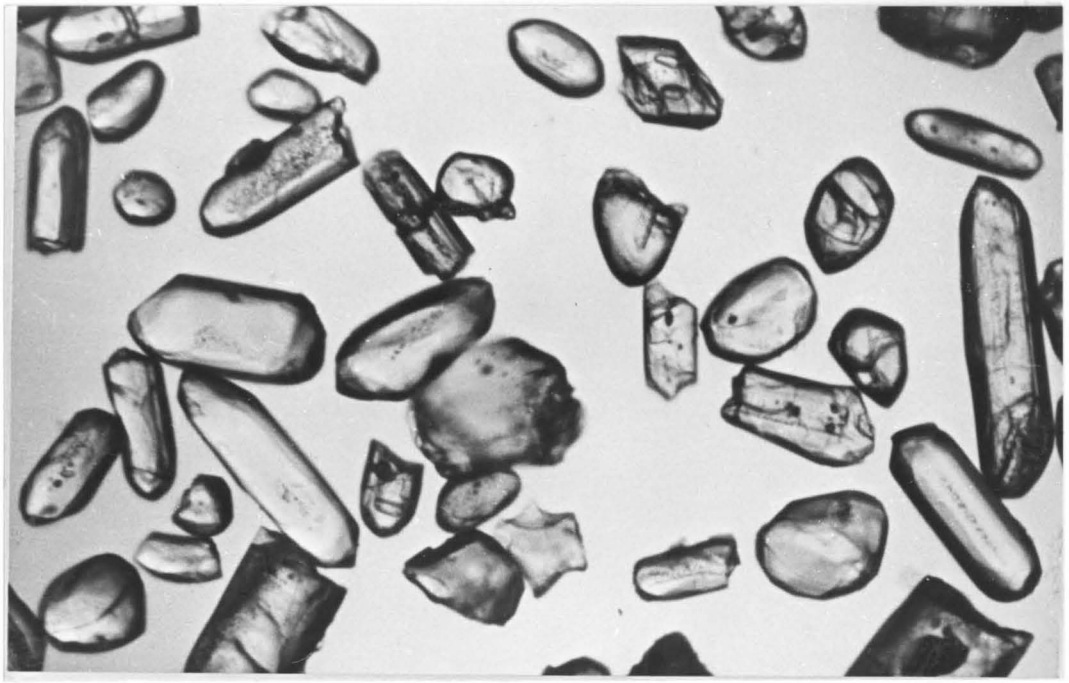


Plate 23. Zircon population in a leucocratic granulite. X120, (no.315, see Fig.47).

Likewise, the age of 840 m.y. should represent the time at which the same threshold was passed at lower T in the more corroded and recrystallised zircons of supracrustal origin.

According to this interpretation, neither would reflect the time of the peak of high-grade metamorphism, which the Rb-Sr whole-rock method, applied to the same samples, dates further back at 1 128 ± 14 m.y. ago.

CHAPTER 8. CONCLUSIONS

Southern Malawi is at the heart of one of the major and least known tectonometamorphic terranes of Africa, namely the Mozambique Belt. Broad expanses in the central and south-eastern parts of the country are characterised by pyroxene or garnet-bearing rocks; and massive granulites, in some cases clearly intrusive, are also present locally. Elsewhere the metamorphic grade is clearly lower and amphibolite and gneisses underlie much of central Malawi and the western part of southern Malawi.

Near the Shire River, west of Blantyre and elsewhere (see Fig.38) transitional rocks occur between the higher and the lower grade terranes and are characterised by the association of pyroxene-bearing gneisses and hornblende-biotite granulites. Three different kinds of textural relationships between amphibolite and granulite facies mineral parageneses have been identified in many different areas of southern and central Malawi and have been designated Types I, II and III. Such textures contributed substantially to the clarification of the development of mineral sequences that are depicted in Fig.50 in which the arrows indicate the direction in which the mineral reactions have proceeded. The thickest line represents a

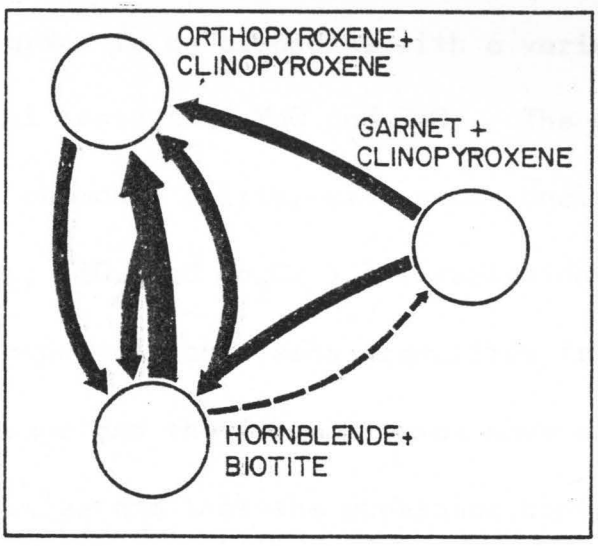


Fig.50. Mineral relationships amongst southern Malawi amphibolite and granulite facies parageneses (see text for explanation).

sequence of prograde development documented by all three types of textures while the thinner, continuous lines refer to reactions only shown by two types of prograde geometries and in a more restricted number of localities. The thinnest, broken arrow indicates a sequence of mineral development only seldom encountered; and the bifurcating arrows represent the multiple mineral reactions present in certain polymetamorphic granulites.

Field and petrographic evidence and an electron-microprobe investigation of the typical minerals of the granulites have demonstrated their metamorphic origin; they also show that the typical orthopyroxene is hypersthene or, more seldom, bronzite and ferrohypersthene while the clinopyroxene is a calcic augite. Analyses of coexisting garnet and clinopyroxene

show that the former is an almandine with a variable, but often substantial content of MgO and CaO. The pyroxene is an augite, less commonly salite, with occasional appreciable amounts of Al_2O_3, TiO_2 and Na_2O. The variation diagrams show that the garnet-clinopyroxene granulites from the northern Kirk Range and the Tengani areas have distinct eclogitic affinities and that the grossular content of garnet is distinctly higher in orthopyroxene-free granulites. Amphibole analyses indicate a substantial chemical difference between hornblendes from different metamorphic environments; those from two-pyroxene granulite terranes are Ti-pargasite with minor edenite, while the Ti-poorer pargasite from garnet-clinopyroxene granulite terranes contains tschermakite as an additional component. Finally, a titaniferous biotite transitional to phlogopite is the typical mica of two-pyroxene granulite terranes.

The petrochemistry of the granulites is characterised by a broad variation in the content of SiO_2 from about 43 to 80 per cent which is paralleled by an increase in alkalis (Na_2O + K_2O) from about 3 to 10 per cent and a decrease in iron, titanium, magnesium and calcium oxides. In a substantial number of mesocratic/leucocratic granulites Na_2O predominates over K_2O, while another group is defined by a pronounced K_2O enrichment, up to nearly 8 per cent , and the resulting

distribution of rocks in the appropriate diagrams is distinctly bimodal. The granulites are also diopside-normative and the calculated plagioclase is relatively sodic, seldom exceeding An_{50}, even in melanocratic rocks which are frequently nepheline- and olivine-normative. Many of the rocks in amphibolite to granulite transitional zones are chemically similar to granulites, but an appreciable number is distinguishable by their corundum-normative composition, a pronounced scatter in the K_2O/Na_2O ratio and a predominance of K_2O over Na_2O. The distribution of Rb relative to K in granulites presents a trend marked by K/Rb ratios of 250 to 1 000 while the amphibolite facies gneisses and the transitional rocks often present a more pronounced Rb enrichment with ratios in the 100 - 500 ppm range.

Reasonable estimates of the different P-T conditions prevailing in a number of areas of southern Malawi are shown in Fig.51 and indicate that the Zomba-Blantyre rocks equilibrated in the medium-pressure granulite field of Green and Ringwood (1967), while the rocks of the Tengani and Ncheu areas fall into the high-pressure granulite field of Green and Ringwood (1967). The granulites of Tengani are especially intriguing as they evolved from earlier metamorphic assemblages at pressures in excess of 12 Kb and temperatures above 800° - $900^{\circ}C$. The other areas of southern and central Malawi often experienced

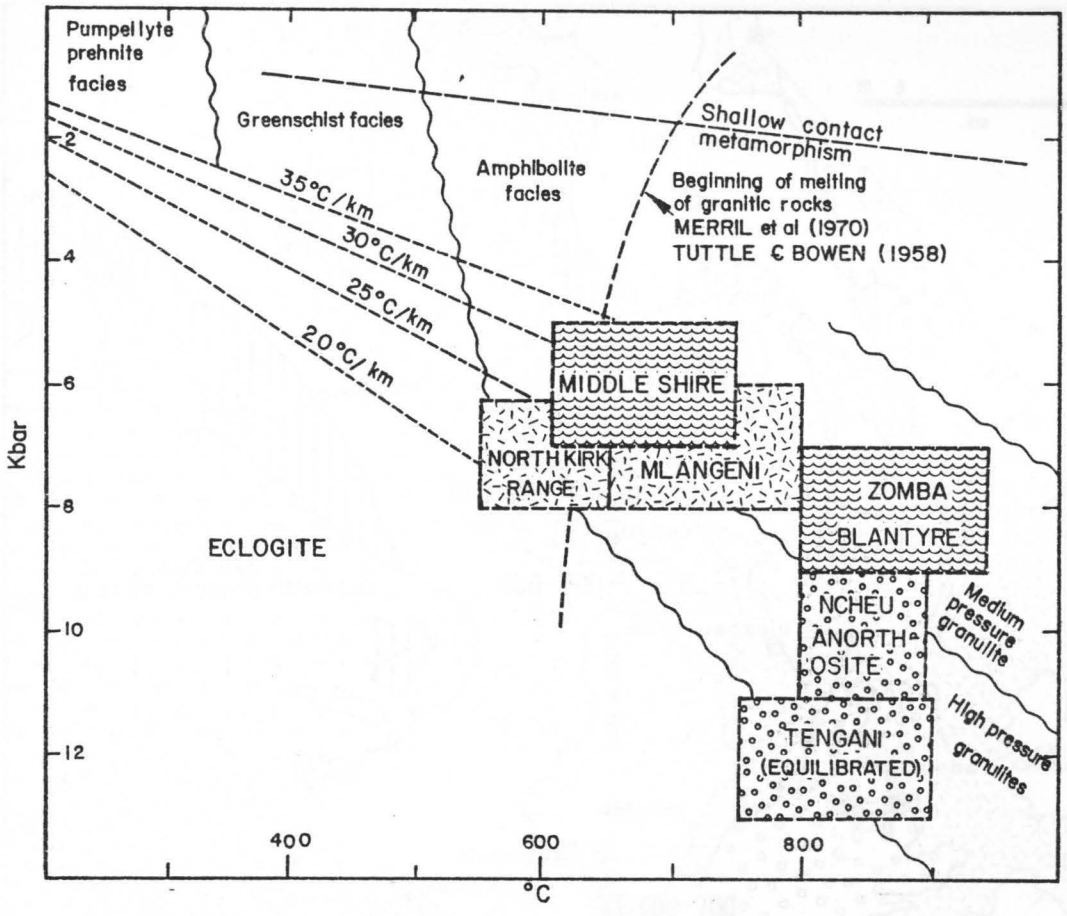


Fig.51. P-T conditions for certain areas in southern Malawi; shown in relation to metamorphic facies and other relevant metamorphic subdivisions and geothermal gradients (after Green and Ringwood, 1967; Winkler, 1974).

metamorphism at considerably lower P and/or T. At Fort Mlangeni (see Fig.52) intermediate conditions between the medium- and high-pressure granulite facies prevailed, resulting in the development of interbanded two-pyroxene and two-pyroxene-garnet rocks with biotite-garnet ± orthopyroxene gneisses. Further south, in the northern Kirk Range (see Fig.52) the P-T conditions straddled the amphibolite/high-pressure granulite facies boundary which are reflected in the widespread

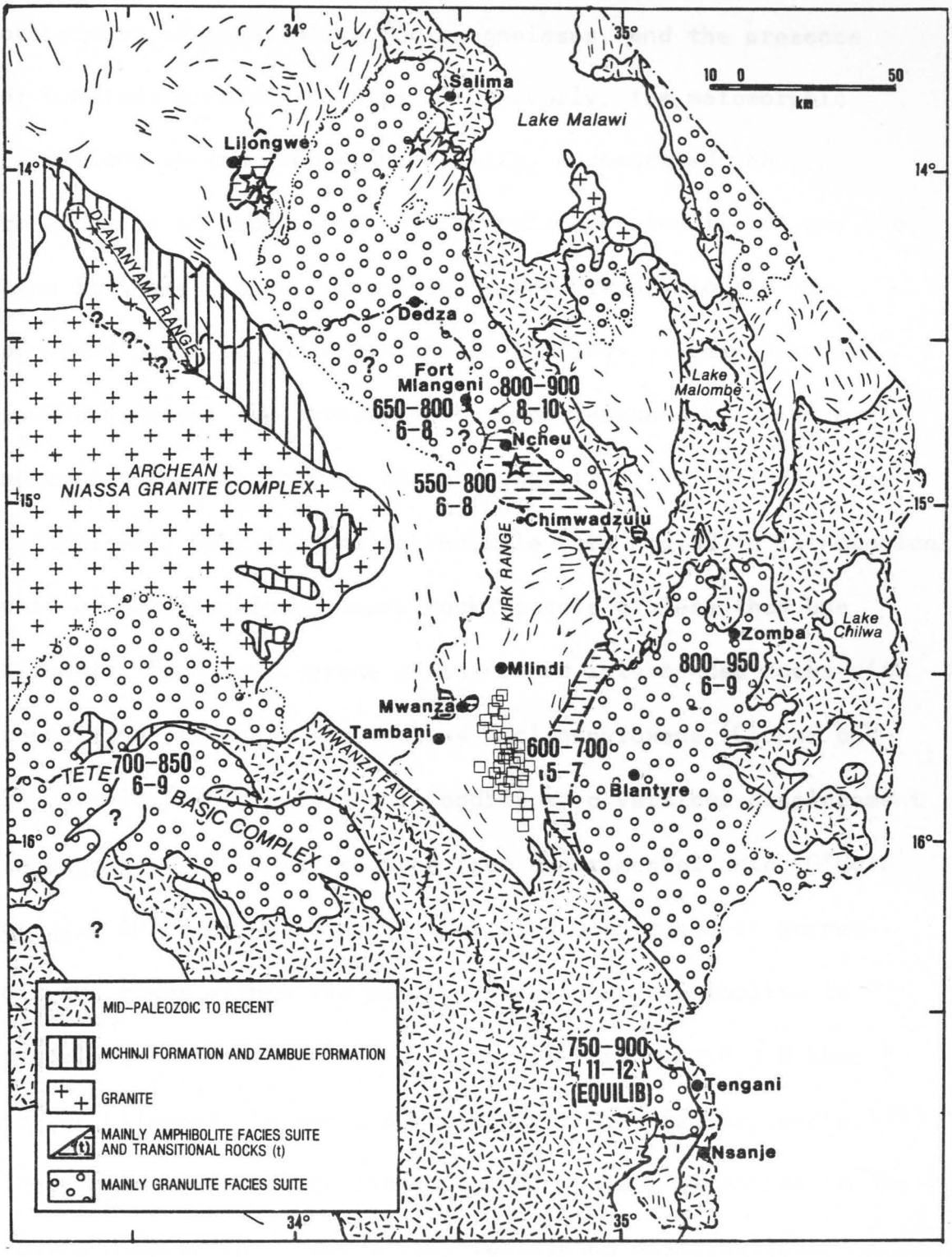


Fig.52. Regional distribution of P-T conditions in southern and central Malawi showing T in °C and P in kbar ; (□) biotitite and (☆) garnet-olivine rocks (after Freitas, 1956; Coelho, 1956, Assunçao and Coelho, 1956; Morel, 1961a; Bloomfield, 1968; Oberholzer, 1968; Saggerson and Turner, 1980 ; see Appendix VII).

occurrence of amphibolite facies gneisses, and the presence of prograde mineral textures. Similarly, the metamorphic conditions in the Middle Shire Valley encompassed the amphibolite to medium-pressure granulite facies fields and the area is therefore characterised by hornblende-biotite pyroxene gneisses and charnockitic gneisses. Elsewhere in southern Malawi the transition between terranes of different metamorphic grade appears abrupt suggesting the influence of tectonism. Near Tambani for example (see Fig.52) a lithological unit of garnet-clinopyroxene rocks occurs at less than one kilometre from lower-grade gneisses and interbanded rocks with coexisting olivine – plagioclase – clinopyroxene (Cooper and Bloomfield, 1961, p.14). In addition, a vertical displacement in excess of 15 km is required from experimental data (O'Hara et al., 1971) to explain the scattered occurrence of garnet-olivine rocks within the mainly gneissic or amphibolite to granulite facies transitional terranes (assuming $P \leq 8$ kbar) of the Lilongwe, Salima and Ncheu areas (see Fig.52, and p.149). These garnet lherzolite rocks deserve special attention in the future because they have a very restricted distribution elsewhere in the world and are usually allochtonous and also generally restricted to the Caledonian and Alpine terranes (O'Hara, 1967; Evans and Trommsdorf, 1978; Obata, 1980).

The available petrographic, chemical and experimental data have produced important constraints on the activity of H_2O in granulites. In melanocratic hornblende granulites, the H_2O was in the 6 - 35 mole per cent range; and the narrowness of the reaction rims in the prograde geometries indicates the restricted mobility of the vapour phase. These conclusions apparently preclude large-scale allochemical processes such as partial melting, metasomatism and metamorphic segregation. The only area of southern Malawi which probably suffered mild metasomatic changes is that of Tengani, where a CO_2, Cl, and H_2O-rich fluid diffused through the sheared granulites causing retrogression to hornblende-biotite-scapolite assemblages akin to those observed in rocks from the Tete region (see Fig.52 and Appendix VII). Finally, deep seated K,Al,H_2O metasomatism was perhaps also active in the Middle Shire terranes to account for the occurrence of a swarm of unusual biotitite lenticular bodies (see Fig.52).

At present, only a partial depletion of Rb relative to K passing from the amphibolite to the granulite facies can be identified; but in general the majority of the granulites and transitional terranes have maintained the composition of basalt or andesite, dacite and rhyolite (see Figs. 53 and 54) and related sediments such as greywacke. This interpretation is particularly interesting because Figs. 53 and 54 also show that

the granulites of southern Malawi have chemical similarities, despite a certain enrichment in alkalis, with 240 hypersthene-bearing rocks from African charnockite-granulite suites investigated by Clifford (1974). In contrast, shale, marl and marly limestone compositions predominate in the lower-grade terranes of the Kirk Range, intruded by comparitively less alkalic and more magnesian amphibolites (see Figs.53 and 54). The area between Fort Mlangeni and Chimwadzulu (see Fig.52) includes rocks of a transitional character. Massive,

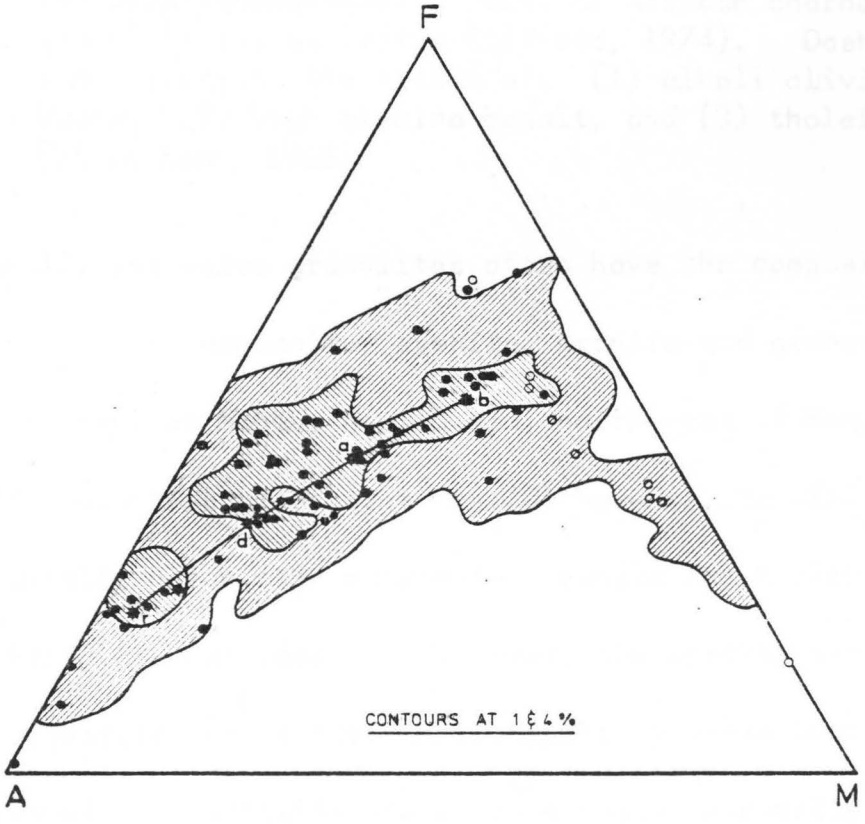


Fig.53. AFM diagram for the southern Malawi granulite facies rocks (●), and Kirk Range amphibolite and metadolerite (○) superimposed on field of 240 hypersthene-bearing rocks of African charnockite-granulite suites (after Clifford, 1974), in relation to Daly's (1933) average rhyolite (r), dacite (d), andesite (a) and basalt (b).

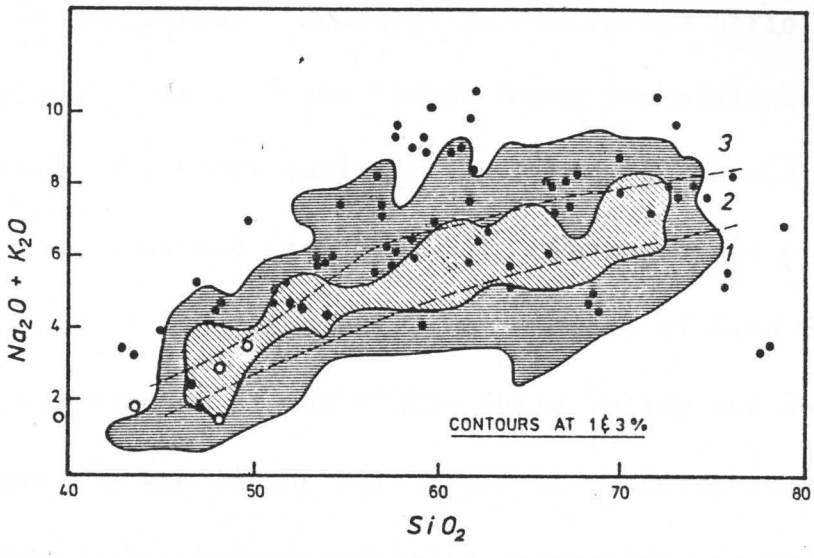


Fig.54. Alkali-silica diagram for the southern Malawi granulites (●) and for the Kirk Range amphibolites and metadolerites (○) superimposed on the field of 240 hypersthene-bearing rocks of African charnockite-granulite suites (after Clifford, 1974). Dashed lines separate the fields of: (1) alkali olivine basalt, (2) high alumina basalt, and (3) tholeiite (after Kuno, 1968).

occasionally intrusive granulites often have the composition of K-rich norite, monzonite, syenite, granite and granodiorite. Those occurring at Ncheu, near Dedza, north-east of Mangochi and in the Blantyre areas (see Fig.20) have strong affinities to the areally associated monzonite, syenite and K-rich granite of the Perthitic Complexes. Moreover, the spatial association of these massifs and of their metamorphic pyroxene-bearing varieties with anorthosite bodies in areas of granulite facies metamorphism is comparable to the intriguing anorthosite-monzonite-syenite-charnockite-K-rich granite suites that are characteristic of many high-grade Precambrian terranes

elsewhere in the world. Rocks of granodioritic affinity, regionally distributed in the Middle Shire transitional terranes could represent early-, to syn-kinematic intrusives or a pre-existing basement (see Fig.52). Petrographic and structural data further indicate that a group of Ring Complexes intruded the terranes of the Middle Shire Valley and Zomba areas before the end of the main regional metamorphic event, which produced orthopyroxene-bearing parageneses in areas of appropriate grade.

The results of Rb-Sr whole-rock and U-Pb (zircon) age determinations carried out on samples from the Middle Shire transition zone are shown in Fig.55. In this diagram some other relevant data are presented, including ages recalculated from unpublished results (Clifford et al., in prep.) on selected southern Malawi granulite and amphibolite facies suites.

Fig.55 indicates that southern Malawi experienced a metamorphic evolution between c. 1 130 m.y. ago and c. 450 m.y. ago. Within this range, hypersthene-bearing granitic magmas were emplaced in the Mchinji region of central Malawi at the same time of the prograde metamorphism in the Middle Shire terranes some 1 100 m.y. ago. Considering the Sr^{87}/Sr^{86} initial ratios (Ro), the Middle Shire transition zone granulites and gneisses have a very low value (Ro = 0,7027),

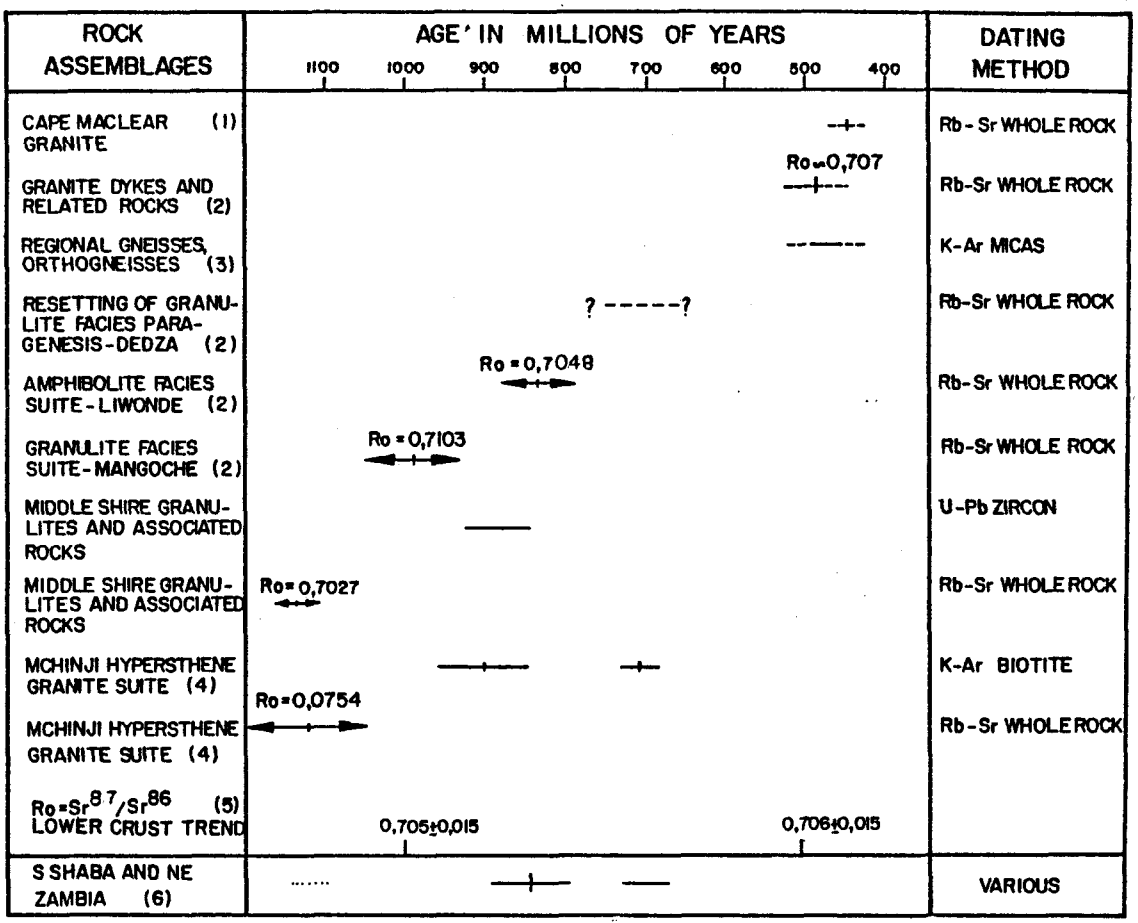


Fig.55. Age determinations in southern Malawi and other relevant areas. (1) Snelling (1963); (2) Clifford et al. (in prep.); (3) Bloomfield (1970); (4) Brewer et al., (1979); (5) Clifford (1974); and (6) Cahen (1970).

consistent with their derivation from (mantle-derived) volcanic rocks (Kistler, 1974; Davies et al., 1970) despite obvious uncertainties. Subsequently, the c. 980 m.y. event in the Mangochi area could represent the intrusion of syenite and pyroxene granite and their recrystallisation under granulite facies conditions. Their high initial ratio (Ro = 0,7103) suggests that the rocks are a granitophile extract rich in Rb and Sr^{87} or reworked high-level crustal material (Heier, 1964;

Lambert and Heier, 1968). The spread of ages in the 920 - 840 m.y. range obtained with the U-Pb zircon method from the Middle Shire transition zone is probably related to an insufficient knowledge of the zircon isotopic systems in rocks of different origin. Similarly, no precise geological significance can yet be attributed to the c. 830 m.y. old event recorded in gneisses from Liwonde and from other localities of southern and central Malawi.

The c. 700 m.y. old age of the retrogression of the granulite facies parageneses in the Dedza area is also obviously crude and speculative and may apply only to that specific area. The late K-Ar mica ages obtained from the Middle Shire Valley area probably indicate the time when temperature fell below about 300° - 400°C (Hunziker, 1979).

The available geochronological and P-T data are combined in Figs.56(a) and (b) in an attempt to synthesize the evolution of metamorphism with time; and curves I and II in Fig.56(b) indicate the thermal profiles prevailing at about 1 100 m.y. ago across the transitional areas of southern Malawi, shown in Fig.56(a). The hypothesized changes of P-T conditions with time in three distinct localities of garnet-clinopyroxene granulites are shown with arrows, A, B and C in Fig.56(b); and since there are no radiometric age determinations for these rocks, the existence of earlier metamorphic cycles cannot be

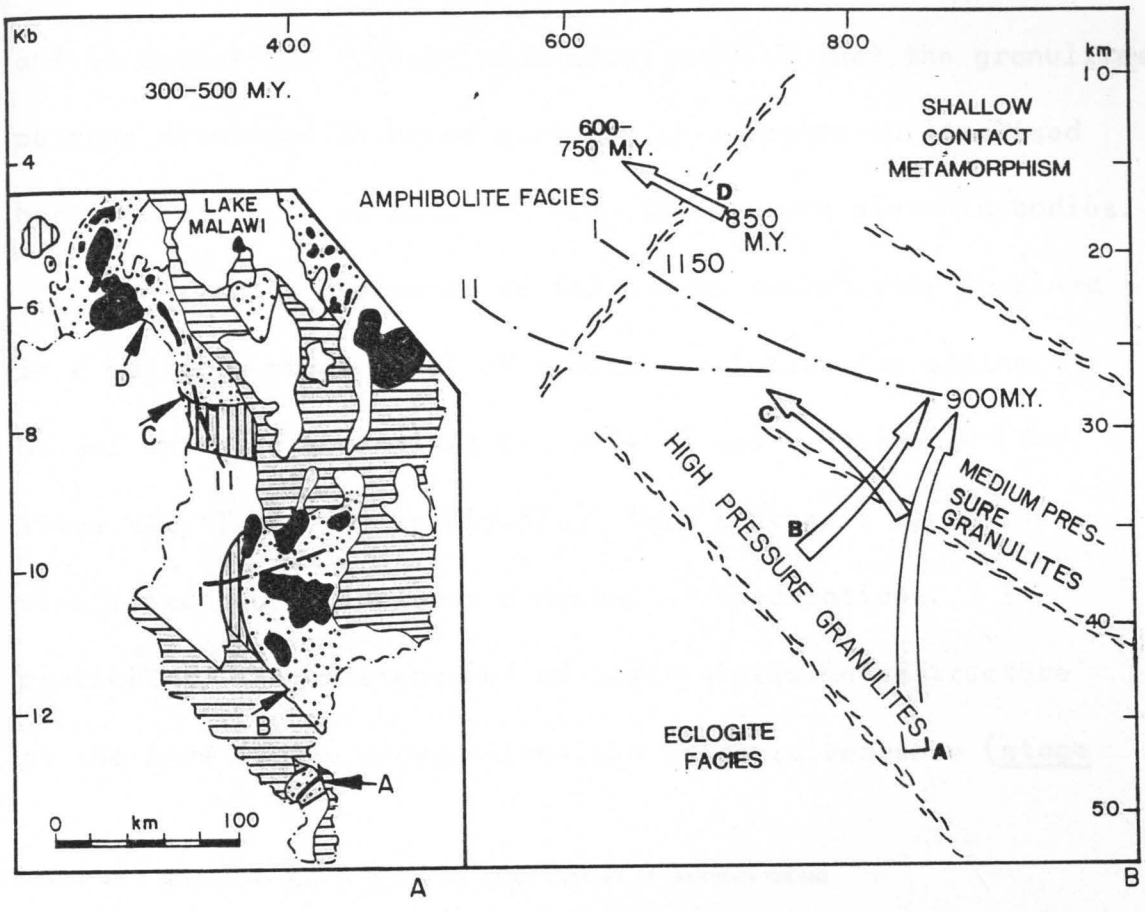


Fig.56(a). Generalised map of metamorphic assemblages in southern Malawi. Horizontal ruling, mid-Paleozoic to Recent; black, metamorphosed plutonic rocks; blank, gneisses; vertical ruling, transitional rocks; and stippled, granulites. Curves (I) and (II) are thermal profiles and (A), (B), (C) and (D) are polymetamorphic terranes shown in Fig.56(b).

Fig.56(b). P-T diagram showing (I) and (II) thermal profiles across transition zones shown in Fig.56(a); (A), (B), (C) and (D) are possible P-T-time pathways followed by granulites in areas shown in Fig.56(a). Ages are in millions of years and the metamorphic subdivisions are after Green and Ringwood (1967).

ruled out. Arrow D is the possible P-T-time evolution pathway followed at a later stage by typical two-pyroxene granulites and by garnet-clinopyroxene granulites (arrows A and B). The steep gradients of 30 - 40°C/km of profiles I

and II across two transitional areas suggest that the granulites perhaps developed in broad aureoles in response to localised heat sources such as massive, high temperature plutonic bodies.

The results discussed so far may be tentatively combined in a multiple-stage model of crustal evolution for southern Malawi which is summarised in Table 43 and represented (see stage VII, Table 43) in Fig.57. This synthesis is obviously very simplified and it includes a number of speculations. In particular, the existence of an older sialic infrastructure at the base of the geosyncline-like volcanic sequence (stage

TABLE 43 - SEQUENCE OF EVENTS IN THE PRE-KAROO HISTORY OF SOUTHERN MALAWI

	Event	Age (m.y.)
XII	Cooling, uplift, and emplacement of post-tectonic Lake Malawi granite stocks and dykes (?)	450
XI	Resetting of granulite facies parageneses and faulting of high-pressure ultramafic rocks into amphibolite facies and transitional terranes	650-750
X	Cooling, uplift, and closure of Rb-Sr isotope systems in amphibolite facies terranes	826 ± 32
IX	Widespread downgrading of high-pressure granulites to lower-pressure (hornblende) granulites, and resetting of U-Pb zircon ages in transitional granulites	840-920
VIII	Shearing, scapolitisation and retrogression of high-pressure granulites of Tengani	
VII	Remobilised Basement rocks crystallised under granulite facies conditions east of Mangochi	981 ± 34
VI	Emplacement of hypersthene granite in the Mchinji region of central Malawi; possible intrusion of Ring Complexes in southern Malawi	1 119 ± 46
V	Folding, prograde medium-pressure granulites in areas of high heat-flow from the magma cushion and from the emplacement of anorthosite and related Perthitic Complexes; prograde high-pressure granulites at greater depth, and in areas of reduced heat-flow	1 128 ± 14
IV	Plagioclase fractionation of the igneous cushion to yield anorthosite and crust-contaminated K-rich magmas, mainly of syenitic composition	
III	Burial, crustal thickening and emplacement of large magmatic cushion at mantle-crust discontinuity or in the lower crust	
II	Deposition of volcanic rocks and greywacke, with minor pelite and carbonate sediments in marine environment	
I	Older Basement (e.g. Ubendian fold belt, Archean granite complex)	

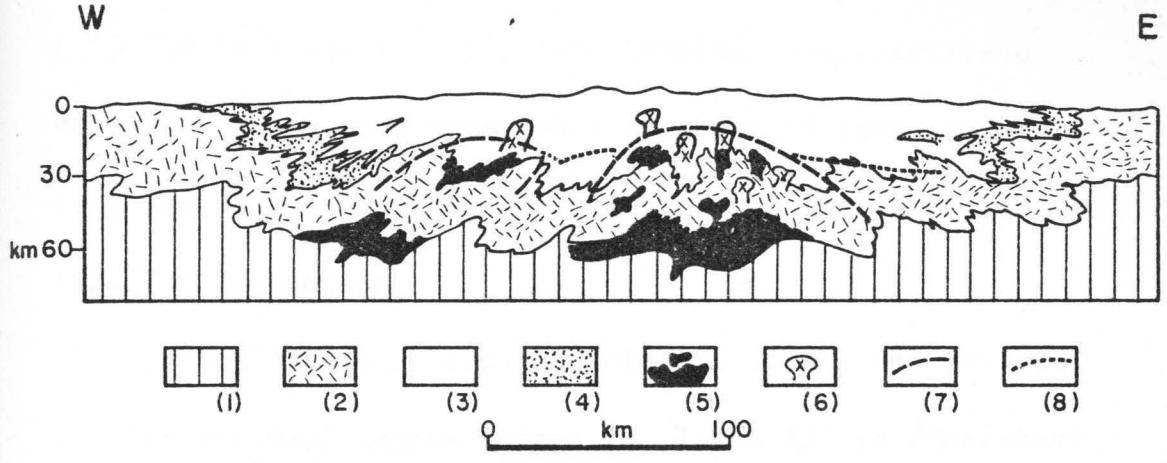


Fig.57. Schematic interpretation of the Mozambique Orogenic Belt at c. 1 000 m.y. ago (episode VII, Table 43). Patterns indicate the: (1) lithospheric upper mantle; (2) pre-Mozambiquian sialic crust; (3) Mozambiquian supracrustal gneisses and granulites; (4) Mozambiquian pelitic and carbonate rocks; (5) high-pressure mafic cumulates, anorthosite and related rocks; (6) syenitic and granitic plutons of remobilised basement and/or cover rocks; (7) orthopyroxene isograd; and (8) garnet-clinopyroxene isograd.

I, Table 43) is postulated according to present views on the evolution of eastern Africa (Piper, 1976; Shackleton, 1976). The intrusion of large, deep-seated, cushion-like igneous bodies (stage III, Table 43) is based on a model for the genesis of anorthosite by Bridgwater et al., (1974) and on hypotheses by Shackleton (1973). This model is also consistent with the hot-spot model of crustal growth proposed by Newton et al., (1980) and is supported by the presence of deep-seated, positive gravity anomalies in the regions of granulite facies metamorphism of southern and central Malawi (Andrews, 1974).

The actual occurrence, in north-west Mozambique, of the huge ($\geq$6 000 km^2) anorthositic Tete Complex, recrystallised under P-T conditions comparable to those of Zomba-Blantyre (see Fig.52 and Appendix VII) provides further evidence for this interpretation.

Contamination by crustal material of the anorthosite-related residual magmas (stage IV, Table 43) is consistent with the observed widespread occurrence of migmatitic granulites. Moreover, the cause-effect relationship between rocks of the anorthosite-K-rich granite/charnockite kindred and high-grade metamorphism (stage V, Table 43) is consistent with similar conclusions reached in southern Greenland by Bridgwater and Watterson (1967) and in the Grenville Belt of eastern Canada by Hargraves (1962) and Berrangé (1966).

The sheared and scapolitised anorthosite and granulites of Tengani might perhaps indicate an important event of regional metasomatism (stage VIII, Table 43). This could perhaps correlate, under the Karoo cover, with (a) the regionally sheared, scapolitised and davidite mineralised anorthosite and granulites of Tete (see Appendix VII; Davidson and Bennett, 1950), and (b) with the davidite-mineralised feldspathic mylonite occurring near the Mwanza fault area south-west of Tambani (see Fig.52 and Appendix VII; Cooper and Bloomfield, 1961). Faulting of high-pressure hypermelanic

rocks is attributed to a relatively late event (stage XI, Table 43) because, had this occurred earlier, the P-T conditions prevailing in the Lilongwe area would have rapidly replaced the garnet-olivine pair with plagioclase or spinel-bearing lower-pressure mineral parageneses (see p.150; O'Hara et al., 1971).

The model presented and the geological processes highlighted in these conclusions will hopefully provide a basis for further studies of a more specialised nature. However two points are worthy of additional mention. The first relates to the possibly important influence exerted by the delivery of (mantle derived) CO_2 into the lower crust during granulite facies metamorphism (Touret, 1975; Newton et al., 1980). Flushing of granulites by a CO_2-rich vapour phase occurred in the Tete and Tengani regions, and CO_2 was also probably the dominant vapour phase in a mafic granulite from Zomba. In addition, the common Type II prograde geometries observed in amphibolite and transitional rocks could also be related to the introduction of CO_2 along discontinuities, with resultant dilution and flushing of H_2O, in accordance with the interpretation given to similar structures in prograde charnockitic gneisses from south India by Janardhan et al. (1979).

The second relevant point appears to be the significance of southern Malawi as a possible link between two distinct

structural regions of the African subcontinent, namely the 600 ± 100 m.y. Damaran-Katangan (Pan-African) orogenic domain and the 1 100 ± 200 m.y. Kibaran orogenic domain (Clifford, 1974). In this regard, the climax of the Mozambiquian tectonothermal event in southern Malawi coincides with a period of low- to very high-grade metamorphism that affected the Namaqualand-Natal Belt of southern Africa (A, Fig.58) between c. 1 200 and 900 m.y. ago (Nicolaysen and Burger, 1965; Joubert, 1971; Clifford et al., 1975). Other coeval regions in central Africa are the Kibaride Belt (B, Fig.58, Cahen, 1970) and the Irumide Belt (C, Fig.58; Shackleton, 1973). In view of the results of this thesis it is worthy of note that Ramsay

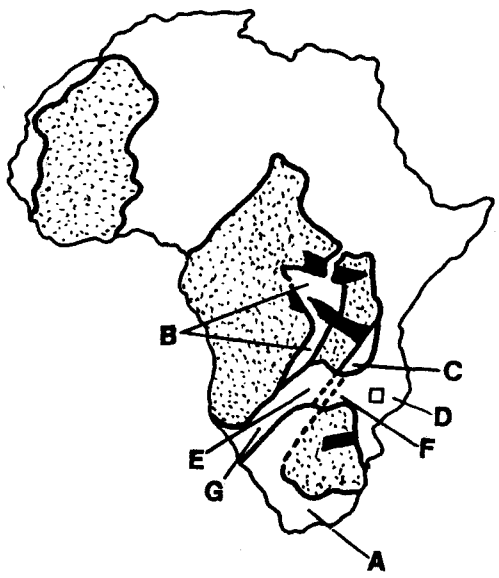


Fig.58. Major structural units of Africa with Archean-lower Proterozoic (≥2 000 m.y. old) mobile belts (black), stable continental crust since 1 500 m.y. ago (stippled), and mobile belts younger than 1 500 m.y. (blank)(after Onstott and Hargraves, 1981). (A) to (G) are mobile belts discussed in the text and (□) is position of southern Malawi.

and Ridgway (1977) found no evidence for an Irumide Belt in eastern Zambia and proposed that the Pan-African Mozambique Belt (D, Fig.58) forms the margins of the Zambian (and Tanzanian) Cratons.

Among the Pan-African terranes, the Lufilian Belt of Zambia (E, Fig.58) experienced an earlier, lower/middle Kundelungu tectonic phase with pegmatite emplacement at c. 800 - 840 m.y. ago and a subsequent major tectonic event, the Kolwezian phase, at c. 700 m.y. ago (Cahen, 1970). These periods of tectonic (and igneous) activity coincide in time with the age of the amphibolite facies rocks and of certain retrograded granulites of southern Malawi respectively (see Fig.55).

The Zambezi Belt of southern Zambia (F, Fig.58) includes scapolitised eclogite facies rocks originally extruded as mafic volcanic rocks at the base of the Lufilian sedimentary sequence not earlier than 1 300 m.y. ago (Cahen, 1970; Vrana et al., 1975; Martin and Porada, 1977). This may possibly provide an indication of the time in which analogous volcanic and sedimentary rocks, the precursor of the granulites, were deposited in southern Malawi.

In contrast, the Namibian Damara Belt (G, Fig.58) experienced sedimentation and mafic marine igneous activity between 810 and 720 m.y. ago, followed by a major cycle of tectonic activity between 560 and 490 m.y. ago (Hawkesworth et al., 1981) corresponding to the period of cooling, uplift

and sporadic emplacement of post-tectonic intrusive rocks in southern Malawi.

In conclusion (see Fig.57), the Mozambiquian Orogenic Cycle of southern Malawi appears characterised by a very complex and perhaps continuous thermotectonic activity in which the following events may be recognized: (a) the c. 1 100 m.y. Kibaran stage; (b) the c. 830 m.y. old 'middle' (lower to middle Kundelungu) stage; (c) the c. 700 m.y. old 'Katangan' (Kolwezian) stage; and finally (d) the c. 450 - 500 'waning' stage of Damaran age. If this interpretation is correct, the Mozambiquian Orogenic Cycle spans the time sequence of two major orogenic events, the Kibaran and Pan African, in southern Africa.

APPENDIX I

LIST OF SAMPLES

In the present thesis 509 samples of granulites and gneisses from southern Malawi have been considered, as shown in Table I-1. The localisation of nearly all samples is shown in Maps 1 to 4, enclosed in a pocket at the back of the thesis. However for some specimens insufficient information was available for them to be plotted on the Maps: they are listed in Table I-2 with some relevant data. Field numbers, thin section (laboratory) numbers, Map reference numbers and the ones used throughout the thesis are listed for all the 509 specimens in Table I-3.

In addition, 10 samples of granulites from the Tete area of Mozambique have been obtained from the Geological Survey of Portugal and their numbers, preceded by a letter T, are listed at the end of Table I-3. In this thesis the original numbers occurring in a paper by Coelho (1969) have been used throughout. This work should be considered for further information on the sampling localities, but the details are however scanty. In addition, no. T19 was not described in the above publication (Coelho, ibid.) but it was collected from the same area as the others (Coelho, personal communication).

TABLE I-1 SAMPLE SOURCES

Group	Thesis no.	Collector/Collection
I	I - 122	T.N.Clifford.
II	123 - 496	M.A.G.Andreoli.
III	497 - 508	Malawi Geological Survey, Zomba.
IV	509	University of the Witwatersrand Geology Department Collection.

TABLE I-2 AREA OF ORIGIN OF UNDETERMINED SAMPLES

Thesis no.	Sheet Area	References
22	-	Manono Bridge (Central Malawi).
64	Lake Malombe	Mpala River, 50Km south of Mangochi (Liwonde Road).
122	Chikwawa	Livingstone Falls.
499	Mulanje	Kafiri Quarry, Nachinjango.
500	Kirk Range	4Km west of Charlie's Court.
503	Dedza	North of Khoma Hill. Grid references: 160502; 50 000 Sheet No. 1434A1.
508	Mchinji	Kapote Hill, Zambia border.
509	Tambani	2Km east of Mwanza Fault.

TABLE 1-3 - SPECIMEN NUMBERS

Thesis no.	Field no.	Slide no.	Map no.	Thesis no.	Field no.	Slide no.	Map no.
1	66-C-3	19647	2	43	69-B-18	23463	2
2	-4	19648	2	44	-19	23464	2
3	-5	19649	2	45	-20	25185	2
4	-6	19650	2	46	-21	25186	2
5	-7	19651	2	47	-22	23465	2
6	-8	19652	2	48	-23	23466	2
7	-9	19653	2	49	-24	25187	2
8	-10	19654	2	50a	-25	25188	2
9	-11	19655	2	50b	-25	25188	2
10	-12	19656	2	51	-26	25189	2
11	-13	19657	2	52	-27	25190	2
12	-17A	19658	2	53	-28	23467	2
13	-17B	19659	2	54	-29	23468	2
14	-18B	19660	2	55a	-30A	23469	2
15	-18C	19661	2	55b	-30B	23469	2
16	-18E	19662	2	56	72-D-1	X19664	2
17	-20	19663	3	57	-2	X19665	2
18	-23	19664	4	58	-3	-	4
19	-24	22246	4	59	-4A	X19666	2
20	-25	19665	4	60	-4B	X19667	2
21	-31C	22247	4	61	-5A	X19746	2
22	-32	22248	-	62	-5B	X19747	2
23	-33	19668	4	63	-5C	X19748	2
24	-34	19669	4	64	-6	X19671	-
25	-36	19670	4	65	-7A	X19672	3
26	-37	19671	3	66	-7B	-	3
27	-38	19672	2	67	-7C	X19674	3
28	68 -NA	22250	2	68	-8A	X19749	3
29	-NB	22251	2	69	-8B	X19750	3
30	-KA	22252	2	70	-9	X19751	3
31	-KB	22253	2	71	-10	X19752	3
32	69-B-1	23452	2	72	-11	X19753	3
33	-2	23453	2	73	-12	X19754	3
34	-3	23454	2	74	-13	X19755	3
35	-4	23455	2	75	-14	X19756	3
36	-7	23456	2	76	-15	X19782	2
37	-8	23457	2	77	-16	X19783	2
38	-9	23458	2	78	-17	X19784	2
39	-11	23459	2	79	-18	X19785	2
40	-12	23460	2	80	-19	-	2
41	-13	23461	2	81	-20	X19786	2
42	-17	23462	2	82	-21	X19787	3

TABLE 1-3 - SPECIMEN NUMBERS (CONTD.)

Thesis no.	Field no.	Slide no.	Map no.	Thesis no.	Field no.	Slide no.	Map no.
83	72-D-22	X19788	2	120	72-D-57	X19986	2
84	-23	X19789	2	121	D-H-20	X19983	4
85	-24	-	2	121a	-20A	X20120	4
86	-25	-	2	to	to	to	4
87	-26	-	2	121i	-20I	X20205	4
88	-27	X19791	2	122	-161A	X20896	1
89	-28	X19792	4	123	MA -2	X21723	1
90	-29	X19793	4	124	-3	-	1
91	-30	X19826	4	125	-4	X21303	1
92	-31A	X19827	3	126	-5	X21304	1
93	-31B	X19828	3	127	-6	-	1
94	-32A	X19829	3	128	-7	X21305	1
95	-32B	X19830	3	129a	-8	X21258	1
				129b		X21384	1
96	-32C	X19831	3	130	-9	X21378	1
97	-33	X19832	3	131	-10	X21266	1
98	-34	X19833	3	132	-11	X21267	1
99	-35	X19834	3	133	-12	X21221	1
100	-36	X19835	3	134	-13	X21765	1
101	-37	X19929	3	135	-14	X21379	1
102	-38	X19930	3	135b	-14B	MA400	1
103	-39	X19931	3	136	-15	X21222	1
104	-40	X19932	3	137	-16	X21380	1
105	-41	X19933	3	138	-17	X21268	1
106	-42	X19934	3	139	-18	X21382	1
107	-43	X19935	3	140	-19	X21223	1
108	-44	X19936	3			X22154	1
109	-45	X19974	3	141	-20	X21390	1
110	-46A	X19975	2	142	-21	X21436	1
111	-46B	X19976	2	143	-22	X21744	1
112	-46C	X19977	2	144	-23	X21745	1
113	-47	X19978	2	145	-24	X21383	1
114	-48	X19979	2	146	-25	-	1
115	-49	X19980	2	147	-26	-	1
		X20678	2	148	-27	X21437	1
116a	-50A	X19981	2	149	-28	-	1
116b	-50B	-	2	150	-29	-	1
117a	-51B	X19982	2	151	-30	X21385	1
117b	-52	X20557	2	152	-31	-	1
118a	-53A	X19984	2	153	-32	-	1
118b	-53B	-	2	154	-33	-	1
118c	-54	X20854	2	155	-34	-	1
119	-55	X19985	2	156	-35	-	1

TABLE 1-3 - SPECIMEN NUMBERS (CONTD.)

Thesis no.	Field no.	Slide no.	Map no.	Thesis no.	Field no.	Slide no.	Map no.
157	MA-36	X21386	1	200	MA-79	-	2
158	-37	-	1	201	-80	-	2
159	-38	-	1	202	-81	-	2
160	-39	X21387	1	203	-82	-	2
161	-40	X22155	1	204	-83	-	2
162	-41	X21388	2	205	-84	-	2
163	-42	X21389	2	206	-85	-	2
164	-43	-	2	207	-86	-	2
165	-44	-	2	208	-87	-	2
166	-45	X21396	2	209	-88	-	2
167	-46	-	2	210	-89	-	2
168	-47	-	2	211	-90	-	2
169	-48	-	2	212	-91	-	2
170	-49	-	2	213	-92	X21320	2
171	-50	X21392	2	214	-93	-	2
172	-51	-	2	215	-94	-	2
173	-52	-	2	216	-95	-	2
174	-53	-	2	217	-96	-	2
175	-54	X21393	2	218	-97	-	2
176	-55	-	2	219	-98	X21321	2
177	-56	X21712	2	220	-99	-	2
178	-57	X21713	2	221	-100	-	2
179	-58	X21589	2	222	-101	X21724	2
180	-59	-	2	223	-102	-	2
181	-60	X21714	2	224	-103	-	2
182	-61	X21715	2	225	-104	X21353	2
183	-62	-	2	226	-105	-	2
184	-63	-	2	227	-106	-	2
185	-64	-	2	228	-107	X21725	2
186	-65	-	2	229	-108	-	2
187	-66	-	2	230	-109	-	2
188	-67	-	2	231	-110	-	2
189	-68	-	2	232	-111	-	2
190	-69	-	2	233	-112	X21354	2
191	-70	-	2	234	-113	-	2
192	-71	-	2	235	-114	X21726	2
193	-72	-	2	236	-115	-	2
194	-73	-	2	237	-116	-	2
195	-74	-	2	238	-117	X22159	2
196	-75	-	2	239	-118	X21837	2
197	-76	-	2	240	-119	X21716	2
198	-77	-	2	241	-120	X22156	2
199	-78	-	2	242	-121	X21590	2

TABLE 1-3 - SPECIMEN NUMBERS (CONTD.)

Thesis no.	Field no.	Slide no.	Map no.	Thesis no.	Field no.	Slide no.	Map no.
243	MA-121a	X21657	2	285	MA-164	-	2
244	-123	-	2	286	-165	-	2
245	-124	-	2	287	-166	-	2
246	-125	-	2	288	-167	-	2
247	-126	-	2	289	-168	-	2
248	-127	-	2	290	-169	-	2
249	-128	-	2	291	-170	-	2
250	-129	X21727	2	292	-171	-	2
251	-130	-	2	293	-172	X21322	2
252	-131	X21838	2	294	-173	-	2
253	-132	-	2	295	-174	-	2
254	-133	X21854	2	296	-175	-	2
255	-134	X21853	2	297	-176	-	2
256	-135	-	2	298	-177	-	2
257	-136	-	2	299	-178	-	2
258	-137	-	2	300	-179	-	2
259	-138	-	2	301	-180	-	2
260	-139	-	2	302	-181	-	2
261	-140	-	2	303	-182	-	2
262	-141	X21728	2	304	-183	-	2
263	-142	-	2	305	-184	X21658	2
264	-143	-	2	306	-185	-	2
265	-144	-	2	307	-186	-	2
266	-145	-	2	308	-187	X21730	2
267	-146	-	2	309	-188	-	2
268	-147	-	2	310	-189	X21355	2
269	-148	-	2	311	-190	X21755	2
270	-149	-	2	312	-191	-	2
271	-150	-	2	313	-192	-	2
272	-151	X21729	2	314	-193	X21756	2
273	-152	-	2	315	-194	X21356	2
274	-153	-	2	316	-195	X21757	2
275	-154	-	2	317	-196	-	2
276	-155	-	2	318	-197	-	2
277	-156	-	2	319	-198	X22157	2
278	-157	-	2	320	-199	X21758	2
279	-158	-	2	321	-200	X21753	2
280	-159	-	2	322	-201	X21731	2
281	-160	X21591	2	323	-202	X21323	2
282	-161	-	2	324	-203	MA-203	2
283	-162	-	2	325	-204	MA-204	2
284	-163	-	2	326	-205	MA-205	2

TABLE 1-3 - SPECIMEN NUMBERS (CONTD.)

Thesis no.	Field no.	Slide no.	Map no.	Thesis no.	Field no.	Slide no.	Map no.
327	MA-206	-	2	366	MA-245	X21750	2
328	-207	X21752	2	367	-246	X21751	2
329	-208	-	2	368	-247	-	2
330	-209	X21244	2	369	-248	X21768	2
		X21259		370	-249	X21438	2
331	-210	X21246	2	371	-250	-	2
		X21260		372	-251	-	2
332	-211	-	2	373	-252	X21439	2
333	-212	-	2	374	-253	-	2
334	-213	X21748	2	375	-254	X21440	2
335	-214	X21247	2			X21040	2
336	-215	-	2	376	-255	-	2
337	-216	-	2	377	-256	-	2
338	-217	-	2	378	-257	-	2
339	-218	-	2	379	-258	-	2
340	-219	X21270	2	380	-259	-	2
341	-220	X21928	2	381	-260	-	2
342	-221	X21747	2	382	-261	-	2
343	-222	X21774	2	383	-262	-	2
344	-223	X21732	2	384	-263	X21735	2
345	-224	X21839	2	385	-264	-	2
346	-225	X21840	2	386	-265	-	2
347	-226	-	2	387	-266	-	2
348	-227	X21929	2	388	-267	-	2
349	-228	-	2	389	-268	-	2
350	-229	X21261	2	390	-269	-	2
351	-230	X21224	2	391	-270	-	2
352a	-231	X21225	2	392	-271	-	2
352b	-231B	X22158	2	393	-272	-	2
353	-232	X21766	2	394	-273	-	2
354	-233	-	2	395	-274	X21734	2
355	-234	X21930	2	396	-275	-	2
356	-235	-	2	397	-276	-	2
357	-236	X21943	2	398	-277	-	2
358	-237	-	2	399	-278	-	2
359	-238	X21944	2	400	-279	-	2
360	-239	-	2	401	-280	-	2
361	-240	-	2	402	-281	-	2
362	-241	X21767	2	403	-282	-	2
363	-242	X21768	2	404	-283	-	2
364	-243	X21243	2	405	-284	X21212	2
365	-244	X21749	2	406	-285	-	3

TABLE 1-3 - SPECIMEN NUMBERS (CONTD.)

Thesis no.	Field no.	Slide no.	Map no.	Thesis no.	Field no.	Slide no.	Map no.
407	MA-286	-	3	447	MA-326	X21741	3
408	-287	-	3	448	-327	-	3
409	-288	X21213	3	449	-328	X21484	3
410	-289	X21717	3	450	-329	-	3
411	-290	X21214	3	451	-330	-	3
412	-291	X21718	3	452	-331	X21485	3
413	-292	-	3	453	-332	-	3
414	-293	X21719	3	454	-333	X21486	3
415	-294	X21720	3	455	-334	X21487	3
416	-295	X21721	3	456	-335	MA335	3
417	-296	-	3	457	-336	X21488	3
418	-297	-	3			X21769	
419	-298	X21736	3	458	-337	X21770	3
420	-299	-	3	459	-338	X21531	3
421	-300	X21737	3	460	-339	X21532	3
422	-301	X21738	3	461	-340	X21533	3
423	-302	X21739	3	462	-341	X21760	3
424	-303	-	3	463	-342	X21324	3
425	-304	-	3	464	-343	X21596	2
426	-305	-	3	465-6	-344	X21761	2
427	-306	-	3	467	-345	X22016	2
428	-307	X21592	3	468	-346	X21762	2
429	-308	X21593	3	469	-347	-	2
430	-309	X21278	3	470	-348	X21763	2
431	-310	X21279	3	471	-349	X21764	3
432	-311	X21215	3	472	-350	-	3
433	-312	X21357	3	473	-351	X21771	3
434	-313	X21280-1	3	474	-352	X21772	2
		X21781		475	-353	X21773	2
435	-314	X21282	3	476	-354	-	2
436	-315	X21483	3	477	-355	X21775	2
437	-316	X21528	3	478	-356	X21776	2
438	-317	-	3	479	-357	X21777	2
439	-318	X21529	3	480	-358	X21778	2
440	-319	-	3	481	-359	X21779	2
441a	-320A	X21216	3	482	-360	X21780	2
441b	-320B	-	3	483	-361	-	2
442	-321	X21351	3	484	-362	-	2
443	322	X21594	3	485	-363	-	4
444	-323	X21530	3	486	-364	X21782	4
445	-324	-	3	487	-365	X22161	4
446	-325	X21740	3	488	-366	-	4

TABLE 1-3 - SPECIMEN NUMBERS (CONTD.)

Thesis no.	Field no.	Slide no.	Map no.
489	MA-367	-	4
490	-368	X21783	4
491	-369	-	2
492	-370	X21659	2
493	-371	X21597	2
494	-372	X21660	2
495	-373	X21661	2
496	-374	X22018	2
496a	-375	X21598	2
497	KB-487	X22013	1
498	KB-507	X21262	1
499	E-418	X21290	-
500	KB-712	X21269	-
501	KB-717	X21742	2
502	T-480	X21289	3
503	T-560	X22014	-
504	P-297	X21293	4
505	P-329	X21291	4
506	P-373	X21292	4
507	P-377	X22015	4
508	Q-34	X21302	-
509	-	MA81-1	

TETE SAMPLES

Thesis no.	Original no.	Slide no.
T8	8	T8
T11	11	T11
T19	19	T19
T37	37	T37
T78	78	T78
T117	117	T117
T180	180	T180
T201	201	T201
T240	240	T240
T257	257	T257

APPENDIX II

PETROGRAPHY

In the various chapters of the thesis only the more interesting or otherwise more typical mineral assemblages found in selected granulites were described. For completeness this Appendix presents in Table II-1 a list of mineral name abbreviations and in Table II-2 a comprehensive tabulation of the minerals present in all thin sections investigated. In addition, short petrographic descriptions of the samples analysed for Rb-Sr geochronology are presented in Table II-3.

TABLE II-1 - LIST OF ABBREVIATIONS

aeg	aegirine	mic	microcline
alb	albite	Nap	oligoclase/Na-andesine[1]
all	allanite	nep	nepheline
and	andesine	oli	oligoclase
ano	anorthite	om	opaque minerals
apa	apatite	opx	orthopyroxene
bio	biotite	phl	phlogopite
bit	bitownite	pla	plagioclase
Cap	Ca-andesine/labradorite[1]	pre	prehnite
car	carbonate	qtz	quartz
cha	chalcopyrite	rut	rutile
chl	chlorite	sca	scapolite
cor	corderite	sil	sillimanite
cpx	clinopyroxene	spe	spessartine
con	corundum	sph	sphene
epi	epidote	spi	spinel (hercynite)
flu	fluorite	tou	tourmaline
gar	garnet	tre	tremolite
gra	graphite	ura	uralite amphibole
hor	hornblende	zir	zircon
Kfl	K-feldspar[2]	zoi	zoisite
kya	kyanite	undet	undetermined
lab	labradorite	tr	traces
mes	mesoperthite	sym	symplectite

(1) Mainly antiperthitic plagioclase with polysynthetic albite twinning.

(2) Mainly perthitic orthoclase-like feldspar unless microcline when it is specified in brackets in the column of the additional minerals.

TABLE II-2 - MINERAL ASSEMBLAGES OF SOUTHERN MALAWI ROCKS

		constituent minerals									accessories			
Slide no.	sample no.	opx	cpx	gar	hor	bio	Kfl	Nap	Cap	qtz	apt	zir	om	additional minerals
19647	1					x	x	x		x	x	x	x	mus; rut = tr
19648	2				x	x		x						
19649	3	x	x			x	x		x	x	x			ura, mus, car; chl = tr
19650	4	x				x	x		x	x	x	x	x	car
19651	5	x	x		x	x		x			x		x	
19652	6	x			x	x			x	x	x	x	x	
19653	7	x	x		x	x			x	x	x	x	x	
19654	8				x	x	x	x		x	x	x	x	(mic), sph, all
19655	9	x			x	x	x	x		x	x	x	x	
19656	10				x	x	x			x				(mic)
19657	11		x		x		x	x			x		x	bio = tr
19658	12				x	x	x	x		x			x	(mic), car
19659	13				x	x	x	x		x	x			sph, om, zir = tr
19660	14			x	x				x					epi, rut
19661	15													tre
19662	16				x				x					zoi, con
19663	17					x		x		x	x	x	x	kya, sil, rut, mus, car
19664	18	x			x	x			x					mus, car
19665	20						x	x	x	x				(mic), aeg, sph
19668	23				x	x		x			x		x	aeg, sph
19669	24							x		x		x	x	all, aeg, sph
19670	25	x	x			x	x	x		x		x		
19671	26				x	x		x	x	x	x		x	nep, sph; Kfl, spi = tr
19672	27			x		x	x		x	x	x	x		
22246	19		x	x		x			x	x	x			mus, radioactive mineral
22247	21				x	x				x				epi
22248	22				x				x					
22250	28	x	x		x	x	x		x	x	x	x	x	
22251	29	x				x	x		x		x	x	x	
22252	30		x		x	x	x	x		x	x	x	x	ura
22253	31				x	x	x	x		x	x	x	x	car
23452	32	x			x	x	x	x		x	x			rut, sph
23453	33				x	x	x	x		x	x	x	x	(mic), all, sph

TABLE II-2 - MINERAL ASSEMBLAGES OF SOUTHERN MALAWI ROCKS (CONTD.)

		constituent minerals									accessories			
Slide no.	sample no.	opx	cpx	gar	hor	bio	Kfl	Nap	Cap	qtz	apt	zir	om	additional minerals
23454	34		x		x	x		x			x		x	sph; Kfl = tr
23455	35						x		x	x				(mic)
23456	36	x		x		x	x	x		x	x	x	x	(mic)
23457	37	x	x		x	x		x		x	x	x	x	
23458	38	x	x		x	x	x	x		x	x		x	
23459	39					x	x	x		x	x	x	x	(mic), mus, chl, tou, car; hor = tr
23460	40	x	x		x	x			x	x	x	x	x	
23461	41				x	x	x	x		x	x	x	x	(mic), all, flu (?)
23462	42		x			x	x	x		x	x	x	x	
23463	43	x		x		x	x		x	x	x		x	rut, car
23464	44	x		x		x	x		x	x	x	x	x	
23465	47					x	x			x				pla = undet
23466	48	x	x		x	x			x		x	x	x	
23467	53					x	x	x		x		x	x	(mic), alb
23468	54				x	x			x		x		x	Kfl = tr
23469	55a	x	x			x	x		x	x	x		x	
ditto	55b	x	x		x				x		x		x	hor = tr
25185	45	x	x		x	x	x		x	x			x	ura, car
25186	46	x	x		x	x	x		x	x	x	x	x	
25187	49	x	x			x	x		x	x	x		x	
25188	50a	x	x		x	x	x		x	x	x	x	x	
ditto	50b	x	x			x			x	x	x		x	
25189	51	x				x			x	x		x	x	
25190	52	x		x		x	x	x		x	x	x	x	
X19664	56						x	x		x		x	x	all; bio = tr
X19665	57					x	x	x		x		x	x	(mes); all, apa = tr
X19666	59		x				x	x		x	x	x	x	(mic), chl, mus
X19667	60		x				x	x		x				
X19671	64			x		x	x	x		x				
X19672	65	x			x		x	x		x	x	x	x	(mic), all, car; bio = tr
X19674	67				x		x	x		x	x	x	x	(mic), all, sph, tou
X19746	61				x	x			x			x	x	tou
X19747	62	x			x	x	x		x	x	x	x	x	pla = undet

TABLE II-2 - MINERAL ASSEMBLAGES OF SOUTHERN MALAWI ROCKS (CONTD.)

		constituent minerals									accessories			
Slide no.	sample no.	opx	cpx	gar	hor	bio	Kfl	Nap	Cap	qtz	apt	zir	om	additional minerals
X19748	63	x	x		x	x	x	x		x				rut
X19749	68		x		x	x			x		x	x		sph, car
X19750	69	x	x				x	x		x	x		x	
X19751	70		x			x	x	x		x	x		x	mus, ura, gra, sph, car
X19752	71		x		x	x	x	x		x	x		x	
X19753	72	x	x		x		x	x		x	x	x	x	(mic)
X19754	73	x	x				x	x		x			x	
X19755	74	x	x				x	x		x	x	x	x	(mic), all
X19756	75		x				x	x		x	x	x	x	all, sph
X19782	76	x	x		x		x	x		x	x	x	x	
X19783	77		x		x		x	x		x	x	x	x	
X19784	78	x	x		x		x	x		x	x	x	x	
X19785	79	x	x		x		x	x		x	x	x	x	
X19786	81	x	x		x	x	x	x		x	x	x	x	
X19787	82	x	x		x		x	x		x	x	x	x	
X19788	83	x	x		x	x	x	x		x	x	x	x	
X19789	84				x		x	x		x	x		x	
X19791	88				x		x	x		x	x	x	x	sph
X19792	89		x		x	x	x	x		x	x	x	x	(mic)
X19793	90		x		x	x	x	x		x	x	x	x	
X19826	91		x				x	x		x	x	x	x	(mic), car
X19827	92					x	x	x		x	x	x	x	chl; opx, car, gar = tr
X19828	93	x				x			x	x	x		x	ura, chl, car; zir = tr
X19829	94				x	x	x		x	x				(mic)
X19830	95				x	x			x	x			x	
X19831	96					x	x		x	x				(mic)
X19832	97				x	x	x	x		x	x	x	x	
X19833	98	x	x				x	x		x			x	apa, gra, car
X19834	99	x	x			x	x		x	x	x		x	chl, ura, car
X19835	100		x		x	x	x		x	x	x	x	x	
X19929	101	x	x			x	x		x	x				hem, rut
X19930	102	x	x						x	x			x	
X19931	103		x			x	x	x			x	x	x	(mes), car

TABLE II-2 - MINERAL ASSEMBLAGES OF SOUTHERN MALAWI ROCKS (CONTD.)

		constituent minerals									accessories			
Slide no.	sample no.	opx	cpx	gar	hor	bio	Kfl	Nap	Cap	qtz	apt	zir	om	additional minerals
X19932	104	x		x		x	x		x	x		x	x	spi, sil, car
X19933	105			x		x	x		x		x	x		
X19934	106		x	x	x	x			x					bit, chl, ura , car
X19935	107	x	x		x	x			x	x	x	x	x	
X19936	108			x		x	x	x		x		x	x	rut
X19974	109			x		x	x			x				
X19975	110						x			x				(mic), alb; om = tr
X19976	111						x			x			x	(mic), bio, alb, mus
X19977	112				x	x	x		x	x	x	x	x	(mic), alb, sph
X19978	113	x	x				x		x	x	x	x	x	
X19979	114						x		x	x	x	x	x	mus
X19980	115						x		x	x				
X19981	116a	x				x	x		x	x	x	x	x	car
X19982	117a	x	x		x	x			x	x	x			
X19983	121		x	x	x	x			x	x				
X19984	118a	x				x	x		x		x		x	qtz; cpx = tr
ditto	118b	x					x		x	x				pla = undet
X19985	119	x	x		x	x			x	x	x			
X19986	120	x				x	x	x		x		x	x	alb
X20197	121a					x	x	x		x	x	x	x	sph, all (?)
X20198	121b				x	x	x	x		x	x	x	x	(mic), sph, all, epi, car, zoi, mus
X20199	121c					x	x			x	x	x		pla = undet; epi
X20199	121d				x	x	x		x	x	x	x		
X20200	121e				x	x	x		x	x				sph, all, epi, mic, chl
X20201	121f				x	x	x			x		x		pla = undet, epi, all
X20202	121g				x	x	x			x		x		pla = undet
X20203	121h		x		x	x			x			x	x	sph
X20204	121i			x	x	x			x	x				sph
X20205	121k			x	x	x		x		x		x	x	
X20523	116 b	x				x			x	x	x		x	pla = undet
X20557	117b						x	x		x	x	x	x	hem; bio = tr
X20586	116 a	x	x			x	x			x		x	x	car, epi
X20854	118c						x	x		x	x		x	(mic), alb; bio = tr

TABLE II-2 - MINERAL ASSEMBLAGES OF SOUTHERN MALAWI ROCKS (CONTD.)

		constituent minerals									accessories			
Slide no.	sample no.	opx	cpx	gar	hor	bio	Kfl	Nap	Cap	qtz	apt	zir	om	additional minerals
X20896	122	x	x							x				pla = undet
X21212	405	x	x		x	x	x		x	x	x		x	
X21213	409	x					x	x		x		x	x	pla = undet
X21214	411	x	x			x	x			x	x		x	pla = undet, ura, sph
X21215	432	x					x		x	x	x	x	x	car
X21216	441a	x					x	x			x		x	qtz = tr
ditto	441b	x					x	x			x		x	
X21221	133		x	x	x	x	x	x		x				opx, chl, ura = tr
X21222	136	x	x	x	x				x					sca, rut
X21223	140		x	x	x	x								pla = undet; opx = tr
X21224	351	x	x		x	x	x		x	x	x	x	x	
X21225	352a	x	x		x		x		x	x			x	K-fl, qtz = tr
X21243	364	x			x	x	x	x		x			x	
X21244	329				x	x	x	x		x	x	x	x	
X21245	330	x	x		x	x	x	x		x	x	x	x	
X21246	331	x			x	x		x		x	x	x	x	
X21247	335				x	x	x	x		x	x	x	x	sph
X21258	129		x	x	x	x			x	x				sca, rut; opx = tr
X21260	331	x			x	x		x		x	x	x	x	
X21261	350		x	x	x	x			x	x			x	
X21262	498	x	x	x	x						x	x		rut
X21266	131	x	x	x	x	x	x		x					rut
X21267	132	x	x	x	x	x			x				x	sca, rut, pyr
X21268	138			x			x							sil, spi
X21269	500		x	x	x	x				x				pla = undet
X21270	340			x		x	x	x		x		x	x	
X21278	430	x	x			x	x		x				x	
X21279	431	x			x	x	x		x	x	x	x	x	car
X21280	434	x	x		x				x				x	lab-bit
X21281	ditto	x	x		x				x				x	lab-bit
X21282	435	x	x		x	x	x		x	x		x	x	car
X21289	502	x				x	x			x			x	cor, sil, spi
X21290	499	x	x		x	x			x	x		x	x	

TABLE II-2 - MINERAL ASSEMBLAGES OF SOUTHERN MALAWI ROCKS (CONTD.)

		constituent minerals									accessories			
Slide no.	sample no.	opx	cpx	gar	hor	bio	Kfl	Nap	Cap	qtz	apt	zir	om	additional minerals
X21291	505	x	x	x	x	x			x	x			x	
X21292	506	x	x	x	x				x				x	rut
X21293	504		x	x	x	x							x	and, Kfl, qtz = tr
X21302	508	x				x								Kfl, Nap, qtz = tr
X21303	125	x	x	x	x				x	x			x	bit
X21304	126	x	x		x	x			x	x	x		x	
X21305	128	x	x				x		x	x	x	x		gar, hor, bio = tr
X21320	213	x	x				x	x		x	x	x	x	hor, bio = tr
* X21322	293	x	x				x	x		x			x	bio = tr
X21323	323	x	x		x			x		x	x		x	bio, Kfl = tr
ditto					x	x		x					x	
X21324	463	x	x		x				x					
X21351	442	x	x		x	x	x		x			x	x	
X21353	225	x	x		x	x	x		x	x		x	x	spi
X21354	233	x	x				x		x	x	x	x	x	spi
X21355	310	x	x			x			x	x			x	Kfl = tr
X21356	315	x	x		x	x	x		x	x	x	x	x	
X21357	433	x					x	x		x			x	
X21378	130		x	x	x	x			x	x	x		x	rut
X21379	135			x		x	x		x		x	x		rut
X21380	137		x		x	x			x	x		x	x	bit, sca, sph, car
X21382	139		x			x	x		x	x				sph, lab-bit, gra, tre, car
X21383	145	x		x		x	x	x		x				rut
X21385	151	x		x	x	x	x		x	x			x	gra
X21386	157	x			x	x			x		x		x	
X21387	160	x	x			x			x		x	x	x	sph, hor = tr
X21388	162	x					x	x		x				spi, rut; bio = tr
X21389	163		x		x	x		x		x			x	Kfl = tr
X21390	141			x										pre, alb , mus
X21392	171		x		x			x		x	x	x	x	bio = tr
X21393	175				x	x		x		x			x	spi
X21396	166				x	x	x			x			x	alb-oli, mes, spi
X21436	142	x	x	x	x	x			x	x	x		x	spi, qtz = tr
* X21321	219	x	x				x	x		x	x	x	x	bio = tr

TABLE II-2 - MINERAL ASSEMBLAGES OF SOUTHERN MALAWI ROCKS (CONTD.)

		constituent minerals									accessories			
Slide no.	sample no.	opx	cpx	gar	hor	bio	Kfl	Nap	Cap	qtz	apt	zir	om	additional minerals
X21437	148			x		x			x	x			x	gra
X21438	370	x		x										alb, bio = tr
X21439	373	x							x	x			x	
X21440	375	x		x		x		x		x			x	
X21483	436	x		x	x	x			x		x	x	x	
X21484	449	x	x		x	x			x					Kfl, qtz = tr
X21485	452	x			x	x	x	x		x				bit, cpx, bio = tr
X21486	454	x		x	x						x	x	x	bit, cpx, bio = tr
X21487	455	x	x	x	x				x				x	
X21488	457	x	x	x	x				x					bit; bio = tr
X21528	437	x		x			x		x	x	x	x	x	rut
X21529	439	x		x			x	x		x	x	x	x	car, bio = tr
X21530	444	x		x		x	x		x					car; apa, zir = tr
X21531	459	x		x		x	x		x	x				rut
X21532	460	x		x		x			x		x	x	x	tre-act, car
X21533	461	x		x		x			x	x		x		tre, chl, rut, apa, car
X21593	429	x							x			x		gra, pyr, sph, cha; Kfl = tr
X21594	443	x	x		x	x			x	x			x	
X21596	464		x	x		x	x		x					sph
X21597	493	x	x		x	x	x		x	x				
X21598	496a	x	x						x					hor, bio, Kfl, qtz = tr
X21657	243						x		x	x				car
ditto		x	x						x		x		x	bio = tr
ditto		x			x	x			x					
X21658	305	x				x	x		x		x		x	qtz = tr
X21659	492	x	x						x		x		x	qtz = tr
X21660	494	x	x						x				x	
ditto		x	x		x	x			x				x	
X21589	179	x			x				x				x	
ditto		x							x				x	sca
ditto		x	x						x					
X21590	242	x			x		x		x	x				bio = tr
X21591	281	x	x		x	x			x	x				

TABLE II-2 - MINERAL ASSEMBLAGES OF SOUTHERN MALAWI ROCKS (CONTD.)

		constituent minerals									accessories			
Slide no.	Sample no.	opx	cpx	gar	hor	bio	Kfl	Nap	Cap	qtz	apt	zir	om	additional minerals
X21592	428	x							x		x		x	
ditto		x	x		x	x			x	x		x		ura, bio, car
X21661	495		x		x				x					car, ura, bio, om = tr
X21712	177	x	x		x	x			x				x	
X21713	178	x				x			x	x			x	spi
X21714	181						x	x		x				
X21715	182	x					x		x	x			x	
X21716	240	x	x			x	x		x	x			x	car
X21717	410	x	x		x	x	x		x	x				
X21718	412			x		x	x	x		x				
X21719	414	x	x		x	x			x					
X21720	415	x	x		x	x	x		x					
X21721	416	x	x		x		x		x		x	x	x	
X21723	123	x	x	x	x								x	pla = undet
ditto				x						x				opx, bio, Kfl = tr
X21724	222			x					x	x				lab-bit
X21725	228	x	x		x								x	pla = undet
ditto										x				ditto
X21726	235	x	x		x								x	pla = undet
ditto							x			x				ditto
X21727	250									x				ditto
ditto		x	x		x	x								ditto
ditto		x	x		x	x								
X21728	262								x	x				
ditto		x							x	x			x	car
X21729	272	x	x		x									pla = undet
ditto		x	x										x	ditto
ditto										x				ditto
X21730	308	x				x				x				ditto
X21731	322				x							x		ditto, spi
ditto		x	x									x		pla = undet
ditto										x				ditto

TABLE II-2 - MINERAL ASSEMBLAGES OF SOUTHERN MALAWI ROCKS (CONTD.)

		constituent minerals									accessories			
Slide no.	sample no.	opx	cpx	gar	hor	bio	Kfl	Nap	Cap	qtz	apt	zir	om	additional minerals
X21732	344				x	x	x			x	x	x	x	pla = undet; sph, car
X21734	395	x							x	x				bio = tr
X21735	384	x				x				x				pla = undet
ditto		x				x						x		ditto
X21736	419		x		x	x	x	x			x		x	ort, cpx = igneous ?
X21737	421		x		x	x	x		x	x	x		x	zir = tr
X21738	422	x	x		x	x			x	x				apa, om = tr
X21739	423				x	x	x	x		x				apa, zir, om = tr
X21740	446		x		x			x	x					apa, zir, om = tr
X21741	447						x		x	x				mus, rut
X21742	501		x	x	x				x	x				om = tr
X21744	143		x						x	x				sph
ditto					x						x		x	pla = undet
X21745	144	x			x	x			x	x				
X21747	342				x	x	x	x		x				
X21748	334				x				x					
ditto					x					x				pla = undet
X21749	365			x		x	x			x				mus
X21750	366	x			x	x			x		x		x	
ditto		x			x				x				x	
ditto		x			x		x		x	x				
X21751	367	x	x		x	x			x	x	x		x	gra ?
X21752	328		x		x	x	x		x	x	x		x	pla = undet
ditto							x	x		x				spi
X21753	321	x				x	x		x	x	x	x	x	Kfl = tr
X21755	311	x	x		x				x	x				
X21756	314	x	x		x	x		x		x				
X21757	316	x	x		x	x	x	x		x				
X21758	320	x	x		x	x	x	x		x				
X21760	462									x				spe, Mn- pyroxene
X21761	465			x	x				x	x				
X21762	468		x	x	x				x	x				sph
X21763	470				x	x	x	x		x			x	cpx = tr

TABLE II-2 - MINERAL ASSEMBLAGES OF SOUTHERN MALAWI ROCKS (CONTD.)

		constituent minerals									accessories			
Slide no.	sample no.	opx	cpx	gar	hor	bio	Kfl	Nap	Cap	qtz	apt	zir	om	additional minerals
X21764	471	x			x	x	x	x		x				chl, car
X21765	134	x	x	x	x	x			x	x				
X21766	353		x	x	x	x	x		x	x	x			ilmenite + cpx sym, car
X21767	362		x		x				x			x	x	(lab-bit), sph
X21768	363						x			x				(mic), alb
X21769	457								x					
ditto		x	x	x	x				x					bio = tr
X21770	458	x								x		x		
X21771	473				x	x	x	x		x	x	x	x	
X21772	474		x		x	x	x	x		x	x			
X21773	475					x	x			x		x	x	alb, all, mic, mus, chl
X21774	343	x	x	x	x	x	x		x	x		x		
X21775	477				x	x		x		x	x			epi, sph
X21776	478				x			x		x		x	x	
X21777	479				x			x		x	x	x		
X21778	480			x		x		x		x			x	kya, sil
X21779	481			x	x				x	x				chl, car
X21780	482				x				x	x		x		
X21781	434			x		x		x		x		x		(alb-oli), kya, sil
X21782	486				x	x				x	x	x		mus, sph, pla = undet
X21783	490		x			x				x			x	
X21837	239		x		x		x	x			x			
X21838	252		x		x	x	x							
ditto		x	x				x	x			x			
X21839	345				x	x	x	x		x				
X21840	346				x	x	x	x		x		x		sph
X21853	255	x	x		x	x	x	x		x	x	x		
X21854	254	x	x				x		x		x	x		
X21928	341		x						x	x				sph
X21929	348				x	x	x	x		x				sph
X21930	355		x	x					x	x				epi, sph
X21943	357													alb-oli, hor = tr
X21944	359				x			x						

TABLE II-2 - MINERAL ASSEMBLAGES OF SOUTHERN MALAWI ROCKS (CONTD.)

		constituent minerals									accessories			
Slide no.	sample no.	opx	cpx	gar	hor	bio	Kfl	Nap	Cap	qtz	apt	zir	om	additional minerals
X22013	497	x	x	x	x				x	x	x		x	rut; bio = tr
X22014	503	x	x	x					x		x		x	
X22015	507		x	x	x				x	x		x	x	gra, ilmenite + cpx syn
X22016	467		x		x				x	x	x		x	
X22018	496	x		x										hor = tr
X22154	140		x		x				x					sph
X22155	161				x	x			x		x		x	ura, opx = tr ?
X22156	241		x		x						x		x	
X22157	319		x											sca
X22158	352b				x	x					x		x	qtz, Kfl = tr
X22159	238	x			x	x	x		x	x	x		x	
X22161	487		x						x	x				sca, epi, sph; zir = tr
MA 81-1	509						x	x					x	sph, davidite
MA 203	324	x	x		x	x			x		x		x	sph
MA 204	325	x	x		x	x		x		x	x		x	ura
MA 205	326	x	x		x	x	x		x	x	x		x	pla = zoned
MA 400	135b	x		x										rut; pla = tr

TABLE II-3 - PETROGRAPHIC DESCRIPTIONS OF SAMPLES USED IN AGE DETERMINATIONS

Sample no.	Petrography
1.	Quartzo-feldspathic granulite
	The medium- to coarse-grained rock has a granulitic texture, and is poorly foliated, with a xenoblastic to polygonal, granoblastic fabric. Poikiloblastic, platy quartz and oligoclase are the main components with minor perthite, skeletal biotite and traces of deuteric muscovite. Opaque minerals, apatite, zircon and rutile are the accessory constituents.
3.	Quartzo-feldspathic granulite
	The rock is medium-grained and characterised by a xenoblastic, granoblastic texture. Lobate boundaries of poikiloblastic, elongated quartz grains are present. Quartz and antiperthitic andesine are the main constituents with minor ortho- and clinopyroxene, skeletal biotite and traces of K-feldspar. Apatite and opaque minerals are the accessory constituents. Little sericite, chlorite and calcite are deuteric.
8.	Gneissic granite dyke
	This rock, fine- to medium-grained, is characterised by a granolepidoblastic, inequigranular, seriate texture. Perthitic microcline, quartz and oligoclase are the main constituents, with minor dark-brown biotite and bluish-green hornblende. Accessory constituents are: very abundant sphene, allanite, opaque minerals, apatite and zircon. The plagioclase may be dusted by sub-microscopic needles as in certain granulites. Feldspar augen-like grains may represent relicts of igneous minerals.
9.	Hypersthene-quartz syenite
	The rock is dark coloured and fine- to medium-grained. The texture is seriate, grading from hypidiomorphic to granoblastic with complex grain boundaries, frequently lobate, scalloped and occasionally with triple-point junctions. Perthite and zoned oligoclase are the main constituents with minor quartz, hornblende, hypersthene and biotite. Accessory constituents are abundant idiomorphic zircon, apatite and opaque minerals. The hypersthene is xenoblastic, interstitial, and occasionally includes some hornblende and quartz grains.

TABLE II-3 - PETROGRAPHIC DESCRIPTIONS OF SAMPLES USED IN AGE DETERMINATIONS (CONTD.)

Sample no.	Petrography
11.	Perthitic gneiss
	The gneiss is medium-to coarse-grained, well foliated and characterised by a granonematoblastic texture and straight, polygonal grain boundaries. Perthitic feldspar (about 60 per cent of the mode) and green hornblende are main constituents with minor oligoclase, augite and traces of biotite. Apatite and little opaque minerals are the accessory constituents. Replacement of sodic plagioclase by perthite and microrapakivi textures are sporadically present.
12.	Quartzo-feldspathic gneiss
	The rock is medium-to coarse-grained and has a xenoblastic, seriate texture with common amoeboid grain boundaries and myrmekites. Large, recrystallised quartz ribbons show undulose extinction. Quartz, antiperthitic feldspar ($\pm An_{10}$) and microcline constitute over 90 per cent of the rock. Dark-brown biotite and green hornblende are the minor constituents, while the accessories are very rare and include carbonate and opaque minerals.
13.	Biotite gneiss
	The gneiss is medium-grained with a granolepidoblastic, equigranular to seriate texture. Myrmekites are common and the grain boundaries between felsic minerals are lobate and amoeboid. Main constituents are oligoclase, and minor brown biotite with a little interstitial quartz, K-feldspar and green hornblende. Apatite, rare zircon, sphene and traces of opaque minerals are the accessory constituents.
26.	Nepheline gneiss
	The gneiss is medium- to coarse-grained, has a granolepidoblastic, seriate to equigranular texture, slightly curved grain boundaries and sporadic triple-point junctions. Antiperthitic, sodic oligoclase is the main constituent with minor nepheline, dark-brown biotite, olive-green hornblende and rare K-feldspar. Accessory constituents are abundant idioblastic apatite, opaque minerals, sphene, carbonate (primary ?) and hercynite.

TABLE II-3 - PETROGRAPHIC DESCRIPTIONS OF SAMPLES USED IN AGE DETERMINATIONS (CONTD.)

Sample no.	Petrography
27.	Biotite gneiss
	This medium-grained gneiss has a granoblastic, equigranular to seriate texture. Grain boundaries between felsic minerals are frequently dentate; triple-point junctions are rare. Main constituents are andesine, feldspar and quartz, occasionally forming elongated grains parallel to foliation. Minor constituents are dark-brown biotite and little garnet. The accessory minerals are little idioblastic zircon and apatite.
30.	Mesocratic granulitic gneiss
	The rock is fine- to medium-grained and mesoscopically resembles a granulite; it is characterised by a granoblastic texture with frequent straight grain boundaries. Antiperthitic plagioclase ($\pm An_{30}$), perthite and brown hornblende are the main components with minor quartz, skeletal biotite, and clinopyroxene. Opaque minerals, zircon, apatite are accessory constituents. Replacement of pyroxene by hornblende and uralite is occasionally present.
31.	Mesocratic granulitic gneiss
	The rock is fine- to medium-grained and mesoscopically it resembles a granulite, and, has a texture transitional from hypidiomorphic to granoblastic. Perthitic, myrmekitic oligoclase and green hornblende are the main components, with minor quartz and biotite. Opaque minerals, apatite and zircon are the accessory constituents, while carbonate replaces hornblende and biotite.
33.	Quartzo-feldspathic gneiss
	The gneiss is fine- to medium-grained and has a granolepidoblastic, seriate texture with irregular, dentate grain boundaries. Sporadic, elongated quartz grains show undulose extinction. Quartz, plagioclase ($\pm An_{30}$), perthitic microcline are the main constituents with minor dark-brown biotite and green hornblende. Sphene, zircon, opaque minerals, apatite and metamictic allanite are accessory constituents. Quartz-plagioclase myrmekites are very common at the plagioclase-K-feldspar contact.

TABLE II-3 - PETROGRAPHIC DESCRIPTIONS OF SAMPLES USED IN AGE DETERMINATIONS (CONTD.)

Sample no.	Petrography
34.	Pyroxene amphibolite dyke
	The rock is medium-grained and presents a granonematoblastic, equigranular texture with curved to straight grain boundaries and common triple-point junctions. Greenish-brown hornblende, clinopyroxene and sodic andesine are the main constituents with minor biotite and traces of K-feldspar. Apatite, opaque minerals and sphene are the accessory constituents. The pyroxene is poikiloblastic and includes hornblende and plagioclase grains.
35.	Granite dyke
	The granite is coarse-grained, hypidiomorphic, granular and with a column index < 5. Myrmekites and microrapakivi textures are common. Perthitic microcline, quartz and sodic feldspar are the main constituents with minor biotite. Zircon and apatite are the accessory minerals.
36.	Garnet granulite
	The granulite is fine- to medium-grained, lineated, and presents a granolepidoblastic texture with irregular grain boundaries. Sodic andesine, perthitic microcline and quartz are the main components with scarcer garnet, biotite and orthopyroxene. Apatite, opaque minerals, and zircon are accessory constituents. Relationships between garnet, biotite and pyroxene are complex and indicate replacement of the latter by quartz-biotite symplectites.
39.	Quartzo-feldspathic granulite
	This unfoliated rock is fine- to medium-grained and characterised by a xenoblastic texture and irregularly sutured grain boundaries. Perthitic microcline, sodic oligoclase and quartz are the main components with only minor amounts of biotite and traces of hornblende. Accessory constituents are apatite, subidioblastic zircon, opaque minerals and tourmaline. Deuteric alteration of feldspars and biotite is shown by some sericite, chlorite and carbonate.

TABLE II-3 - PETROGRAPHIC DESCRIPTIONS OF SAMPLES USED IN AGE DETERMINATIONS (CONTD.)

Sample no.	Petrography
40.	Melanocratic hornblende granulite
	The granulite is rather fine-grained, well lineated and slightly foliated. The texture is grano-nematoblastic with frequent straight boundaries and triple-point junctions. Andesine, brown hornblende, and clinopyroxene are the main constituents with minor uralitised orthopyroxene and brown biotite. Accessory constituents are apatite, opaque minerals and zircon. Replacements of pyroxenes by biotite or hornblende (and vice versa) are occasionally present.
41.	Microgranite
	The rock has a fine-grained, seriate, granoblastic texture with many myrmekites and sporadic triple-point grain boundaries. Main constituents are perthitic microcline, quartz and subordinate albite-oligoclase, with minor dark-brown biotite and bluish-green hornblende. Accessory constituents are apatite, opaque minerals, zircon, allanite, and fluorite (?). Inclusions of quartz are present in the feldspar while perthite, quartz and hornblende are intensely recrystallised.
42.	Syenite
	The rock is coarse-grained, with a granoblastic texture and extremely complex grain boundaries, indicating three phases of mutual replacements and recrystallisation. Main constituents are perthitic K-feldspar and sodic plagioclase with minor amounts of quartz, clinopyroxene and biotite. Accessory components are zircon, an unidentified high-relief, high birifrangence mineral, opaque grains and apatite. Biotite seems to be secondary after the pyroxene.
48.	Melanocratic hornblende granulite
	The granulite is fine-grained, foliated with a grano-nematoblastic texture and frequent straight grain boundaries. Sodic labradorite and brown hornblende are the main constituents, followed by hypersthene, biotite and augite. Accessory constituents are opaque minerals, apatite and rounded zircon. Pyroxenes replace biotite while augite is infrequently included in hornblende.

TABLE II-3 - PETROGRAPHIC DESCRIPTIONS OF SAMPLES USED IN AGE DETERMINATIONS (CONTD.)

Sample no.	Petrography
57.	Quartzo-feldspathic rock
	The rock is fine-grained, unfoliated with a granoblastic, mainly equigranular texture and rounded, interlobate grain boundaries. Mesoperthitic feldspar and quartz constitute up to 95 per cent of the mode. Sodic oligoclase and biotite are minor constituents while opaque grains, zircon, metamictic allanite and traces of apatite are the accessory minerals.
59.	Quartzo-feldspathic rock
	The rock is fine-grained, with a granoblastic, equigranular texture and occasional myrmekites. Main constituents are quartz, perthitic microcline and sodic oligoclase which, in equal proportions, form over 90 per cent of the mode. Opaque minerals, zircon, and apatite make up for the remainder.
65.	Quartzo-feldspathic granulite
	The granulite, slightly lineated, has a fine- to medium-grained, granoblastic and inequigranular to seriate texture with common myrmekites. Perthitic microcline, quartz, and oligoclase are the main constituents, followed by a little orthopyroxene, olive-green hornblende and traces of biotite. Frequent idiomorphic zircon, metamictic allanite, carbonate, opaque minerals, and apatite are the accessory constituents.
67.	Quartzo-feldspathic granulite
	The rock is well lineated and resembles a granulite in hand specimen. It is characterised by an inequigranular, flaser fabric and ribbon-like quartz grains in a fine-grained felsic matric. Quartz, perthitic K-feldspar and oligoclase are main constituents with little dark olive-green hornblende. Opaque minerals, allanite, idiomorphic zircon, apatite, sphene, and tourmaline are the accessory constituents.

TABLE II-3 - PETROGRAPHIC DESCRIPTIONS OF SAMPLES USED IN AGE DETERMINATIONS (CONTD.)

Sample no.	Petrography
70.	Biotite-diopside gneiss
	The gneiss is fine-grained and presents a granolepidoblastic, seriate texture with interlobate, sutured grain boundaries and widespread myrmekites. Cryptic and recrystallised mortar fabric is sporadically developed. Main components are, in the order, orange-brown biotite, plagioclase (An_{30}), perthite, colourless clinopyroxene and quartz. Opaque grains, graphite (?), apatite and sphene are accessory minerals. Biotite and clinopyroxene generally coexist but occasionaly disequilibrium textures are preserved, while the uralitisation of the pyroxene is widespread.
75.	Leucocratic augite granulite
	The rock, fine-to medium-grained, is poorly lineated, unfoliated, and with a granoblastic, seriate texture. Boundaries are straight to lobate while myrmekitic textures of quartz and sodic feldspar frequently rim the K-feldspar. Perthitic microcline, antiperthitic, sodic andesine and quartz are the main constituents with minor, xenoblastic, greenish augite. Accessory constituents are quite abundant and include opaque minerals, sphene, zircon, apatite and allanite.
92.	Melanocratic rock
	The rock is fine- to medium-grained, greenish in colour, with a granolepidoblastic, seriate texture and curved, irregular grain boundaries. Occasional quartz grains are amoeboid to poikiloblastic. Sodic, antiperthitic andesine, quartz, and dark-brown biotite are the main constituents with minor K-feldspar and uralite which possibly replaces pyroxene. Orthopyroxene and garnet were not found in the thin section but are present in the sample. Zircon, carbonate, apatite, and opaque minerals are accessory constituents.
93.	Mesocratic granulite
	The rock, fine- to medium-grained, presents a granolepidoblastic, seriate texture, with rare platy quartz grains. The constituents are, in the order, antiperthitic andesine, quartz, orthopyroxene, and biotite. Accessory components are opaque grains, carbonate, apatite and rare zircon. Biotite and orthopyroxene appear in general to coexist, but some mica forms from the pyroxene which is also affected by uralitisation and is replaced by carbonate.

TABLE II-3 - PETROGRAPHIC DESCRIPTIONS OF SAMPLES USED IN AGE DETERMINATIONS (CONTD.)

Sample no.	Petrography
97.	Perthitic orthogneiss
	The gneiss is fine- to medium-grained, with a granoblastic texture, curved, irregular grain boundaries and myrmekites. Quartz may form elongated grains with slightly embayed boundaries. Perthitic microcline, quartz, Na-oligoclase are the main constituents, followed by minor green hornblende and dark-brown biotite. Zircon, apatite and opaque minerals are the accessory constituents.
108.	Garnet gneiss
	The gneiss is poorly foliated, fine- to medium-grained and with a granolepidoblastic texture. The grain boundaries of quartz are frequently embayed and this mineral forms sporadic, flattened blebs, parallel to the foliation and showing, in places, incipient development of mortar fabric. Myrmekitic textures of quartz and plagioclase are also present. Quartz, perthite and sodic feldspar ($\pm An_{30}$) are the main constituents with minor garnet and biotite. Opaque minerals, zircon and rutile (as needles in the quartz) are the accessory constituents.
110.	Granite dyke
	The granite is coarse-grained with an hypidiomorphic to xenomorphic texture and a colour index (M) next to 0. Main constituents are slightly perthitic microcline, antiperthitic albitic feldspar (slightly zoned) and quartz. Specks of opaque minerals are rare.
117b.	Granite vein
	The granite is medium- to coarse-grained, with $M < 10$, a xenomorphic texture and very frequent myrmekites. K-feldspar, sodic feldspar and quartz are the main constituents followed by very little biotite. Opaque minerals, apatite, hematite, and zircon are the accessory components.
118c.	Granite vein
	The granite is medium-grained, with an hypidiomorphic to xenomorphic texture and a $M < 10$. Main constituents are perthitic K-feldspar (microcline), quartz and albitic feldspar. Biotite is a very minor component and the accessory constituents are opaque minerals and rare apatite.

TABLE II-3 - PETROGRAPHIC DESCRIPTIONS OF SAMPLES USED IN AGE DETERMINATIONS (CONTD.)

Sample no.	Petrography
121a.	Biotite gneiss
	The gneiss has a granolepidoblastic, seriate texture with scalloped, amoeboid grain boundaries. Xenoblastic, poikiloblastic, and amoeboid quartz, dark-brown biotite and oligoclase are the main constituents with minor K-feldspar. Opaque minerals, apatite, zircon, sphene and metamictic allanite (?) are the accessory constituents.
121b.	Hornblende-biotite gneiss
	The gneiss is fine-to medium-grained and presents a granolepidoblastic, inequigranular-seriate texture with grain boundaries that are generally irregular. Myrmekites and triple-point junctions are also present. Dark-brown biotite and quartz are the main constituents, followed by minor (antiperthitic) plagioclase ($\pm An_{30}$), microcline and green hornblende. Accessory sphene, zircon, opaque minerals, apatite and allanite are accompanied by traces of late-formed carbonate, epidote, zoisite and white mica.
315.	Quartzo-feldspathic granulite
	The granulite has a fine-grained, subequigranular, granoblastic texture and interlobate, curved grain boundaries. Antiperthitic andesine is the main constituent with minor quartz, orthopyroxene, biotite, perthite and hornblende. Relationships between hornblende, biotite and pyroxenes are unclear. Opaque minerals, zircon and apatite are the accessory constituents. Biotite is included in orthopyroxene.
321.	Granulite with leucocratic bands
	The granulite has a fine- to medium-grained granolepidoblastic, subequigranular texture with curved and interlobate grain boundaries. Antiperthitic andesine is the main constituent with minor amounts of quartz, biotite, orthopyroxene and traces of K-feldspar. Opaque minerals, apatite, zircon and hercynite are accessory constituents. Green spinel (hercynite) is rimmed by an opaque mineral and biotite is replaced in a few cases by orthopyroxene. The reverse reaction is also present but more often the two minerals coexist.

TABLE II-3 - PETROGRAPHIC DESCRIPTIONS OF SAMPLES USED IN AGE DETERMINATIONS (CONTD.)

Sample no.	Petrography
324.	Mesocratic granulite
	The rock is fine-grained and its texture is granonematoblastic, seriate with frequent myrmekites and curved, rather irregular grain boundaries. Main constituents are hornblende, intermediate plagioclase and perthitic K-feldspar followed by biotite and minor ortho- and clinopyroxene. Apatite, opaque grains, rare sphene and carbonate are accessory minerals. Mineral textures provide evidence of prograde mineral development.
325.	Mesocratic granulite
	The granulite is medium-grained and with a seriate, granoblastic texture showing irregular and interlocking grain boundaries grading to curve or straight. Main components are orthopyroxene, clinopyroxene, hornblende, biotite, antiperthitic andesine and quartz. Apatite and opaque grains are accessory minerals. Some uralite is also present and the rock presents evidence of both prograde and retrograde mineral developments.
326.	Mesocratic granulite
	The rock is medium-to coarse-grained and presents a granoblastic, inequigranular to seriate texture with interlocking to curved grain boundaries. Main constituents are zoned, intermediate plagioclase, quartz, orthopyroxene, clinopyroxene, K-feldspar, hornblende and biotite with apatite and opaque grains as accessory minerals. The rock provides clear indications of prograde mineral development.
328.	Pyroxene gneiss
	In hand specimen the rock is characterised by a dark colour typical of granulite, and, in thin section it is fine-grained with curved to straight grain boundaries and a granonematoblastic texture. Main constituents are intermediate plagioclase and hornblende followed by clinopyroxene, K-feldspar, minor biotite and quartz. Accessories are apatite and opaque minerals. A cross-cutting quartz-rich vein with biotite-rich selvedges carries perthitic K-feldspar, antiperthitic oligoclase and quartz. Clinopyroxene appears to replace hornblende.

TABLE II-3 - PETROGRAPHIC DESCRIPTIONS OF SAMPLES USED IN AGE DETERMINATIONS (CONTD.)

Sample no.	Petrography
330.	Granitic gneiss
	The gneiss is medium-grained, poorly foliated with a granolepidoblastic, seriate texture and with curved to interlobate grain boundaries. There is no evidence of a relict igneous texture; antiperthitic oligoclase, perthite and quartz are the main constituents with minor hornblende and biotite. Opaque grains, apatite, and zircon are the accessory minerals.
331.	Quartzo-feldspathic granulite
	The granulite is fine to medium-grained with a granolepidoblastic, seriate texture and interlobate, curved grain boundaries between felsic minerals. Sodic andesine, quartz and dark-brown biotite are the main constituents with minor orthopyroxene and hornblende. Biotite and orthopyroxene generally coexist but, in places, the former seems to replace the latter. Opaque minerals, apatite and zircon are the accessory constituents.
335.	Mesocratic gneiss
	The rock, banded and foliated, has a granonematoblastic, seriate texture with curved, lobate grain boundaries and myrmekites. Antiperthitic plagioclase ($\pm An_{30}$), quartz, biotite and green hornblende are the main constituents with minor K-feldspar. Hornblende replaces biotite in places and the latter mineral is rimmed by sphene. Opaque grains, apatite, sphene and zircon are the accessory constituents.
351.	Granulite
	The rock is fine grained, unfoliated with a granolepidoblastic, seriate texture and complex grain boundaries from straight to interlobate. Antiperthitic andesine, quartz, K-feldspar and biotite are the main constituents, followed by clinopyroxene, hornblende, and orthopyroxene. Pyroxene, hornblende and biotite are in general coexisting but biotite is occasionally replaced by pyroxenes. Opaque minerals, apatite and zircon are accessory constituents.

TABLE II-3 - PETROGRAPHIC DESCRIPTIONS OF SAMPLES USED IN AGE DETERMINATIONS (CONTD.)

Sample no.	Petrography
366.	Melanocratic hornblende granulite
	The rock is subequigranular, fine grained with a granonematoblastic texture and generally curved to straight mineral boundaries. Main constituents are hornblende, intermediate plagioclase with minor orthopyroxene, biotite and accessory apatite and opaque grains. The rock is cut by a quartz-myrmekitic andesine acidic vein with scattered pyroxenes, hornblende and K-feldspar grains. At the contact between the melanocratic rock and the leucocratic vein an orthopyroxene-plagioclase reaction rim is developed (Type 1 prograde geometry).
367.	Mesocratic granulite
	The rock presents a fine-grained, inequigranular to seriate, granoblastic texture with straight to curved mineral boundaries. Main constituents are andesine, orthopyroxene, hornblende, biotite, clinopyroxene and quartz. Apatite, opaque grains and graphite (?) are accessory minerals and there is evidence for prograde mineral development.

APPENDIX III

ELECTRON-MICROPROBE MINERAL ANALYSES

(i) Analytical Equipment Employed

The programme of mineral analyses on rocks from southern Malawi and related areas was carried out in the following laboratories:

1) National Institute for Metallurgy, Johannesburg.

2) Anglo-American Corporation Research Laboratories, Johannesburg.

3) Geological Survey, Pretoria.

4) Geology Department, Witwatersrand University.

In the above laboratories[4] different microprobes and analytical techniques were used and these are referred to separately. In all cases the probed sections were coated under vacuum by a thin film of high purity carbon.

1) National Institute for Metallurgy

In this laboratory 97 silicate and 8 opaque minerals were probed. The electron-microprobe used was an ARL EMX model; the working conditions for silicates were as follows: 15 KV accelerating voltage, 0,5 μA sample current measured on brass,

---

(4) A list of the abbreviations used in this Appendix to define the different analytical laboratories is as follows:

N.I.M.= National Institute for Metallurgy.
A.A.C.= Anglo-American Corporation, Research Laboratories.
G.S. = Geological Survey, Pretoria.
G.D. = Geology Department, Witwatersrand University.

focused beam for all the minerals. Counts were accumulated against a constant total beam current collected over a period of time of ± 10 seconds. Ka radiation was measured for all elements. In the case of the opaque minerals the working conditions differ in the accelerating voltage: 20 KV and the beam current: 0,04 μA; the other parameters did not change.

In each marked grain three different areas were probed, each a few microns in area; the average of the X-ray counts from each area was used in the calculation of the percentage of each element. For the analysis of the standards, 10 readings were measured on peak, but for the unknown samples the probe took 5 readings on the peak plus 3 readings on each side of it to calculate the background. The X-ray intensities, expressed as counts, were automatically punched on a computer paper-tape and converted into oxide mass percentages by the computer programme EMPDAR VII. This programme applied corrections for fluorescence, absorption, atomic number, dead time and background. In Tables III-1 and III-2 the standards used for the analysis of the silicate and oxide (opaque) minerals are presented.

The microprobe operators of the electron-microprobe were Miss E. Gasparrini and Dr. E. A. Viljoen.

2) Anglo-American Corporation Research Laboratories

The electron-microprobe used to obtain 23 quantitative

TABLE III-I
SILICATE STANDARDS (N.I.M.)

Element	Standard
Si,Mg,Ca	Synthetic diopside
Al	" anorthite
Ti	" rutile
Fe	" ferrosilite
Mn	" tephroite
K	" microcline
Na	" plagioclase An_{50}

TABLE III-2
OXIDE MINERAL STANDARDS (N.I.M.)

Element	Standard
Fe	Synthetic magnetite
Ti	" ilmenite
Cr,Al,Mg	Analyzed chromite
Mn	" tephroite

TABLE III-3
PYROXENE STANDARDS (A.A.C.)

Element	Standards
K	orthoclase
Mn	hedembergite
Na	anorthoclase
Mg	forsterite
Al	enstatite glass + 10% Al_2O_3
Fe	hedembergite
Ca	diopside
Si	enstatite glass
Ti	diopside glass + 2% TiO_2
Cr	chromite

TABLE III-4
SILICATE STANDARDS (G.S.)

Element	Standard
Si	quartz (natural)
Ti	rutile "
Al	corundum "
Fe	hematite "
Mn	pyrolusite "
Mg	periclase (synthetic)
Ca	wollastonite (natural)
N	albite "
K	sanidine "

TABLE III-5 - SILICATE STANDARDS (G.D.)

Si,Mg,Al:	Synthetic enstatite glass containing 10% Al_2O_3
Mn:	Rhodocrosite
Ca:	Anorthite
Na:	Sanidine
Cr:	Stillwater chromite
Fe,Ti:	Apollo 11 ferric glass (synthetic)

mineral analyses is an ARL SEMQ equipped with 3 scanning spectrometers used for K, Mn, Na, Al, Mg and 6 fixed channel spectrometers measuring Fe, Si, Ti, Ca, Cr. The accelerating voltage was 20 KV with a sample current of 0,05 μA (measured on brass). One reading of 20 seconds was taken on the standard peak, and 3 counts of 20 seconds each on the unknown. Background counts were taken once only for 10 seconds on each side of the peak. Only Kα radiation was measured, and the same conditions were used for both silicate and opaque mineral grains (1 analysis only).

The raw data was processed on line using a computer programme which applied an empirical matrix correction according to Albee and Ray (1970). Standards used in the analyses of silicates (except garnet) are presented in Table III-3. In the case of garnet, Al, Fe, Mg were calibrated against an analysed pyrope. One ilmenite was analysed with the above standards. The electron-microprobe operator was Mr. G. Hutchenson.

3) Geological Survey of South Africa, Pretoria

The electron-microprobe used by this laboratory is a JEOL, JXA50A model, fitted with 3 spectrometers. It was operated under the following conditions: 15 KV accelerating voltage and 0,05 μA of specimen current, measured on brass. The diameter of the beam ranged between 3 and 5 μ. On the peaks counts were taken 3 times for 10 seconds each and on background

counting was made twice for 5 seconds on both sides of the peak.

The electron-microprobe was computer controlled and the raw data were immediately processed by applying Bence and Albee (1968) corrections. The standards used are given in Table III-4 and they were analysed by the National Institute for Metallurgy and the McLachlan and Lazar analytical laboratories of Johannesburg. The electron-microprobe operator at the Geological Survey laboratory was Mr. L.W. Esterhuyse.

4) Geology Department, Witwatersrand University Johannesburg

Only two analyses were carried out in this laboratory using an electron-microprobe ARL SEMQ model fitted with 3 scanning spectrometers. Operating conditions were as follows: 15 KV accelerating voltage and 0,05 μA specimen current (on brass); the beam was focused with a resolution of 5μ. Radiation measured was the Kα of elements and the time of accumulation was 1 x 20 seconds on peak and 2 x 10 seconds on background on each side. All data processing was done on line and the counts were compared against the peak of the standards. Corrections were done according to the method of Albee and Ray (1970). The standards used are listed in Table III-5 and were cross-checked with the Anglo-American Research Laboratories electron-microprobe. The electron-microprobe operator was Mr. G. Davies.

(ii) Precision and Accuracy of Electron-microprobe Analyses

No data on precision and/or accuracy were directly provided by the National Institute for Metallurgy analytical laboratory but more information is available for the Anglo-American and Geological Survey microprobes. In particular in Table III-6 the analysis of a standard clinopyroxene provided by the Australian National University, Canberra, (A) is compared with the average composition determined by the Anglo-American laboratory electron-microprobe. This mineral was analysed occasionally to monitor instrumental drift. The reproducibility of the analyses seems adequate for the present purpose despite a deterioration in the precision for the minor elements e.g. Mn shows a 12,5 per cent variation calculated as $\Delta\ \% = \frac{(A-B) \times 100}{AB/2}$ The precision and accuracy of the Geological Survey Laboratory electron-microprobe may be evaluated from Tables III-7 and III-8 in which are compared the analyses of a standard clinopyroxene and garnet (A) with the average composition (B) determined during a run. The quality of the analyses is below that from the Anglo-American probe, particularly for the minor elements. The only major oxide with a large $\Delta\%$ (6 per cent) is Al_2O_3 in garnet. To evaluate the quality of the analyses obtained from N.I.M. and to provide a cross-reference between the three electron-microprobes, the same garnet, hypersthene and augite were analysed in the different laboratories. The

TABLE III-6

CLINOPYROXENE STANDARD* COMPOSITION(A) AND A.A.C. ANALYSIS (B)

	A	B	Δ%
SiO_2	51,4	51,65	1
TiO_2	0,53	0,50	6
Al_2O_3	5,51	5,20	6
Cr_2O_3	0,61	0,65	7
FeO	3,80	4,00	5
MnO	0,08	0,07	12
MgO	16,07	15,93	1
CaO	21,06	20,91	1
Na_2O	0,95	0,92	3
K_2O	0,05	t	n.c.

*Clinopyroxene from garnet-clinopyroxenite nodule, University of Canberra, AUS.

All iron as FeO; t=traces; n.c. = not calculated.

TABLE III-7

CLINOPYROXENE STANDARD* COMPOSITION (A) AND G.S. ANALYSIS (B)

	A	B	Δ%
SiO_2	55,05	54,72	1
TiO_2	0,16	0,12	25
Al_2O_3	1,12	0,85	24
FeO	3,14	2,81	10
MnO	0,16	0,13	19
MgO	15,47	15,89	3
CaO	24,13	23,96	1
Na_2O	0,6	1,04	42
K_2O	0,04	0,03	25
Total	99,87	99,55	

*Pitcairne, New York, USA (Diop-1).

All iron as FeO.

TABLE III-8

GARNET STANDARD* COMPOSITION (A) AND G.S. ANALYSIS (B)

	A	B	Δ %
SiO_2	40,46	40,06	1
TiO_2	0,1	0,06	40
Al_2O_3	23,48	22,07	6
FeO	15,2	15,55	2
MnO	0,69	0,55	20
MgO	14,77	15,06	2
CaO	4,27	4,05	5
Na_2O	0,03	t	n.c.
K_2O	0,04	t	n.c.
Total	99,04	97,4	

*Magdala, Scuppansberg, S.A.

All iron as FeO; t = traces; n.c. = not calculated.

compositions of these minerals are presented in Tables III-9, 10 and 11, with the different percentages between the analyses. These same tables provide also a more precise evaluation on the accuracy of the analytical data obtained from the Geological Survey electron-microprobe.

TABLE III-9
ORTHOPYROXENE *ANALYSES BY DIFFERENT LABORATORIES

	1-N.I.M.	2-G.S.	3-A.A.C.	Δ%1-2	Δ%1-3	Δ% 2-3
SiO_2	51,09	53,16	50,83	4	-	5
TiO_2	0,11	0,16	0,08	48	30	67
Al_2O_3	1,32	2,03	1,63	54	21	22
FeO	27,60	25,29	27,41	4	1	8
MnO	1,26	0,59	0,90	53	33	41
MgO	18,37	18,37	18,60	-	1	1
CaO	0,80	0,81	0,77	1	4	5
Na_2O	0,05	0,04	0,01	20	133	100
K_2O	-	0,04	-	-	n.c.	n.c.
Total	100,60	100,49	100,23			

*Sample locality (55a) shown in Fig.9.
All iron as FeO; t= traces; n.c.= not calculated.

TABLE III-10
CLINOPYROXENE *ANALYSES BY DIFFERENT LABORATORIES

	1-N.I.M.	2-G.S.	3-A.A.C.	Δ%1-2	Δ%1-3	Δ%2-3
SiO_2	50,44	51,21	50,53	1	-	1
TiO_2	0,31	0,33	0,28	6	10	16
Al_2O_3	2,76	3,17	2,81	15	2	12
FeO	12,61	12,50	12,35	1	2	1
MnO	0,57	0,54	0,43	5	28	22
MgO	11,58	11,96	11,91	3	3	-
CaO	20,51	19,68	21,27	2	4	8
Na_2O	0,48	0,44	0,46	8	4	4
K_2O	-	0,04	-	n.c.	n.c.	n.c.
Total	99,26	99.87	100,04			

*Sample locality (55a) shown in Fig.9.
All iron as FeO; n.c.= not calculated.

TABLE III-11
GARNET *ANALYSES BY DIFFERENT LABORATORIES

	1-N.I.M.	2-G.S.	3-A.A.C.	Δ%1-2	Δ%1-3	Δ%2-3
SiO_2	38,83	39,52	38,50	2	1	3
TiO_2	t	0,09	-	n.c.	n	n.c.
Al_2O_3	22,31	21,25	22,49	5	1	6
FeO	29,11	27,22	29,61	6	2	8
MnO	1,18	1,11	0,81	6	37	31
MgO	7,67	7,57	7,44	1	3	2
CaO	2,29	2,35	2,40	3	5	2
Na_2O	t	0,04	0,01	n.c.	n.c.	100
K_2O	t	0,04	-	n.c.	n.c.	n.c.
Total	101,41	99,19	101,25			

* Sample locality (104) shown in Fig.9.
All iron as FeO; n.c. not calculated; t = traces.

(iii) Mineral Analyses

Orthopyroxene — Table III-12

Clinopyroxene — Table III-13

Garnet — Table III-14

Hornblende — Table III-15

Biotite — Table III-16

Plagioclase — Table III-17

Prehnite, ilmenite, magnetite — Table III-18

TABLE III-12 - ORTHOPYROXENE ANALYSES

Locality no.	7						55a			5			46		
SiO_2	50,30	50,22	49,68	49,17	48,80	49,20	51,13	50,97	51,09	52,37	51,55	51,55	51,76	52,07	51,39
TiO_2	0,08	0,04	0,08	0,07	0,06	0,08	0,06	0,07	0,11	0,14	0,15	0,14	0,09	0,10	0,12
Al_2O_3	0,88	0,76	0,72	0,78	0,80	0,99	0,89	0,86	1,32	1,71	1,58	1,39	1,41	1,07	1,20
FeO	33,20	32,53	33,22	32,95	32,74	32,17	27,44	27,30	27,60	29,98	30,49	29,88	23,09	23,53	23,39
MnO	1,26	1,26	1,16	1,16	1,16	1,16	1,26	1,26	1,26	0,04	0,74	0,74	1,24	1,07	1,14
MgO	15,01	15,01	14,70	14,85	15,16	14,83	18,89	18,56	18,37	16,28	16,38	16,08	21,26	21,94	21,78
CaO	1,04	0,91	0,82	1,00	0,94	1,06	0,86	0,85	0,80	1,17	0,84	1,71	0,60	0,75	0,62
Na_2O	0,06	0,06	0,04	0,04	0,04	0,04	0,05	0,05	0,05	0,10	0,09	0,12	0,07	0,09	0,07
K_2O	-	-	-	-	-	-	-	-	-	-	-	-	-	-	-
Total	101,84	100,80	100,42	100,02	99,70	99,53	100,58	99,92	100,60	101,79	101,82	101,61	99,52	100,62	99,71

Sample localities shown in Fig.9 and in Map 2 in the pocket at the back of the thesis.

All iron as FeO. All analyses by N.I.M.

TABLE III-12 - ORTHOPYROXENE ANALYSES (CONTD.)

Locality	48			55b			104				436		456	135b
SiO_2	51,11	51,34	51,08	50,41	50,64	49,99	49,84	50,19	50,14	49,98	50,13	50,41	51,95	52,76
TiO_2	0,17	0,17	0,18	0,13	0,13	0,12	0,12	0,08	0,14	0,11	0,25	0,19	0,12	0,00
Al_2O_3	1,01	1,15	1,10	1,96	2,14	1,78	2,49	2,56	2,53	2,68	1,71	1,25	3,30	1,67
Cr_2O_3	n.d	n.d	n.d	n.d.	n.d	n.d	n.d	n.d	n.d	n.d	n.d	n.d	0,11	0,05
FeO	29,09	29,80	28,71	26,30	26,53	26,64	28,62	29,20	29,48	29,42	28,93	30,02	18,37	32,14
MnO	0,99	0,96	0,97	1,19	1,19	1,25	0,46	0,45	0,45	0,45	0,65	0,70	0,18	0,15
MgO	17,33	17,78	17,03	17,77	18,05	17,73	17,64	17,51	18,09	17,07	16,35	16,51	25,13	23,77
CaO	0,91	1,29	1,26	1,34	1,41	1,28	0,37	0,41	0,37	0,38	1,01	0,83	0,64	0,29
Na_2O	0,09	0,09	0,09	0,0	0,12	0,10	0,09	0,09	0,09	0,10	0,0	0,2	0,04	0,00
K_2O	-	-	-	-	-	-	-	-	-	-	-	-	-	-
Total	100,70	102,58	100,42	99,10	100,21	98,89	99,63	100,49	101,29	100,19	99,03	100,29	99,84	100,82
Analyst	N.I.M.	N.I.M.	N.I.M.	N.I.M.	N.I.M.	N.I.M.	N.I.M.	N.I.M.	N.I.M.	N.I.M.	G.S.	G.S.	G.S.	A.A.C.

Sample localities shown in Fig.9 and in Maps 1 to 3 in the pocket at the back of the thesis.
All iron as FeO; n.d.: not determined.

TABLE III-12 - ORTHOPYROXENE ANALYSES (CONTD.), MOZAMBIQUE

Locality no.	T37	T78	T19	T19
SiO_2	50,14	51,31	52,75	53,25
TiO_2	0,18	0,05	0,03	0,03
Al_2O_3	4,81	3,43	2,6	2,72
Cr_2O_3	-	-	0,04	0,08
FeO	21,66	19,43	16,16	17,81
MnO	0,34	0,30	0,33	0,37
MgO	22,63	24,15	26,52	26,6
CaO	0,57	0,37	0,63	0,12
Total	100,85	99,04	99,09	100,94
Analyst	A.A.C.	A.A.C.	G.S.	G.S.

For sample localities see Appendix I-3 and Coelho (1969).

All iron as FeO.

TABLE III-13 CLINOPYROXENE ANALYSES

Locality no.	7		55a						5				46	
SiO_2	49,36	50,19	50,15	49,26	49,71	50,19	50,44	50,31	50,06	50,09	50,47	50,66	50,25	51,36
TiO_2	0,27	0,29	0,33	0,24	0,34	0,30	0,31	0,27	0,36	0,36	0,35	0,32	0,32	0,23
Al_2O_3	2,10	2,40	2,75	2,20	2,80	2,65	2,76	2,84	3,06	3,07	2,79	3,09	2,28	2,08
FeO	14,68	15,96	12,60	13,01	12,82	12,37	12,61	12,63	13,39	13,42	13,20	12,85	9,86	10,46
MnO	0,51	0,51	0,57	0,57	0,57	0,57	0,57	0,57	0,43	0,37	0,44	0,33	0,52	0,48
MgO	10,64	10,50	11,73	11,04	11,55	11,86	11,58	11,61	11,02	11,09	10,91	11,42	13,08	13,26
CaO	20,11	19,46	19,02	19,62	20,03	20,79	20,51	20,00	21,21	20,74	21,82	21,50	21,40	20,90
Na_2O	0,52	0,53	0,48	0,49	0,48	0,48	0,48	0,48	0,58	0,57	0,54	0,61	0,74	0,75
K_2O	-	-	-	-	-	-	-	-	-	-	-	-	-	-
Total	98,19	99,84	97,63	96,43	98,30	99,21	99,26	98,71	100,11	99,71	100,52	100,78	98,45	99,52

Sample localities shown in Fig.9 and in Map 2 in the pocket at the back of the thesis.

All iron as FeO. All analyses by N.I.M.

TABLE III-13- CLINOPYROXENE ANALYSES (CONTD.)

Locality no.	436		*	353			121	19	468	456	48	55b		
SiO_2	48,62	48,47	50,96	50,13	50,34	52,48	50,29	50,85	53,93	50,30	50,33	49,19	49,68	61,13
TiO_2	0,39	0,45	0,73	0,54	0,48	0,18	0,19	0,29	0,24	0,64	0,59	0,30	0,34	0,31
Al_2O_3	2,19	2,34	1,31	1,45	3,15	1,53	5,93	5,76	2,88	5,15	2,62	2,79	3,06	3,12
Cr_2O_3	n.d	n.d	n.d	n.d	n.d	n.d	n.d	n.d	n.d	0,17	n.d	n.d	n.d	n.d
FeO	11,28	11,00	12,98	12,76	14,13	12,10	10,85	11,49	6,79	7,0	11,60	11,91	10,65	11,82
MnO	0,50	0,58	0,16	0,19	0,18	0,20	0,26	0,31	0,23	0,07	0,46	0,60	0,57	0,68
MgO	13,03	12,85	11,09	11,69	10,72	11,29	11,68	12,03	12,89	13,52	12,13	11,41	12,29	11,79
CaO	22,03	22,13	23,22	23,51	20,42	21,26	22,10	20,94	22,53	21,75	21,83	21,57	22,55	21,28
Na_2O	0,43	0,38	0,40	0,41	0,58	0,46	0,64	0,42	0,73	0,81	0,42	0,51	0,50	0,53
K_2O	-	-	-	-	-	-	-	-	-	-	-	-	-	-
Total	98,47	98,20	100,86	100,69	100,00	99,50	101,06	102,08	100,22	99,41	99,98	98,28	99,64	100,66
Analyst	G.S.	G.S.	A.A.C.	A.A.C.	A.A.C.	A.A.C.	N.I.M.	N.I.M.	G.S.	A.A.C	N.I.M.	N.I.M.	N.I.M.	N.I.M.

Sample localities shown in Fig.9 and in Maps 2 to 4 in the pocket at the back of the thesis.
All iron as FeO.
*Analysis from a clinopyroxene-ilmenite symplectite; n.d. not determined.

TABLE III-13 - CLINOPYROXENE ANALYSES (CONTD.)

											MOZAMBIQUE		
Locality no.	132	136	133					498		140	T37		T78
SiO_2	49,49	49,46	50,87	50,39	51,82	49,76	50,93	50,96	50,71	50,59	48,04	47,92	47,83
TiO_2	0,74	1,09	0,95	0,95	0,90	0,89	0,43	0,65	0,53	0,30	1,64	1,46	1,11
Al_2O_3	4,8	6,83	3,66	4,69	4,69	6,60	5,96	3,98	3,85	2,35	7,79	7,63	7,08
Cr_2O_3	0,09	n.d.	n.d.	n.d.	n.d.	n.d.	n.d.	0,03	0,03	0,04	0,03	0,03	0,11
FeO	7,88	7,14	8,69	10,64	9,36	9,46	8,63	8,06	8,12	13,23	8,33	8,70	7,01
MnO	0,09	0,28	0,29	0,33	0,33	0,27	0,25	0,08	0,08	0,20	0,18	0,17	0,10
MgO	13,65	12,34	12,77	11,57	10,23	11,89	10,79	15,09	14,26	11,03	11,77	12,12	12,72
CaO	21,47	22,23	21,78	19,85	21,38	17,87	21,03	18,80	20,53	21,27	20,93	20,49	21,19
Na_2O	0,83	0,91	0,65	0,80	0,79	1,14	0,97	0,65	0,55	0,35	1,30	1,06	0,79
K_2O	-	-	-	-	-	-	-	-	-	-	-	-	-
Total	99,04	100,28	99,66	99,22	99,50	98,08	98,11	98,3	98,66	99,36	100,01	99,58	97,97
Analyst	A.A.C.	G.S.	G.S.	G.S.	G.S.	G.S.	G.S.	A.A.C.	A.A.C.	A.A.C.	A.A.C.	A.A.C.	A.A.C.

Sample localities for nos. 132, 133, 136, 140 and 498 shown in Fig.9 and Map 1 in the pocket at the back of the thesis.
For samples nos. T37 and T78: see Appendix I-3 and Coelho (1969).
All iron as FeO; n.d. not determined.

TABLE III-14 GARNET ANALYSES

Locality no.	456	104			436			468		353		506	121	19
SiO_2	39,81	38,76	38,83	38,39	38,23	36,82	37,05	38,32	37,69	38,02	38,31	37,92	37,84	38,29
TiO_2	0,09	0,02	0,02	0,03	0,26	0,20	0,26	0,17	0,19	0,02	0,01	0,03	0,05	0,04
$Al2O_3$	23,01	22,21	22,31	21,33	20,60	20,67	21,68	19,51	21,08	20,17	20,86	20,30	19,79	20,16
Cr_2O_3	0,03	n.d.	n.d.	n.d.	n.d.	n.d.	n.d.	n.d.	n.d.	n.d.	n.d.	n.d.	n.d.	n.d.
FeO	20,8	29,84	29,11	29,70	27,54	27,81	27,94	23,86	24,05	25,93	26,43	26,83	25,29	25,24
MnO	0,4	1,16	1,18	1,29	1,64	1,62	1,65	0,82	0,70	1,19	1,29	1,03	0,99	1,27
MgO	10,82	8,02	7,67	7.56	5,12	4,97	4,57	4,19	4,56	3,49	3,38	5,25	4,40	5,60
CaO	6,34	2,18	2,29	2,08	5,92	6,42	6,58	11,83	11,23	9,01	8,66	8,19	10,00	7,54
Na_2O	0,01	-	-	-	0,16	0,1	0,10	0,11	0,11	0,04	0,03	-	-	0,09
K_2O	-	-	-	-	-	-	-	-	-	-	-	-	-	-
Total	101,32	102,19	101,14	100,38	99,47	98,62	99,83	98,81	99,61	97,99	98,99	99,28	98,36	98,53
Analyst	A.A.C.	N.I.M.	N.I.M.	N.I.M.	G.S.	G.S.	G.S.	G.S.	G.S.	A.A.C.	A.A.C.	N.I.M.	N.I.M.	N.I.M.

Sample localities shown in Fig.9 and in Maps 2 to 4 in the pocket at the back of the thesis.
All iron as FeO; n.d. not determined.

TABLE III-14 - GARNET ANALYSES (CONTD.)

Locality no.	132		498		135b	140	141
SiO_2	39,24	38,68	38,72	38,60	38,72	38,11	38,87
TiO_2	0,1	0,11	0,12	0,10	0,06	0,07	0,05
Al_2O_3	22,79	22,47	22,56	22,63	22,38	22,0	21,39
Cr_2O_3	0,33	0,22	0,04	0,04	0,19	0,05	0,01
FeO	20,38	22,03	22,27	22,20	26,08	27,67	24,17
MnO	0,48	0,59	0,32	0,30	0,53	0,62	0,42
MgO	9,32	7,92	8,15	8,24	8,63	5,23	6,42
CaO	8,89	8,96	8,89	8,73	4,85	7,47	9,18
Na_2O	0,01	0,04	0,02	0,03	0,03	0,01	-
K_2O	-	-	-	-	-	-	-
Total	101,54	101,02	101,08	100,86	101,47	101,23	100,51

Sample locality shown in Fig.9 and in Map 1 in the pocket at the back of the thesis.

All iron as FeO. All analyses by A.A.C.

TABLE III-15 - HORNBLENDE ANALYSES

Locality no.	5			46				48					55b			
SiO_2	40,84	42,28	41,76	41,55	42,21	41,99	42,03	41,55	41,66	41,62	41,58	42,01	40,47	40,58	40,37	41,24
TiO_2	2,60	2,54	2,75	2,11	2,24	2,10	2,31	3,19	3,24	3,23	3,29	3,35	2,26	2,26	2,29	2,15
Al_2O_3	10,73	11,23	11,40	10,80	10,93	10,76	10,59	11,65	11,57	11,90	11,82	11,48	12,40	12,23	12,19	11,87
FeO	17,44	17,78	17,59	14,92	15,04	14,74	14,62	15,85	16,10	16,32	16,21	16,38	17,41	17,72	17,27	16,97
MnO	0,19	0,20	0,59	0,31	0,34	0,30	0,30	0,25	0,26	0,22	0,25	0,26	0,28	0,36	0,31	0,30
MgO	10,62	10,04	10,12	11,81	12,04	12,38	12,48	9,68	9,85	10,00	10,22	10,41	9,14	9,36	9,30	9,71
CaO	11,45	11,09	11,41	11,28	11,22	11,19	11,35	11,50	11,15	11,46	11,31	10,92	11,72	11,94	11,35	11,15
Na_2O	1,76	1,82	1,72	1,76	1,76	1,75	1,64	1,84	1,70	1,58	1,71	1,91	1,43	1,07	1,53	1,40
K_2O	1,38	1,43	1,51	1,74	1,61	1,56	1,63	1,87	1,79	1,78	1,81	1,91	2,27	1,43	2,31	2,29
Total	97,01	98,41	98,85	96,28	97,39	96,77	96,95	97,38	97,32	98,11	98,20	98,63	97,58	96,95	96,92	97,08

Sample localities shown in Fig.9 and in Map 2 in the pocket at the back of the thesis.

All iron as FeO, all analyses by N.I.M.

TABLE III-15 - HORNBLENDE ANALYSES (CONTD.)

Locality no.	436		468			353	132				498		54			
SiO_2	40,47	40,17	44,44	49,68	44,15	41,31	42,23	39,02	40,1	40,2	45,42	45,42	42,04	41,14	41,46	41,96
TiO_2	2,90	3,09	1,32	0,85	1,3	2,07	2,06	2,27	2,11	1,94	1,67	2,06	2,15	2,09	1,90	1,75
Al_2O_3	12,60	13,31	11,68	8,52	11,65	11,69	14,17	13,58	17,00	16,95	11,09	10,60	12,70	12,01	11,91	11,29
Cr_2O_3	n.d.	n.d.	n.d.	n.d.	n.d.	n.d.	n.d.	n.d.	0,06	0,07	0,04	0,03	n.d.	n.d.	n.d.	n.d.
FeO	16,11	16,18	14,49	15,38	14,41	21,21	13,15	13,62	10,57	10,41	10,91	9,65	14,23	14,35	14,33	14,87
MnO	0,31	0,46	0,26	0,27	0,25	0,09	0,27	0,34	0,03	0,04	0,07	0,06	0,29	0,28	0,29	0,35
MgO	8,95	8,88	10,51	8,70	11,72	8,01	12,41	13,30	12,75	12,67	14,08	14,84	11,35	11,88	11,51	11,38
CaO	10,81	10,53	11,83	13,18	12,26	11,62	10,85	11,54	11,55	11,52	11,34	11,56	11,65	11,21	11,57	11,29
Na_2O	1,16	1,89	1,58	1,66	1,37	0,70	2,15	2,39	2,63	2,63	1,81	1,75	1,87	1,82	1,74	1,85
K_2O	2,67	2,30	0,50	0,20	0,51	1,73	1,05	1,76	0,73	0,65	0,49	0,51	1,91	1,83	1,81	1,89
Total	95,98	96,81	96,61	98,24	97,62	98,43	98,34	97,82	97,53	97,08	96,92	96,48	98,19	96,61	96,52	96,63
Analyst	G.S.	G.S.	G.S.	G.S.	G.S.	A.A.C	G.S.	G.S.	A.A.C.	A.A.C.	A.A.C.	A.A.C.	N.I.M.	N.I.M.	N.I.M.	N.I.M.

Sample localities shown in Fig.9 and in Maps 1 to 3 in the pocket at the back of the thesis.
All iron as FeO; n.d. not determined.

TABLE III-16 - BIOTITE ANALYSES

Locality no.	48			54			104		
SiO_2	36,35	36,59	36,21	36,69	36,66	37,60	35,96	36,31	36,26
TiO_2	5,48	5,47	5,85	4,72	4,52	4,38	5,40	5,44	5,15
Al_2O_3	13,84	13,55	13,19	13,56	13,64	13,95	15,12	15,10	14,49
FeO	16,38	16,67	17,36	15,07	15,07	14,27	16,35	16,34	17,71
MnO	0,10	0,11	0,11	0,16	0,15	0,14	0,07	0,05	0,05
MgO	13,13	13,04	12,16	13,78	14,07	15,12	12,61	12,32	11,61
CaO	0,0	0,0	0,01	0,0	0,0	0,0	0,0	0,0	0,0
Na_2O	0,12	0,14	0,15	0,25	0,18	0,16	0,06	0,09	0,08
K_2O	10,69	10,78	10,30	10,41	10,89	10,62	10,56	10,38	10,40
Total	96,09	96,35	95,34	94,64	95,18	96,24	96,13	96,03	95,75

Sample localities shown in Fig.9 and in Maps 2 and 3 in pocket at the back of the thesis.

All iron as FeO, all analyses by N.I.M.

TABLE III-17 - PLAGIOCLASE ANALYSES

Locality no.	55a			5			55b		
SiO_2	57,52	55,95	56,58	57,53	58,18	57,73	55,97	55,78	55,31
Al_2O_3	26,30	26,16	27,04	25,08	25,52	26,09	26,23	27,31	25,99
CaO	8,82	9,45	8,76	7,99	7,70	8,78	8,92	10,09	9,53
Na_2O	6,18	5,58	5,97	6,61	7,00	6,75	5,45	5,81	5,91
K_2O	0,41	0,37	0,33	0,49	0,42	0,43	0,19	0,24	0,26
Total	99,23	97,51	98,68	97,90	98,82	99,78	96,76	99,23	97,00

Sample locality shown in Fig.9 and in Map 2 in the pocket at the back of the thesis.

All analyses by N.I.M.

TABLE III-18 - PREHNITE, ILMENITE AND MAGNETITE ANALYSES

	PREHNITE		ILMENITE				MAGNETITE
Locality no.	141		55a	46	104	353	46
SiO_2	43,41	43,53	n.d.	n.d.	n.d.	n.d.	n.d.
TiO_2	-	-	48,85	49,09	51,22	48,96	0,12
Al_2O_3	23,61	23,68	0,28	-	-	0,03	0,40
Cr_2O_3	-	-	0,02	-	-	0,08	0,23
FeO	0,09	0,15	51,41	51,32	45,31	47,57	93,52
MnO	0,02	-	1,11	0,80	0,29	0,52	-
MgO	-	-	0,20	1,18	1,68	0,06	0,20
CaO	26,77	26,79	n.d.	n.d.	n.d.	n.d.	n.d.
Na_2O	-	0,02	n.d.	n.d.	n.d.	n.d.	n.d.
K_2O	0,02	0,02	n.d.	n.d.	n.d.	n.d.	n.d.
Total	93,93	94,19	101,87	102,39	98,61	97,22	94,47
Analyst	A.A.C.	A.A.C.	N.I.M.	N.I.M.	N.I.M.	A.A.C.	N.I.M.

Sample localities shown in Fig.9 and in Maps 1 to 3 in the pocket at the back of the thesis.

All iron as FeO. n.d. not determined.

APPENDIX IV

X-RAY FLUORESCENCE ROCK ANALYSES

(i) Analytical techniques for petrochemistry and geochemistry

All whole-rock analyses reported in this thesis were conducted by X-ray fluorescence spectrometry (with the exception of FeO). Information on preparatory and analytical techniques is presented herewith:

1. Sample preparation

The samples used for analytical work were sufficiently large to encompass compositional inhomogeneities. The weight of each of these samples was of the order of 5Kg. Only in a few cases (samples 129, 132, and 50b) the samples were rather small.

Care was taken to avoid weathered material and the samples were reduced to $\leq$ 1cm in size in a rock-splitter and jaw crusher. This material was successively split by coning and quartering. No less than one quarter was then kept for further crushing by a jaw crusher which reduced the fragments to $\leq$ 3mm, followed by final crushing in an agate-lined Siebteknik mill. A representative portion of each sample was thus reduced to $\leq$ 120 mesh. Samples from localities nos. 4 to 55 were supplied to the author, in powder form, by Professor T. N. Clifford; these were crushed in a nickel-chromium vessel in the Department of Geology, Leeds University.

2. Analytical equipment

Analytical work was conducted using a Philips model PW1410 X-ray fluorescence spectrometer, equipped with a 3Kw generator (PW1140). In this thesis, 32mm diameter samples were used against the normal sample diameter of 45mm, because the additional intensity obtained using the larger samples (about 20%) did not justify the larger amount of powder (especially standards) and flux required.

Raw data from the X-ray fluorescence spectrometer were either punched onto cards or captured directly on paper tape for subsequent processing on the IBM 370 computer at the University of the Witwatersrand Computer Centre. All computer programs used for data reduction were written by Dr. T.S. McCarthy (Geology Department, University of the Witwatersrand).

3. Major and minor elements

The elements Fe, Mn, Ti, Ca, K, P, Si, Al and Mg were determined using the fusion method of Norrish and Hutton (1969), with slight modifications. Samples were preheated at 110°C and 1 000°C in vitreosil crucibles to a constant mass and the variations in weight were measured. Na was determined on undiluted sample powder, pelletized in the manner referred to by Norrish and Hutton (1969).

The instrumental conditions used for these analyses are

listed in Table IV-1. A Cr target tube was used for all elements. Spectral interferences on Mn and Fe were eliminated by a primary radiation filter.

Following the procedure of Norrish and Hutton (1969), SiO_2 and Fe_2O_3 - CaO blanks have been used to estimate backgrounds.

The spectrometer was calibrated using the international standards W-1, BR, BCR-1, G-2, GR, SY-1, GSP-1, DTS-1, PCC-1 and mixtures of G-2 and PCC-1, G-2 and DTS-1, following the concentrations recommended by Flanagan (1973). A reference disc was counted from time to time to check instrumental drift. This drift was always below 5%. All counting was done under vacuum.

FeO was determined by dichromate titration, after dissolution of the sample in a nitrogen atmosphere. Details of the method are described by Schaffer (1966).

The content of CO_2 was determined by wet method according to the method by Shapiro and Brannock (1962).

4. Trace elements: Rb, Sr, Y, Zr, Nb, Cl, S

These trace elements were analysed on undiluted powder pellets and the instrumental conditions employed, with the exception of Cl and S, are listed in Table IV-2. Background positions were measured on both sides of the peaks, taking care to avoid tailing effects. Blanks were used to determine the relationship between background intensities and the background in the peak positions.

TABLE IV-1 - EXPERIMENTAL CONDITIONS FOR THE DETERMINATION OF MAJOR AND MINOR ELEMENTS ON THE PHILIPS PW1410 SPECTROMETER

Element	Fe	Mn	Ti	Ca	K	P	Si	Al	Mg	Na	Bgnd*	Bgnd*
Spectral line	K	K	K	K	K	K	K	K	K	K	-	-
Crystal	LiF	LiF	LiF	LiF	PET	PET	PET	PET	ADP	RAP	RAP	RAP
Angle	85,73	95,20	86,14	113,09	50,69	89,66	109,21	145,12	136,72	54,79	54,70	58,00
Collimator	C	F	F	F	F	C	C	C	C	C	C	C
Detector	Flow proportional counter											
Counting time (seconds)	40	100	20	20	20	40	20	100	200	200	100	100
Tube target	Chromium											
KV	50											
MA	50											
Filter	IN	IN	OUT	OUT	OUT	OUT	OUT	OUT	OUT	OUT	OUT	OUT
Inter-ferences	-	-	-	-	-	Ca K_β	-	-	-	-	-	-

*Background

TABLE IV-2 - INSTRUMENTAL CONDITIONS FOR THE DETERMINATION OF Rb, Sr, Y, Zr, and Nb

Element	Bgnd*	Bgnd*	Nb	Bgnd*	Zr	Bgnd*	Y	Bgnd*	Sr	Bgnd*	Rb	Bgnd*
Spectral line	-	-	K_α	-	K_α	-	K_α	-	K_α	-	K_α	-
Crystal						LIF (220)						
Angle	28,00	29,50	30,44	30,90	32,10	33,15	33,90	34,80	35,85	36,80	37,99	38,80
Collimator						150 µm						
Detector						Scintillator counter						
Counting time (seconds)	40	40	80	40	80	40	80	40	80	60	80	40
Tube target						Tungsten						
Kv						65						
MA						40						
Filter						OUT						
Inter-ference	-	-	YK_β	-	SrK_β	-	RbK_β	-	-	-	-	-

*Background

Absorption corrections were applied to samples and standards, according to the method of Reynolds (1963, 1967).

Calibration was carried out with international standards W-1, BCR-1 and AGV-1 (Flanagan, 1973).

Cl, S Uncalibrated semi-quantitative analyses of chlorine and sulphur were carried out on a few selected samples, following instrumental conditions listed in Table IV-3.

TABLE IV-3 - INSTRUMENTAL CONDITIONS FOR THE SEMI-QUANTITATIVE DETERMINATION OF Cl, S

Element	Bgnd*	Cl	Bgnd*	Bgnd*	S	Bgnd*
Crystal			PET(3)			
Angle	58,50	65,58	68,00	73,00	75,92	81,00
Collimator			fine			
Counting Time (seconds)	40	100	40	40	100	40
Tube target			Cr			
Kv			50			
MA			50			
Filter			out			

*Background

(ii) Quality of the analytical data

1. Major and minor elements

Five international standards, obtained by the National Institute for Metallurgy (N.I.M.), Johannesburg, were analysed by Dr. T. S. McCarthy (1977) for major and minor elements (Fe, Mn, Ti, Ca, K, P, Si, Al, Mg and Ba) to assess analytical accuracy over a wide range of abundance of the elements. The results obtained by the above investigator are listed in Table IV-4, together with mean composition of these standards reported by Russel et al. (1972). The general close correspondence between the two sets of data attests to the accuracy of the methods used in this work.

Analytical precision was determined by McCarthy (1977) by replicate analysis of samples of granite, basalt and a feldspathic pyroxenite from the Bushveld Igneous Complex. Average compositions and standard deviations obtained on these three samples are listed in Table IV-5 for major constituents. The precision is generally good, although for minor elements, the precision is less satisfactory as is evident for example from the large standard deviation of MgO in the granite Wits-G (40 per cent) and P_2O_5. Also the gravimetric loss on ignition is particularly imprecise at low levels, reflecting the difficulty in evaluating small changes in mass.

TABLE IV-4 - ANALYTICAL RESULTS OBTAINED ON N.I.M. INTERNATIONAL STANDARDS

STANDARD	N.I.M.-G		N.I.M.-S		N.I.M.-N		N.I.M.-P		N.I.M.-D	
SOURCE	WITS	N.I.M.	WITS	N.I.M.	WITS	N.I.M.	WITS	N.I.M.	WITS	N.I.M.
SiO_2	75,69	75,59	64,02	63,72	51,98	52,43	38,25	38,86	51,52	50,88
TiO_2	0,107	0,09	0,062	0,05	0,186	0,17	0,034	0,04	0,202	0,20
Al_2O_3	12,42	12,08	17,81	17,33	16,71	16,64	0,44	0,44	4,45	4,38
Fe_2O_3(tot)	1,98	2,02	1,44	1,40	8,98	9,00	17,07	16,97	12,91	12,29
MgO	0,08	0,10	0,57	0,48	7,69	7,43	44,42	43,30	26,41	25,19
MnO	0,03	0,02	0,02	0,01	0,19	0,17	0,22	0,20	0,23	0,18
CaO	0,79	0,80	0,69	0,70	11,44	11,55	0,27	0,31	2,69	2,68
Na_2O	3,76	3,32	0,49	0,43	2,82	2,44	0,34	0,10	0,76	0,37
K_2O	4,99	4,98	14,93	15,34	0,26	0,26	0,019	0,04	0,103	0,10
P_2O_5	0,02	0,03	0,12	0,13	0,02	0,04	0,01	0,03	0,02	0,04
FeO	1,25	1,29	0,31	0,29	6,96	7,24	14,11	14,27	8,08	9,20

WITS = McCarthy(1977). N.I.M. = Results of Russel et al. (1972) reported by Flanagan (1973).

TABLE IV-5-ANALYTICAL PRECISION FOR MAJOR AND MINOR ELEMENTS

	WITS-P		WITS-B		WITS-G	
	Concentration	σ	Concentration	σ	Concentration	σ
SiO_2	55,13	0,20	57,71	0,36	75,34	0,34
TiO_2	0,217	0,001	0,916	0,004	0,292	0,004
Al_2O_3	5,83	0,03	8,89	0,074	11,98	0,08
Fe_2O_3 (tot)	11,95	0,12	9,12	0,04	3,47	0,05
MgO	21,80	0,12	10,97	0,07	0,04	0,02
MnO	0,20	0,007	0,13	0,005	0,05	0,01
CaO	4,01	0,03	6,86	0,03	1,51	0,01
Na_2O	1,12	0,04	2,55	0,08	3,09	0,10
K_2O	0,157	0,001	0,079	0,002	4,46	0,03
P_2O_5	0,020	0,002	0,094	0,004	0,04	0,003
FeO	7,40	0,36	7,23	0,27	1,75	0,12
L.O.I	0,06	0,02	0,21	0,23	0,02	0,01

L.O.I. = Loss on ignition.

σ = standard deviation.

2. Trace elements

International standard, released by the U.S. Geological Survey were used to define the accuracy of trace elements data.

The concentrations obtained for some of the trace elements on a few of these standards are listed in Table IV-6 along with values quoted by Flanagan (1973). A generally good agreement has been obtained by McCarthy (1977) relatively to other analysts.

The abovementioned samples of granite, basalt and pyroxenite were used by Dr. T. S. McCarthy to assess analytical precision by replicate trace element analyses on ten pellets of each rock type. Mean concentrations, standard deviations and coefficients of variation determined are listed in Table IV-7. While the precision is less satisfactory toward the detection limits, reproducibility is more than adequate for the needs of this thesis.

TABLE IV-6 - TRACE ELEMENT RESULTS OBTAINED ON INTERNATIONAL STANDARDS

	Sr		Rb		Zr		Y		Nb	
Standard	A	R.V.1.	A	R.V.1.	A	R.V.1.	B	R.V.2	B	R.V.2.
G-2	467	479	164	168	327	300	-	-		
GSP-1	234	233	246	254	570	500	-	-		
BCR-1	-			-		-	33	34	7,6	11,5
W-1	-			-		-	5,2	6,9	18,6	20,5

A: Measured value (McCarthy, 1977).

B: Measured value (this thesis).

R.V.1. Recommended value (Flanagan, 1973).

R.V.2 Recommended value (McCarthy, Personal communication).

TABLE IV-7 - ANALYTICAL PRECISION FOR TRACE ELEMENTS

	Wits-P		Wits-B		Wits-G	
	Concentration	σ	Concentration	σ	Concentration	σ
Rb	12	0,9	<d.l.*		99	1,5
Sr	80	1,8	99	1,5	108	1,4
Zr	26	2,3	77	0,9	354	10,6
Y	6	0,6	14	1,1	80	1,2
Nb	<d.l.*		3	1	24	0,6

*below detection limit.
σ: standard deviation.

(iii) Whole rock analyses and trace element compositions - Presentation of the data

Major, minor elements, expressed as weight per cent of the oxide, and trace elements, expressed in parts per million, analysed in each sample during the course of this thesis are presented in Table IV-8.

In a few cases no trace elements, nor FeO have been determined, all iron being given as Fe_2O_3.

Table IV-9 lists all published analyses of southern Malawi rocks discussed in the text in tables IV-10 to IV-16. Available published geochemical data (Bloomfield, 1965b) are presented in Table IV-17.

Most of the analyses listed in Table IV-8 were carried out by the author; however, the following were made by Mr. A.Bemath: nos. 15, 31, 41, 42, 44, 50b, 53, 56, 58, 59, 60, 61, 62 and 64. In addition, U1 and U2 are unpublished analyses by E.Pinkney of Leeds University.

TABLE IV-8 WHOLE ROCK ANALYSES AND TRACE ELEMENT COMPOSITIONS

Locality no.	48	34	46	29	93	61	99	28	40	38	107	102	101	104	69
SiO_2	43,56	47,94	48,20	43,01	47,37	48,14	50,99	51,13	51,03	51,70	51,92	56,63	54,76	59,17	57,71
TiO_2	2,48	1,72	1,69	4,30	1,92	1,75	1,76	2,08	1,63	1,73	1,57	0,91	1,83	1,54	1,13
Al_2O_3	15,89	13,54	15,02	14,62	15,20	14,51	15,76	15,27	14,47	13,91	15,48	16,87	20,22	15,53	15,11
Fe_2O_3	1,94	3,42	5,70	3,60	2,46	4,53	2,56	1,55	4,07	7,01	4,08	3,92	2,82	1,89	10,73*
FeO	11,68	9,31	7,22	13,22	10,50	9,12	7,13	8,90	8,35	7,88	9,02	4,67	3,05	8,80	
MnO	0,26	0,23	0,21	0,23	0,23	0,22	0,17	0,20	0,21	0,26	0,16	0,18	0,06	0,19	0,21
MgO	7,15	6,97	6,75	5,48	9,33	7,07	5,28	5,11	5,60	4,24	6,52	3,81	2,27	3,94	1,73
CaO	10,15	11,41	9,78	9,70	7,56	9,10	6,24	9,85	8,31	7,50	5,14	6,98	6,47	3,28	7,07
Na_2O	2,13	2,85	3,63	2,76	2,28	3,17	4,25	3,88	3,85	4,66	3,70	4,60	5,52	3,76	4,58
K_2O	1,21	1,14	0,99	0,60	2,05	1,40	1,55	0,85	1,18	0,61	1,01	1,00	1,97	1,02	1,19
P_2O_5	0,19	0,13	0,17	0,91	0,28	0,24	0,44	0,25	0,28	0,20	0,24	0,15	0,47	0,02	0,31
H_2O	0,04	0,02	0,06	0,06	0,10	0,05	0,06	0,06	0,04	0,00	0,05	0,10	0,06	0,06	0,06
H_2O+	0,09	0,30	0,17	0,49	0,09	0,29	0,59	0,18	0,30	0,00	0,46	0,13	0,19	0,05	0,77
CO_2	0,26	n.d.	n.d.	n.d.	n.d.	n.d.	1,65	n.d.	n.d.	n.d.	n.d.	n.d.	n.d.	n.d.	0,5
Total	97,03	98,71	99,59	98,98	99,37	99,59	98,43	99,31	99,32	99,70	99,35	99,85	99,69	99,25	101,1
Rb	22	11	7	11	118	13	13	13	12	8	14	13	28	9	-
Sr	208	144	269	238	125	177	389	344	177	150	476	389	2527	697	-
Y	29	30	29	68	32	37	29	32	43	37	26	29	20	58	-
Zr	109	90	85	273	118	104	78	220	144	52	65	78	159	580	-
Nb	5	0	5	31	15	6	4	14	6	-	4	4	10	12	-

Sample localities shown in Fig. 19 and in Maps 2 and 3 in the pocket at the back of the thesis.
*All iron as Fe_2O_3

TABLE IV-8 - WHOLE ROCK ANALYSES AND TRACE ELEMENTS COMPOSITIONS (CONTD.)

Locality no.	93	98	116a	118a	43	45	49	63	4	44	37	51	39	52	370	3	50b
SiO_2	61,96	59,83	64,05	58,12	60,91	63,96	61,52	68,91	68,93	68,40	70,38	71,94	73,15	75,73	75,87	77,97	74,35
TiO_2	0,97	1,57	1,32	0,96	1,19	0,73	0,83	0,45	0,54	0,85	0,49	0,31	0,25	0,24	0,30	0,24	0,43
Al_2O_3	15,59	15,03	14,38	17,86	16,90	16,64	16,82	16,05	14,74	15,13	13,49	12,96	13,86	12,04	11,84	11,28	11,88
Fe_2O_3	1,31	3,25	2,34	1,17	2,59	1,72	0,19	1,00	1,40	0,94	1,79	2,16	2,14	0,79	4,04*	1,19	0,93
FeO	5,95	5,18	4,70	5,46	4,86	2,88	5,27	1,87	3,78	4,02	2,95	3,19	0,87	2,77		2,02	2,61
MnO	0,11	0,10	0,11	0,12	0,13	0,10	0,10	0,06	0,11	0,09	0,09	0,10	0,07	0,07	0,09	0,06	0,07
MgO	3,75	2,23	2,68	3,86	2,15	2,63	3,33	0,96	1,18	1,54	1,08	1,29	0,0	0,58	1,04	0,42	1,74
CaO	3,82	4,44	4,27	5,72	4,18	5,20	5,39	4,09	4,32	3,63	3,68	2,19	1,91	2,21	1,49	3,46	3,46
Na_2O	3,79	4,71	3,86	4,48	4,51	4,67	4,12	4,85	3,90	3,72	4,72	4,67	4,71	4,04	5,05	3,06	3,43
K_2O	1,91	2,17	1,20	1,53	1,11	1,00	1,68	1,11	0,51	1,20	0,48	1,24	2,89	1,13	0,56	0,37	0,54
P_2O_5	0,18	0,41	0,20	0,28	0,12	0,21	0,17	0,10	0,18	0,11	0,09	0,07	0,06	0,06	0,03	0,02	0,10
H_2O-	0,11	0,06	0,13	0,04	0,13	0,08	0,06	0,05	0,03	0,09	0,04	0,04	0,04	0,01	0,09	0,02	0,05
H_2O+	0,23	0,61	0,36	0,0	1,00	0,49	0,0	0,35	0,32	0,54	0,18	0,13	0,52	0,38	0,06	0,25	0,24
Total	99,68	99,59	99,60	99,60	99,78	100,31	99,48	99,85	99,94	100,26	99,46	100,29	100,47	100,05	100,46	100,36	99,83
Rb	64	17	23	27	6	6	31	11	5	22	4	14	32	28	-	3	9
Sr	335	257	350	605	326	570	504	382	314	257	130	172	215	127	-	142	513
Y	26	40	20	15	23	9	8	7	34	21	35	22	15	25	-	12	15
Zr	189	157	172	148	116	99	68	109	100	190	121	118	140	95	-	101	214
Nb	9	7	9	8	4	1	3	3	2	5	2	1	2	4	-	-	3

Sample localities shown in Fig.19 and on Maps 2 and 3 in the pocket at the back of the thesis.
*All iron as Fe_2O_3.

TABLE IV-8 – WHOLE ROCK ANALYSES AND TRACE ELEMENT COMPOSITIONS (CONTD.)

Locality no.	56	36	55	1	57	60	113	116b	405	441a	76	81	82
SiO_2	78,56	67,57	69,71	71,37	76,18	74,12	72,36	74,67	54,05	56,82	59,40	58,89	57,94
TiO_2	0,16	0,92	0,40	0,44	0,27	0,20	0,42	0,06	2,36	1,35	1,42	1,56	1,65
Al_2O_3	12,22	14,81	15,60	14,79	12,07	13,08	13,56	14,21	15,13	16,67	17,08	16,47	16,47
Fe_2O_3	0,79	0,98	0,44	0,98	1,63	1,84	1,31	0,25	1,84	8,02*	3,01	3,38	3,21
FeO	0,34	4,38	1,55	1,59	0,81	0,53	1,22	0,48	9,81		2,90	3,03	3,43
MnO	0,03	0,09	0,04	0,06	0,04	0,06	0,0	0,02	0,16	0,00	0,11	0,11	0,12
MgO	0,0	1,39	0,38	0,68	0,17	0,10	0,54	0,12	2,49	3,18	1,29	2,30	2,31
CaO	1,50	2,72	2,77	2,73	1,12	1,77	1,96	2,24	6,80	4,86	4,32	4,34	4,40
Na_2O	4,57	3,01	3,54	3,67	3,98	3,94	3,29	2,87	3,35	4,44	4,40	4,35	4,70
K_2O	2,22	4,20	4,25	3,48	4,13	4,03	4,57	4,77	2,48	3,72	4,41	4,59	4,85
P_2O_5	0,03	0,25	0,11	0,09	0,02	0,05	0,12	0,01	1,26	0,93	0,66	0,71	0,75
H_2O-	0,05	0,02	0,03	0,02	0,03	0,02	0,06	0,07	0,11	0,16	0,05	0,05	0,04
H_2O+	0,19	0,0	0,55	0,34	0,05	0,49	0,51	0,23	0,00	0,29	0,34	0,36	0,30
Total	100,66	100,34	99,37	100,24	100,50	100,23	99,92	100,00	99,84	100,44	99,39	100,14	100,17
Rb	26	107	79	73	86	63	89	122	–	–	102	–	102
Sr	54	205	251	240	57	304	475	405	–	–	1430	–	1215
Y	32	32	13	19	54	15	8	3	–	–	29	–	30
Zr	346	407	180	202	335	133	184	51	–	–	360	–	438
Nb	16	14	5	6	16	2	2	–	–	–	21	–	24

Sample localities shown in Fig.19 and in Maps 2 and 3 in the pocket at the back of the thesis.
*All iron as Fe_2O_3.

TABLE IV-8 - WHOLE ROCK ANALYSES AND TRACE ELEMENT COMPOSITIONS (CONTD.)

Locality no.	83	84	30	31	441b	74	75	432	65	73	375	67	115
SiO_2	57,74	58,69	57,88	61,38	59,69	61,80	61,32	62,14	66,82	65,77	67,85	69,92	71,78
TiO_2	1,63	1,60	1,76	1,37	0,50	0,63	0,63	1,0	0,85	0,76	0,31	0,37	0,09
Al_2O_3	17,19	16,30	16,42	15,99	18,37	17,68	17,25	18,29	14,69	14,37	18,71	13,80	14,48
Fe_2O_3	3,07	3,46	3,29	2,85	4,43*	1,69	5,09	4,1*	0,95	0,98	2,83*	1,73	2,53*
FeO	3,25	3,02	3,51	2,84		3,96	2,60		4,48	5,60		1,71	
MnO	0,11	0,10	0,10	0,10	0,00	0,15	0,23	0,00	0,10	0,17	0,06	0,07	0,00
MgO	2,37	2,19	2,32	1,98	2,55	0,23	0,03	1,10	0,91	0,96	0,30	0,06	0,00
CaO	4,35	4,23	4,60	4,00	3,99	3,52	3,47	2,73	2,75	2,76	2,17	1,47	1,08
Na_2O	4,55	4,40	4,21	4,08	4,83	4,74	3,49	3,64	3,78	3,58	6,72	3,04	2,53
K_2O	4,64	4,88	4,57	4,59	4,68	5,00	5,46	6,91	4,30	4,42	1,52	5,66	7,86
P_2O_5	0,75	0,73	0,81	0,66	0,73	0,17	0,14	0,32	0,06	0,19	0,07	0,08	0,05
H_2O-	0,0	0,09	0,00	0,11	0,24	0,04	0,03	0,11	0,17	0,05	0,07	0,08	0,13
H_2O+	0,44	0,32	0,44	0,46	0,36	0,0	0,14	0,45		0,00	0,26	0,31	0,26
Total	100,09	100,01	99,91	100,41	100,36	99,61	99,88	100,79	99,86	99,61	100,96	98,30	100,79
Rb	104	106	52	59	-	82	113	-	132	108	-	140	-
Sr	1266	1152	1016	877	-	236	259	-	177	226	-	96	-
Y	31	37	35	30	-	45	57	-	36	39	-	64	-
Zr	471	458	419	369	-	999	1309	-	390	516	-	514	-
Nb	25	27	27	21	-	38	44	-	19	24	-	44	-

Sample localities shown in Fig.19 and in Maps 1 and 3 in the pocket at the back of the thesis.
*All iron as Fe_2O_3.

TABLE IV-8 - WHOLE ROCK ANALYSES AND TRACE ELEMENTS COMPOSITIONS (CONTD.)

Locality no.	433	132	129	133	106	135	71	70	50a	105	108	58	118b	120	U1	U2
SiO_2	73,10	46,17	46,69	53,51	52,17	57,87	54,70	57,33	59,49	66,68	72,63	58,51	62,00	62,69	68,28	77,58
TiO_2	0,15	1,41	3,41	1,35	0,15	0,11	1,02	0,83	1,16	0,67	0,69	1,18	0,7	0,85	0,42	0,17
Al_2O_3	14,51	14,23	14,10	17,89	28,43	26,87	17,27	14,97	12,79	16,19	12,78	17,38	17,48	17,67	15,14	12,16
Fe_2O_3	0,94*	1,51	1,56	9,11*	0,34	0,16*	2,12	1,10	1,40	1,06	1,20	2,08	0,72	0,77	1,90	1,64
FeO		11,22	14,00		0,98		4,55	5,75	6,41	2,80	3,35	2,80	4,07	3,64	3,15	1,56
MnO	0,00	0,11	0,17	0,05	0,02	0,00	0,11	0,14	0,15	0,06	0,07	0,08	0,08	0,08	0,09	0,04
MgO	0,00	9,49	6,14	3,88	1,14	0,00	4,47	4,85	6,77	1,41	1,78	2,51	2,79	2,51	1,39	0,48
CaO	1,37	13,14	10,26	8,54	12,18	9,09	8,06	6,42	5,60	2,60	2,24	3,69	5,11	4,91	4,13	3,29
Na_2O	3,83	2,17	1,23	4,53	4,00	5,18	4,91	2,38	2,21	3,60	2,75	3,72	4,32	4,37	4,17	2,90
K_2O	5,85	0,42	0,48	1,26	0,56	1,03	1,84	4,92	1,78	4,19	2,28	7,57	2,09	2,33	0,50	0,35
P_2O_5	0,04	0,09	0,68	0,32	0,01	0,09	0,30	0,20	1,01	0,27	0,14	0,53	0,25	0,26	0,16	0,01
H_2O-	0,16	0,06	0,07	0,10	nil	0,11	0,05	0,04	0,07	0,07	0,03	0,05	0,06	0,03	0,03	0,03
H_2O+	0,45	0,1	0,50	0,08	0,4	0,24	0,19	0,96	0,67	0,42	0,04	0,18	0,41	0,03	0,29	0,12
Total	100,40	100,21	100,39	100,62	100,38	100,75	99,59	99,89	99,51	100,02	99,98	100,28	99,88	100,14	99,65	100,00
Rb	-	-	-	-	6	-	51	171	65	86	60	286	41	45	-	-
Sr	-	-	-	-	449	-	855	118	897	315	302	827	602	662	-	-
Y	-	-	-	-	3	-	19	30	46	43	14	22	12	11	-	-
Zr	-	-	-	-	33	-	171	189	293	321	212	360	104	171	-	-
Nb	-	-	-	-	-	-	10	15	16	5	6	22	6	6	-	-

Sample localities shown in Fig. 19 and in Maps 1 to 3 in the pocket at the back of the thesis.
*All iron as Fe_2O_3.

TABLE IV-9 - REFERENCES OF PUBLISHED ANALYSES DISCUSSED IN THE TEXT

Locality no.	Original no.	Reference/Table where mentioned	Locality no.	Original no.	Reference/Table where mentioned
P1	E245	Listed in Table IV-10.	P33	KB1149	Listed in Table IV-12.
P2	-	Thatcher (1968, p.40).	P34	W244	ditto.
P3	-	Thatcher (ibid.).	P35	KB1097	ditto.
P4	E194	Listed in Table IV-10.	P36	KB845	ditto.
P5	KB1500	ditto.	P37	KB1784	ditto.
P6	-	ditto.	P38	KB849	ditto.
P7	-	ditto.	P39	KB1099	Listed in Table IV-13.
P8	-	ditto.	P40	KB832	ditto.
P9	KB1797	ditto.	P41	KB1843	ditto.
P10	KB1538	ditto.	P42	KB1179	ditto.
P11	KB1541c	ditto.	P43	KB1791	ditto.
P12	-	ditto.	P44	KB1780	ditto.
P13	-	ditto.	P45	KB1786	ditto.
P14	H2225	ditto.	P46	W379	Listed in Table IV-14.
P15	T556	ditto.	P47	KB2130	ditto.
P16	KB1516	ditto.	P48	H4213	ditto.
P17	C779	ditto.	P49	H2288	ditto.
P18	H2279	ditto.	P50	KB1983	ditto.
P19	KB1377	ditto.	P51	KB1877	ditto.
P20	H4206	ditto.	P52	E279A	ditto.
P21	H4263	ditto.	P53	W109	Listed in Table IV-15.
P22	G1453	ditto.	P54	KB1979	ditto.
P23	KB640	ditto.	P55	-	ditto.
P24	KB966	Listed in Table IV-11.	P56	-	ditto.
P25	KB725	ditto.	P57	-	Listed in Table 16.
P26	KB746	ditto.	P58	-	ditto.
P27	KB726	ditto.	P59	-	ditto.
P28	KB690	ditto.	P60	-	ditto.
P29	KB666	ditto.	P61	-	ditto.
P30	KB118	ditto.	P62	-	ditto.
P31	KB688	ditto.	P63	-	Listed in Table IV-10.
P32	KB1520	ditto.			

Sample approximate localities shown in Fig.20.

TABLE IV-10 - PUBLISHED ANALYSES OF AMPHIBOLITE FACIES GNEISSES AND GRANULITES, AFTER BLOOMFIELD (1968, p.121)

	(a)	(b)	(c)	(d)	(d)	(f)	(g)	(h)	(i)	(j)	(k)	(l)	(m)	(n)	(o)	(p)	(q)	(r)	(s)	(t)	(u)	(v)
SiO_2	62,99	63,88	54,44	55,39	58,29	53,67	61,62	61,27	66,55	61,80	57,72	50,30	66,00	77,53	67,40	58,28	62,43	67,06	68,98	68,78	72,08	64,06
TiO_2	0,82	0,58	1,38	0,65	0,89	0,98	1,03	1,03	0,74	0,88	0,41	1,41	0,87	0,06	0,51	0,13	0,72	0,42	0,62	0,80	0,31	0,99
Al_2O_3	16,37	17,68	14,97	17,79	16,84	16,24	15,93	15,81	14,91	16,63	20,47	17,33	16,63	12,58	17,12	21,67	15,92	13,88	16,76	18,56	14,50	12,39
Fe_2O_3	2,01	1,49	4,43	3,40	1,73	1,13	1,82	2,15	1,27	1,34	1,54	3,97	1,58	1,45	1,93	1,12	3,04	2,70	2,39	6,53	1,85	2,07
FeO	4,79	3,06	5,35	8,41	5,86	7,73	4,77	4,71	4,88	4,34	3,58	5,61	2,70	0,94	1,94	5,58	5,58	4,46	5,47	1,78	0,49	5,70
MnO	0,09	0,08	0,19	0,22	0,14	0,16	0,11	0,11	0,11	0,09	0,16	0,23	0,07	nil	nil	0,26	0,10	0,08	0,11	0,03	0,02	0,19
MgO	3,37	2,13	4,82	5,15	3,04	6,20	2,39	2,41	1,45	2,19	2,45	4,52	1,28	0,48	1,19	0,01	3,05	2,02	1,46	0,25	0,26	2,88
CaO	4,55	5,00	7,93	4,18	6,38	9,26	4,58	4,81	2,60	4,03	7,19	8,40	4,56	0,73	2,08	1,44	0,44	1,45	0,22	nil	1,48	7,89
Na_2O	2,37	4,58	4,63	4,40	4,05	3,36	3,42	3,27	2,71	3,72	5,20	3,95	5,15	4,37	4,49	7,06	2,29	2,33	0,73	0,36	4,02	2,38
K_2O	2,44	1,32	1,34	0,10	2,40	1,01	4,02	4,05	4,55	4,63	1,09	3,07	0,95	1,82	3,15	4,27	6,30	5,28	3,21	2,81	4,98	1,25
P_2O_6	0,19	0,20	0,52	0,31	0,38	0,26	0,29	0,35	0,22	0,35	0,19	1,21	0,21	0,03	0,13	0,09	0,13	0,32	0,05	0,10	0,10	0,20
Totals*	100	100	100	100	100	100	100	100	100	100	100	100	100	100	100	100	100	100	100	100	100	100

*Analyses recalculated water-CO_2-free to 100 per cent; n.d. = not determined.

(g) includes 0,02 per cent ZrO_2; (h) includes 0,03 per cent ZrO_2; and (p) includes 0,08 per cent ZrO_2.

(a) Garnetiferous biotite gneiss: (P16).
(b) Hornblende-biotite-plagioclase gneiss: (P17).
(c) Biotite-hornblende gneiss: (P11).
(d) Garnet-hornblende-anthophyllite gneiss: (P12).
(e) Biotite-hornblende-clinopyroxene-plagioclase gneiss with garnet: (P7).
(f) Granulitic hornblende-clinopyroxene-plagioclase gneiss with garnet - a basic inclusion in (e): (P6).
(g) Biotite-hornblende-clinopyroxene-plagioclase gneiss with potash feldspar and garnet: (P8).
(h) Biotite-hornblende-plagioclase gneiss with potash feldspar - from the foliated border of (g): (P63).
(i) Hypersthene-biotite-garnet gneiss with potash feldspar: (P10).
(j) Biotite-hypersthene granulite: (P5).
(k) Intermediate charnockitic granulite: (acid type): (P4).
(l) Intermediate charnockitic granulite: (P1).
(m) Leucocratic hypersthene (charnockitic) granulite: (P9).
(n) Quartzo-feldspathic biotite-muscovite schist: (P23).
(o) Quartzo-feldspathic muscovite-biotite gneiss (P19).
(p) Biotite-muscovite-plagioclase gneiss: (P13).
(q) Biotite-garnet-quartz gneiss: (P14).
(r) Biotite-garnet-quartz gneiss: (P18).
(s) Biotite-garnet-quartz-sillimanite gneiss: (P20).
(t) Biotite-garnet-quartz-sillimanite gneiss: (P21).
(u) Quartzo-feldspathic granulite: (P22).
(v) Hornblende-epidote quartzite: (P15).

Approximate sampling localities shown in Fig.20.
Original sample numbers listed in Table IV-9.

TABLE IV-11 - PUBLISHED ANALYSES OF AMPHIBOLITE, METAGABBRO AND RELATED ROCKS AFTER BLOOMFIELD (1968, pp.137-142).

	(a)	(b)	(c)	(d)	(e)	(f)	(g)	(h)	(i)
SiO_2	37,36	39,75	44,18	45,49	48,63	48,66	50,02	50,12	50,44
TiO_2	0,60	0,76	1,25	0,98	3,43	0,82	1,44	1,08	0,79
Al_2O_3	29,07	20,70	10,57	0,21	13,42	11,09	13,98	16,41	6,59
Fe_2O_3	4,89	6,87	7,30	3,77	4,94	3,03	0,19	3,50	3,09
FeO	3,26	6,43	6,02	4,66	11,54	6,84	9,21	8,90	7,82
MnO	0,11	0,20	0,19	0,09	0,32	0,20	0,31	0,17	0,19
MgO	5,26	7,85	19,02	44,45	5,23	13,51	9,05	6,24	16,00
CaO	17,62	15,00	9,34	t	9,15	14,32	13,07	9,87	13,00
Na_2O	1,22	1,52	1,45	0,02	2,36	1,11	2,16	2,94	1,17
K_2O	0,49	0,81	0,3	0,02	0,61	0,40	0,39	0,42	0,66
P_2O_5	0,12	0,10	0,30	-	0,35	-	0,18	0,35	0,15
Totals**	100,00	100,00	100,00	100,00*	100,00	100,00	100,00	100,00	100,00
CIPW NORMATIVE MINERALS (MOLECULAR PERCENTAGES)									
q	-	-	-	-	-	4,55	-	0,01	-
or	-	-	2,09	-	2,32	3,78	3,88	2,54	2,32
ab + an	72,13	47,58	33,61	-	33,88	47,17	20,56	57,29	46,65
ne	6,55	8,24	-	-	-	-	-	-	-
le	-	3,86	-	-	-	-	-	-	-
ka	1,73	-	-	-	-	-	-	-	-
di + he	0,72	16,45	18,12	-	37,36	15,70	42,23	13,23	29,10
lar	4,25	1,83	-	-	-	-	-	-	-
fo + fa	11,58	13,53	26,32	57,55	11,51	-	10,57	-	11,04
en + fe	-	-	10,05	36,82	10,67	17,69	17,63	20,97	8,32
ap	0,25	0,21	0,62	-	0,77	-	0,30	0,73	0,36
ma	5,09	7,23	7,48	5,62	3,15	5,37	3,20	3,70	0,20
il	0,83	1,07	1,71	-	1,14	4,96	1,1	1,52	2,00
An%	100	100	63	-	71	53	49	54	59

* includes 0,09 Cr_2O_3 and 0,32 NiO % ; ** analyses recalculated water-free to 100; t: traces.

(a) Corundum amphibolite: : (P24).
(b) Garnet amphibolite : (P25).
(c) Hypersthene amphibolite : (P26).
(d) Serpentinised peridotite : (P27).
(e) Garnetiferous metadolerite: (P28).
(f) Clinopyroxene amphibolite : (P29).
(g) Biotite metagabbro : (P30).
(h) Garnetiferous metadolerite : (P31).
(i) Biotite hornblende metagabbro: (P32).

Approximate sampling localities shown in Fig.20.
Original sample numbers listed in Table IV-9.

TABLE VI-12 - PUBLISHED ANALYSES OF MELANOCRATIC AND HYPERMELANIC ROCKS FROM THE RING COMPLEXES, AFTER BLOOMFIELD (1968, p.151)

	(a)	(b)	(c)	(d)	(e)	(f)
SiO_2	40,20	42,50	41,68	47,26	47,89	49,65
TiO_2	1,64	1,62	2,08	1,31	1,16	0,74
Al_2O_3	6,82	6,84	9,34	8,29	8,48	3,60
Fe_2O_3	5,06	2,68	4,26	3,24	5,35	2,88
FeO	10,49	8,19	5,62	8,69	8,36	5,79
MnO	0,20	0,16	0,11	0,15	0,23	0,19
MgO	18,14	22,11	19,23	12,73	12,16	16,12
CaO	11,13	10,69	7,28	12,66	13,29	19,01
Na_2O	1,02	0,54	0,41	1,76	0,67	0,57
K_2O	0,79	1,81	6,97	0,49	0,13	nil
H_2O+	0,54	0,53	0,85	0,39	0,88	0,46
H_2O-	nil	0,09	0,24	0,18	0,21	0,19
P_2O_5	2,21	1,25	0,75	1,82	0,03	0,08
CO_2	1,50	0,65	0,01	0,57	0,94	0,59
Cr_2O_3	0,06	n.d.	0,04	0,16	0,01	0,19
NiO	0,05	n.d.	0,07	0,11	0,06	0,19
Totals	*99,83	99,66	100,25	99,85	99,81	99,85

AVERAGE CIPW NORMATIVE MINERALS (MOLECULAR PERCENTAGES)

or	7,72	-	-	1,91
ab + an	16,14	3,02	12,48	28,22
ne	1,32	2,19	-	-
le	-	32,64	-	-
c	-	-	-	-
di + he	25,29	13,13	69,76	34,40
lar	-	3,45	-	-
fo + fa	39,59	36,74	8,09	0,41
en + fe	-		5,44	26,46
ap	3,62	1,54	0,17	2,00
il	2,27	2,87	1,04	1,77
ma	4,05	4,41	3,03	4,62
hem	-	-	-	-
An%	71	100	59	60

*Analysis includes 0,89 per cent BaO; normative calcite not calculated.

(a) Metapyroxenite: (P34).
(b) Biotite-olivine-metapyroxenite: (P33).
(c) Biotite-metapyroxenite: (P35).
(d) Hypersthene-metagabbro: (P36).
(e) Hornblende-hypersthene metagabbro: (P37).
(f) Hypersthene-metadiallagite: (P38).

Approximate sampling localities shown in Fig.20.
Original sample numbers listed in Table IV-9.

TABLE IV-13 - PUBLISHED ANALYSES OF LEUCOCRATIC ROCKS FROM THE RING COMPLEXES AFTER BLOOMFIELD (1968, p.152)

	(a)	(b)	(c)	(d)	(e)	(f)	(g)
SiO_2	50,44	54,12	57,61	59,61	57,48	67,37	68,97
TiO_2	1,45	0,87	1,11	0,86	1,16	0,71	0,40
Al_2O_3	15,18	15,88	18,03	18,38	16,07	13,88	13,09
Fe_2O_3	3,99	2,29	1,48	1,76	3,88	1,49	1,41
FeO	3,88	5,24	2,17	2,22	4,91	3,74	3,45
MnO	0,08	0,17	0,05	0,01	0,14	0,11	0,07
MgO	3,91	4,37	1,90	1,74	1,03	0,29	0,22
CaO	7,01	6,34	4,17	3,08	4,21	2,00	1,80
Na_2O	1,91	3,83	4,95	4,84	3,99	3,27	3,02
K_2O	7,82	4,92	6,24	6,71	5,86	6,71	6,71
H_2O+	0,61	0,06	0,15	0,26	0,36	0,29	0,35
H_2O-	0,23	0,27	0,07	0,11	0,12	0,12	0,04
P_2O_5	2,19	1,27	0,81	0,38	0,53	0,18	0,12
CO_2	0,01	0,14	0,18	0,10	0,13	0,08	0,27
Totals	*99,77	99,77	99,04	**100,06	99,87	100,24	99,92

AVERAGE CIPW NORMATIVE MINERALS (MOLECULAR PERCENTAGES)

q	-	-	18,35
or	37,80	37,20	40,45
ab + an	35,47	49,73	31,78
ne	1,11	0,05	-
c	-	-	4,58
di + he	9,02	5,29	4,44
fo + fa	7,98	2,6	-
en + fs	-	-	2,49
ap	3,63	1,20	0,32
il	1,65	1,45	0,79
ma	3,35	2,48	1,55
An%	33	18	10

* total includes 1,06 per cent BaO; ** total includes 0,28 per cent F_2O; calcite not calculated.

(a) Biotite-pyroxene perthitic syenite: (P39).
(b) Pyroxene-perthitic syenite: (P40).
(c) Biotite-pyroxene perthitic syenite: (P41).
(d) Biotite-hornblende perthite gneiss: (P42).
(e) Quartz syenite: (P43).
(f) Microcline granite: (P44).
(g) Microcline granite: (P45).

Approximate sampling localities shown in Fig.20.
Original sample numbers listed in Table IV-9.

TABLE IV-14 - PUBLISHED ANALYSES OF SYENITES AND RELATED GNEISSES FROM PERTHITIC COMPLEXES, AFTER BLOOMFIELD (1968, p.144)

	(a)	(b)	(c)	(d)	(e)	(f)	(g)
SiO_2	61,36	60,98	62,91	61.86	56,10	55,60	58,25
TiO_2	0,47	0,60	0,76	0,49	0,82	0,83	0,76
Al_2O_3	17,77	19,03	16,73	18,23	15,85	15,67	18,55
Fe_2O_3	2,86	3,08	3,47	3,53	3,45	3,29	1,59
FeO	1,58	0,96	1,99	1,15	2,88	3,01	2,56
MnO	0,07	0,05	0,16	0,07	0,11	0,08	0,12
MgO	0,79	0,63	0,89	0,68	2,76	2,81	2,14
CaO	1,97	1,78	0,99	0,63	5,85	5,66	4,39
Na_2O	3,74	5,36	6,17	4,79	4,02	3,49	4,49
K_2O	8,21	6,88	5,16	7,48	5,75	7,08	6,09
H_2O+	0,31	0,39	0,17	0,62	0,31	0,48	0,09
H_2O-	0,26	nil	0,19	0,16	0,25	0,06	0,33
CO_2	0,38	nil	nil	nil	nil	0,68	0,05
P_2O_5	0,37	0,09	0,07	0,35	1,52	1,32	0,44
Totals	100,14	99,83	99,66	100,04	99,67	100,06	99,85

AVERAGE CIPW NORMATIVE MINERALS (MOLECULAR PERCENTAGES)*

q	2,47	-
or	40,84	37,43
ab + an	50,06	44,20
ne	-	0,46
c	0,28	-
di + he	-	8,28
fo + fa	-	3,33
en + fs	2,08	-
ap	0,46	2,27
ilm	2,80	2,91
ma	0,80	1,21
hem	0,72	-
An%	11	21

* Normative calcite not calculated.

(a) Hornblende-biotite-perthite gneiss: (P46).
(b) Biotite-hornblende-perthite gneiss: (P47).
(c) Biotite-hornblende perthitic syenite: (P48).
(d) Biotite perthitic syenite: (P49).
(e) Foliated pyroxene-hornblende perthitic syenite: (P50).
(f) Biotite-hornblende-diopside perthitic syenite: (P51).
(g) Hornblende perthitic syenite: (P52).

Approximate sample localities shown in Fig.20.
Original sample numbers listed in Table IV-9.

TABLE IV-15 - PUBLISHED ANALYSES OF GRANITOID GNEISSES

	(a)	(b)	(c)	(d)
	1	2	3	
SiO_2	69,32	69,09	69,54	75,70
TiO_2	0,08	0,17	0,17	0,17
Al_2O_3	14,78	14,45	14,30	12,95
Fe_2O_3	2,06	1,74	1,90	1,87
FeO	1,01	1,67	1,84	0,14
MnO	0,02	0,06	0,06	0,14
MgO	0,79	0,29	0,24	-
CaO	1,12	2,06	0,88	0,20
Na_2O	3,96	3,39	4,11	4,40
K_2O	6,32	6,16	6,22	4,06
H_2O^+	0,44	0,65	0,04	-
H_2O^-	0,01	0,22	0,69	-
P_2O_5	0,28	0,11	0,22	0,37
CO_2	0,07	nil	0,01	-
Totals	100,26	100,26	100,22	100,00*

* Analysis recalculated water-free to 100,00.

(a) Leucocratic granitoid gneiss (Herdsman, 1963, p.134): (P53).
(b) Sheared and epidotized biotite granite (Bloomfield, 1965, p.52): (P54).
(c) Granite (Walshaw, 1965, p.61): (P55).
(d) Granite (Bloomfield, 1965, p.53): (P56).

Approximate sampling localities shown in Fig.20.
Original sample numbers listed in Table IV-9.

TABLE IV-16 - PUBLISHED ANALYSES OF POST-KINEMATIC GRANITE AND SYENITE AFTER BLOOMFIELD (1968, p.158)

	(a)	(b)	(c)	(d)	(e)	(f)
SiO_2	70,30	66,01	62,09	62,31	66,40	59,18
TiO_2	0,13	0,38	0,75	0,51	0,36	0,85
Al_2O_3	15,05	15,89	17,18	17,04	15,39	16,14
Fe_2O_3	1,40	3,05	2,34	2,50	3,14	4,15
FeO	1,01	0,86	1,87	1,72	1,15	2,59
MnO	0,06	0,06	0,12	0,08	0,09	0,18
MgO	0,24	0,43	1,12	1,04	0,77	1,51
CaO	1,06	1,24	2,54	2,84	1,56	2,46
Na_2O	3,56	4,03	4,23	4,03	4,08	4,48
K_2O	6,48	7,38	7,14	7,14	6,35	6,96
H_2O+	0,68	0,63	0,22	0,24	0,38	0,36
H_2O-	0,14	0,29	0,18	0,11	0,18	0,20
P_2O_5	0,04	0,04	0,12	0,27	0,26	0,57
CO_2	nil	nil	0,29	0,21	nil	0,10
F	-	-	-	-	-	-
	100,15	100,29	100,19	100,04	100,11	99,73

(a) Muscovite-biotite granite: (P60).
(b) Biotite granite: (P61).
(c) Biotite-quartz syenite (P57).
(d) Hornblende biotite-quartz syenite: (P58).
(e) Biotite granite: (P62).
(f) Biotite-hornblende-quartz syenite: (P59).

Approximate sampling localities shown in Fig.20.
Original sample numbers listed in Table IV-9.

TABLE IV-17 - PUBLISHED TRACE ELEMENT CONCENTRATIONS IN METAPLUTONIC ROCKS AFTER BLOOMFIELD (1965, pp.48 and 58)

locality no.	P35	P33	P38	P42	P39	P40	P43	P44	P45	P52
Rb ppm	900	60	50	350	500	290	n.d.	380	220	240
Sr ppm	350	450	300	850	2 000	1 100	1 100	450	700	1 300
Y ppm	35	40	40	85	55	60	70	50	70	70
Zr ppm	130	120	75	1 000	80	350	1 000	500	800	1 000
Nb ppm	70	50	35	45	50	65	110	45	55	40

Approximate sampling localities shown in Fig.20.
Original sample numbers listed in Table IV-9.
Whole-rock analyses and rock designation are reported in Tables IV-11, IV-12, and IV-13.

APPENDIX V

DETERMINATION OF P-T METAMORPHIC CONDITIONS

In this short Appendix the partitioning coefficient, mole fractions and other calculated values used to solve geothermometer and geobarometer equations are reported.

Table V-1 lists the values which were used in the definition of the P-T conditions in the areas of two-pyroxene granulites according to formulae: (no.2), Wood and Banno (1973); (no.4), Wells (1977); and (no.7), Powell (1978). Mole fractions, partitioning coefficients and other thermodynamic parameters used to define metamorphic conditions in the Tengani and Ncheu areas are shown in Tables V-2 and V-3 respectively.

TABLE V-1 - ACTIVITIES AND MOLE FRACTIONS OF CATIONS IN COEXISTING PYROXENES FROM TWO-PYROXENE GRANULITES

Area	Sample nos.	a^{cpx}_{enst}	a^{opx}_{enst}	x^{opx}_{Fe}	x^{cpx}_{Ca,M_2}	x^{cpx}_{Mg,M_2}	x^{opx}_{Fe,M_2}	x^{opx}_{Ca,M_2}	$x^{opx}_{M_2}$
Zomba	(5)	0,0268	0,2120	0,510	0,862	0,065	0,469	0,051	0,452
	(7)	0,0360	0,1837	0,552	0,823	0,0662	0,5063	0,039	0,4107
	(48)	0,0279	0,2389	0,486	0,887	0,0436	0,4705	0,047	0,4435
	(55a)	0,0431	0,2752	0,547	0,823	0,0662	0,4157	0,037	0,5023
	(55b)	0,0213	0,2591	0,454	0,890	0,034	0,415	0,055	0,498
Blantyre	(46)	0,0326	0,3599	0,377	0,862	0,075	0,3511	0,025	0,5809
Tete	(T37)	0,0342	0,3806	0,349	0,830	0,0557	0,3379	0,021	0,6301
	(T78)	0,0394	0,4366	0,311	0,860	0,0604	0,3037	0,015	0,6723

Sample localities for the Zomba and Blantyre areas shown in Fig.9 and in Map 2 in the pocket at the back of the thesis; for the Tete area see Appendix I-3 and Coelho (1969).

TABLE V-2 - MOLE FRACTIONS AND PARTITIONING VALUES (K) FOR GEOTHERMOMETRY-GEOBAROMETRY IN TENGANI GARNET-CLINOPYROXENE GRANULITES

		Sample no.			
Equation no.		(132)	(498)	(140)	(135b)
(16)	In K_D	1,5724	1,6256	1,4841	-
(21)	X^{ga}_{Ca}	0,2380	0,2331	0,2028	-
(23)	ΔVr	-	-	-	-7,964
(24)	X^{Ml}_{Al}	-	-	-	0,036
(25)	(1-Y)	-	-	-	0,860
(3)	X^{opx}_{Fe}	-	-	-	0,341

Sample localities shown in Fig. 9 and in Map 1 in the pocket at the back of the thesis.

TABLE V-3 - MOLE FRACTIONS AND PARTITIONING VALUES (K) FOR GEOTHERMOMETRY-GEOBAROMETRY IN TRANSITIONAL ROCKS FROM NCHEU AREA

		Sample no.			
Equation no.		436	468	456	104
(2)	$^{cpx}_{a\ enst}$	0,0169	-	0,0367	-
	$^{cpx}_{a\ enst}$	0,2247	-	0,4605	-
-	X^{opx}_{Fe}	0,5018	-	0,29096	0,4822
(7)	$X^{cpx}_{Ca,\ M_2}$	0,917	-	0,871	-
	$X^{cpx}_{Mg,\ M_2}$	0,0229	-	0,0527	-
	$X^{opx}_{Fe,\ M_2}$	0,4682	-	0,2811	-
	$X^{opx}_{Ca,\ M_2}$	0,038	-	0,025	-
	$X^{opx}_{Mg,\ M_2}$	0,4648	-	0,6849	-
(16)	ln K_D	1,8825	2,3389	1,3110	-
(21)	X^{ga}_{ca}	0,17498	0,3122	0,1671	-
(23)	ΔVr	-7,97	-	-8,1732	-8,0948
(24)	X^{Ml}_{Al}	0,034	-	0,072	0,058
(25)	(1-Y)	0,4914286	-	0,5607	0,9151

Sample localities shown in Fig. 9 and in Maps 2 and 3 in the pocket at the back of the thesis.

APPENDIX VI

GEOCHRONOLOGY

(i) Previous Age Determinations

To date, only nine mineral age determinations from rocks of southern Malawi have been published (Bloomfield, 1968) and they are listed in Table VI-1.

TABLE VI-1 - PUBLISHED MINERAL AGES FROM THE AMPHIBOLITE FACIES TERRANES OF SOUTHERN MALAWI, AFTER BLOOMFIELD (1968)

Locality	Rock	Mineral	Method	Age (m.y.)
A	Nepheline gneiss	zircon	Pb-Alpha	551 ± 55
B	Aegirine pegmatite	monazite	Pb-Alpha	542 ± 55
C	Metapyroxenite	biotite	K-Ar	493 ± 20
D	Biotitite	biotite	K-Ar	490 ± 20
E	Calc-pelitic schist	phlogopite	K-Ar	470 ± 20
F	Marble	phlogopite	K-Ar	460 ± 20
G	Quartz-mica schist	muscovite	K-Ar	440 ± 20
H	Anatectic syenite	biotite	K-Ar	395 ± 16
I	Metapyroxenite	biotite	K-Ar	380 ± 55

Localities of dated rocks are shown in Fig.47, Chapter 7.

(ii) Sampling details and petrographic data

The programme of age determinations was carried out on 51 samples from localities shown in Figs.VI-A and VI-B. Detailed information on rock-type designations, thin section numbers and sampling areas are listed in Table VI-2; and short petrographic descriptions were provided in Appendix II-3.

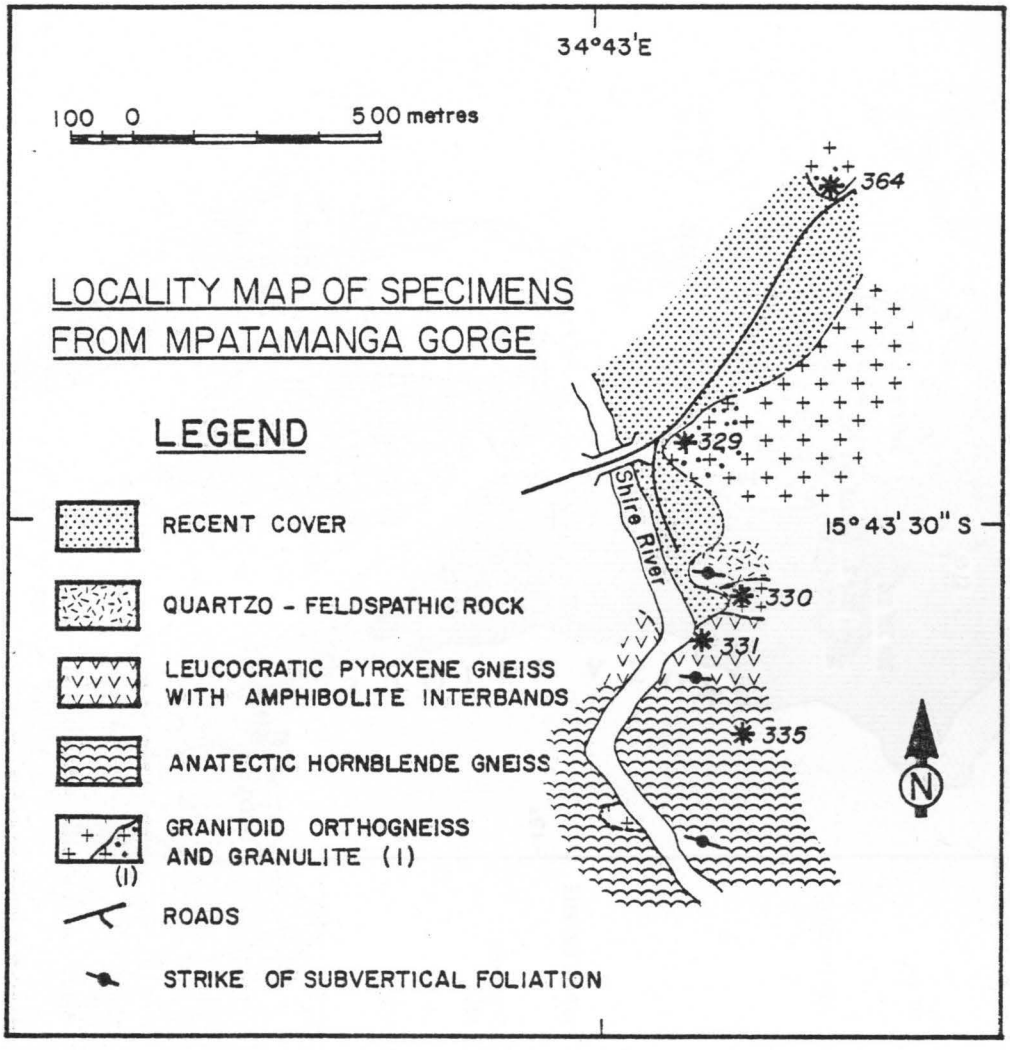


Fig.VI-A. Geological map of the Mpatamanga Gorge in the Middle Shire transition zone with localities of samples used in age determinations.

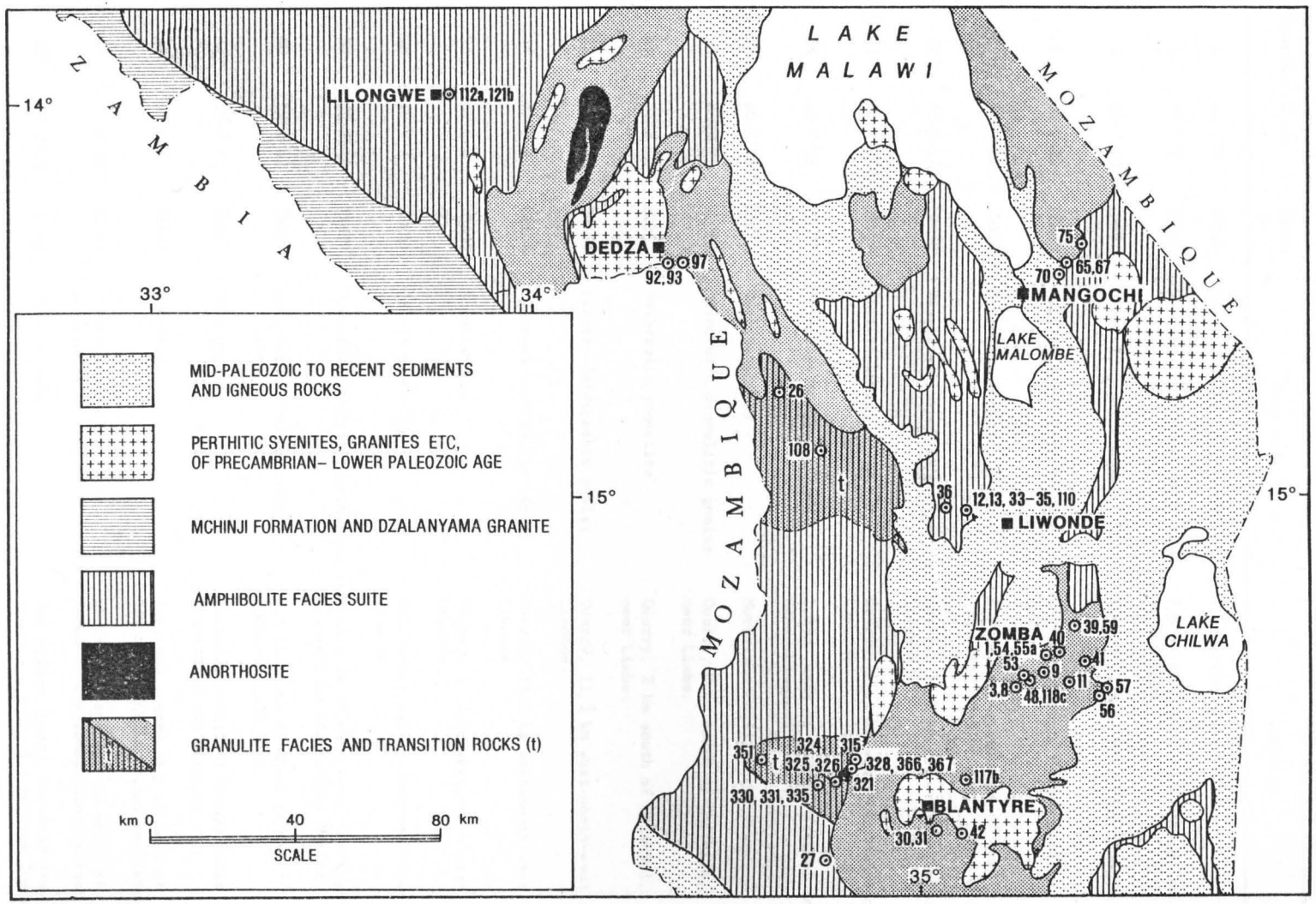


Fig.VI-B. Generalised locality map for samples used in age determinations (after Clifford et al., in prep.; Bloomfield, 1968).

TABLE VI-2 - LIST OF SAMPLES, PETROGRAPHIC TYPES AND LOCALITIES FOR GNEISSES, GRANULITES AND IGNEOUS ROCKS USED IN AGE DETERMINATIONS

Sample no.	Field no.	Slide no.	Rock type	Locality
1	66-C-3	19647	Quartzo-feldspathic granulite	Old Prison quarry, Zomba.
3	66-C-5	19649	Quartzo-feldspathic granulite	9,6 km on the main road from Zomba to Blantyre.
8	66-C-10	19654	Gneissic granite dyke	11,3 km on main road from Zomba to Blantyre.
9	66-C-11	19655	Hypersthene-quartz syenite	Chiloni's Court, Ntonya Complex, near Zomba.
11	66-C-13	19657	Perthitic gneiss	2,8 km east-south-east of the Namikango Trading Post, Zomba district.
12	66-C-17A	19658	Quartzo-feldspathic gneiss	Quarry, 11,3 km west-north-west of Liwonde.
13	66-C-17B	19659	Biotite gneiss	Quarry, 11,3 km west-north-west of Liwonde.
26	66-C-37	19671	Nepheline gneiss	1,6 km west of Muluma Mission, in the Ncheu-Livelezi River.
27	66-C-38	19672	Biotite gneiss	Murchison Falls, Shire River.
30	68KA	22252	Mesocratic granulitic gneiss	Quarry, 2 km south of Chichiri, near Limbe.
31	68KB	22253	Mesocratic granulite	Quarry, 2 km south of Chichiri, near Limbe.
33	69-B-2	23453	Quartzo-feldspathic gneiss	Quarry, 11,3 km west-north-west of Liwonde.
34	69-B-3	23454	Pyroxene amphibolite (dyke)	Quarry, 11,3 km west-north-west of Liwonde.
35	69-B-4	23455	Granite dyke	Quarry, 11,3 km west-north-west of Liwonde.
36	69-B-7	23456	Garnet granulite	Uhikombola quarry, west-north-west of Liwonde.
39	69-B-11	23459	Quartzo-feldspathic granulite	West side of main road from Zomba to Liwonde, behind Songani Market.
40	69-B-12	23460	Melanocratic hornblende granulite	0,8 km south of Chopi on the Zomba-Liwonde Road.
41	69-B-13	23461	Microgranite	East-south-east of Mikuyo Radio Station, Zomba District.
42	69-B-17	23462	Syenite	Sekoloma quarry, 3,2 km west of Malabwi Mountain, Blantyre District.
48	69-B-23	23466	Melanocratic hornblende granulite	Chikala quarry, 9,6 km south of Zomba on the Zomba-Blantyre Road.
53	69-B-28	23467	Granite dyke	New Prison quarry, northern end of Namilongo Hill, 6,4 km from Zomba.
54	69-B-29	23468	Amphibolite dyke	Old Prison quarry, Zomba.

TABLE VI-2 - LIST OF SAMPLES, PETROGRAPHIC TYPES AND LOCALITIES FOR GNEISSES, GRANULITES AND IGNEOUS ROCKS USED IN AGE DETERMINATIONS (CONTD.)

Sample no.	Field no.	Slide no.	Rock type	Locality
55a	69-B-30	23469	Quartzo-feldspathic granulite	Old Prison quarry, Zomba .
56	72-D-1	X19664	Quartzo-feldspathic rock	Ntondwe-Namiwawa River at the crossing of the Palombe Road, 21,7 km east-south-east of Zomba .
57	72-D-2	X19665	Quartzo-feldspathic rock	Piriwit Mountain 21,7 km east-south-east of Zomba .
59	72-D-4A	X19666	Quartzo-feldspathic rock	Zomba-Lilongwe road, cutting east of Songani Mountain, 14,5 km north of Zomba .
65	72-D-7A	X19672	Quartzo-feldspathic granulite	1,9 km west of Chowe School on the Mangoche-Namwera Road .
67	72-D-7C	X19674	Quartzo-feldspathic granulite	1,9 km west of Chowe School on the Mangoche-Namwera Road .
70	72-D-9	X19751	Biotite-diopside gneiss	3,4 km west-south-west of Chowe School on the Mangoche-Namwera Road, in the Mpiriri River .
75	72-D-14	X19756	Leucocratic augite granulite	3,2 km west of Jalasi Court on the Mangoche-Namwera Road .
92	72-D-31A	X19827	Melanocratic rock	2,4 km south-east of Dedza on the Dedza-Ncheu Road .
93	72-D-31B	X19828	Mesocratic granulite	2,4 km southeast of Dedza on the Dedza-Ncheu Road .
97	72-D-33	X19832	Perthitic orthogneiss	6,4 km east-south-east of Dedza .
108	72-D-44	X19936	Garnet gneiss	2,4 km east of Kampepuza Trading centre on the Ncheu-Balaka Road .
110	72-D-46A	X19975	Granite dyke	Quarry, 11,2 km west-north-west of Liwonde .
117b	72-D-52	X20557	Granite vein	Njuli quarry, 46,7 km. south of Zomba .
118c	72-D-54A	X20894	Granite vein	Chikala quarry, 9,6 km south of Zomba .
121a	72-D-59	X20199	Biotite gneiss	Lilongwe borehole DH20 (depth 27 m) .
121b	72-D-59	X20200	Hornblende-biotite gneiss	Lilongwe borehole DH20 (depth 30,5 m).
315	MA194	X21356	Quartzo-feldspathic granulite	4 Km west of Kunthembwe Court, Middle Shire district .
321	MA200	X21753	Granulite with leucocratic bands	6 Km west-south-west of Kunthembwe Court Middle Shire District .
324	MA203	MA203	Mesocratic granulite	8,7 Km west-south-west of Kunthembwe Court Middle Shire District .
325	MA204	MA204	Mesocratic granulite	9,2 Km west-south-west of Kunthembwe Court Middle Shire District.
326	MA205	MA205	Mesocratic granulite	9,8 Km west-south-west of Kunthembwe Court Middle Shire District .
328	MA207	X21752	Mesocratic pyroxene gneiss	10,5 Km west-south-west of Kunthembwe Court Middle Shire District .

TABLE VI-2 - LIST OF SAMPLES, PETROGRAPHIC TYPES AND LOCALITIES FOR GNEISSES, GRANULITES AND IGNEOUS ROCKS USED IN AGE DETERMINATIONS (CONTD.)

Sample no.	Field no.	Thin Section no.	Rock types	Locality
330	MA209	X21245	Granitic gneiss	Mpatamanga Gorge, Shire River .
331	MA210	X21246	Quartzo-feldspathic granulite	Mpatamanga Gorge, Shire River .
335	MA214	X21247	Mesocratic gneiss	Mpatamanga Gorge, Shire River .
351	MA230	X21224	Granulite	Wakurumadzi River, 8 Km south-east of Mwanza, Middle Shire .
366	MA245	X21750	Melanocratic hornblende granulite	11,3 Km west-south-west of Kunthembwe Court, Middle Shire District .
367	MA246	X21751	Mesocratic hornblende granulite	11,6 Km west-south-west of Kunthembwe Court, Middle Shire District .

(iii) Analytical techniques and isochron calculating methods

The Rb and Sr concentrations for the Middle Shire samples were measured at the University of Leeds, U.K., by D.C.Rex, using standard laboratory procedures, and the precision of each determination is about ± 1 per cent (1σ); the Sr^{87}/Sr^{86} ratios were obtained by mass spectrometry and the precision of these measurements is ± ,01 per cent (1σ). In addition, analyses of the N.B.S. S.R.M. - 987 and Eimer and Amend $SrCO_3$ standards yielded Sr^{87}/Sr^{86} ratios of 0,71033 $\pm 4E^{-5}$ and 0,70804 $\pm 3E^{-5}$ respectively. All age determinations were carried out using a Rb^{87} decay constant of $1,42 \times 10^{-11} y^{-1}$ and in accordance with Brooks et al. (1972) the term isochron, when applied to the samples from the Middle Shire, is reserved for regression lines, the data points of which scatter less than that amount predicted by experimental uncertainties. The degree of scatter is expressed by a value:

$$MSUM = \sqrt{\frac{SUMS}{N-2}}$$

where N is the number of data points and SUMS is a statistical function defined by York (1969); an isochron therefore is defined here as a regression line with MSUM less than 2,5.

In contrast, unpublished age determinations for the regional granulite and amphibolite facies suites were obtained with a computer programme available at Leeds University, which relates the scatter of the points on the Rb-Sr isotope diagrams to primary differences in Sr^{87}/Sr^{86} initial ratios and then calculates the most likely isochron slope accordingly (Clifford et al., in prep.).

However, the scatter presented by a suite of granite and syenite dykes and intrusive bodies was found to be excessive and the calculated ages should only be considered as indicative. In two restricted areas of southern and central Malawi, (namely Liwonde and Mangoche) the rather close association of samples with petrographic and petrochemical affinities suggest homogeneity of Sr^{87}/Sr^{86} initial ratios; and their age was calculated with the regression technique of York (1969). Analytical data obtained from regional granulites, gneisses and intrusive bodies (with the exception of the data for the rocks of the Middle Shire transition zone presented in Chapter 7) are listed in Tables VI-3 to VI-5); and the relative isochron diagrams are shown in Figs.VI-C to VI-G.

Considering then the U-Pb mineral age determinations, the lead and uranium isotopic analyses were performed by Dr. C. Burger at the C.S.I.R. (Pretoria) by mass spectrometry on samples prepared using the laboratory procedures described by Clifford et al. (1975). Precision for the above elements is better than ± 1 per cent, while for Pb-isotopic ratios it is better than ± 2 per cent; the decay constants used are: U^{235}, $0{,}9722 \times 10^{-9}\ y^{-1}$; and U^{238}, $0{,}1537 \times 10^{-9}\ y^{-1}$.

(iv) Tables of results and isochron diagrams

Rb-Sr isochron diagram (regional granulites)	Fig.VI-C
Rb-Sr analytical data (regional granulites)	Table VI-3
Rb-Sr isochron diagram (Mangochi area)	Fig.VI-D
Rb-Sr analytical data (regional gneisses)	Table VI-4
Rb-Sr isochron diagram (regional gneisses)	Fig.VI-E
Rb-Sr isochron diagram (Liwonde area)	Fig.VI-F
Rb-Sr analytical data (intrusive bodies)	Table VI-5
Rb-Sr isochron diagram (intrusive bodies)	Fig.VI-G

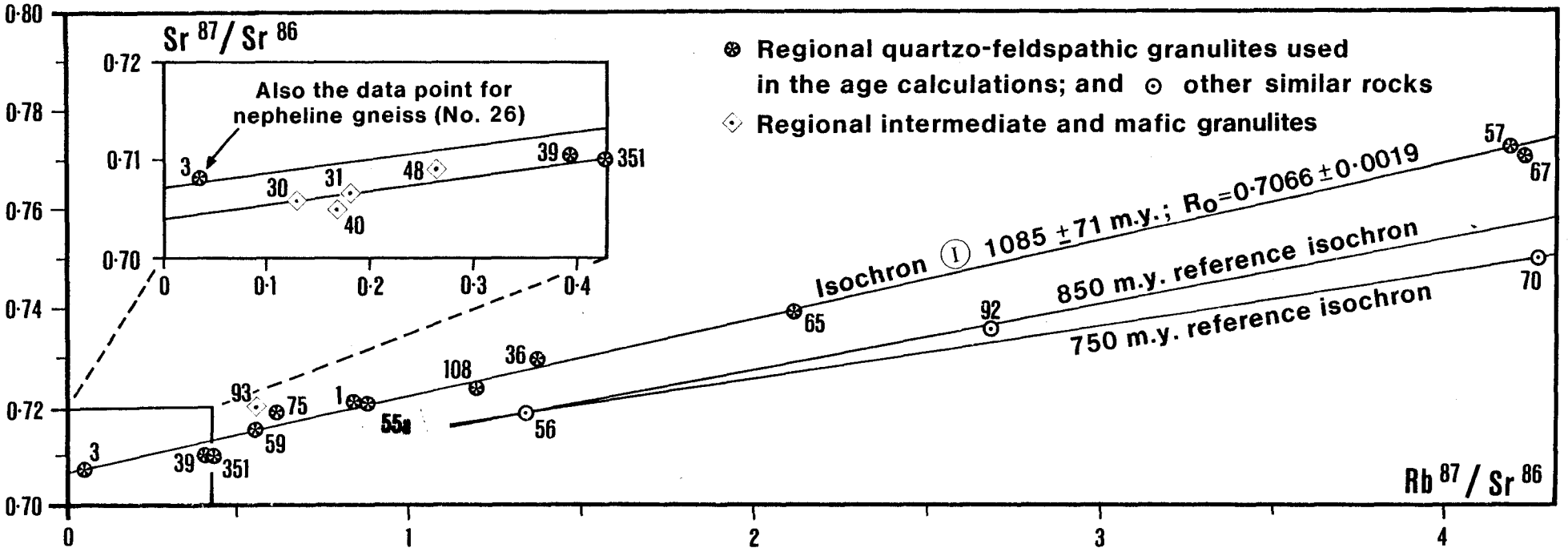


Fig.VI-C. Rb-Sr whole-rock isochron diagram, after Clifford et al. (in prep.), for the regional quartzo-feldspathic granulites of southern Malawi (see Appendices VI-B and VI-2 for sample localities and Appendix II-3 for petrographic descriptions).

TABLE VI-3-Rb-Sr ISOTOPIC DATA FOR REGIONAL GRANULITE FACIES AND RELATED ROCKS (AFTER CLIFFORD ET AL., IN PREP.)

Sample no.(1)	Slide no.	Name	Rb_{ppm}	Sr_{ppm}	Rb^{87}/Sr^{86}	Sr^{87}/Sr^{86}
1	19647	Quartzo-feldspathic granulite	62	213	0,840	0,7212
3	19649	Quartzo-feldspathic granulite	2	157	0,039	0,7076
26	19671	Nepheline gneiss	30	2 240	0,039	0,7077
30	22252	Mesocratic granulite	52	1 143	0,132	0,7061
31	22253	Mesocratic granulite	64	1 015	0,182	0,7066
36	23456	Garnet granulite	100	212	1,366	0,7303
39	23459	Quartzo-feldspathic granulite	33	241	0,397	0,7104
40	23460	Melanocratic granulite	10	171	0,169(2)	0,7047(2)
48	23466	Melanocratic granulite	21	220	0,267(3)	0,7090(3)
55 a	23469	Quartzo-feldspathic granulite	85	281	0,869(2)	0,7211(2)
56	X19664	Quartzo-feldspathic rock	26	57	1,323	0,7184
57	X19665	Quartzo-feldspathic rock	90	62	4,202	0,7727
59	X19666	Quartzo-feldspathic rock	62	331	0,540	0,7149
65	X19672	Quartzo-feldspathic granulite	141	194	2,107	0,7390
67	X19674	Quartzo-feldspathic granulite	134	91	4,235	0,7709
70	X19751	Biotite-diopside gneiss	169	114	4,285	0,7498
75	X19756	Leucocratic augite granulite	78	375	0,602	0,7188
92	X19827	Melanocratic rock	111	120	2,675	0,7357
93	X19828	Mesocratic granulite	63	327	0,560	0,7197
108	X19936	Garnet gneiss	88	217	1,182	0,7226
351	X21224	Granulite	69	464	0,428	0,71035

Analysts: J. Gronow (nos. 1, 3, 26, 30, 31, 36, 39, 40, 48 and 49); and for all other samples A. Gledhill.

(1) See Appendices VI-B and VI-2 for localities and Appendix II-3 for petrographic descriptions.

(2) Mean of duplicate analyses.

(3) Mean of triplicate analyses.

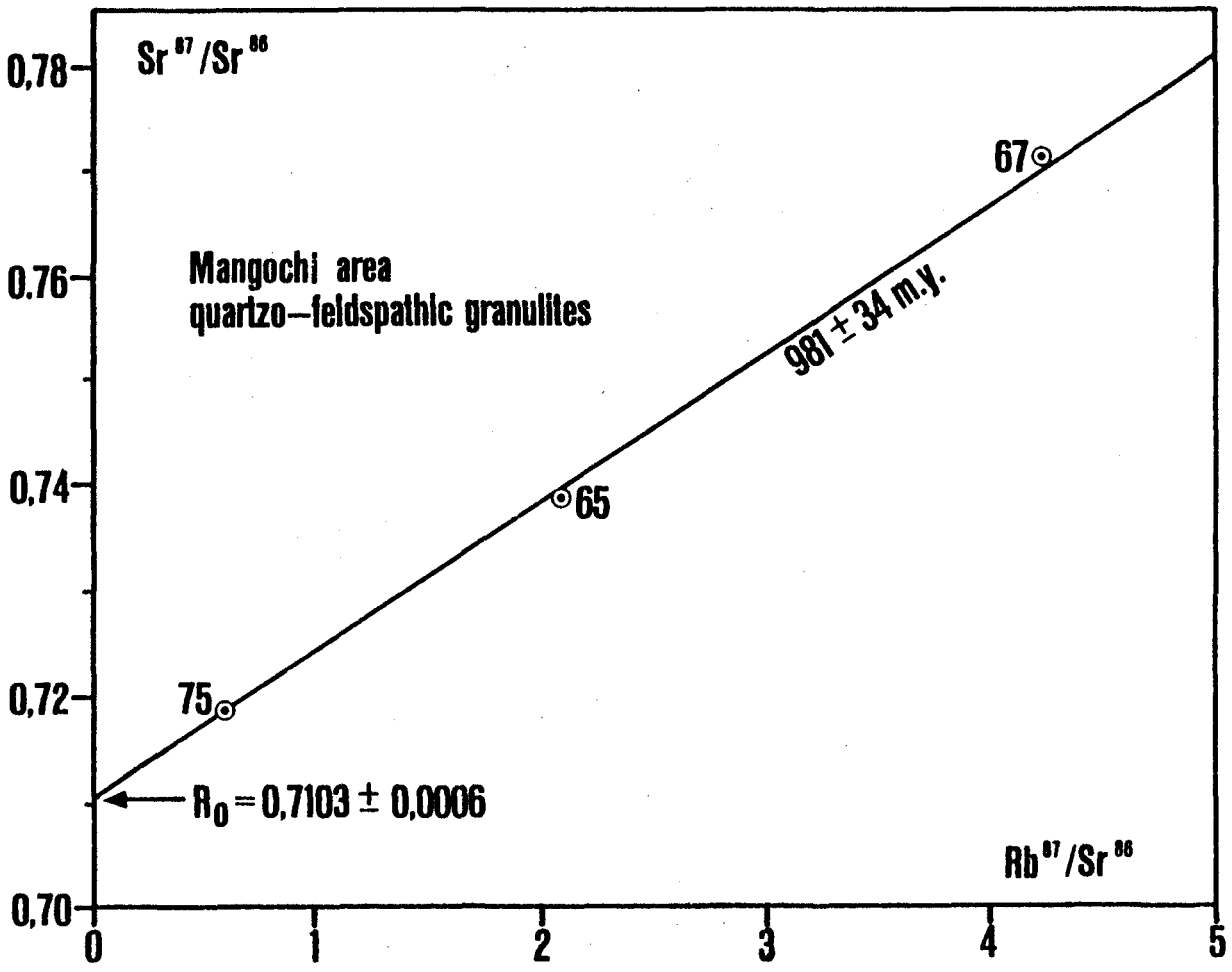


Fig.VI-D. Rb-Sr whole-rock isochron diagram for the Mangochi area granulites and related rocks (see Appendices VI-B and VI-2 for sample localities and Appendix II-3 for petrographic descriptions).

TABLE VI-4 - Rb-Sr ISOTOPIC DATA FOR AMPHIBOLITE FACIES ROCKS (AFTER CLIFFORD ET AL., IN PREP.)

Sample[1] no.	Slide no.	Name	Rb_{ppm}	Sr_{ppm}	Rb^{87}/Sr^{86}	Sr^{87}/Sr^{86}
11	19657	Perthitic gneiss	303	994	0,8844	0,7165
12	19658	Quartzo-feldspathic gneiss	120	342	1,018	0,7169
13	19659	Biotite gneiss	159	621	0,740[2]	0,7132[2]
27	19672	Biotite gneiss	78	695	0,324	0,7097
33	23453	Quartzo-feldspathic gneiss	135	748	0,523	0,7112
34	23454	Pyroxene amphibolite	9	166	0,149[2]	0,7065[2]
54	23468	Amphibolite	20	275	0,213[2]	0,7077[2]
121a	X20199	Biotite gneiss	94	177	1,544	0,72357
121b	X20200	Hornblende-biotite gneiss	93	215	1,250	0,72005

Analysts: J. Gronow (nos. 11, 12, 13, 26, 27, 33, 34 and 54); and for the remaining samples A. Gledhill (121a and 121b).

(1) See Appendices VI-B and VI-2, for localities and Appendix II-3 for petrographic descriptions.

(2) Mean of duplicate analyses.

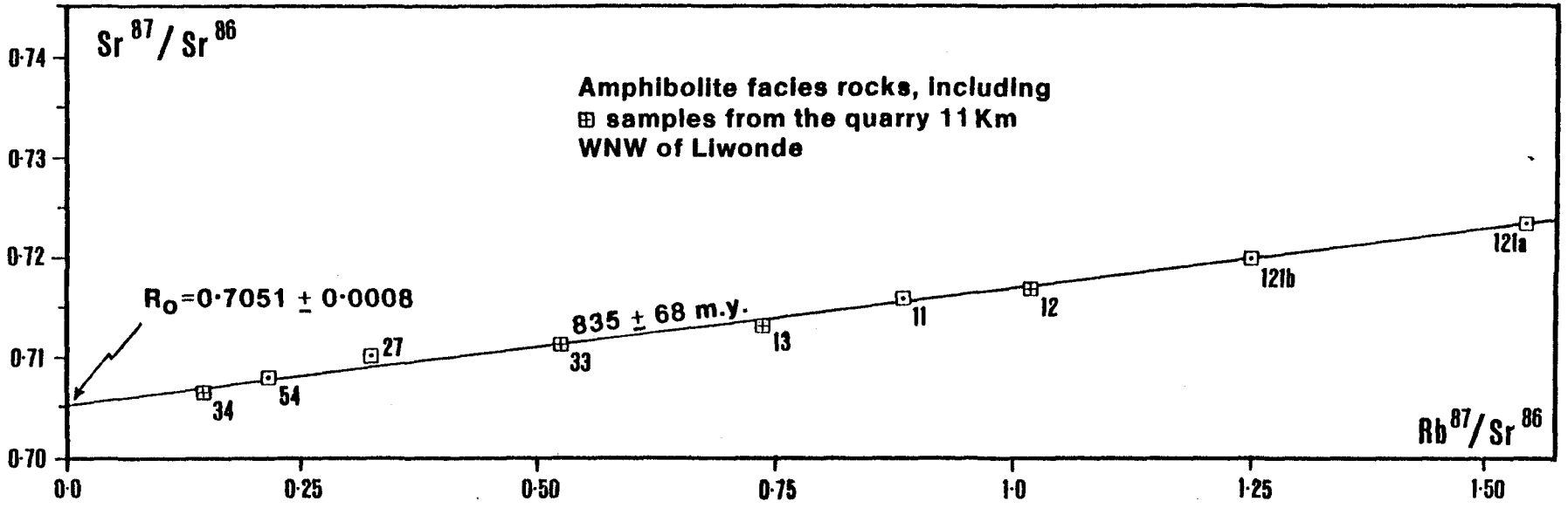


Fig.VI-E. Rb-Sr whole-rock isochron diagram, after Clifford et al. (in prep.), for the southern Malawi regional amphibolite facies gneisses (see Appendices VI-B and VI-2 for sample localities and Appendix II-3 for petrographic descriptions).

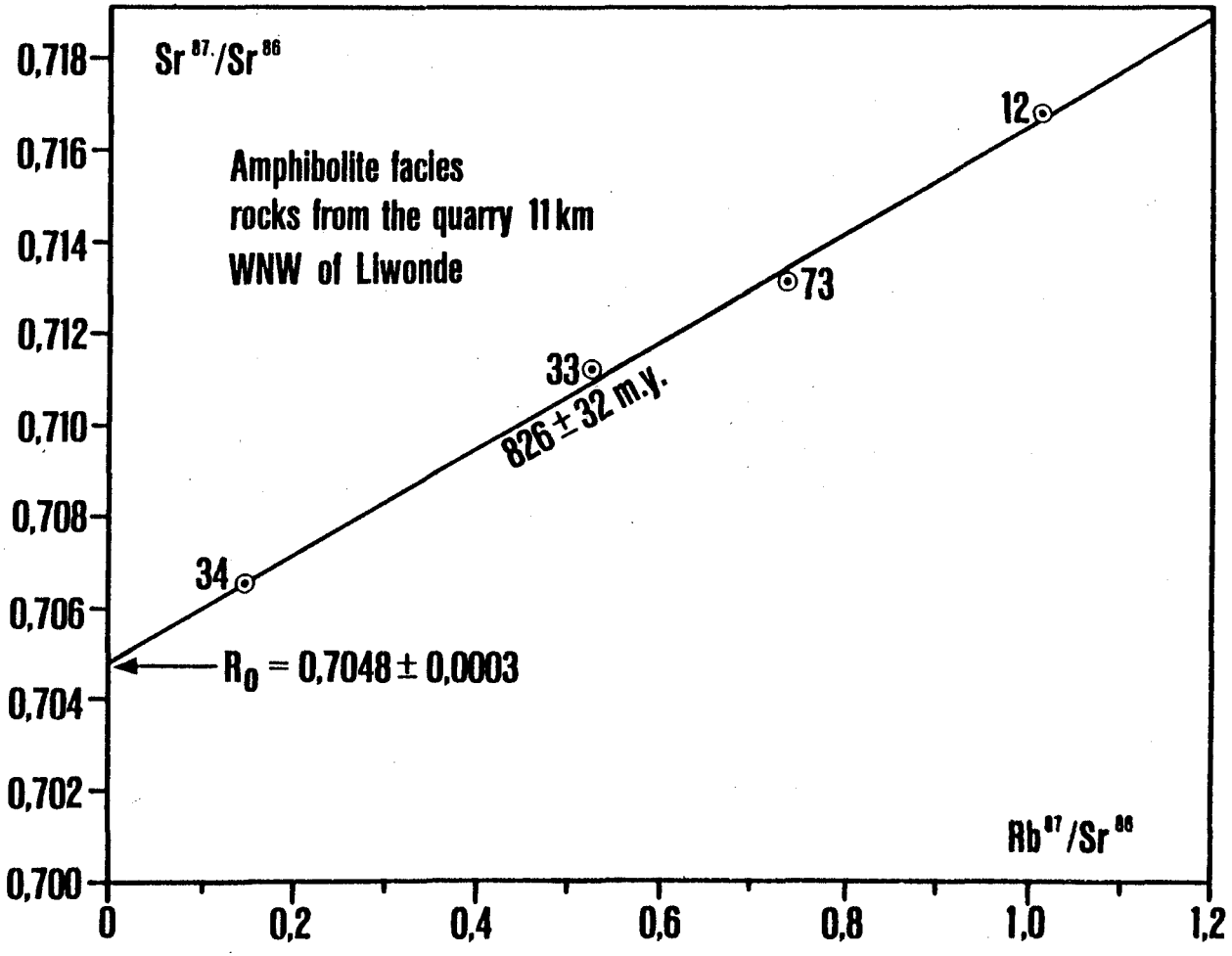


Fig.VI-F. Rb-Sr whole-rock isochron diagram for the Liwonde quarry gneisses and amphibolite (see Appendices VI-B and VI-2 for sample localities and Appendix II-3 for petrographic descriptions).

TABLE VI-5 - Rb-Sr ISOTOPIC DATA FOR GRANITE DYKES, VEINS AND INTRUSIVE BODIES (AFTER CLIFFORD ET AL., IN PREP.)

Sample[1] no.	Slide no.	Name	Rb_{ppm}	Sr_{ppm}	Rb^{87}/Sr^{86}	Sr^{87}/Sr^{86}
8	19654	Gneissic granite	173	183	2,752	0,7329
9	19655	Hypersthene-quartz syenite	114	256	1,289	0,7183
35	23455	Granite	162	547	0,859	0,7140
41	23461	Microgranite	187	77	7,015	0,7555
42	23462	Syenite	132	905	0,423	0,7092
53	23467	Granite	152	138	3,19 [2]	0,7280[2]
97	X19832	Perthitic orthogneiss	161	777	0,602	0,71027
110	X19975	Granite	99	538	0,531	0,71106
117b	X20557	Granite	192	197	2,826	0,72515
118c	X20894	Granite	135	299	1,307	0,71755

Analysts: J. Gronow (nos. 8, 9, 35, 41, and 53); and for the remaining samples A. Gledhill (nos. 97, 110, 117b and 118c).

(1) See Appendix VI-B and VI-2 for localities, and Appendix II-3, for petrographic descriptions.

(2) Mean of duplicate analyses.

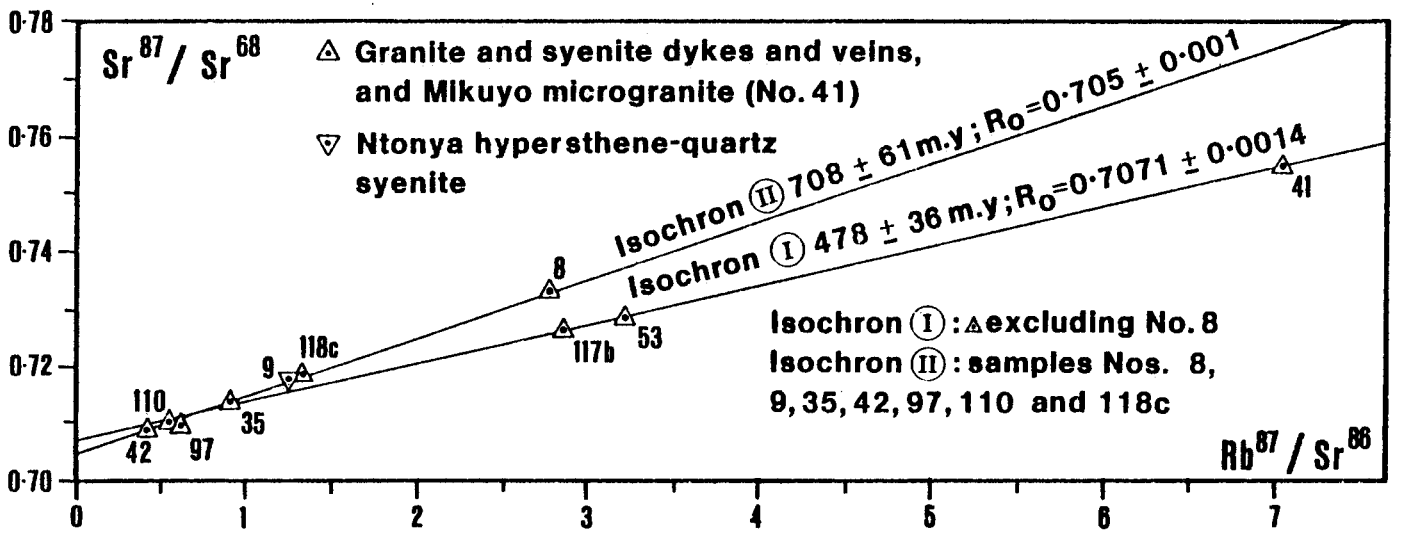


Fig.VI-G. Rb-Sr whole-rock isochron diagram, after Clifford et al. (in prep.), for the southern Malawi granite and syenite dykes and veins (see Appendices VI-B and IV-2 for sample localities and Appendix II-3 for petrographic descriptions).

APPENDIX VII

THE GRANULITES OF THE TETE AREA, MOZAMBIQUE

1. Introduction

In order to improve the understanding of the regional geological framework of southern Malawi, it was considered useful to determine the metamorphic overprint on the Tete Complex of north-west Mozambique (see Fig.VII-A). For this reason a brief study was carried out on a suite of samples, listed in Appendix I, which were kindly provided by Mr.P.Coelho of Lisbon Geological Museum. Coelho (1969) provided generalised sampling localities and extended petrographic and petrochemical information for these samples, and his original specimen numbers, preceded by the letter T have been maintained in the present study.

2. Regional setting

Rocks of the Tete Complex constitute an extension of the Basement suite of southern Malawi situated some 20 km south-west of the Mwanza Fault (see Fig.VII-A). Its contacts with the regional gneisses of the Mwanza area are hidden below younger Karoo sediments. Rock exposures of the Tete Complex outcrop over an area of about 6 000 km^2 on either side of the Zambezi River north of the town of Tete. The only known exposures of the intrusive contact between the Complex and the Basement paragneisses and granodioritic rocks are in the south-west and

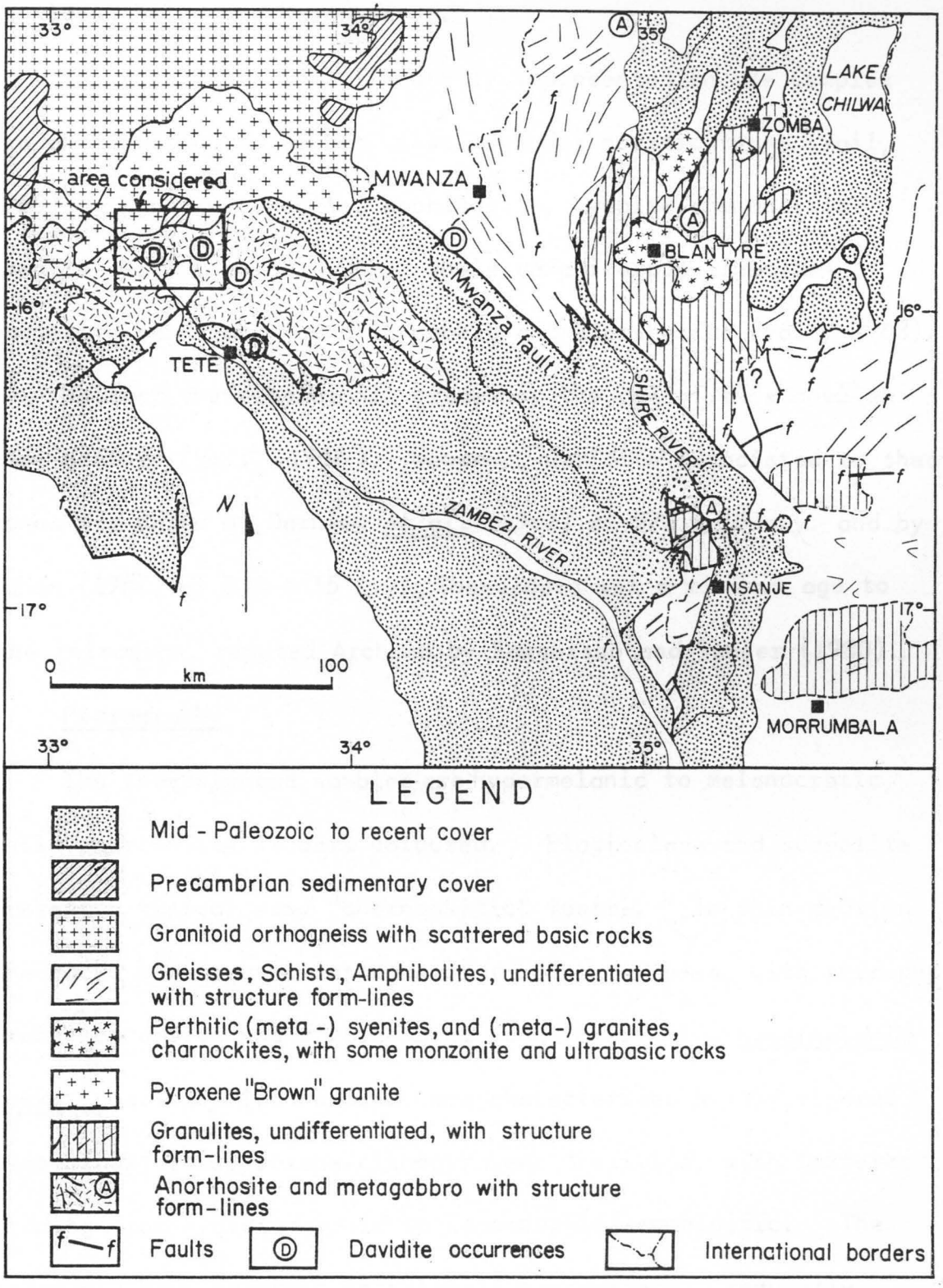


Fig.VII-A. Generalized geology of southern Malawi and the adjacent Tete area of north-west Mozambique (after Davidson and Bennett, 1950, Freitas, 1956; Oberholzer 1968, Bloomfield, 1968; and Vail 1968).

in the north (Real, 1966; Vail, 1968). Elsewhere this contact is hidden below the Karoo cover.

The rock types most frequently represented in the Complex are anorthosite and gabbro, that includes noritic types (Vail, 1968). Minor pyroxenite, amphibolite, syenite and aplitic granite occur (Coelho, 1969), while vanadiferous ilmenite-magnetite bands are found in gabbro and anorthosite (Vail, 1968).

Neither the metamorphic grade nor the age of this complex were defined (Vail, 1968); however, davidite associated to shear zones was dated by Darnley et al. (1961) at 578 ± 15 m.y. and by Cahen (1957) at 330 ± 15 m.y., These data set a minimum age to the intrusion, reputed Archean by Saggerson and Turner (1980).

3. Petrography

The investigated samples are hypermelanic to melanocratic, while anorthosite is dark coloured. Plagioclase and scapolite present a typical waxy "charnockitic" lustre. In thin section the rocks show granoblastic, equigranular textures, with straight grain boundaries and triple-point junctions. The hypermelanic rocks nos. T117, T180 and T240 are characterised by the mineral assemblage orthopyroxene-clinopyroxene ± olivine, with textures grading from hypidiomorphic to xenomorphic/xenoblastic. The pyroxenes have frequent interlobate boundaries. Regularly spaced exsolution lamellae of orthopyroxene (Plate 24) are very frequent in the clinopyroxene, which is often clouded by an

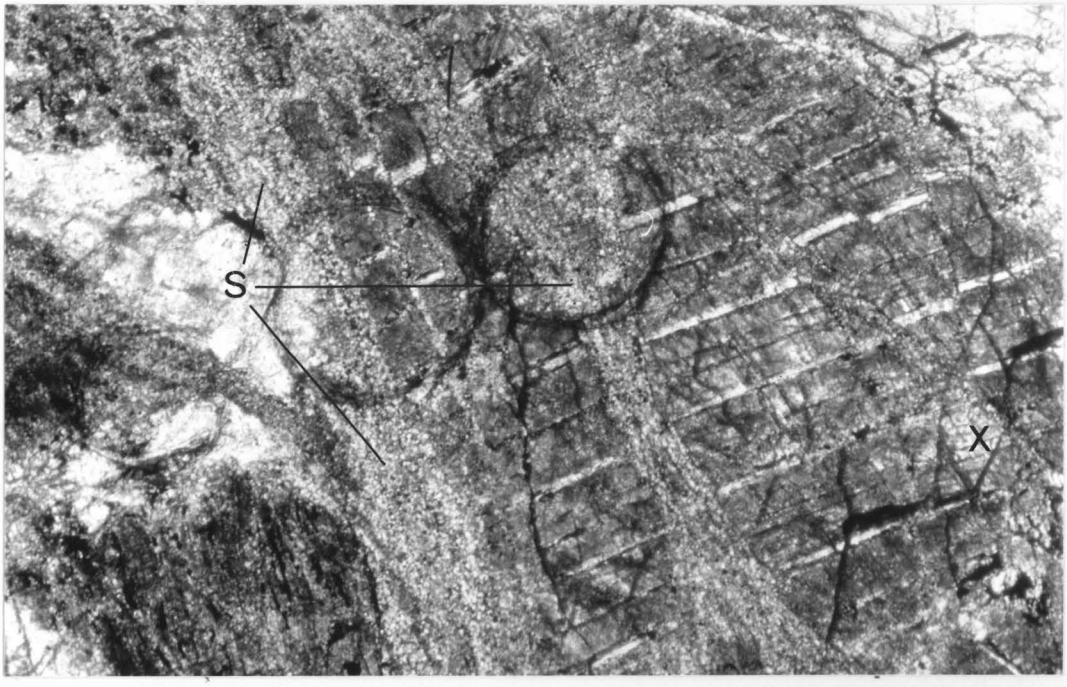


Plate 24. Pyroxenite, detail of clinopyroxene (X), with scapolite-hornblende-microshears (S) off-setting exsolution lamellae of orthopyroxene. X50, Tete area (sample no.T117; Coelho, 1969).

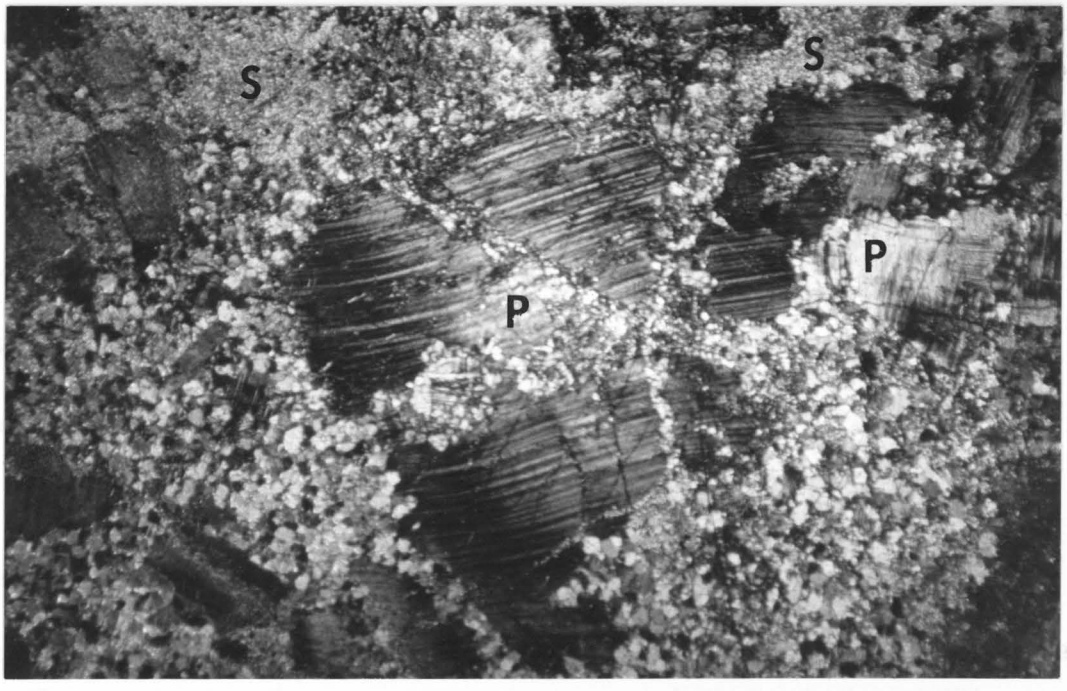


Plate 25. Anorthosite, detail of sheared plagioclase (P); note scapolite (S), and size breakdown of feldspar along cross-cutting shears. X10, crossed nicols, Tete area (sample no.T11; Coelho, 1969).

opaque dusting. The assemblage orthopyroxene-clinopyroxene-plagioclase is preserved in the melanocratic granulites nos. T37 and T78. Clinopyroxene, which occasionally hosts small feldspar inclusions, displays a distinctive pale-pink to pale-purple hue. The orthopyroxene is distinctly pleochroic from apple-green to salmon-pink. Plagioclase has a composition from An_{50} to An_{60}. The only accessory minerals are ilmenite and magnetite, and the texture is typically granoblastic.

The gabbro no.T257 is characterised by the partly preserved igneous assemblage: labradorite-olivine-clinopyroxene. The rock texture is medium-grained, hypidiomorphic-idiomorphic, with intensely clouded feldspars and kelyphitic and embayed crystals of olivine. The clinopyroxene is zoned with a pale-green core and a colourless rim, while small orthopyroxene grains are locally developed at the contact between olivine and plagioclase. In the anorthosites nos.T8 and T11 the assemblage antiperthitic Na-labradorite-clinopyroxene ± sphene is preserved. The texture is very coarse and porphyritic with plagioclase often attaining megacrystic dimensions.

Textures indicative of retrogression are present in the majority of the samples and are characteristically associated to cross-cutting shear zones or areas of ductile deformation (see Plates 24 to 26). The original assemblage of clinopyroxene-intermediate plagioclase is still clearly recognizable in the



Plate 26. Two-pyroxene granulite; detail of clinopyroxene showing ductile deformation. Note small plagioclase inclusions (P). X50, Tete area (sample no.T78, Coelho, 1969).

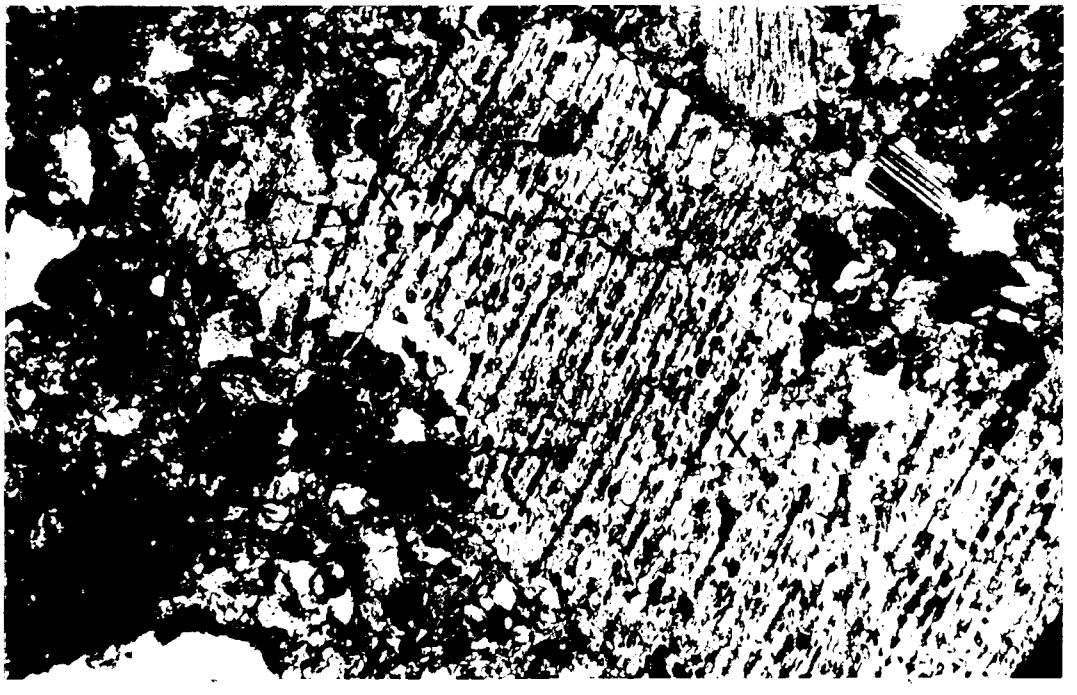


Plate 27. Metagabbro; detail of clinopyroxene (X) with regularly distributed grains of plagioclase, sphene and hornblende. X50, Tete area (sample no.T201; Coelho, 1969).

metagabbro no.T201 in which the pyroxene is generally filled by minute plagioclase, hornblende and sphene inclusions (see Plate 27) and is surrounded by a rim of amphibole. The original plagioclase in contrast has undergone widespread size breakdown and replacement by scapolite. The process of scapolitisation is locally almost complete, and in the melanocratic scapolite granulite no.T19 relicts of orthopyroxene are occasionally preserved within a medium- to coarse-grained granonematolepidoblastic ground-mass characterised by the stable paragenesis scapolite-hornblende-orthopyroxene ± biotite. In extreme cases, anorthosite and metagabbro are converted to scapolite rock or to calcite ± scapolite rock. (Davidson and Bennett, 1950).

More than one event of shearing, mylonitisation and fabric annealing has also been identified. The complex polymetamorphic mineral relationships are summarised in Table VII-1 where olivine, colourless clinopyroxene and plagioclase are shown as primary magmatic phases. In contrast, Event 1 is marked by the development of granoblastic orthopyroxene from the reaction of olivine with plagioclase in gabbro no.T257; therefore indicating the onset of the granulite facies metamorphism (see Chapter 5, p.128 and Fig.36). Event 2 is defined by subsequent widespread shearing, generally accompanied by the growth of scapolite, hornblende, biotite from plagioclase and pyroxenes.

Davidite is the typical oxide mineral formed during this event in zones of more intense scapolitisation (Davidson and Bennett, 1950).

A later episode, presented in Table VII-1, is defined by the growth of epidote and of kyanite from plagioclase and of plagioclase, hornblende and sphene grains from the clinopyroxene (see Plate 27). In particular, kyanite occurs in sample no.T8 in a set of cataclastic bands quite distinguished from an early set of polygonised shears like those of Plate 25.
A list of the minerals occurring in the investigated samples is presented in Table VII-2.

TABLE VII-1 SEQUENCE OF METAMORPHIC MINERAL DEVELOPMENTS IN ROCKS FROM TETE

Event (1)	magmatic	1	2	3
Shearing (x)			xxxxxxxx	x
Minerals				
olivine				
clinopyroxene				
orthopyroxene				
plagioclase				
scapolite				
hornblende				
biotite				
sphene				
rutile, davidite				
kyanite, epidote				

(1) Event magmatic: see samples nos. T180, T240.
" 1 : see samples nos. T37, T78.
" 2 : see samples nos. T117, T180, T19, T8, T11.
" 3 : see samples nos. T201, T8 .

TABLE VII-2 - MINERAL ASSEMBLAGES OF ROCKS FROM THE TETE AREA, NORTH-WESTERN MOZAMBIQUE

		constituent minerals									accessories			
Slide no.	sample no.	opx	cpx	gar	hor	bio	Kfl	Nap	Cap	qtz	apt	zir	om	additional minerals
T8	T8	x							x					sca, ky
T8	ditto	x	x						x				x	
T11	T11	x				x			x					sca, chl, epi, sph, rut
T19	T19	x			x	x								sca, rut
T37	T39	x	x			x			x				x	ura
T78	T78	x	x						x					bio = tr
T117	T117	x	x											hor, sca = tr
T180	T180	x	x											pla, ura = tr
T201	T201		x						x					hor, sca, zoi, sph
T240	T240	x	x										x	olivine
T257	T257	x	x		x				x				x	olivine

The abbreviations used are the same as in Appendix II-2.

4. Mineral Chemistry

Electron-microprobe analyses of coexisting ortho- and clinopyroxene, from two samples of granulitic metagabbros (nos. T37 and T78), and of orthopyroxenes from a scapolite rock (no.T19), are presented in Table VII-3. More specific details on the techniques or equipment used, and a list of the individual analyses are presented in Appendix III.

Data presented in Table VII-3 indicate that in the two-pyroxene granulites, a magnesian hypersthene coexists with an aluminous and titaniferous augite with an appreciable Na_2O

TABLE VII-3 - ELECTRON-MICROPROBE ANALYSES OF PYROXENES FROM GRANULITE AND SCAPOLITE ROCKS OF THE TETE AREA - MOZAMBIQUE

	opx				cpx	
Sample[1] no.	T37	T78	T19	T19	T37	T78
No. of analyses	1	1	a-1	b-1	2	2
SiO_2	50,14	51,31	52,75	53,25	47,98	47,83
TiO_2	0,18	0,05	0,03	0,03	1,55	1,11
Al_2O_3	4,81	3,43	2,6	2,72	7,71	7,08
FeO	21,66	19,43	16,16	17,81	8,52	7,01
MnO	0,34	0,30	0,33	0,37	0,18	0,10
MgO	22,68	24,15	26,52	26,6	11,95	12,72
CaO	0,57	0,37	0,63	0,12	20,71	21,19
Na_2O	-	-	-	-	1,18	0,79
Total	100,38	99,03*	99,09**	100,94	99,78	97,83□
CATIONS ON THE BASIS OF 6 OXYGENS						
Si	1,859	1,903	1,927	1,920	1,795	1,812
Al^{iv}	0,141	0,097	0,073	0,080	0,205	0,188
Al	0,069	0,053	0,039	0,036	0,135	0,128
Ti	0,005	0,001	0,001	0,001	0,044	0,032
Fe	0,672	0,603	0,494	0,537	0,267	0,222
Mn	0,011	0,009	0,01	0,011	0,006	0,003
Mg	1,253	1,335	1,444	1,430	0,666	0,718
Ca	0,021	0,015	0,025	0,005	0,830	0,860
Na	-	-	-	-	0,086	0,058
Σxyz	4,031	4,017	4,015	4,021	4,033	4,022

(1) Generalized sampling area is shown in Fig.VII-A (see Coelho, 1969).

Total iron as FeO; *total includes 0,08 per cent Cr_2O_3; **total includes 0,04 per cent Cr_2O_3; and □ total includes 0,11 per cent Cr_2O_3.

content. The composition of the Tete pyroxenes is compared in Table VII-4 with the variation range of the main oxides in the hypersthene and augites from southern Malawi granulites. Table VII-4 clearly indicates the pronounced enrichment in Al_2O_3, and in TiO_2, MgO and Na_2O of the Tete pyroxenes.

The remaining mineral analyses in Table VII-3 refer to sample T19. They indicate that in this scapolite rock a relict and older bronzite (no.T19-a)is similar to a younger bronzite (no.T19-b), stable with scapolite. Qualitative electron-microprobe scans were traversed in a few samples. In pyroxenite no.T117 (see Plate 24) a scan over scapolite-hornblende-bearing microshears displayed K and Al concentrations well above background values, indicating a 'metasomatic'

TABLE VII-4 - OXIDES VARIATION RANGE IN METAMORPHIC PYROXENES FROM THE TETE AREA AND FROM SOUTHERN MALAWI

	Hypersthene		Augite	
	Tete	Malawi*	Tete	Malawi*
SiO_2	50,1 - 51,3	50,3 - 51,1	47,8 - 48,0	50,0 - 50,8
TiO_2	0,1 - 0,2	0,1 - 0,2	1,1 - 1,5	0,3 - 0,6
Al_2O_3	3,4 - 4,8	1,0 - 2,0	7,1 - 7,7	2,2 - 3,0
FeO	19,4 - 21,7	23,3 - 28,9	7,0 - 8,5	10,2 - 12,7
MgO	22,7 - 24,1	17,2 - 21,7	11,9 - 12,7	11,1 - 13,2
CaO	0,4 - 0,6	0,7 - 1,3	20,7 - 21,2	20,0 - 21,8
Na_2O	-	-	0,8 - 1,2	0,5 - 0,7

*The compared granulites of southern Malawi are samples nos. 46, 48, 55a, and 55b.
Sample localities for southern Malawi granulites are shown in Fig.9 and for the Tete area granulites see note (1) to Table VII-3.

introduction of elements. Moreover, the same results were obtained with a scan across a bright-green uralite band in pyroxenite no.180. In the two-pyroxene granulite no.T78 (see Plate 26) concentrations of Al were detected in a scan over feldspar-like grains in clinopyroxene. In addition, there is a certain number of published analyses for the oxide mineral davidite which, as previously explained (see Table VII-I) is often paragenetically associated to scapolite ± calcite or to diopside (Davidson and Bennett, 1950). From analytical data this mineral is a titanate of iron with rare earths (REE_2O_3 + ThO_2 ≈ 6,1 per cent) and uranium (e U_3O_8 ≈ 9,6 per cent) as essential constituents, and, vanadium (V_2O_5 ≈ 1,4 per cent) and chromium (Cr_2O_3 up to 4,8 per cent) as accessory constituents (Bannister and Horne, 1950; Hayton, 1960; Butler and Hall, 1960).

5. Determination of P-T metamorphic conditions

Although minimum electron-microprobe analytical data are available, temperatures ranging from 700° to 800°C have been calculated (see Table VII-5; Appendix V-1) by substituting mineral chemical data listed in Table VII-3 in equations (2), (4) and (7) of Chapter 5. A minimum pressure estimate of 5 - 7 kbar is provided in gabbro no.T257 by the reaction of olivine and plagioclase to yield orthopyroxene. This is based on published experimental results on olivine basaltic

TABLE VII-5 - GEOTHERMOMETRY OF TWO-PYROXENE GRANULITES FROM THE TETE AREA

	T-A	T-B	T-C	
Sample no.			5kbar	10kbar
T37	835	836	740	750
T78	862	853	719	726

A, B and C refer to geothermometer equations (2), (4) and (7) of Chapter 5 respectively; temperature in °C.
For sample localities see note (1) to Table VII-3.

compositions (see Table 32 and Fig.36, Chapter 5; Green and Ringwood, 1967). A reasonable estimate of the upper limit to pressure may be argued from the stability of orthopyroxene + plagioclase rather than garnet + clinopyroxene in the rocks investigated (see Fig.36, Chapter 5; Green and Ringwood, 1967).

In addition, the high Al_2O_3 content of the Tete pyroxenes relative to those from southern Malawi might have some significance, if Wilson (1976b) hypothesized correctly that Al_2O_3 content of pyroxenes tends to increase with pressure. Finally garnet-clinopyroxene-andesine rocks are associated to metagabbro in the south-western parts of the Basic Complex (Vail, 1968). From all the above data and Fig.36 it is likely that in the Tete area pressures ranged between 6 and 9 kbar at temperatures of 700 - 850°C.

6. Discussion and Conclusions

The Tete Complex is a large igneous mass characterised by anorthosite and metagabbro with minor, mainly hypermelanic rocks.

The similarity between this intrusion and the anorthosite masses of Madagascar (Boulanger, 1957) and the Kunene Complex of southern Angola (Simpson, 1970) was noted by Vail (1968), while Coelho (1969) compared it to the Bushveld Igneous Complex of South Africa. The granulite-facies metamorphic overprint, and the often megacrystic, antiperthitic nature of the constituent intermediate plagioclase (An_{50} - An_{60}) suggest, however, that the Tete Complex has distinctive affinities with the massif-type anorthosites described by Anderson and Morin (1969). In addition, the Tete Complex presents some affinity with the much smaller Linthipe anorthosite mass, characterised towards its margins by a gradation into a gabbroic rock (Bloomfield, 1968, p.136).

Petrographic and mineral chemical data, applied to published experimental results, suggest that the Tete area was metamorphosed at temperatures of between 700° - 850°C and at pressures of 6 to 9 kbar. Subsequently, the anorthosite and granulites of the Tete area underwent regional ductile deformation, shearing and mylonitisation, with development of shear zones oriented north-south (Davidson and Bennett, 1950). Subsequently, a fluid composed mainly of CO_2, Cl, H_2O and SO_3 (Coelho, 1969) migrated through the shear zones causing regional metasomatism and forming scattered mineralisations of occasional economic significance (Davidson and Bennett, 1950).

A list of the minerals associated to the metasomatised rocks is presented in Table VII-6 which also indicates some of the elements probably introduced by the fluid.

Although the overall extent of the regional metasomatism is unknown, davidite occurrences are only found within the outcrop of the Complex and were recognized over an area of ± 800 km^2; and they possibly extend below the Karoo cover ± 10 km east of Tete (see Fig.VII-A; Davidson and Bennett, 1950).

TABLE VII-6 - ORE MINERALS OF METASOMATIC ORIGIN IN THE TETE COMPLEX AREA

		GANGUE					
	Minerals	A	B	C	D	Main (minor elements)	Refs.*
oxides:	davidite	x	x	x		Ti, Fe, U, La (Ce, Cr, V, Y)	(1)
	rutile, ilmenite, magnetite	x				Ti, Fe	(1)
	pechblende				x□	U (Pb, Th)	(2)
	stibio-, niobo-tantalite				x	Ta, Sb, Nb, (U)	(2), (3)
sulphides:	pyrite, pyrrhotite	x				Fe	(1)
	chalcopyrite	x				Fe, Cu	(1)
	molybdenite	x				Mo	(1)

A, Scapolite-calcite/dolomite (± apatite, tourmaline, siderite).
B, Diopside (± vermiculite, scapolite, hornblende, tourmaline, apatite).
C, Albite ± calcite (± tourmaline).
D, Uncertain; □: as nodules in plagioclase of (meta-) gabbro.

*References: (1) Davidson and Bennett, 1950; (2), Real, 1966; (3) Coelho, 1969.

The stability of the paragenesis scapolite-bronzite-hornblende in sample no.T19 tentatively suggests that the metasomatic event took place under high-grade metamorphic conditions and that at least occasionally the activity of H_2O in the vapour was

rather low. These conclusions are supported by (a) the observed reaction of dolomite with quartz to yield diopside (and CO_2) (Davidson and Bennett, 1950) which moves to the right if $T > 625^{o}C$ and a $\overset{vapour}{CO_2} \geq 95$ moles per cent at $P_{vapour} \approx 5$ kbar (in: Winkler, 1976, p.121); and (b) the pegmatite-like dimensions attained by davidite, frequently found in shattered crystals with a diameter exceeding 30 cm (Davidson and Bennett, 1950).

The age of the granulite facies metamorphism is unknown at present but the available data do not support the implication by Saggerson and Turner (1980) that the Tete Complex is part of a small Archean craton older than 2 500 m.y. In particular, (a) the P-T conditions of the Tete area are comparable to those of Zomba-Blantyre; (b) typical Mozambiquian amphibolite and granulite facies rocks occur in the Tambani area of Malawi at less than 20 km from the Tete Complex (see Fig.VII-A); (c) there is a substantial similarity between the shearing and scapolitisation events which affected the regions of Tete and of Tengani in southern Malawi (see Table 2, Chapter 2); (d) davidite-bearing feldspathic mylonite occurs within the gneisses of the Tambani area in proximity of the Mwanza fault (see sample no.509, Table II-2; Fig.VII-A; Cooper and Bloomfield, 1961); and finally (e) the Complex intrudes into the Fingoé System (Mouta and Dias, 1957), correlable, if Vail (1965b) is correct, with the Umkondo System; and according

to this reasoning the Complex is younger than 1 800 m.y. (Professor T.N. Clifford, personal communication). From the above considerations it is tentatively concluded that the Tete Complex is akin to the massif-type anorthosite bodies in orogenic terranes and it was affected by medium-pressure granulite facies metamorphism during the Mozambiquian Orogenic cycle.

LIST OF REFERENCES

ALBEE, A.L., AND RAY, L. (1968). Correction factors for electron probe microanalysis of silicates, oxides, carbonates, phosphates and sulphates. Anal. Chem., 42: 382-403.

_____ (1970). Correction factors for electron probe microanalysis of silicates, oxides, carbonates, phosphates and sulphates. Anal. Chem., 42: 1408-1414.

ALTHAUS, E. (1967). The triple point andalusite-sillimanite-kyanite. Contrib. Mineral. Petrol., 16: 29-44.

_____ (1969a). Das System Al_2O_3-SiO_2- H_2O. Experimentelle Untersuchungen und Folgerungen für die Petrogenese der metamorphen Gesteine. Neues Jahrb. Mineral. Abhand., 111: 74-161.

_____ (1969b). Experimental evidence that the reaction of kyanite to form sillimanite is at least bivariant. Am. J. Sci., 267: 273-277.

ALTHAUS, E., KAROTKE, E., NITSCH, K.H., AND WINKLER, H.G.F. (1970). An experimental re-examination of the upper stability limit of muscovite + quartz. Neues Jahrb. Mineral. Monatsh., 1970: 325-336.

ANDERSON, C.A. (1941). Volcanoes of the Medicine Lake Highlands, California. Univ. California Dept. Geol. Sci. Bull., 25: 347-422.

ANDERSON, A.T.Jr., AND MORIN, M. (1969). Two types of massif anorthosites and their implications regarding the thermal history of the crust. In: Isachsen, Y.W., ed., Origin of anorthosite and related rocks. New York State Mus. Sci. Serv. Mem., 18: 57-69.

ANDREW, A.R., AND BAILEY, T.E.G. (1910). The geology of Nyasaland. J. Geol. Soc. London, 66: 189-251.

ANDREWS, E.M. (1974). Gravity survey of Malawi, fieldwork and processing. Inst. Geol. Sci. London Rep., 74/15.

AOKI, K., AND KUSHIRO, I. (1968). Some clinopyroxenes from ultramafic inclusions in Dreiser Weiher, Eifel. Contrib. Mineral. Petrol., 18: 325-337.

AOKI, K. (1975). Origin of phologopite- and potassic richterite-bearing peridotite xenoliths from S. Africa. Contrib. Mineral. Petrol., 53: 145-156.

ARAUJO, J.R.F. (1967). The Mozambique Belt in the Barue area, Manica and Sofala District, Mozambique, with special reference to the petrology, stratigraphy and metamorphism. Univ. Leeds Inst. African Geol., 11th Ann. Rept.: 19.

ASSUNÇAO, C.F. TORRE DE, AND COELHO, A.V.P. (1956). The rocks with charnockitic affinities in Mozambique. Moçambique Serviços Indústria e Geologia Bol., 19: 173-181.

BANNISTER, F.A., AND HORNE, J.E.T. (1950). A radioactive mineral from Mozambique related to davidite. Mineral. Mag., 29: 101-112.

BARTHOLOME, P. (1962). Iron-magnesium ratios in associated pyroxenes and olivines. In: Engel, A.E.J., James, H.L., and Leonard, B.F., eds., Petrologic studies: a volume in honor of A.F. Buddington. New York, Geol. Soc. Am.: 1-20.

BARTRUM, S.A. (1936). Spilitic rocks of New Zealand. Geol. Mag., 73: 414-423.

BEHR, H.J. ET AL. (1971). Granulites - results of a discussion. Neues Jahrb. Mineral. Monatsh., 3: 97-123.

BELLINGHAM, K.S. AND BROOMLEY, J. (1973). The geology of the Ntchisi-Middle Bua area. Geol. Surv. Malawi Bull., 27.

BENCE, A.E., AND ALBEE, A.L. (1968). Empirical correction factors for the electron microanalysis of silicates and oxides. J. Geol., 76: 382-403.

BERRANGE, J.P. (1966). Some critical differences between orogenic-plutonic and gravity stratified anorthosites. Geol. Rdsch., 55: 617-642.

BLATT, H., MIDDLETON, G., AND MURRAY, R. (1972). Origin of Sedimentary Rocks. Englewood-Cliffs, N.J., Prentice Hall.

BLOOMFIELD, K. (1958). The geology of the Port Herald area. Geol. Surv. Nyasaland Bull., 9.

_____ (1965a). The geology of the Zomba area. Geol. Surv. Malawi Bull., 16.

_____ (1965b). Infracrustal Ring-Complexes of southern Malawi. Geol. Surv. Malawi Mem., 4.

_____ (1966). A major east-north-east dislocation zone in central Malawi. Nature, 211: 612-614.

_____ (1967). Aegirine gneisses in central Malawi. J. Geol. Soc. London, 123: 93-98.

_____ (1968). The pre-Karroo geology of Malawi. Geol. Surv. Malawi Mem., 5.

_____ (1970). Orogenic and post-orogenic plutonism in Malawi. In: Clifford, T.N., and Gass, I.G., eds., African magmatism and tectonics, Edinburgh, Oliver and Boyd: 119-155.

BLOOMFIELD, K., AND GARSON, M.S. (1965). The geology of the Kirk Range-Lisungwe Valley area. Geol. Surv. Malawi Bull., 17.

BORLEY, G.D. (1974). Oceanic Island. In: Sorensen, H., ed., The alkaline rocks. London, J. Wiley and Sons: 311-330.

BOULANGER, J. (1957). Les anorthosites de Madagascar. C.C.T.A., 2nd Meeting Regional Comm. for Geol., Tananarive: 55-60.

BOWES, D.R., AND PARK, R.G. (1966). Metamorphic segregation and banding in the Loch Kerry basite sheet from the Lewisian of Gairloch, Ross-shire, Scotland. J. Petrol., 7: 306-333.

BREWER, M.S., HASLAM, H.M., DARBYSHIRE, D.P.F., AND DAVIS, A.E. (1979). The petrology and geochronology of hypersthene granites in the Mchinji area, Malawi. Inst. Geol. Sci. London Rep., 79/1.

BRIDGWATER, D. AND WATTERSON, J.S. (1967). Igneous intrusions and associated rocks of the mangerite-charnockite suite. Nature, 213: 897.

BRIDGWATER, D. AND WINDLEY, B.F. (1973). Anorthosites, post-orogenic granites, acid volcanic rocks and crustal development in the North Atlantic shield during the mid-Proterozoic. In: Lister, L.A., ed., Symposium on granites, gneisses and related rocks. Geol. Soc. S. Afr., Spec. Publ., 3: 307-317.

BRIDGWATER, D., SUTTON, J., AND WATTERSON, J. (1974). Crustal downfolding associated with igneous activity. Tectonophysics, 21: 57-77.

BROOKS, C., HART, S.R., AND WENDT, I. (1972). Realistic use of two error regression treatments as applied to rubidium-strontium data. Rev. Geophys. Space Phys., 10: 551-577.

BROWN, G.C., AND FYFE, W.S. (1970). The production of granitic melts during ultrametamorphism. Contrib. Mineral. Petrol., 28: 310-318.

BUDDINGTON, A.F. (1939). Adirondack igneous rocks and their metamorphism. Geol. Soc. Am. Mem., 7.

BÜSCH, W., SCHNEIDER, G., AND MEHNERT, K.R. (1974). Initial melting at grain boundaries. Part III: Melting in rocks of granodioritic, quartz-dioritic and tonalitic composition. Neues Jahrb. Mineral. Monatsh., 1974: 345-370.

BUTLER, J.R., AND HALL, R. (1960). Chemical characteristics of davidite. Econ. Geol., 55: 1541-1550.

CABY, R. (1970). La chaine pharusienne dans le nord-ovest de l'Ahaggar (Sahara central, Algérie); sa place dans l'orogenèse du Précambrien supérieur en Afrique. (D.Sc. thesis) Montpellier, France, Univ. Montpellier.

CAHEN, L. (1957). L'age de la 'davidite' de Mavuzi (Tete). Mocambique Servicos Industria e Geologia Bol., 19: 35-38.

_____ (1970). Igneous activity and mineralisation episodes in the evolution of the Kibaride and Katangide orogenic belts in Central Africa. In: Clifford, T.N., and Gass, I.G., eds. African Magmatism and Tectonics. Edinburgh, Oliver and Boyd: 97-117.

CANNON, R.T., HOPKINS, D.R., THATCHER, E.C., PETERS, E.R., KEMP, J., GASKELL, J.L., AND RAY, G.C. (1969). Polyphase deformation in the Mozambique Belt. Northern Malawi. Geol. Soc. Am. Bull., 80: 2615-2622.

CARMICHAEL, I.S.E., TURNER, F.J., AND VERHOOGEN, J. (1974). Igneous Petrology. New York, McGraw-Hill.

CARTER, G.S., AND BENNETT, J.D. (1973). The geology and mineral resources of Malawi (2nd revised edition). Geol. Surv. Malawi Bull., 6.

CAWTHORN, R.G., AND COLLERSON, K.D. (1974). The recalculation of pyroxene end-members parameters and the estimation of ferrous and ferric iron content from electron-microprobe analyses. Am. Mineral., 59: 1203-1208.

CLARK, L. (1967) Differential retrogressive metamorphism in granulites of the Karasuk Group, Karamonga, Uganda. Geol. Mag., 104: 289-297.

CLIFFORD, T.N. (1974). Review of African granulites and related rocks. Geol. Soc. Am. Spec. Pap., 156.

CLIFFORD, T.N., GRONOW, J., REX., D.C., AND BURGER, A.J. (1975). Geochronological and petrogenetic studies of high-grade metamorphic rocks and intrusives in Namaqualand, South Africa. J. Petrol., 16: 154-188.

COELHO, A.V.P. (1956). Breves notas petrologicas referentes à regiao de Angonia. Moçambique Serviços Indústria e Geologia Bol., 19: 97-111.

_____ (1969). O complexo gabro-anorthositico de Tete (Moçambique). Moçambique Serviços Geologia e Minas Bol., 35: 63-78.

COOPER, W.G.G., AND BLOOMFIELD, K. (1961). The geology of the Tambani-Salambidwe area. Geol. Surv. Nyasaland Bull., 13.

DALY, R.F. (1933). Igneous rocks and the depth of the earth. New York, McGraw-Hill.

DARNLEY, A.G., HORNE, M.A., SMITH, G.H., CHANDLER, T.R.D., DANCE, D.F., AND PREECE, E.R. (1961). Ages of some uranium and thorium minerals from East Central Africa. Mineral. Mag., 32: 716-724.

DAVIDSON, C.F., AND BENNETT, J.A.E. (1950). The uranium deposits of the Tete District, Mozambique. Mineral. Mag., 32: 291-303.

DAVIES, R.D., ALLSOPP, H.L., ERLANK, A.J. AND MANTON, W.I. (1970). Sr-isotopic studies on various layered mafic intrusions in Southern Africa. Geol. Soc. S. Afr. Spec. Publ., 1: 576-593.

DAWSON, A.L., AND KIRKPATRICK, I.M. (1968). The geology of the Cape Maclear Peninsula - Lower Bwanje Valley area. Geol. Surv. Malawi Bull., 28.

DEER, W.A., HOWIE, R.A., AND ZUSSMAN, J. (1962 & 1963). Rock forming minerals. 5 volumes. London, Longmans, Green and Co.

DELHAL, J. (1957). Les massifs cristallins de la Lulua et de la Lueta (Masai). Univ. Louvain Inst. Geol. Mem., 20: 211-281.

_____ (1963). Le socle de la region de Luiza (Masai). Annales Mus. Roy. de l'Afrique Centrale, 45.

DODSON, M.H., CAVANAGH, B.J., THATCHER, E.G., AND AFTALION, M. (1975). Age limits for the Ubendian metamorphic episode in northern Malawi. Geol. Mag., 112: 403-410.

ELLIS, D.J., AND GREEN, D. (1979). An experimental study of the effect of Ca upon garnet-clinopyroxene Fe-Mg exchange equilibria. Contrib. Mineral, Petrol., 71: 13-22.

EMSLIE, R.F. (1973). Some chemical characteristics of the anorthosite suites and their significance. Can. J. Earth Sci., 10: 54-71.

_____ (1975). Pyroxene megacrysts from anorthositic rocks: new clues to the sources and evolution of the parent magma. Can. Mineral., 13: 138-145.

EVANS, R.K. (1965). The geology of the Shire Highlands. Geol. Surv. Malawi Bull., 18.

EVANS, B.W., AND LEAKE, B.E. (1960). The composition and origin of the striped amphibolites of Conemara, Ireland. J. Petrol., 1: 337-363.

EVANS, B.W., AND TROMMSDORF, V. (1978). Petrogenesis of garnet lherzolite, Cima di Gagnone, Lepontine Alps. Earth and Planetary Sci. Letters, 40: 333-348.

ESKOLA, P. (1921). On the eclogites of Norway. Skr. Vidensk. Selsk. Kristiania, 8: 1-118.

FERRY, J.M., AND SPEAR, F.S. (1978). Experimental calibration of the partitioning of Fe and Mg between biotite and garnet. Contrib. Mineral. Petrol., 66: 113-117.

FIELD, D., AND CLOUGH, P.W.L. (1976). K/Rb ratios and metasomatism in metabasites from a Precambrian amphibolite-granulite transition range. J. Geol. Soc. London, 132: 277-288.

FISHER, J.R. AND ZEN, E-AN (1971). Thermochemical calculations from hydrothermal phase equilibrium data and the free energy of H_2O. Am. J. Sci., 270: 297-314.

FITCHES, W.R. (1968). New K-Ar age determinations from the Precambrian Mafingi Hills area of Zambia and Malawi. Univ. Leeds Inst. African Geol., 12th Ann. Rept: 12-14.

FLANAGAN, F.J. (1973). 1972 values for international geochemical reference samples. Geochim. Cosmochim. Acta, 37: 1189-1200.

FREITAS, A.J. DE, compiler (1956). Esboço Geologico Provincia de Moçambique Lourenco Marques, Junta de Comercio Externo. Scale 1 : 2 000 000; 1 sheet.

FREITAS, A.J. DE (1957). Noticia explicativa do esboço geologico de Moçambique (1 : 2 000 000). Moçambique Serviços Indústria e Geologia Bol., 23.

_____ (1959). A geologia e o desenvolvimento economico e social de Moçambique. Lourenço Marques, Junta de Comercio Externo.

GARSON, M.S., AND WALSHAW, R.D. (1969). The geology of the Mlanje area. Geol. Surv. Malawi Bull., 21.

GILL, J.B. (1970). Geochemistry of Viti Levu, Fiji and its evolution as an island arc. Contrib. Mineral. Petrol., 27: 179-203.

GILLULY, J. (1935). Keratophyres of eastern Oregon and the spilitic problem. Am. J. Sci., 229: 225-252.

GITTINS, J., ALLEN, C.R., AND COOPER, A.F. (1975). Phlogopitization of pyroxenite; its bearing on the composition of carbonatite magmas. Geol. Mag., 112: 503-507.

GREEN, D.H., AND RINGWOOD, A.E. (1967). An experimental investigation of the gabbro to eclogite transformation and its petrological applications. Geochim. Cosmochim. Acta., 31: 767-833.

GREEN, T.H. (1969). High pressure experimental studies on the origin of anorthosite. Can. J. Earth Sci., 6: 427-440.

GROOME, D.R., AND HALL, H. (1974). The geochemistry of the Devonian lavas of the northern Lorne Plateau, Scotland. Mineral. Mag., 39: 621-640.

HABGOOD, F. (1959). The geology of the Cholo area. Geol. Surv. Nyasaland, Ann. Rept. for 1958: 14-15.

HABGOOD, F., HOLT, D.N., AND WALSHAW, R.D. (1973). The geology of the Thyolo area. Geol. Surv. Malawi Bull., 22.

HARGRAVES, R.B. (1962). Petrology of the Allard Lake anorthosite suite, Quebec. In: Engel, A.E.J., James, H.L., and Leonard, B.F., eds., Petrologic studies. New York, Geol. Soc. Am.: 163-190.

HARME, M. (1965). On the potassium migmatites of southern Finland. Com. Geol. Finland Bull., 219.

HASLAM, H.W., HARDING, R.R., AND TRESHAM, A.E. (1976). Chromite-chlorite intergrowths in peridotite at Chimwadzulu Hill, Malawi. Mineral. Mag., 40: 695-701.

HAYTON, J.D. (1960). The constitution of davidite. Econ. Geol. 55: 1030 - 1038.

HAWKESWORTH, C.J., KRAMERS, J.D., AND MC G. MILLER, R. (1981). Old model Nd ages in Namibian Pan-African rocks. Nature, 289: 278-282.

HEDGE, C.H. (1966). Variations in radiogenic strontium found in volcanic rocks. J. Geophys. Res., 71: 6119-6126.

HEIER, K.S. (1964). Rubidium-strontium and strontium-87/strontium-86 ratios in deep crustal material. Nature, 202: 477-478.

HERDSMAN, W.H., analyst (1963). Analyses of rocks carried out in 1963. Geol. Surv. Malawi Rec., 5: 133-135.

HERZ, N. (1968). Anorthosite belts, continental drift, and the anorthosite event. Science, 164: 944-946.

HIETANEN, A. (1969). Metamorphic environment of anorthosite in the Boehls Butte area, Idaho. In: Isachsen, Y.W., ed., Origin of anorthosite and related rocks. New York State Mus. Sci. Serv. Mem., 18: 371-386.

HIGGINS, M.D., AND DOIG, R. (1977). 540 m.y. old anorthosite complex in the Grenville Province of Quebec, Canada. Nature, 267: 40-41.

HOLT, D.N. (1961). The geology of part of Fort Johnston District, east of Lake Nyasa. Geol. Surv. Nyasaland Rec., I: 23-39.

HORROCKS, P.C. (1980). Ancient Archaean supracrustal rocks from the Limpopo Mobile Belt. Nature, 286: 596-599.

HOSCHEK, G. (1969). The stability of staurolite and chloritoid and their significance in metamorphism of pelitic rocks. Contrib. Mineral. Petrol., 22: 208-232.

HUNZIKER, J.C. (1979). Potassium-argon dating. In: Jäger, E., and Hunziker, J.C. eds., Lectures in isotope geology. Berlin, Springer-Verlag: 52-76.

IRVING, A.J. (1974). Geochemical and high-pressure experimental studies of garnet pyroxenite and pyroxene granulite xenoliths from the Delegate basaltic pipes, Australia. J. Petrol., 15: 1-40.

ISACHSEN, Y.W. (1969). Origin of anorthosite and related rocks, a summarization. In: Isachsen, Y.W., ed., Origin of anorthosite and related rocks. New York State Mus. Sci. Serv. Mem., 18: 435-445.

JAKES, V.P., AND WHITE, A.J.R. (1970). K/Rb ratios of rocks from island arcs. Geochim. Cosmochim. Acta, 34: 849-856.

JANARDHAN, A.S., NEWTON, R.C., AND SMITH, J.V. (1979). Ancient crustal metamorphism at low P_{H_2O}: charnockite formation at Kabbaldurga, south India. Nature, 278: 511-514.

JOUBERT, P. (1971). The regional tectonism of the gneisses of part of Namaqualand. Univ. Cape Town Dept. Geol. Chamber Mines Precambrian Res. Unit Bull., 10.

KEMP, J. (1974). The Precambrian geology of two areas in Malawi, its significance for the Mozambiquian and Ubendian Belts. Univ. Leeds Inst. African Geol. 18th Ann. Rep.: 30-31.

KISTLER, R.W. (1974). Phanerozoic batholiths in western North America. Am. Rev. Earth Plan. Sci., 2: 403-418.

KNABE, W. (1970). Anatexis von Quartz-Plagioklas-Biotit-Metamorphiten. Geol. Jahrb., 89: 1-32.

KRANCK, E.H. (1969). Anorthosites and rapakivi, magmas from the lower crust. In: Isachsen, Y.W., ed., Origin of anorthosite and related rocks. New York State Mus. Sci. Serv. Mem., 18: 93-97.

KRÖNER, A. (1977). Precambrian mobile belts of southern and eastern Africa - Ancient sutures or sites of ensialic mobility? A case for crustal evolution towards plate tectonics. Tectonophysics, 40: 101-135.

KUNO, H. (1950). Petrology of the Hakone Volcano and the adjacent areas, Japan. Geol. Soc. Am. Bull., 61: 957-1020.

_____ (1968). Differentiation of basalt magmas. In: Hess, H.H., and Poldervaart, A., eds., Basalts - the Poldervaart treatise on rocks of basaltic composition, vol. 2. New York, Interscience Pubs.: 623-688.

LAMBERT, I.B., AND HEIER, K.S. (1968). Geochemical investigations of deep seated rocks in the Australian Shield. Lithos, 1: 30-53.

LAMBERT, R. st. J., AND HOLLAND, J.G. (1974). Yttrium geochemistry applied to petrogenesis utilizing calcium-yttrium relationships in mineral and rocks. Geochim. Cosmochim. Acta, 38: 1393-1414.

LA ROCHE, H. DE (1966). Sur l'existence de plusiers facies geochimiques dans les shists paleozoiques des Pyrenees Luchonnaises. Geol. Rdsch., 55: 274-301.

LEWIS, J.D., AND SPOONER, C.M. (1973). K/Rb ratios in Precambrian granulite terraines. Geochim. Cosmochim. Acta, 37: 1111-1118.

LIOU, S.G. (1971). Synthesis and stability relations of prehnite, $Ca_2Al_2Si_2O_{10}(OH)_2$. Am. Mineral., 56: 507-531.

LLOYD, F.E., AND BAILEY, D.K. (1973). Light element metasomatism of the continental mantle: the evidence and the consequences. Physics and Chem. of the Earth, 9: 389-416.

LUNA, I.R. DE, E FREITAS, F. (1953). Geologia e metalogenia dos depositos de uranio do vale de Mavudzi. Moçambique Serviços Indústria e Geologia Bol., 11.

MACDONALD, G.A. (1968). Composition and origin of Hawaiian lavas. Geol. Soc. Am. Mem., 116: 477-522.

MACGREGOR, I.D. (1964). The reaction 4 enstatite + spinel = fosterite + pyrope. Carnegie Inst. Wash. Yearbook, 63: 157.

MARTIN, H., AND PORADA, H. (1977). The infracratonic branch of the Damara Orogen in South West Africa. II-Discussion of relationships with the Pan-African mobile belt system. Precambrian Res., 5: 339-357.

McCARTHY, T.S. (1976). Chemical interrelationships in a low pressure granulite terrain in Namaqualand, South Africa and their bearing on granite genesis and the composition of the lower crust. Geochim. and Cosmochim. Acta, 40: 1057-1068.

_____ (1977). Geochemical studies of selected granitic terrains in South Africa. (Unpublished Ph.D. thesis) Johannesburg, Univ. of the Witwatersrand.

McCARTHY, T.S., AND CAWTHORN, R.G. (1980). Changes in initial $^{87}Sr/^{86}Sr$ ratio during protracted fractionation in igneous complexes. J. Petrol., 21: 245-264.

MEHNERT, K.R. (1968). Migmatites and the origin of granitic rocks. Amsterdam, Elsevier.

MERRILL, R.B., ROBERTSON, J.K., AND WYLLIE, P.S. (1970). Melting reactions in the system $NaAlSi_3O_8$-$KAlSi_3O_8$-SiO_2-H_2O to 20 Kilobars compared with results for other feldspar-quartz-H_2O and rock-H_2O systems. J.Geol., 78: 558-569.

MISCH, P., AND RICE, J.M. (1975). Miscibility of tremolite and hornblende in progressive Skagit metamorphic suite, north Cascades, Washington. J. Petrol., 16: 1-21.

MOREL, S.W. (1958). The geology of the Middle Shire area. Geol. Surv. Nyasaland Bull., 10.

_____ (1961a). Amphibolite-granulite facies assemblages in southern Nyasaland. Mineral.Mag., 32: 725-730.

_____ (1961b). Pre-Cambrian perthosites in Nyasaland. Geol. Mag., 98: 235-244.

MOUTA, F., AND DIAZ, F.B. (1957). Quelques elements nouveax sur les formations anciennes du Mozambique (Système Mozambiquien). Moçambique Serviços Indústria e Geologia Bol., 24: 39-46.

NEWTON, R.C., SMITH, J.V., AND WINDLEY, B.F. (1980). Carbonic metamorphism, granulites and crustal growth. Nature, 288: 45-50.

NICOLAYSEN, L.O., AND BURGER, A.J. (1965). Note on an extensive zone of 1 000 million-year old metamorphic and igneous rocks in southern Africa. Sci. Terre, 10: 500-518.

NOCKOLDS, S.R. (1954). Average chemical composition of some igneous rocks. Geol. Soc. Am. Bull., 65: 1007-1032.

NOCKOLDS, S.R. AND ALLEN, R. (1954). The geochemistry of some igneous rock series, Part II. Geochim. Cosmochim. Acta. 5: 245-285.

NORRISH, K., AND HUTTON, J.T. (1969). An accurate X-ray spectrographic method for the analysis of a wide range of geological materials. Geochim. Cosmochim. Acta., 93: 431-453.

OBATA, M. (1980). The Ronda peridotite: garnet-, spinel-, and plagioclase-lherzolite facies and the P-T trajectories of a high-temperature mantle intrusion. J.Petrol., 21: 533-572.

OBERHOLZER, W.F., compiler (1968). Carta geologica do Moçambique. Direcção Provincial Serviços Geologia e Minas, scale 1 : 2 000 000; 1 sheet.

O'HARA, M.J. (1967). Garnetiferous ultrabasic rocks of orogenic regions. In: Wyllie, P.J., ed., Ultramafic and related rocks. New York, J. Wiley and Sons: 167-172.

_____ (1968). The bearing of the phase equilibria studies in synthetic and natural systems on the origin and evolution of basic and ultrabasic rocks. Earth Sci. Rev., 4: 69-133.

O'HARA, M.J., RICHARDSON, S.W., AND WILSON, G. (1971). Garnet peridotite stability and occurrence in crust and mantle. Contrib. Mineral. Petrol., 32: 48-68.

O'HARA, M.J., AND YARWOOD, G. (1978). High pressure-temperature point on an Archaean geotherm, implied magma genesis by crustal anatexis and consequences for garnet-pyroxene thermometry and barometry. Phil. Trans. Roy. Soc. London, A288 : 441-456.

OLIVER, R.L., AND SCHULTZ, P.K. (1968). Colour in charnockites. Mineral.Mag., 36: 1135-1138.

ONSTOTT, T.C., AND HARGRAVES, R.B. (1981). Proterozoic transcurrent tectonics: paleomagnetic evidence from Venezuela and Africa. Nature, 289: 131-136.

PETERS, E.R. (1969). The geology of the Kasungu area. Geol. Surv. Malawi Bull., 25.

PETTIJOHN, F.J., POTTER, P.E., AND GIEVER, R. (1972). Sand and Sandstone. Berlin, Springer-Verlag.

PICHAMUTHU, C.S. (1969). Nomenclature of charnockites. Indian Minerals, 10: 23-35.

PIPER, J.D.A. (1976). Palaeomagnetic evidence for a proterozoic super-continent. Phil. Trans. Roy. Soc. London, A280: 469-490.

POWELL, R. (1975). Thermodynamics of coexisting cummingtonite-hornblende pairs. Contrib. Mineral.Petrol., 51: 29-37.

_____ (1978). The thermodynamics of pyroxene geotherms. Phil. Trans. Roy. Soc. London, A288: 457-469.

RAHEIM, A., AND GREEN, D.H. (1974). Experimental determination of the temperature and pressure dependence of the Fe/Mg partitioning coefficient for co-existing garnet and clinopyroxene. Contr. Mineral. Petrol., 48: 179-203.

RAMSAY, C.R., AND RIDGWAY, J. (1977). Metamorphic patterns in Zambia and their bearing on problems of Zambia metamorphic history. Precambrian Res., 4: 321-337.

RAY, G.E. (1974). The structural and metamorphic geology of northern Malawi. J. Geol. Soc. London, 130: 427-440.

REAL, F. (1966). Geologia da bacia do rio Zambeze (Moçambique) - caracteristicas geológico-mineiras da bacia do em Zambese, em territorio moçambicano. Lisboa, Junto de Investigaçoes do Ultramar.

REYNOLDS, R.C. (1963). Matrix correction in X-ray analysis. Am. Mineral. 48: 1133-1143.

_____ (1967). The estimation of mass absorption coefficients by Compton scattering: improvements and extensions of the method. Am. Mineral., 48: 1133-1143.

RICHARDSON, S.W., BELL, P.M., AND GILBERT, M.C. (1968). Kyanite-sillimanite equilibrium between 700° and 1500°. Am. J. Sci., 266: 513-541.

_____ (1969). Experimental determination of kyanite-andalusite and andalusite-sillimanite equilibria: the aluminium triple point. Am. J. Sci., 26: 259-272.

ROBINSON, D., AND LEAKE, B.E. (1975). Sedimentary and igneous trends on AFM diagrams. Geol. Mag., 112: 305-307.

RUSSEL, B.G., ET AL. (1972). Preliminary report on the analysis of the six NIMROC geochemical standard samples. (S.Afr.)National Institute for Metallurgy, Res. Rep. No. 1351.

SAGGERSON, E.P. (1973). Metamorphic facies series in Africa: a contrast. In: Lister, L.A., ed., Symposium on granites, gneisses and related rocks. Geol. Soc. S. Africa Spec. Publ., 3: 227-334.

SAGGERSON, E.P., AND TURNER, L.M. (1980). Distribution of regional metamorphism in Africa. Geol. Rdsch., 69: 745-756.

SCHAFFER, H.N.S. (1966). The determination of iron (II) oxide in silicate and refractory materials. The Analyst, 91: 755-770.

SEN, S.K., AND RAY, S. (1971). Hornblende-pyroxene granulites versus pyroxene granulites: A study from the type charnockite area. Neues Jahrb. Mineral. Abhand., 115: 291-314.

SHACKLETON, R.M. (1973). Correlation of structures across Precambrian orogenic belts in Africa. In: Tarling, D.H., and Runcorn, S.K., eds., Implications of continental drift to the Earth Sciences, 2. London, Academic Press: 1091-1095.

_____ (1976). Pan-African structures. Phil. Trans. Roy. Soc. London, A280: 491-497.

SHAPIRO, L., AND BRANNOCK, W.W. (1962). Rapid analysis of silicate, carbonate and phosphate rocks. U.S. Geol. Surv. Bull., 114-A.

SHAW, D.M. (1968). A review of K-Rb fractionation trends by covariance analysis. Geochim. Cosmochim. Acta, 32: 573-601.

SHARFMAN, R.S. (1968). On the average chemical composition of spilites. Doklady, A.N., USSR, 180-1: 202-203 (in Russian).

SHERATON, J.W., SKINNER, A.C., AND TARNEY, J. (1973). The geochemistry of the Scourian gneisses of the Assynt district. In: Park, R.G., and Tarney J., eds. The early Precambrian of Scotland and related rocks of Greenland. Lewisian conferences, 2nd, Newcastle, University of Keele, England: 13-30.

SIGHINOLFI, G.P. (1969). K/Rb ratios in high-grade metamorphism: a confirmation of the hypothesis of a continual crustal evolution. Contrib. Mineral. Petrol., 21: 346-356.

SIGHINOLFI, G.P., AND GORGONI, C. (1975). Genesis of massif-type anorthosites - the role of high grade metamorphism. Contrib. Miner. Petrol., 51: 119-126.

SIMPSON, E.S.W. (1970). The anorthosite of southern Angola: a review of present data. In: Clifford, T.N., and Gass, I.G., eds., African magmatism and tectonics. Edinburgh, Oliver and Boyd: 89-96.

SMITH, E.B. (1973). Basic chemical thermodynamics. Oxford, Clarendon Press.

SNELLING, N.J. (1963). Age Determination Unit. Inst. Geol. Sci. London Overseas Geol. Surv., Ann. Rep. for 1962: 30-39.

SNELLING, N.J., JOHNSON, R.L., AND DRYSDALL, A.R. (1972). The geochronology of Zambia. Geol. Surv. Zambia Rec., 12: 19-30.

STANTON, R.L. (1972). Ore petrology. New York, McGraw-Hill.

STEUHL, H.H. (1962). Die experimentelle metamorphose und anatexis eines parabiotitgneisses auf dein Schwarzwald. Chem. Erde, 21: 413-418.

STORRE, B., AND KAROTKE, E. (1972). Experimental data on melting reactions of muscovite + quartz in the system K_2O-Al_2O_3-SiO_2- H_2O to 20 Kb water pressure. Contrib. Mineral. Petrol., 30: 343-345.

STRECKEISEN, A. (1976). To each plutonic rock its proper name. Earth Sci. Rev., 12: 1-33.

SUNDIUS, N. (1930). On the spilitic rocks. Geol. Mag., 67: 1-17.

SWARDT, A.M.J. DE, GARRAND, P., AND SIMPSON, J.G. (1965). Major zones of transcurrent dislocation and superimposition of orogenic belts in parts of Central Africa. Geol. Soc. Am. Bull., 76: 89-102.

TARNEY, J. (1976). Geochemistry of Archaean high-grade gneisses, with implications as to the origin and evolution of the Precambrian crust. In: Windley, B.F., ed., The early history of the earth. London, J. Wiley and Sons: 405-417.

TARNEY, J., SKINNER, A.C., AND SHERATON, J.W. (1972). A geochemical comparison of major Archaean gneiss units from north-west Scotland and east Greenland. Montreal, 24th Int. Geol. Congress Rept., 1: 162-174.

TAYLOR, S.R., CAPP, A.C., GRAHAM, A.L., AND BLAKE, D.H. (1969). Trace element abundances in andesite. II-Saipan, Bouganville and Fiji. Contrib. Mineral. Petrol., 23: 1-26.

THATCHER, E.C. (1968). The geology of the Dedza area. Geol. Surv. Malawi Bull., 29.

_____ (1973). Gneisses and granites in the Malawi province of the Mozambique belt. In: Lister, L.A., ed., Symposium on granites, gneisses and related rocks. Geol. Soc. S.Afr. Spec. Publ., 3: 149-156.

THATCHER, E.C., AND WALTER, M.J. (1968). The geology of the South Lilongwe Plain and Dzalanyama Range. Geol. Surv. Malawi Bull., 23.

THATCHER, E.C., AND WILDERSPIN, K.E. (1968). The geology of the Mchinji-Upper Bua area. Geol. Surv. Malawi Bull., 24.

THOMPSON, R.N. (1974). Some high pressure pyroxenes. Mineral. Mag., 39: 768-782.

TOURET, M.J. (1975). Facies granulite et fluid carbonique. In: Bellière, J., and Duelesne, J.C., eds., Geologie des Domaines Cristallins. Liège, Soc. Geol. Belgique: 267-287.

TUTTLE, O.F., AND BOWEN, N.J. (1958). Origin of granite in the light of experimental studies in the system $NaAlSi_3O_8$-SiO_2-H_2O. Geol. Soc. Am. Mem., 74.

VAIL, J.R. (1965a). An outline of the geochronology of the late Precambrian formations of eastern Central Africa. Roy. Soc. London Proc., A284: 354-369.

VAIL, J.R. (1965b). Progress report on regional studies of the Umkondo System and Fingoé Series, Central Africa. Univ. Leeds, Inst. African Geol., 9th Ann. Rep.: 11-14.

VAIL, J.R. (1968). Preliminary investigation of the Tete Complex, Mozambique. Univ. Leeds Inst. African Geol., 12th Ann. Rep.: 23-25.

VORE, G.W. DE (1975). The role of partial melting of metasediments in the formation of the anorthosite-norite-syenite complex, Laramic range, Wyoming. J. Geol., 83: 749-762.

VRANA, S., PRASAD, R., AND FEDIUKOVA, E. (1975). Metamorphic kyanite eclogites in the Lufilian arc of Zambia. Contrib. Mineral. Petrol., 51: 139-160.

WAARD, D. DE (1969). The anorthosite problem, the problem of anorthosite and related rocks. In: Isachsen, Y.W., ed., Origin of anorthosite and related rocks. New York State Mus. Sci. Serv. Mem., 18: 71-97.

WACRENIER, P., AND WOLFF, J.P. (1965). Notice explicative sur la feuille Bangui ouest, carte geologique de reconnaissance a l'echelle du 1/500 000. French Equatorial Africa, Dir. Mines et Géologie, Inst. Equatoriale Recherches Etudes Geol. et Minières.

WALSHAW, R.D. (1965). The geology of the Ncheu-Balaka area. Geol. Surv. Malawi Bull., 19.

WALTER, M.J. (1972a). The geology of the Lilongwe-Dowa area. Geol. Surv. Malawi Bull., 26.

_____ (1972b). The geology of the Salima-Mwera Mission area. Geol. Surv. Malawi Bull., 30.

WELLS, P.R.A. (1977). Pyroxene geothermometry in simple and complex systems. Contrib. Mineral. Petrol., 62: 129-139.

_____ (1979). Chemical and thermal evolution of Archaean sialic crust, southern west Greenland. J. Petrol., 20: 187-226.

WILSON, A.F. (1976a). A normalizing procedure for comparing chemical variations in pyroxenes in mafic granulites. Contrib. Mineral. Petrol., 55: 131-138.

_____ (1976b). Aluminium in coexisting pyroxenes as a sensitive indicator of changes in metamorphic grade within the mafic granulite terrain of the Fraser Range, Western Australia. Contrib. Mineral. Petrol., 56: 255-277.

WINKLER, H.G.F. (1967). Petrogenesis of metamorphic rocks. 2nd edition, Berlin, Springer-Verlag.

_____ (1974). Petrogenesis of metamorphic rocks. 3rd edition, Berlin, Springer-Verlag.

_____ (1976). Petrogenesis of metamorphic rocks. 4th edition, Berlin, Springer-Verlag.

WINKLER, H.G.F., AND SEN, S.K. (1973). Nomenclature of granulites and other high grade metamorphic rocks. Neues Jahrb. Mineral. Monatsh., 1973: 393-402.

WOOD, B.J. (1974). The solubility of alumina in orthopyroxene coexisting with garnet. Contrib. Mineral. Petrol., 46: 1-15.

WOOD, B.J., AND BANNO, S. (1973). Garnet-orthopyroxene and orthopyroxene-clinopyroxene relationships in simple and complex systems. Contrib. Mineral. Petrol., 42: 109-125.

WYNNE-EDWARDS, H.R. (1976). Proterozoic ensialic orogenesis: the millipede model of ductile plate tectonics. Am. J. Sci., 276: 927-953.

YODER, H.S. Jr., AND TILLEY, C.E. (1962). Origin of basalt magmas: an experimental study of natural and synthetic rocks systems. J. Petrol., 3: 342-532.

YORK, D. (1969). Least squares fitting of a straight line with correlated errors. Earth and Planetary Sci.Letters, 5. 320-324.

MAP 1

34°45 161 35°00' 35°15' 35°30' 35°45'

CHIKWAWA ■

156-158 159-160 154-155 145-153

142-144

■THYOLO

123-124

125

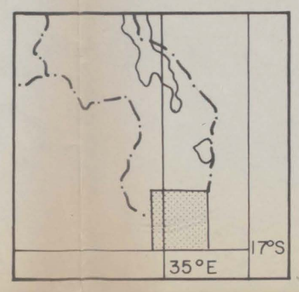
126 127

MOZAMBIQUE

16°15'

128

LOCATION



16°30'

16°30'S

5 0 5 10 15 20 20 30km

497 141

TENGANI
135 135b

129-130 131 132-134,136

498

16°45'

MOZAMBIQUE

137-140

■NSANJE

LEGEND

- Mid-Paleozoic to Recent
- Perthitic syenite
- Hypermelanic rocks
- Anorthosite
- Undifferentiated gneiss and granulite
- Geological boundaries
- International border

Geology after Bloomfield, 1958; Habgood et al., 1973

34°45' 35°00'E 35°15' 35°30' 35°45'

MAP SHOWING SAMPLE LOCALITIES

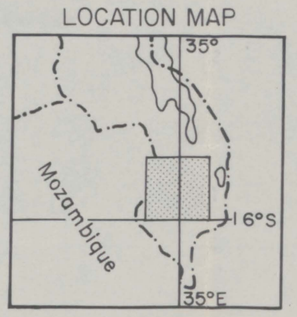
LEGEND

- Mid-Paleozoic to Recent
- Perthite-rich rocks
- Hypermelanic rocks
- Anorthosite
- Undifferentiated gneiss and granulite
- International border

501
464
470
474
14-16
465,467
469
468
47,36
483-484
12,13,110-112
32-35
475-476
480-481
482
477
478-479
27
37,38
39,59,60
40
496
491
492
493-495
61-63
7
ZOMBA
1-2;396-404; 54,55
41
50-53;369-395
9
10
405
23
3,4
11,58
5,6,8
24,174-178;281-308 48,49,118-120
57
56
346-347
345
348-350,353
354-355
351-352
344
343
342
359
339
356-358
341
340
337-338
339
330-336; 362-363
360-361
364
365
366
367
326
327
328
315
368
316
317
314
313
311-312
309-310
323
322
318-320
324
325
321
226-237
238-239
217-225
28-29; 113-117; 244-280
CHIMWADZULU MOUNTAIN
240-243
86-88
BLANTYRE
30-31
213-216
42
177-182
76-85; 183-212
45-46
162-176
43-44
499

15°15'
15°30'S
15°45'
34°30'
34°45'
35°00E
35°15'
35°30'

LOCATION MAP



5 0 5 10 15 20 25 30 km

Geology after Bloomfield, 1965a; Bloomfield and Garson, 1965; Morel, 1958

MAP SHOWING SAMPLE LOCALITIES

34°30' 34°45'

LAKE MALAWI

14°15'

502

DEDZA

92-93

94-97

422

420-421

419

418

416 417 415 414 413

411

412

410

14°30'S

423

424-426

427

428-430

98-99

100-101

431

432

433

102

434-435

103

MOZAMBIQUE

436-438

104

105

439-440

26

14°45'

448

449

450 453-454

106;455-457

453-452

458

NCHEU

107

441-442

443-444

446-447

445

462

108;459-461

109

17

463

471-473

BALAKA

14°30

14°45'

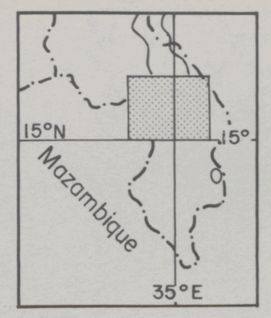
N

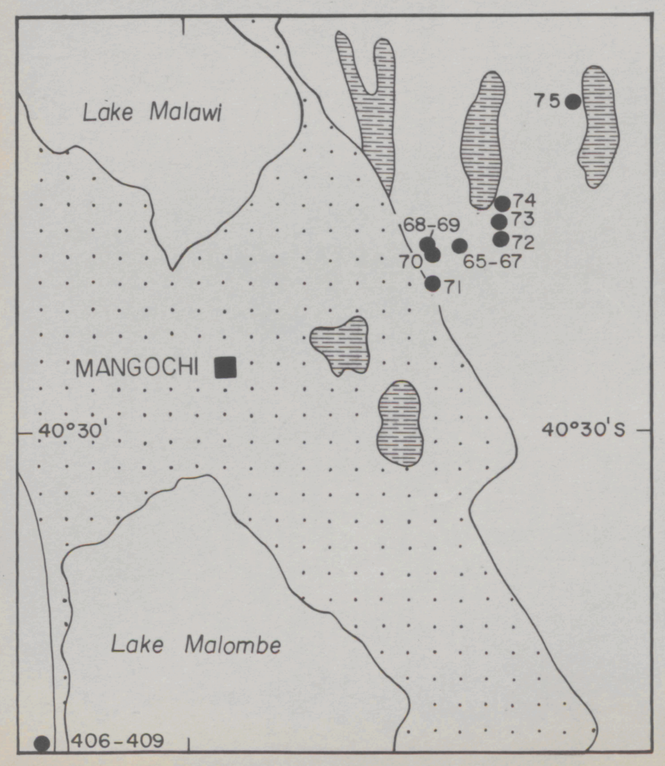
Geology after Walshaw, 1969; Thatcher, 1968

5 0 5 10 15 20 25 30 km

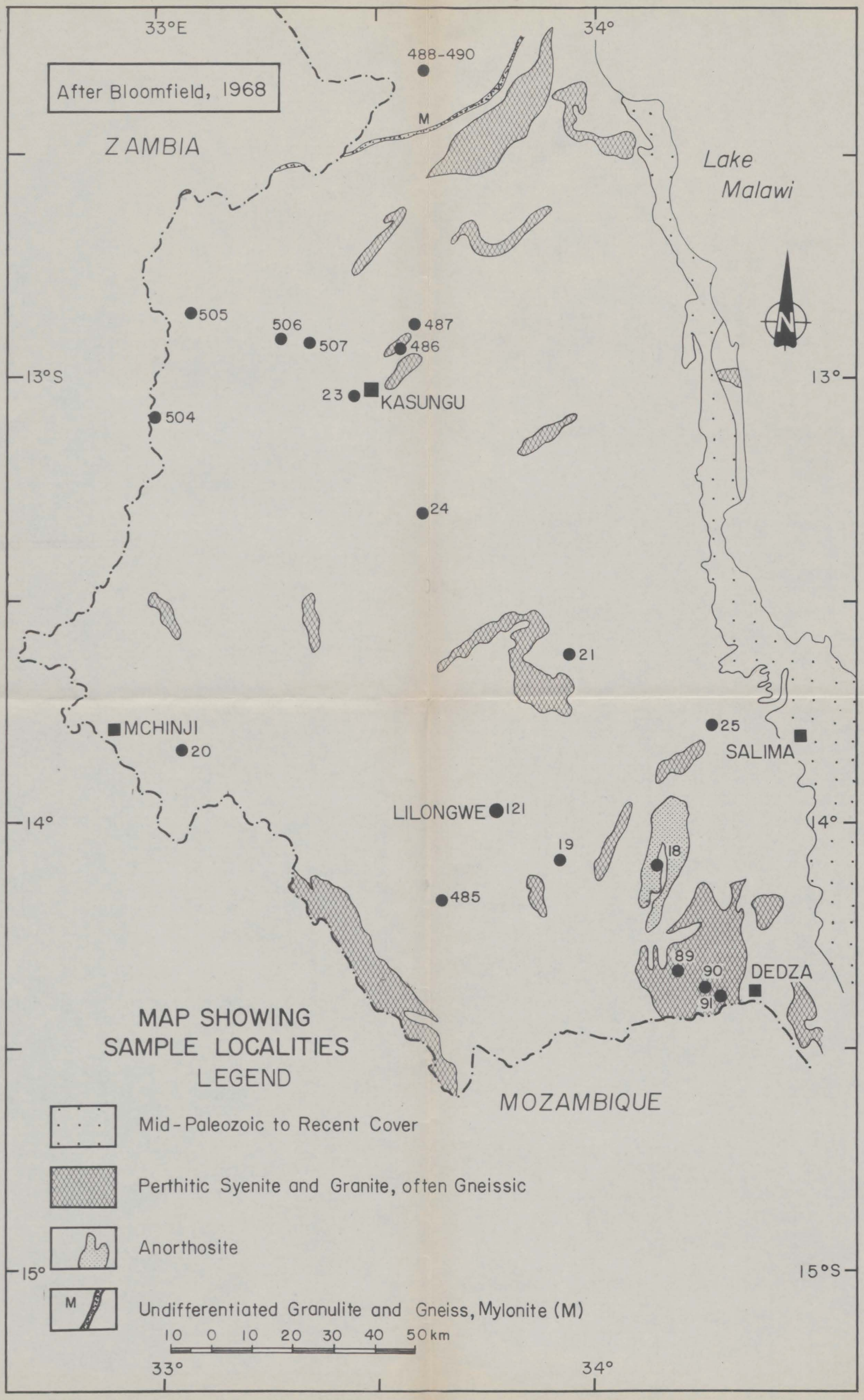
LEGEND

- Mid-Paleozoic to Recent
- Perthite-Rich rock and Granite
- Hypermelanic rocks
- Anorthosite
- Undifferentiated Gneiss and Granulite
- International border
- Geological boundary





MAP 4


33°E
34°
After Bloomfield, 1968
488-490
M
ZAMBIA
Lake
Malawi
N
505
506
507
487
486
13°S
13°
23
KASUNGU
504
24
21
MCHINJI
20
25
SALIMA
LILONGWE
121
14°
14°
19
18
485
89
90
91
DEDZA
MAP SHOWING
SAMPLE LOCALITIES
LEGEND
MOZAMBIQUE
Mid-Paleozoic to Recent Cover
Perthitic Syenite and Granite, often Gneissic
Anorthosite
15°
15°S
M
Undifferentiated Granulite and Gneiss, Mylonite (M)
10 0 10 20 30 40 50 km
33°
34°

MAP OF METAMORPHIC ASSEMBLAGES

LEGEND

- Middle-Paleozoic to Recent
- Mchinji formation and Dzalanyama granite
- Perthitic syenite, granite, monzonite, perthite-rich granulite, orthogneiss with occasional hypermelanic rocks
- Medium-pressure granulite facies suite, hypersthene-plagioclase rock, two-pyroxene granulite
- Amphibolite facies gneiss transitional to medium-pressure hornblende granulite (prograde)
- Gneiss and amphibolite transitional to garnet-clinopyroxene-plagioclase high-pressure granulite
- High-pressure granulite facies suite partly inverted to medium-pressure granulite
- (1) (2) Garnet-cordierite-(sillimanite)-granulite, (1), partly inverted to gneiss and thence to hypersthene granulite (2) (central Malawi)
- Amphibolite facies suite, undifferentiated gneiss and granulite, with structure form-lines shown
- Anorthosite
- ◇ Biotitite
- □ Garnet-olivine rock
- ▲ Hypersthene granite (Mchinji)
- ■ Melanocratic volcanic rock (Tambani)
- Aegirine-bearing gneiss

ZAMBIA

MOZAMBIQUE

MYLONITES OF THE CHIMALIRO BELT

Lake Malawi

KHOTA KOTA

KASUNGU

CHIPATA

MCHINJI

LILONGWE

DEDZA

SALIMA

Cape Maclear

MANGOCHI

Lake Malombe

Lake Chiuta

FORT MLANGENI

NCHEU

BALAKA

CHIMWADZULU

LIWONDE

Shire River

ZOMBA

Lake Chilwa

MWANZA

TAMBANI

BLANTYRE

MYLONITES OF THE MWANZA FAULT

OTHYOLO

TENGANI

NSANJE

10 0 20 40 60 80 100 km

International border

Geological boundaries

N

13°S

14°

15°

16°

17°

33°E

34°

35°

36°

TANZANIA

ZAMBIA

MOZAMBIQUE

GEOLOGY MODIFIED AFTER BLOOMFIELD, 1968; MOREL, 1961 a